REPORT NO.
EERC 76-30
DECEMBER 1976

EARTHQUAKE ENGINEERING RESEARCH CENTER

CONTRIBUTION OF A FLOOR SYSTEM TO THE DYNAMIC CHARACTERISTICS OF REINFORCED CONCRETE BUILDINGS

by

LINCOLN E. MALIK
VITELMO V. BERTERO

Report to Sponsor:
National Science Foundation

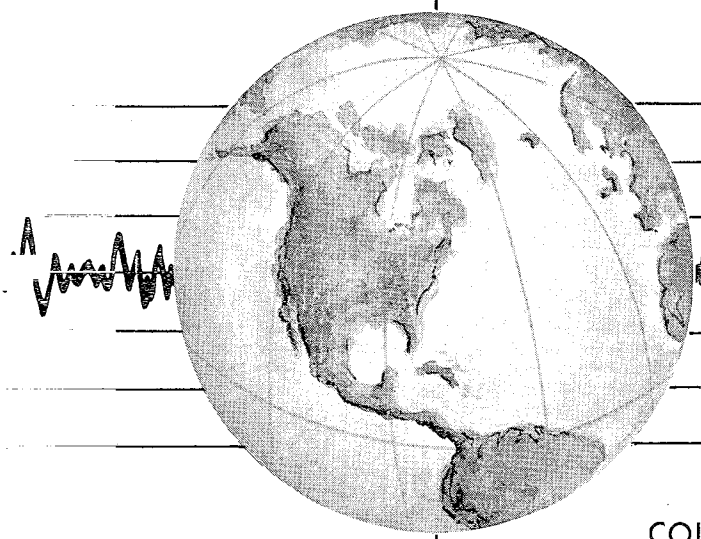

COLLEGE OF ENGINEERING

UNIVERSITY OF CALIFORNIA · Berkeley, California

BIBLIOGRAPHIC DATA SHEET	1. Report No. EERC 76-30	2.	3. Recipient's Accession No.

4. Title and Subtitle

Contribution of a Floor System to the Dynamic Characteristics of Reinforced Concrete Buildings

5. Report Date: December 1976

6.

7. Author(s): Lincoln E. Malik and Vitelmo V. Bertero

8. Performing Organization Rept. No. 76-30

9. Performing Organization Name and Address

Earthquake Engineering Research Center
University of California, Berkeley
1301 South 46th Street
Richmond, California 94804

10. Project/Task/Work Unit No.

11. Contract/Grant No.
AEN-307732 A02
ENV76-01419

12. Sponsoring Organization Name and Address

National Science Foundation
1800 G Street, N.W.
Washington, D.C. 20550

13. Type of Report & Period Covered

14.

15. Supplementary Notes

16. Abstracts

A practicable and sufficiently accurate stiffness matrix method for estimating the contribution of a floor system to the overall elastic stiffness of moment-resisting space frames is developed. The floor system considered consisted of a two-way reinforced concrete slab supported on beams between columns. This stiffness matrix method is achieved by performing extensive parametric finite element analyses to identify the main parametersaffecting and, therefore, controlling the stiffness of individual floor panels of the floor system. The stiffness of a two-way slab floor panel has been investigated by establishing an 8 x 8 panel stiffness matrix based on two rotational degrees of freedom (DOF) at each panel support. Stiffness matrix elements are determined by computing the moments necessary to produce a unit rotation at one support DOF while restraining the other seven DOF in the panel. Existing finite element computer programs are used in these computations. A series of rectangular finite elements models the bending and membrane stress-strain relations of the floor slab. The beams are modeled as uniaxial, prismatic members, connected by rigid links to the slab finite element nodes along the beam's center line. Analytical tests confirm this method's accuracy in estimating the beam-slab composite action in flexible floors.

Floor panels are classified in different categories according to their location in the floor system. To identify the principal parameters controlling the stiffness of these different types of floor panels, a total of 122 two-way slab floor panels, including 70 single panels, 14 corner panels, 28 interior panels and 1 exterior panel, are analyzed. The range of parameters included in the investigation encompasses most of the two-way reinforced concrete floors to be encountered in practice.

The stiffness matrix method, which is based on the results of parametric studies, estimates the elastic rotational stiffness of a floor as that of equivalent, uniaxial members between adjacent column floor supports. This method does not identify a physical cross section for the equivalent members; rather, it establishes a procedure by which the position of the neutral axis of the member in relation to the top of the slab and the member stiffness matrix is computed directly from a set of graphs. Each equivalent member has a 3 x 3 stiffness matrix based on one torsional and two flexural DOF.

The accuracy and practicability of the stiffness matrix method as well as of those methods currently in use, such as the ACI 318-71 equivalent frame method and an effective slab width method for predicting the lateral stiffness of moment-resisting space frames, are evaluated by applying all these methods to 27 single-story, single-panel structures
(continued on next page)

18. Availability Statement	19. Security Class (This Report)	21. No. of Pages
Release unlimited	UNCLASSIFIED	392
	20. Security Class (This Page) UNCLASSIFIED	22. Price A13 - A01

BIBLIOGRAPHIC DATA SHEET	1. Report No. EERC 76-30	2.	3. Recipient's Accession No.
4. Title and Subtitle Contribution of a Floor System to the Dynamic Characteristics of Reinforced Concrete Buildings			5. Report Date 6.
7. Author(s) Lincoln E. Malik and Vitelmo V. Bertero			8. Performing Organization Rept. No.
9. Performing Organization Name and Address Page 2 -- continued from page 1			10. Project/Task/Work Unit No. 11. Contract/Grant No.
12. Sponsoring Organization Name and Address			13. Type of Report & Period Covered 14.

15. Supplementary Notes

16. Abstracts

(continued from page one)
and 1 single-story, multi-panel structure. The results are compared with those from analyses using a finite element method. These methods, with the exception of the finite element method, are also used to predict the dynamic response of two multistory buildings. The results obtained raise serious questions as to the accuracy of equivalent frame and effective slab width methods for such predictions. The developed stiffness matrix method is found to be not only sufficiently accurate, but also simple and economical to use in practice because it can be applied directly in existing frame analysis computer programs or in manual calculations using techniques such as moment distribution. A number of recommendations for improving the method developed herein as well as for extending it to other reinforced concrete floor systems are also suggested.

17. Key Words and Document Analysis. 17a. Descriptors

17b. Identifiers/Open-Ended Terms

17c. COSATI Field/Group

18. Availability Statement	19. Security Class (This Report) UNCLASSIFIED	21. No. of Pages
10	20. Security Class (This Page) UNCLASSIFIED	22. Price

CONTRIBUTION OF A FLOOR SYSTEM TO THE DYNAMIC CHARACTERISTICS OF A REINFORCED CONCRETE BUILDING

by

Lincoln E. Malik
Research Assistant
University of California, Berkeley

and

Vitelmo V. Bertero
Professor of Civil Engineering
University of California, Berkeley

A report on research sponsored by
the National Science Foundation

Report No. EERC 76-30
Earthquake Engineering Research Center
College of Engineering
University of California
Berkeley, California

December 1976

ABSTRACT

A practicable and sufficiently accurate stiffness matrix method for estimating the contribution of a floor system to the overall elastic stiffness of moment-resisting space frames is developed. The floor system considered consisted of a two-way reinforced concrete slab supported on beams between columns. This stiffness matrix method is achieved by performing extensive parametric finite element analyses to identify the main parameters affecting and, therefore, controlling the stiffness of individual floor panels of the floor system. The stiffness of a two-way slab floor panel has been investigated by establishing an 8 x 8 panel stiffness matrix based on two rotational degrees of freedom (DOF) at each panel support. Stiffness matrix elements are determined by computing the moments necessary to produce a unit rotation at one support DOF while restraining the other seven DOF in the panel. Existing finite element computer programs are used in these computations. A series of rectangular finite elements models the bending and membrane stress-strain relations of the floor slab. The beams are modeled as uniaxial, prismatic members, connected by rigid links to the slab finite element nodes along the beam's centerline. Analytical tests confirm this method's accuracy in estimating the beam-slab composite action in flexible floors.

Floor panels are classified in different categories according to their location in the floor system. To identify the principal parameters controlling the stiffness of these different types of floor panels, a total of 122 two-way slab floor panels, including 70 single panels, 14 corner panels, 28 interior panels and 1 exterior panel, are analyzed. The range of parameters included in the investigation encompasses most of the two-way reinforced concrete floors to be encountered in practice.

The stiffness matrix method, which is based on the results of parametric studies, estimates the elastic rotational stiffness of a floor as that of equivalent, uniaxial members between adjacent column floor supports. This method does not identify a physical cross section for the equivalent members; rather, it establishes a procedure by which the position of the neutral axis of the member in relation to

the top of the slab and the member stiffness matrix is computed directly from a set of graphs. Each equivalent member has a 3 x 3 stiffness matrix based on one torsional and two flexural DOF.

The accuracy and practicability of the stiffness matrix method as well as of those methods currently in use, such as the ACI 318-71 equivalent frame method and an effective slab width method for predicting the lateral stiffness of moment-resisting space frames, are evaluated by applying all these methods to 27 single-story, single-panel structures and 1 single-story, multi-panel structure. The results are compared with those from analyses using a finite element method. These methods, with the exception of the finite element method, are also used to predict the dynamic response of two multistory buildings. The results obtained raise serious questions as to the accuracy of equivalent frame and effective slab width methods for such predictions. The developed stiffness matrix method is found to be not only sufficiently accurate, but also simple and economical to use in practice because it can be applied directly in existing frame analysis computer programs or in manual calculations using techniques such as moment distribution. A number of recommendations for improving the method developed herein as well as for extending it to other reinforced concrete floor systems are also suggested.

ACKNOWLEDGMENTS

This report is based on the dissertation written for the degree of Doctor of Philosophy by L. E. Malik (published under the name of L. J. Edgar) under the direct supervision of Professor Vitelmo V. Bertero. The valuable suggestions of Professor Graham H. Powell are gratefully acknowledged.

Financial support for this research was provided in part by the National Science Foundation under Grant Nos. AEN-307732 A02 and ENV-76-01419. The facilities of the University of California Computer Center and the Lawrence Berkeley Laboratory Computer Center were used in the course of this research.

The efforts in preparation of this manuscript by Lucia Tsai and Ellen Hill, and technical illustrations by Leonard Hashizume are greatly appreciated.

TABLE OF CONTENTS

TABLE OF CONTENTS (Continued)

TABLE OF CONTENTS (Continued)

TABLE OF CONTENTS (Continued)

LIST OF TABLES

LIST OF TABLES (Continued)

LIST OF TABLES (Continued)

LIST OF TABLES (Continued)

LIST OF TABLES (Continued)

LIST OF TABLES (Continued)

LIST OF FIGURES

LIST OF FIGURES (Continued)

LIST OF FIGURES (Continued)

LIST OF FIGURES (Continued)

NOTATIONS

A = axial area

A_g = gross area of beam

A_{sh} = shear area of beam

b = width of floor beam

b_f = overhanging flange width

CF_{ij} = carryover factors in a floor panel $[\frac{(K_{ij})_s}{(K_{ii})_s}]$

$(C_{ij})_{IP}$ = contribution of an interior panel to floor carryover factor CF_{ij}

d_s = slab thickness

D = depth of floor beams

Diff. % = percentage difference between two values

e = eccentricity between slab mid-plane and beam neutral axis $(\frac{D-d_s}{2})$

E = modulus of elasticity

f'_c = concrete compressive strength in psi

G = shear modulus

H = height of moment-resisting frame

I = moment of inertia

I^r_{FB} = transformed moment of inertia of flexural beam $(I_{FB} + A_{FB}\,\xi^2)$

I_{FB}, I_{xx}, I_B = moment of inertia of floor beam

I_s = moment of inertia of slab strip from centerline to centerline of floor panel on either side of floor beam

J = polar moment of inertia

J_{TB}, J_B = polar moment of inertia of floor beam

k_F = flexural stiffness of floor beam ($\frac{4EI_B}{L}$ for a uniform beam)

k_{ij} = off-diagonal terms of equivalent member stiffness matrix in "Stiffness Matrix Method"

k_T = torsional stiffness of floor beam ($\frac{GJ_B}{L}$ for a uniform beam)

K = stiffness of prismatic member

K_c = flexural stiffness of column

K_{ec} = flexural stiffness of equivalent column as defined in the ACI 318-71 Code, section 13-4

K_i^* = generalized stiffness in ith mode

K_{ii}, K_{ij} = elements of floor stiffness matrix based on two orthogonal degrees of freedom at each support

K_{lc} = lateral stiffness of column

K_L = lateral stiffness of moment-resisting frame

K_t = torsional stiffness of equivalent torsional member in two-way slab system as defined in the ACI 318-71 Code, section 13-4

$(K)_{em}$ = scalar term of equivalent member stiffness matrix in "Stiffness Matrix Method"

$(K_{11})_S$ = first element of floor panel stiffness matrix

$(K_{11})_B$ = rotational stiffness of two orthogonal floor beams $(\frac{4EI_{FB}}{L_1} + \frac{GJ_{TB}}{L_2})$

$(K_{11})_B^r$ = transformed bare beam stiffness $n(\frac{4EI_{FB}^r}{L_1} + \frac{GJ_{TB}}{L_2})$, where

n = 1 at exterior supports
n = 2 at interior supports

$(K_{11})_{IP}$ = contribution of interior panel to floor stiffness $(K_{11})_S$

$[K]$ = stiffness matrix

$< K_s >_1$ = first row of floor panel stiffness matrix

L_{cm} = span of orthogonal (cross) member to equivalent member in "Stiffness Matrix Method"

L_{em} = span of equivalent member in "Stiffness Matrix Method"

L_1, L_2 = span of equivalent member in "Stiffness Matrix Method"

M_i^* = generalized mass in ith mode

$[M]$ = mass matrix

P = static load

S = factor which is a function of β and L_{em}/L_{cm} and is used to compute S_{11}

S_{ii} = diagonal terms of equivalent member stiffness matrix in "Stiffness Matrix Method"

T_i = ith natural period of vibration

U_{xm}, U_{ym}, U_{zm} = displacement of master nodes as used in computer program SAP IV

U_{xs}, U_{ys}, U_{zm} = displacement of slave nodes as used in computer program SAP IV

α = ratio of flexural stiffness of flexural beam to flexural stiffness of a strip of slab from centerline to centerline of floor panels on either side of beam

$$\left(\frac{4EI_{FB}/L_1}{4EI_s/L_1}\right)$$

β = $\dfrac{\text{torsional stiffness of torsional beam}}{\text{flexural stiffness of flexural beam}} \left(\dfrac{GJ_{TB}/L_2}{EI_{FB}/L_1}\right)$

γ = $\dfrac{\xi}{e}$

Δ_T = lateral displacement of top of slab

$\Delta x, \Delta y, \Delta z$ = translation of slab mid-plane at point in floor panel

δ = distance between floor neutral axis and slab mid-plane at floor supports

$\theta_{sm}, \theta_{ym}, \theta_{zm}$ = rotations of master nodes as used in computer program SAP IV

$\theta_{xs}, \theta_{yy}, \theta_{zz}$ = rotations of slab mid-plane at point in floor panel

λ = distance from top of slab to neutral axis of equivalent beam

ν = Poisson ratio

ξ = distance between floor neutral axis and beam neutral axis of beam at floor supports

ϕ = member parameter in "Stiffness Matrix Method" which is equal to 1.0 for equivalent members framing into a corner support and is assumed equal to 0.5 for all other edge members

$\langle\phi_i\rangle$ = ith mode shape

ψ_{ij} = value of CF_{ij} as $d_s \rightarrow 0$

1. INTRODUCTION

1.1 Statement of Problem

Improvement of currently available earthquake response analysis capabilities and construction techniques assumes added urgency as more tall buildings, nuclear facilities, and other critical structures are being built in seismically-active regions. Such structures are required to have sufficient lateral stiffness and strength to avoid structural damage during minor and moderate earthquake shaking and to avoid structural collapse during severe earthquake ground motions. A rational seismic design must include a realistic estimate of the magnitude and character of the seismic forces that the structure might experience, and of the structure-soil interaction in order to be able to formulate a practical analytical model of the building-soil system.

Reinforced concrete buildings employing a moment-resisting frame usually have floor slabs that are cast monolithically with the beams or joists. Such slabs become an integral part of the moment-resisting frame. The most commonly used floor systems in reinforced concrete buildings are flat slabs and two-way slabs.

A flat slab floor system consists of a flat slab reinforced for flexure in more than one direction, with or without drop panels and column capitals. The flat ceiling surface and economy in the formworks make such floors especially attractive to architects and builders. However, there are problems with shear transfer between the floor slab and columns (even when drop panels and column capitals are used). These floors have fared poorly during recent severe earthquakes. In some cases, brittle shear failures at the floor supports have occurred, as in the Olive View Medical Center during the 1971 San Fernando Earthquake [1], and in other cases, the flexibility of this type of floor has been attributed as the cause of excessive nonstructural damage. These problems have prompted an increasing number of experts to recommend limitations on the use of flat slab floors. The 1973 Uniform Building Code [2] and the 1971 ACI Building Code [3] have both adopted provisions that limit the slab width through which moments can be transferred from the floor system to the columns. The provisions of the 1973 code

recommended by the Structural Engineers Association of California [4] are much more explicit as the commentary on section 2630-d.1 states:

> This provision limits the use of flat slab (plate) floor framing with a wide portion of the slab or even the entire column strip being considered as the framing member. Transfer of moments in structures such as these may involve relatively high shear and torsional stresses which should in general be avoided since these do not exhibit ductile characteristics.

Two-way slab floor systems consist of a slab reinforced for flexure in more than one direction and supported on beams spanning the columns. This type of floor has been found to be very suitable for construction in seismic regions. The beams, with proper web reinforcement, relieve the problem of shear transfer between the floor and columns, which minimizes the probability of shear failures around the columns and ensures more ductile behavior during an earthquake. The beams also contribute considerably to the lateral stiffness of the building as well as help limit the amount of cracking in the slab, thus reducing earthquake-related damage to the floor. The slab contributes to the rotational stiffness and strength of the beams, and also acts as a rigid diaphragm in its own plane which ties the planar building frames together and helps distribute the lateral loads among them. These favorable characteristics of two-way slab floor systems have increased the incidence of their use in buildings in seismically-active regions.

The overall lateral stiffness of moment-resisting frame buildings is primarily governed by the lateral and rotational stiffness of the columns, and the rotational stiffness of the floor system at the supports (Fig. 1.1). The degree to which the floor restrains the column rotations at the floor levels has a considerable influence on the overall lateral stiffness of a building. This influence becomes clear considering that the lateral stiffness of a column fixed at both ends is four times greater than that of a cantilever column, and hence it is usually more efficient to increase a building's lateral stiffness by increasing the stiffness of the floor rather than that of the columns.

In buildings where the floor slab is poured monolithically with beams or joists, studies have shown [5,6] that the lateral stiffness of

moment-resisting frames, which is an essential parameter in determining the dynamic response of the structure, is very sensitive to the assumed participation of the floor slab. Hence an accurate estimation of a building's response to dynamic loading requires accurate analytical models for the contribution of the floor slab to the lateral stiffness of the structure.

In the direct stiffness method, the overall building stiffness matrix can be assembled by appropriately adding the individual column and floor stiffness matrices. Currently, there are accurate and efficient formulations for the elastic and inelastic stiffness matrices of prismatic members [6] which can be used for the individual column stiffness matrix. If, as is usual, the slab is assumed rigid in its own plane, thus neglecting the influence of axial strains and in-plane rotations, and if the floor contribution to the overall building stiffness due to the uneven settlement of supports (column shortening) is also neglected, then the stiffness matrix of the floor can be defined by two rotational degrees of freedom at each support, as is shown in Fig. 1.2. Notice that due to the two-way action and continuity of the floor slab, all these floor degrees of freedom are coupled. As the floor moves into the inelastic range, the stiffness matrix at any loading interval will depend on the pattern and extent of cracking and yield lines in the floor slab.

1.2 Current Floor Stiffness Models

Despite the critical need for analytical models of these different floor types very few are available. Furthermore, most of the available research, both theoretical and experimental, concerns flat slabs. This is partially due to the complexity of analyzing floors which combine the composite action of slabs and beams.

Ideally, an analytical floor model must accurately represent the steel-concrete composite action, the composite beam-slab action, and the slab continuity and its capacity to distribute stresses in more than one direction. The finite element method comes closest to fulfilling these criteria. Some of the available finite elements have great versatility in modeling complex states of stress and strain, and the elasto-

plastic material properties of the slab, and some can even handle the composite action of the concrete and reinforcing steel. Finite element models are the most accurate models available, provided a fine enough mesh is used. However, even a coarse mesh increases the degrees of freedom in the model to such an extent that the cost of a dynamic analysis is prohibitive for tall buildings.

At present this problem is handled by modeling the two-dimensional floor system with prismatic equivalent beams between the supports. Two such currently used models are the Equivalent Frame Method and the Effective Slab Width Method.

The ACI 318-71 Code [3] recommends the Equivalent Frame Method for analyzing buildings with floors consisting of slabs reinforced for flexure in more than one direction with or without beams between supports. The equivalent frame method is based on studies conducted at the University of Illinois [7,8,9] and was to provide a better representation than other available models of the torsional and flexural rotations of the slab as well as the influence of the column size. This method models a structure as two-dimensional equivalent frames on column lines taken longitudinally and transversely through the building which are then analyzed for loads, vertical or horizontal, acting in the plane of the frames. These frames (Fig. 1.3) consist of slab-beam strips bounded laterally by the centerline of the panel on each side of the column line. The moment of inertia of the slab-beam strip is based on the gross cross section of the slab and beam except at the ends where this moment of inertia is increased [Fig. 1.3(b)] to account for the additional stiffness introduced by the column [10].

According to the ACI 318-71 Code [3] the equivalent columns (Fig. 1.4) are assumed to consist of the actual column above and below the slab-beam plus an attached torsional member transverse to the direction in which moments are being determined, and extending to the bounding lateral panel centerlines on each side of the column. The column is assumed to be rigid from the top to the bottom of the slab-beam at the joint. The flexibility of the equivalent column is defined as the sum of the flexibility of the columns above and below the floor and the flexibility of the torsional member.

Several assumptions are made in defining the way that the column and the torsional beam interact to produce the stiffness (inverse of flexibility) of the equivalent column. This is illustrated in the simplified physical model of Figs. 1.4 and 1.5 [10],

> which represents a Column AB, extending above and below the slab, with a portion of the slab CD attached thereto. A moment M applied along CD will cause a torsional rotation of the 'cross beam' CD as well as a flexural rotation of column AB. Thus the rotational restraint on the slab-beam which spans in a direction perpendicular to AB and CD, depends on both the torsional rotation of CD and the flexural rotation of AB.

The overall flexibility $1/K_{ec}$ of the equivalent column is assumed to be the sum of the column flexibility $1/\Sigma K_c$ and the torsional flexibility of the "beam" $1/K_t$. The stiffness K_c is based on the length of the column from centerline to centerline of slab and including the area of infinite moment of inertia from top to bottom of the slab-beam. The torsional stiffness K_t of the "beam" is based on several simplifying assumptions. These include the definition of an "equivalent torsional beam," and a linear moment distribution along the torsional beam which is assumed to vary from a maximum at the column to zero at the middle of the panel. Figure 1.5 shows the assumed linear distribution of the twisting moment applied along the column centerline, the resulting twisting moment diagram of the "torsional beam," and the resulting unit rotation diagram. Notice also that torsional rotation is assumed to be absent in the beam over the width of the support. The development of the expressions to calculate K_t, the assumptions on which they are based, and the justification for their use are discussed in references 7, 8, and 9.

Notice that the method does not explicitly state the level at which the slab-beam joins the column. However, the code's commentary [10] implicitly places the joint at the mid-plane of the slab when it defines the column height as being "from middepth of slab above to middepth of slab below."

As seen from the above discussion the model defined by this method is very complicated and its use in an analysis is by no means

simple. The method lends itself, though with some difficulty, to a moment distribution type of analysis, but it cannot be directly used with most existing computer programs. Such programs usually assign a column stiffness matrix based on prismatic beam theory. However, due to the rigid sections assumed at the top and bottom of the columns, the torsional beam that is attached to the column (Fig. 1.4) only changes the rotational stiffness K_c [Fig. 1.3(c)] to a value of K_{ec} but does not influence the terms associated with the lateral stiffness K_{lc} [Fig. 1.3(c)] or the off-diagonal terms of the column stiffness matrix. Hence, most frame analysis computer programs must be modified such that only the diagonal terms of the column stiffness matrix associated with the rotational degrees of freedom at the two column ends will be modified from K_c to K_{ec}.

It should also be noted that this method was developed on the basis of experiments on the behavior of flat slabs under gravity loads. The method was then generalized to apply to all floor systems employing two-way slabs under gravity and lateral loads. This generalization has not been tested and its applicability is yet to be proven.

The widely-used Effective Slab Width Method models a structure as a series of plane frames where the floor system is considered as uni-axial, prismatic equivalent beams between supports. The equivalent beams are defined as the floor beams or joists plus an effective slab width. Several effective slab width ratios have been suggested [11], ranging from 0.50 of the half panel width on each side of the column line to values greater than unity. There are some studies of flat slabs [12, 13], and others on composite slab-beam floors [14, 15, 16], but most of these deal with defining an effective slab width for designing floors with sufficient strength to carry static gravity loads rather than for defining the contribution of the floor to the lateral stiffness of a moment-resisting frame.

Often the effective slab width in floors with a two-way slab supported on beams between supports is assumed to be equal to that defined for strength design by the ACI 318-71 Code [3], sections 8.7.2 and 8.7.4a, which state:

> 8.7.2 - The effective flange width to be used in the design of symmetrical T-beams shall not exceed one-fourth of the span length of the beam, and its overhanging width on either side of the web shall not exceed eight times the thickness of the slab nor one-half the clear distance to the next beam.

and

> 8.8.4a - For beams having a flange on one side only, the effective overhaning flange width shall not exceed 1/12 of the span length of the beam, nor six times the thickness of the slab, nor one-half the clear distance to the next beam.

As noted in the 1963 edition of the UBC [17], these requirements are the same as in the 1928 code. The limitations on the flange width are empirical but were originally determined by experimental studies of T-beams. The provisions are intended to reflect the fact that shearing deformations relieve the sections of flange farthest from the web of some of the normal stresses due to flexural moments. This relieving limits the flange width that can be considered to participate with the web in resisting the applied flexural moments.

The code is very clear that these flange widths are intended for use in the strength design of T- and L-shaped beams. However, due to the complexity of the equivalent frame analysis and the lack of better alternatives, some analysts extend the application of this code provision to estimate the stiffness of two-way slab floors. An effective slab width equal to the maximum allowable flange width is used along with the beams to represent the composite action of the floor system. Thus, a two-way slab floor is modeled as a series of interior T-beams and edge L-beams.

This and other effective slab widths used are as much a product of tradition as of results of studies on design requirements for floor strength under gravity loads. This method greatly simplifies the analysis but is open to serious questions as to its underlying assumptions and to its accuracy in predicting building responses.

1.3 Objectives of Investigation

Section 1.1 discusses the importance of formulating accurate analytical models for floor systems to estimate adequately the dynamic response of moment-resisting frame structures. Section 1.2 further elaborates that currently available models either require prohibitive computational effort, such as the finite element model, or else are of questionable applicability and accuracy. This investigation was intended to study the stiffness of floors consisting of two-way slabs supported on beams between columns (Fig. 1.6) with the following specific objectives:

1. The methodology should be general enough to cover the vast majority of such floors encountered by engineers in practice.

2. To identify and study all the floor structural parameters that have a primary influence on the stiffness.

3. To develop an accurate and practicable stiffness model based on the results of this investigation which would also be suitable for use by practicing engineers.

4. To assess the accuracy of this model and other currently available models in estimating the lateral stiffness of moment-resisting frames. This would be accomplished by comparing the results from using the different models with those from a finite element analysis which is considered to be the most accurate analytical tool available for such studies.

1.4 Scope of the Investigation

The investigation considered the above objectives with the following limitations:

1. Only the initial elastic stiffness of two-way slab floors was considered.

2. All floors studied were considered to consist of rectangular panels, with a slab of uniform thickness and cast monolithically with the beams of an homogeneous, isotropic, and linear-elastic material.

3. In defining the floor stiffness, only two rotational degrees of freedom are considered at each support (Fig. 1.2). This is based on the assumption that the slab is rigid in its own plane and hence the contribution of in-plane bending and axial strains in the slab can be neglected, as well as the assumption that the slab's contribution to the building stiffness due to uneven settlement of the supports (column shortening) can also be neglected.

4. The floor is assumed to have point supports which neglects the increased stiffness of the floor across the width of the column. The corners of the two-way slab floor panels investigated herein are fairly stiff due to the intersection of the two orthogonal floor beams. Hence the influence of the column in increasing the rotational stiffness of the floor will not be as significant as in the case of flat slabs. However, this assumption might not be justified in buildings with very short spans and wide columns.

2. ELASTIC PARTIAL COMPOSITE ACTION IN A TWO-WAY SLAB FLOOR SYSTEM

2.1 Introduction

Floors consisting of a two-way slab supported on beams between the columns are usually cast monolithically, hence, the slab and the beams resist the applied loads as a single unit which is generally referred to as "composite action" [14]. "Full composite action" between the slab and the beams takes place when there is an eccentricity between the beam neutral axis and the slab neutral surface and then both vertical and horizontal shears are transmitted between the edges of the slab and beams. "Partial composite action" is a special case and occurs when the beam and slab neutral surfaces coincide (Fig. 2.1) and only vertical shears are transmitted between the beams and the slab. This greatly simplifies the analysis especially since membrane forces in the slab can be neglected.

This chapter deals with the elastic stiffness of a single-panel two-way slab floor with partial composite action, i.e., the beams are cast symmetrically above and below the slab neutral surface. Using a single-panel floor further simplifies the analysis as it avoids the problem of modeling the continuity conditions at the panel edges.

2.2 Parameters Affecting Stiffness of a Two-Way Floor System

It is clear that many different parameters can affect the stiffness of a two-way floor system, and that some of them have a greater influence than others. It is necessary in an investigation such as this to identify those parameters that have a primary effect and to limit the investigation to them. Given that this investigation is restricted to the initial elastic rotational stiffness (to first cracking of the floor system), the following parameters are identified as the primary ones to be studied:

1. Slab Thickness-to-Span Ratio (d_s/L_1). - Thickness and span are certainly primary parameters in determining the stiffness of the slab. A thick slab will be stiffer than a thin one. Also, the larger the span the more flexible will be the slab.

2. Length-to-Width Ratio of Slab (L_1/L_2). - A slab reinforced for flexure in two directions carries the load, in the small deflection elastic range, mainly by internal flexure and torsion in two directions (Fig. 2.2). To visualize the performance of such a slab, it is convenient to think of it as consisting of two intersecting sets of parallel strips [Fig. 2.2(a)]. Each strip carries part of an applied load by a combination of flexural and torsional moments. These sets of internal stresses are necessary to maintain strain compatibility within the slab. The stiffnesses of the strips are inversely proportional to their spans (L_1 and L_2), so that when one span is shortened, the strips in that direction become stiffer in both flexure and torsion and carry a higher proportion of the applied load. Thus the ratio L_1/L_2 has an important and direct bearing on the distribution of stresses within a floor slab and in the latter's overall contribution to the stiffness of the entire floor system.

The ratio L_1/L_2 is also a factor in determining the relative stiffnesses of the flexural and torsional beams. This is important inasmuch as these beams determine the boundary conditions along the edges of the slab and thus influence the overall floor stiffness.

3. Flexural and Torsional Stiffnesses of Edge Beams (k_F and k_T). - Since a two-way slab floor system consists of a floor slab and a set of beams (Fig. 2.1), the stiffness and strength of the floor can be considered to be made up of the contribution of the slab plus that of the beams. A moment applied to a column (Fig. 2.3) will primarily cause bending in one set of beams and twisting in the orthogonal set of beams. The contribution of the beams to resisting the applied moment depends on the flexural and torsional stiffnesses of the beams which are determined by material properties, cross-sectional geometry, and span length. The stiffnesses are usually defined as:

$$k_F = \frac{4EI_B}{L} \tag{2.1}$$

and

$$k_T = \frac{GJ_B}{L} \qquad (2.2)$$

The relative slab-beam stiffness in a floor system (i.e., d_s vs. k_F and k_T) has an important bearing on the behavior of the floor. It is clear that if a set of very stiff beams is covered by a thin slab, the overall stiffness and strength of the floor will consist mainly of the beam's contribution. On the other hand, a set of flexible beams supporting a very thick slab will have very little to contribute, and the floor will essentially act as a flat slab.

Another important aspect of the beam stiffnesses is the ratio of k_F of the flexural beam (AB in Fig. 2.3) to k_T of the cross beam (CD in Fig. 2.3). If the flexural stiffness of beam AB is very large compared to the torsional stiffness of beam CD, then the applied moment will be resisted primarily by flexure in beam AB which will in turn transmit the moments to the slab along its length. If the opposite were true, then the applied moment will be resisted primarily by twisting in beam CD.

The ratio of the two stiffnesses k_F/k_T has an important influence on the distribution of stresses in the slab since the beams have a major bearing on the degree of slab restraint at the edges (i.e., the boundary conditions of slab along orthogonal edges).

2.3 Method of Analysis and Computer Program Used

The contribution of a single-panel floor system to the lateral stiffness of a moment-resisting frame, as defined by the objectives and scope of this investigation (sections 1.3 and 1.4), is sufficiently defined by considering eight rotational degrees of freedom at the supports (Fig. 2.1). The direct method to establish the panel stiffness matrix is to determine the terms of each row by applying a unit rotation at the appropriate degree of freedom while restraining the other seven. The external moment to produce the unit rotation gives the diagonal term K_{ii} while the support moments give the rest of the terms of a row of the stiffness matrix.

This part of the investigation was conducted using the finite-element program PLATE [19]. The program analyzes bending in thin and moderately thick plates using linear curvature compatible triangular finite elements, which have a cubic transverse displacement expansion with piecewise-continuous second derivatives. The program also has a beam element so that it admits beams embedded in the plane of the slab.

The program PLATE refers the slab to a global right-handed Cartesian system x-y-z, with the x-y coordinates in the undeformed midsurface. The basic slab mesh unit used is the Q-19 quadrilateral [20] which is assembled with four LCCT-11 triangles [Fig. 2.4(a)]. Each has eleven bending degrees of freedom and five nodal points. The seven internal bending degrees of freedom are eliminated by a static condensation process. The program also contains a triangular mesh element [Fig. 2.4(b)], the LCCT-9, which has three nodal points and nine bending degrees of freedom.

When shear distortions are considered, six more internal degrees of freedom are added to each triangle corresponding to a linear kinematic expansion of the two mean shear distortion components.

Prismatic beam elements [Fig. 2.4(c)] used in the program are assumed to bend on the neutral axis of the slab. This has the effect of neglecting any in-plane bending interaction between slab and beam.

Two reservations might be raised in using this particular program: first, it considers homogeneous material properties for analyzing reinforced concrete structures; and secondly, it does not have a plane stress element that could model membrane forces in the slab. However, since this investigation is limited only to the initial elastic stiffness, the assumption of a homogeneous isotropic material for the floor is acceptable. Also, since the beams in this section of the investigation are symmetrical with respect to the mid-plane of the slab, the membrane stresses in the slab will be small.

2.3.1 Modeling of Floor System

The floor system shown in Fig. 2.5 was modeled of homogeneous, elastic, isotropic material where:

$$f'_c = 3.0 \text{ ksi}$$

$$E = w^{1.5}\, 33\sqrt{f'_c} = 3320.56 \text{ ksi}$$

(This is based on recommendations of the Uniform Building Code [2]).

in which

f'_c = concrete compressive strength (in psi)

$$\nu = 0.17$$

$$G = \frac{E}{2(1+\nu)} = 1419.06 \text{ ksi}$$

The beams were all of a rectangular cross-section (Fig. 2.1), and the following properties were used in the analysis:

Moment of Inertia $(I_{xx}) = \frac{D^3 b}{12}$

Polar Moment of Inertia $(J) = \frac{Db^3}{5}$

Gross Area $(A_g) = Db$

Shear Area $(A_{sh}) = \frac{5A_g}{6}$

The values for the flexural and torsional moments of inertia and the shear area are based on standard derivations that satisfy equilibrium and compatibility conditions [21].

The plate was modeled as a set of quadrilateral and triangular finite elements of uniform thickness. After a study of several meshes it was found that a relatively fine mesh close to the unrestrained degree of freedom, becoming coarser farther away from that degree of freedom, resulted in fairly good convergence.

Three sets of floors were analyzed corresponding to L_1/L_2 equal to 0.5, 1.0, and 2.0. In the case of L_1/L_2 equal to 1.0, the symmetry of the floor can be used to construct the full 8 x 8 stiffness matrix of each panel from the first row of the matrix alone. In rectangular floors with L_1/L_2 not equal to 1.0, the first two rows are necessary to construct the full stiffness matrix. In the case of panels with L_1/L_2 equal to 0.5 and 2.0, however, the first row of the stiffness matrix of one can be used to define the second row of the other. As an example, rearranging the terms of the first row of the matrix for L_1/L_2 equal to 2.0 as follows:

$$< K_{12} \; K_{11} \; K_{16} \; K_{15} \; K_{14} \; K_{13} \; K_{18} \; K_{17} >$$

yields the second row of the matrix for $L_1/L_2 = 0.5$.

2.3.2 Rotational Stiffness of Two-Way Slab Floors with Beams Symmetrical About Mid-Plane of Slab

Analyzing the single-panel floor system shown in Fig. 2.5 according to the method described in section 2.3.1 yields an array of eight terms which make up the top row of the complete (8 x 8) rotational stiffness matrix of the floor system:

$$< K_s >_1 = < K_{11} \; K_{12} \; K_{13} \; K_{14} \; K_{15} \; K_{16} \; K_{17} \; K_{18} > \qquad (2.3)$$

This can be normalized by dividing all terms by $(K_{11})_S$ to yield seven carryover factors. Hence the first row of the stiffness matrix can be presented as:

$$< K_s >_1 = (K_{11})_S < 1.0 \; CF_{12} \; CF_{13} \; CF_{14} \; CF_{15} \; CF_{16} \; CF_{17} \; CF_{18} > \qquad (2.4)$$

2.3.3 Influence of Structural Parameters on Floor Stiffness

a) Influence of d_s/L_1. - To determine the influence of d_s/L_1 on the value of $(K_{11})_S$, a series of 240 in. x 240 in. slabs (Fig. 2.5)

supported on beams with the following structural properties* was analyzed:

I_{xx} = 2250.0 in.^{4}

J = 2560.0 in.^{4}

A_g = 136.34 in.^{2}

A_{sh} = 113.62 in.^{2}

for D = 14.07 in.

b = 9.69 in.

Only the depth of slab d_s was varied. The results of the analysis are given in Table 2.1.

Another set of floor slabs with 240 in. x 240 in. spans and uniform beams with the following beam properties were analyzed:

I_{xx} = 5333.33 in.^{4}

J = 3413.33 in.^{4}

A_g = 181.78 in.^{2}

A_{sh} = 151.49 in.^{2}

for D = 18.76 in.

b = 9.69 in.

The results of the analysis with this second set of beams are also shown in Table 2.1. They clearly indicate that for both sets of beams, $(K_{11})_S$ increases as the slab depth is increased. It is of interest to find the contribution of the slab to the total stiffness of the floor system, and how this contribution is affected by changing d_s/L_1. If the slab in the floor system is neglected, then the rotational stiffness of the bare beams at the columns $(K_{11})_S$ will consist of the flexural stiffness of the flexural beam plus the torsional stiffness of the cross-beam, thus:

---

* This is the only set where a 2:1 depth-to-width of beam ratio was not maintained.

$$(K_{11})_B = \frac{4EI_{FB}}{L_1} + \frac{GJ_{TB}}{L_2} \qquad (2.5)$$

If the total stiffness $(K_{11})_S$ is now divided by $(K_{11})_B$, the results will reflect the slab contribution. The ratio $(K_{11})_S/(K_{11})_B$ is given in Table 2.1 and also plotted in Fig. 2.6. Notice that since the beams for each set maintain their structural properties, $(K_{11})_B$ remains constant, and the plots in Fig. 2.6 have the same shape as that of $(K_{11})_S$ vs. d_s/L_1. These plots show that the contribution of the slab picks up dramatically as its depth increased beyond certain values, as evidenced by the sharp increase in the slope of the plots. This could be explained qualitatively in that for slabs that are shallow relative to beam depth, floor stiffness comes mainly from the value of $(K_{11})_B$, while as the slab depth increases the contribution of the slab dominates. This latter portion of the plot is very close to a cubic equation, as to be expected since the stiffness of the slab is directly proportional to d_s^3/L_1. This relationship is confirmed in Fig. 2.7 where plotting $(K_{11})_S$ vs. d_s^3/L_1 yields a straight line beyond values of d_s^3/L_1 equal to 1.5.

The plots in Fig. 2.6 also show that the relationship between $(K_{11})_S/(K_{11})_B$ and d_s/L_1 is not unique, but is dependent on the relative stiffness of the beams used. This indicates that the influence of slab thickness on the total floor stiffness is coupled with the relative size of the beams.

Hence, the results of this section clearly show that:

1. Beyond a certain slab thickness the slab contribution dominates the value of $(K_{11})_S$ and the total stiffness coefficient becomes directly proportional to d_s^3/L_1.

2. The exact relationship between $(K_{11})_S$ and d_s/L_1 is strongly dependent on the size of the floor beams, and for quantitative relationships the two variables (floor beam size, and d_s/L_1) must be studied together.

b) Influence of d_s/L_1, α, and β. - In this section, a 240 in. x 240 in. two-way slab floor (Fig. 2.1) is analyzed by varying slab

thickness and beam flexural and torsional stiffnesses. In each case, parallel beams are assumed to have the same structural properties, and a 2:1 depth-to-width ratio. It is clear that in this analysis, where the first degree of freedom (Fig. 2.1) is the only one unrestrained, beam AB will be predominantly in bending while beam AC will be predominantly in torsion. Thus it will be convenient to call AB the flexural beam and AC the torsional beam. The importance of the ratio of the torsional stiffness of the torsional beam to the flexural stiffness of the flexural beam has already been discussed in section 2.2c, and this ratio will be labeled β herein, where:

$$\beta = \frac{\text{Torsional Stiffness of Torsional Beam}}{\text{Flexural Stiffness of Flexural Beam}}$$

$$\beta = \frac{GJ_{TB}/L_2}{4EI_{FB}/L_1} \tag{2.6}$$

In the special case where $L_1 = L_2$, eq. 2.6 reduces to:

$$\beta = \frac{G\,(Db^3)_{TB}/5}{4E(bD^3)_{FB}/12}$$

Given that in all the beams used $b = \frac{D}{2}$, then

$$\beta = 0.256\,\frac{D_{TB}^4}{D_{FB}^4} \qquad \text{For } L_1 = L_2 \tag{2.7}$$

$$\nu = 0.17$$

Another variable, α, is defined as the ratio of the flexural stiffness of the flexural beam to the stiffness of a strip of slab along the length of the beam. The width of the slab strip is defined as half a panel width when the slab extends to only one side of the beam and from centerline to centerline of adjacent panels when the slab extends to both sides of the beam. Thus:

$$\alpha = \frac{4EI_{FB}/L_1}{4EI_S/L_1} \tag{2.8}$$

and in the case of a single-panel floor, with a 2:1 depth-to-width beam ratio:

$$\alpha = \frac{(4E/L_1)[(D_{FB})^4/24]}{(4E/L_1)(L_2 d_s^3/24)} \qquad (2.9)$$

$$\alpha = \frac{D_{FB}^4}{L_2 d_s^3}$$

The variable α, defined above, can be viewed as a measure of the relative stiffnesses of the slab and flexural beam and, together with the variable β, relates three primary factors in the stiffness of the floor (slab thickness, flexural stiffness of the flexural beam, and torsional stiffness of the torsional beam).

A total of 21 floor systems with varying values of α, β, and d_s (Fig. 2.1), whose dimensions are given in Table 2.2, were analyzed. Notice that as α is a ratio involving slab thickness and flexural beam depth, it will be constant only if an increase in slab thickness is related to a proportional increase in beam size. This is also similar to the case of β where to keep a constant value of β any increase in the size of the flexural beam should be coupled with a proportional increase in the size of the torsional beam. It should also be noted that for the different values of β used, the following relationships hold true for square slab floors:

β	I_{TB}/I_{FB}
0.064	1.00
0.107	1.67
0.160	2.50

Considering that when $\beta = 0.160$ the flexural moment of inertia of the cross-beam is 2.5 times that of the flexural beam, the range of β chosen for the analysis covers the range usually encountered in square panels.

The results of analyzing the floor systems mentioned above are given in Table 2.3. The results of the previous section (Table 2.1) are presented in Table 2.4 in terms of the variables d_s, α, and β.

The most important result shown in Table 2.3 is that the ratio $(K_{11})_S/(K_{11})_B$, for the ranges of α, β, and d_s studied, is primarily dependent on α, the relative beam-to-slab flexural stiffness. If the slab depth is kept constant and β is varied, the ratio $(K_{11})_S/(K_{11})_B$ for a given value of α will be fairly stable with a variation of less than 2%. This is clear in Table 2.3 for floors with d_s equal to 6.5 in. or 9.0 in.

Table 2.3 also shows that the ratio $(K_{11})_S/(K_{11})_B$ remains stable as α and β are held constant and d_s is varied. This is a very important relationship since the values of $(K_{11})_B$ and α are readily available for any given floor and, by using a plot of α vs. $(K_{11})_S/K_{11})_B$, the value of $(K_{11})_S$ can be obtained directly. Such a plot is given in Fig. 2.8, which includes the results shown in Tables 2.3 and 2.4.

2.3.4 Influence of Structural Parameters on Carryover Factors

The first term of the rotational stiffness matrix of a floor system $(K_{11})_S$, which was discussed in the previous section, is very important in the analysis and design of structures and perhaps the single most important term in the total stiffness matrix. However, it alone is not sufficient and the values of at least several other terms are also necessary for a rational design. This section will deal with the influence of the three structural factors studied (d_s, α, and β) on the "Carryover Factors" CF_{ij}, which are the normalized terms of the stiffness matrix where:

$$CF_{ij} = \frac{(K_{ij})_S}{(K_{11})_S} \tag{2.10}$$

The present practice is to use carryover factors based on prismatic beam theory so that in the floor shown in Fig. 2.1 term CF_{13} would be equal to 0.50 and CF_{17} and CF_{18} would be equal to zero. The Commentary to the 1971 ACI Code [10] has two tables (13-1 and 13-2) which attempt to correct the carryover factors for the added stiffness due

to a rigid joint across the width of the column as compared to a point support. This method for assigning carryover factors totally neglects the effect of the slab, which distributes the moments in two, rather than one, orthogonal directions. In the case of a floor system with a slab fairly stiff relative to the beams (i.e., floors with small values of α), there will be considerable divergence in the carryover factors from those assuming prismatic members between the columns. Besides the influence of the relative slab-to-beam stiffnesses, the carryover factors also depend on the relative stiffnesses of the torsional and flexural beams (i.e., the value of β). As the size of the torsional beam is increased relative to the flexural beam the carryover factors are also expected to change, with CF_{13} decreasing and CF_{15} increasing. This means that more of the moment applied in the first degree of freedom (Fig. 2.1) is transferred in torsion along the torsional beam than in flexure along the flexural beam. As we approach the limit $\beta \to \infty$, CF_{13} approaches zero while CF_{15} approaches 1.0.

Previous sections dealt with the influence of d_s/L_1, α, and β on $(K_{11})_s$ through studying the results for the 21 floors given in Table 2.2. In each of these cases the carryover factors CF_{12} through CF_{18} were also calculated according to eq. 2.10, and the results are given in Table 2.5. These results bring out several important aspects about the carryover factors, in general, and the influence of the three parameters studied (α, β, and d_s/L_1) in particular. Most striking is the fact that for the range of parameters studied, CF_{13} is by far the largest and hence the most important. In a descriptive sense this means that of the moment $(K_{11})_s$ applied at the first degree of freedom, over 35% is transferred along the flexural beam and slab to the third degree of freedom (Fig. 2.1), while less than 10% is transferred through the slab and torsional beam to the fifth degree of freedom. Also important is the fact that within the range of parameters studied, CF_{17} and CF_{18} are fairly small (less than 4%), which means that the cross coupling between columns along a diagonal is small. Hence, the practice of modeling a moment-resistant structure with a two-way slab floor as a series of planar frames is adequate.

Since CF_{13} and CF_{15} are the larger of the factors given in Table 2.5, and as they represent the amount of moment transferred along the flexural and torsional beams, a more detailed discussion of these factors follows.

a) Influence of d_s/L_1, α, and β on CF_{13}: Within the range of parameters studied, Table 2.5 shows that CF_{13} varies little with respect to d_s/L_1 and β, and that its value is primarily dependent on α. It is important to note here that, as mentioned previously, CF_{13} will approach zero as $\beta \to \infty$. This is confirmed by the results on Table 2.5 where the values of CF_{13} decrease as d_s/L_1 and α are constant and β is increased. However, in the range used, which includes the range most likely to be encountered in the field (see section 2.3.3) the influence of β is not predominant. It should be noted that the values of CF_{13} are more sensitive to variations in β as α is increased. This can be explained qualitatively considering that α approximates the relative stiffnesses of the flexural beam and slab, and β is the ratio of the torsional stiffness of the torsional beam to the flexural stiffness of the flexural beam. In cases with small values of α, the slab is considerably stiffer than the beams and dominates the behavior. Thus, changes in the relative stiffnesses of the torsional and flexural beams do not have a major influence on the value of CF_{13}. This is reversed in floors with larger values of α where the beams dominate the behavior. Figure 2.9 gives a plot of CF_{13} vs. α, and as seen in this figure the curve becomes flatter as α increases. For large values of α the curve will approach asymptotically the value ψ_{13}, which is the carryover factor if the slab is neglected. If shear distortions in beams are not taken into account:

$$\psi_{13} = \frac{2EI_{FB}/L_1}{(4EI_{FB}/L_1) + (GJ_{TB}/L_2)} \qquad (2.11)$$

$$\psi_{13} = \frac{0.5}{1+\beta}$$

The difference between CF_{13} and ψ_{13} is due to the effect of the slab in redistributing the moments.

The results of the analysis also show the inadequacy of computing carryover factors on the basis of prismatic members (ψ_{13}) and that the error in doing so can be substantial for low values of α. As an example, there is a 20% difference between the values of ψ_{13} and CF_{13} in the first case given in Table 2.5.

b) Influence of d_s/L_1, α, and β on CF_{15}: The values of CF_{15} given in Table 2.5 are much smaller than those of CF_{13}. This is especially true for low values of α and β (i.e. shallow beams). In such cases, modeling the structure as independent parallel frames with the floor stiffness properties based on $(K_{11})_S$ and CF_{13} will give adequate results. However, as α and β are increased, values of CF_{15} also increase making it necessary to take into account cross-frame coupling through the action of slab and torsional beam.

The results of Table 2.5 shows that for the range of parameters studied, CF_{15} is not sensitive to variations in d_s/L_1, but rather depends on both of the values of α and β, unlike $(K_{11})_S/(K_{11})_B$ and CF_{13} studied above which were found to vary primarily with α. When β equals 0.160, CF_{15} goes from -0.064 to -0.096 as α is increased from 0.80 to 3.0. This phenomenon is clearly shown in Fig. 2.10, where the spread of values of CF_{15} due to changes in α increases with β. To interpret this behavior, consider that as α approaches infinity the value of CF_{15} will approach ψ_{15}, which is the carryover factor based on a floor having four beams and no slab. If shear distortions in beams are neglected,

$$\psi_{15} = \frac{GJ_{TB}/L_2}{(4EI_{FB}/L_1) + (GJ_{TB}/L_2)} \qquad (2.12)$$

$$\psi_{15} = \frac{\beta}{1 + \beta}$$

The limiting values ψ_{15} are represented in Fig. 2.10 by the dashed line. As shown in eq. 2.12, CF_{15} depends solely on β which defines the relative stiffnesses of the torsional and flexural beams. On the other hand, α determines the rate of convergence of CF_{15} toward its limit ψ_{15}. The larger α gets, the closer the results will approximate the case of a four-beam floor with no slab. This is clear in Fig. 2.10 where the curves for larger values of α are closer to the limiting value given by the dashed line.

Despite the divergent values of CF_{15}, it should be noted that in square slabs it is not very common to find a cross-beam with a moment of inertia more than double that of the flexural beam (i.e., $\beta = 0.128$), and for this value of β, CF_{15} varies between -0.055 and 0.113 when α goes from 0.8 to infinity. As this divergence is not very large, linear interpolation based on the value of α will yield an adequate approximation of CF_{15} to be used in an analytical model of the floor system.

2.3.5 Influence of L_1/L_2 on Stiffness and Carryover Factors of a Single-Panel Floor.

The importance of L_1/L_2 to the stiffness and carryover factors of a two-way slab were discussed in section 2.2b. To study the significance of this parameter, two sets of single-panel floors with L_1/L_2 equal to 0.5 and 2.0 were analyzed. These two values of L_1/L_2 can be considered as upper and lower bounds since accepted practice is to consider floors with span ratios larger than 2:1 as one-way slabs. The structural properties of the floors analyzed are given in Tables 2.6 and 2.7. The values of β used in each set of slabs reflect the following relations between the flexural and torsional beams for $L_1/L_2 = 0.5$:

β	I_{TB}/I_{FB}
0.032	1.0
0.064	2.0
0.128	4.0

and for $L_1/L_2 = 2.0$,

β	I_{TB}/I_{FB}
0.064	0.50
0.128	1.00
0.600	4.68

a) Effect on Floor Stiffness. - The first term $(K_{11})_S$ of the stiffness matrix and the ratio $(K_{11})_S/(K_{11})_B$ for these two sets of floors are given in Tables 2.8 and 2.9. It is important to note that, just as in the case of a square panel, the ratio $(K_{11})_S/(K_{11})_B$ is primarily dependent on α. Varying the size of the torsional beam (i.e., varying β) causes only small variations in the ratio $(K_{11})_S/(K_{11})_B$. To study the effect on the stiffness of the floor by changing L_1/L_2, the results of Tables 2.8 and 2.9 along with those for a square floor from Tables 2.3 and 2.4 are all plotted in Fig. 2.11. This plot makes it clear that the general behavior of the floors for all three L_1/L_2 ratios studied is the same, where the participation of the slab as reflected by $(K_{11})_S/(K_{11})_B$ increases as α decreases and this ratio approaches a value of 1.0 as α approaches infinity. The difference in the three curves of Fig. 2.11 is the degree of slab participation, which increases with L_1/L_2. To show that this behavior is structurally consistent, consider the three panels shown in Fig. 2.12 where α, d_s, and L_1 are held constant and L_2 is varied. As L_1/L_2 goes from 2.0 to 0.5, the following takes place: (1) the value of L_2 increases by a factor of 4, and (2) to maintain a constant α, d_s, and L_1, the flexural stiffness of beam AB must also increase by a factor of 4 (see Eq. 2.8).

The results of Fig. 2.11, where $(K_{11})_S/(K_{11})_B$ is found to decrease with L_1/L_2 as α is held constant, indicate that the increase in beam flexural stiffness described above is not matched by a proportional increase in slab stiffness. Hence, as L_1/L_2 decreases, the relative slab-beam stiffnesses also decrease resulting in a higher relative contribution from the beams to the total stiffness of the floor.

Finally, it is of interest in Table 2.9 to examine the influence of an extremely stiff torsional beam on the ratio $(K_{11})_S/(K_{11})_B$. The four floors with values of β equal to 0.60 include torsional beams with moments of inertia 4.68 times larger than that of the flexural beams. Since the flexural beam of a floor with $L_1/L_2 = 2.0$ is twice as long as the torsional beam, the usual case would be for the flexural beam to be the larger. Hence, the case of $\beta = 0.60$ has a much stiffer torsional beam than is to be expected in practice. Nevertheless, the influence on the ratio $(K_{11})_S/(K_{11})_B$ vs. α is not very large. The largest difference in this ratio for $\alpha = 0.80$ is only 10.6% and decreases to 6.1% for $\alpha = 3.0$. These differences indicate that as the torsional beam becomes stiffer, it forces more of the slab to participate in resisting a rotation at the corner support and hence increases the total stiffness of the floor. However, this increase in $(K_{11})_S$ is at a lower rate than the increase in $(K_{11})_B$ due to the stiffer torsional beam; hence, the ratio $(K_{11})_S/(K_{11})_B$ drops as β is increased. As α increases, the beams dominate the stiffness of the floor and the influence of a larger slab participation due to stiffer torsional beams becomes less important. These results point out that even for floors with fairly stiff, short cross-beams, the stiffness of the floor can be adequately approximated from such plots as shown in Fig. 2.11.

b) Effect on Carryover Factors. - The carryover factors CF_{12} through CF_{18} for single-panel floors with L_1/L_2 equal to 0.5 and 2.0 are given in Tables 2.10 and 2.11, respectively. These tables confirm the basic conclusions about the carryover factors arrived at in the case of $L_1/L_2 = 1.0$, i.e., that the most significant carryover factors are CF_{13} and CF_{15}. Notice that CF_{17} and CF_{18} are well below 10% in all cases studied, which further confirms the acceptability of modeling structures as a series of planar frames since the coupling along a diagonal is not very large. Notice also that CF_{17} falls off sharply with L_1/L_2, so that it is less than 2% for $L_1/L_2 = 0.5$ while it rises to over 7% for $L_1/L_2 = 2.0$. This is due to the fact that as L_1/L_2 increases (Fig. 2.12), the floor has shorter, hence stiffer, torsional beams which force more of the slab along beam AC to rotate due to a rotation at the corner support. This distributes more of the moments and rotations through the slab. On the other hand, the stiff flexural beams due to lower values of L_1/L_2 force

most of the floor action to be concentrated along the flexural beam, resulting in high values of CF_{13} and low values for the other carry-over factors.

Influence of L_1/L_2 on CF_{13}. - The results shown in Tables 2.10 and 2.11 generally confirm the conclusion reached in section 2.3.5, that given L_1/L_2, the primary factor is α, while the variations in β have only secondary effects on CF_{13}. Notice that in the case $L_1/L_2 = 2.0$, when β increases from 0.064 to 0.60, the variation of CF_{13} for a given value of α can be as high as 25%. It should be pointed out, however, that this high variation occurs when the stiffness of the torsional beam is increased to ten times that expected in usual cases. Theoretically, if β approaches infinity the value of CF_{13} will approach zero. The values of CF_{13} for the three sets of floors analyzed are plotted in Fig. 2.13. The three are similar in that they level off into fairly flat curves for $\alpha > 1.0$ and very gradually approach ψ_{13} asymptotically. The plot also shows that the value of CF_{13} varies inversely with L_1/L_2 (CF_{13} increases as L_1/L_2 decreases). Hence, the curve of CF_{13} as a function of α approaches its asymptote ψ_{13} faster for lower values of L_1/L_2. The reasons for this behavior are the same as those given in section 2.3.6a. Notice that in eq. 2.11, the asymptote ψ_{13} is independent of L_1/L_2. Tables 2.10 and 2.11 and Fig. 2.13 further clarify the observation made in section 2.3.5a about the inadequacy of assigning values for CF_{13} based on prismatic member theory (ψ_{13}). For low values of α and $L_1/L_2 = 2.0$, the difference between CF_{13} and ψ_{13} can be more than 30%.

Influence of L_1/L_2 on CF_{15}. - The values of CF_{15} for the three sets of floors analyzed are plotted in Fig. 2.14. These results again confirm the observations made above in the case of $L_1/L_2 = 1.0$ where it was found that CF_{15} is dependent on both α and β with the latter being the more important. Figure 2.14 shows that for $L_1/L_2 = 0.5$, CF_{15} is very small for the range of values studied, and could be neglected for most of these cases. This is also true for $L_1/L_2 = 1.0$ where the torsional beams are the same size as the flexural beams or smaller. CF_{15} increases when $L_1/L_2 = 2.0$, where the torsional beams are short relative to the flexural beams and, as expected, more of the moments will be resisted by these

torsional beams. Along with the results from Table 2.11, Fig. 2.14 also shows the limiting values ψ_{15} (see eq. 2.12). Notice that for $L_1/L_2 = 2.0$ and low values of β, CF_{15} is larger than ψ_{15} but that this relationship is reversed as β increases. This means that for low values of β (flexible torsional beams) a greater amount of moment reaches the corner supporting the torsional beams than would be the case if the beams acted without the slab. This sheds some light on the complex interaction of the beams and slab. When the torsional beams are very flexible, the torsional stiffness of the slab in the short span dominates the behavior of the floor and brings a greater amount of torsion to the support than would be the case with beams alone. However, as the torsional beams become stiffer, the slab acts as an elastic support distributing the torsion away along the length of the beam and redistributing it to the other supports. Thus, the slab acts as a redistributing element which distributes torsional moments to support C (Fig. 2.1) when the torsional beams are very flexible, and redistributes torsional moments away from support C when the torsional beams are very stiff.

Figures 2.13 and 2.14 also show that as L_1/L_2 increases, a structure cannot in general be adequately modeled as a series of parallel planar frames since the moments transferred along the torsional beams can be even larger than those transferred along the flexural beams. In this case, a series of intersecting orthogonal planar frames would be a much more realistic model.

2.4 Summary and Conclusions

To make a scientific assessment of existing models for the contribution of a floor system to the overall lateral stiffness of a building, and to develop new and more realistic models, it was necessary to study a fairly simple two-way floor slab. This chapter has investigated the stiffness properties of a single-panel rectangular floor supported at its four corners. The two-way slab floor was further simplified by:

1. Considering only point supports, thus eliminating the effect of varying column sizes.

2. Considering only beams symmetrical about the centerline of the slab, thus eliminating the effects of beam-slab eccentricity and the resulting in-plane slab stresses.

3. Fixing the depth-to-width ratio of the beams at 2:1, thus fixing also the relationship between the flexural and torsional stiffnesses of the individual beams.

The stiffness of the floor is defined by an 8 x 8 stiffness matrix based on two orthogonal rotational degrees of freedom in the plane of the slab at each of the four supports (Fig. 2.1). Due to the two axes of symmetry in a rectangular single-panel floor, the stiffness matrix is fully defined by the first two rows and, in the special case of a square bay, by just the top row.

The floors were modeled as a series of rectangular two-dimensional finite elements for the slab, and uniaxial prismatic elements for the beams. The program PLATE, used to solve the equations, utilizes linear curvature compatible triangular finite elements which have a cubic transverse displacement expansion with piecewise continuous derivatives, and uniaxial beam elements embedded in the slab.

The study considers the influence of the following floor parameters on the values of the coefficients of the stiffness matrix:

1. The slab depth-to-span ratio (d_s/L_1).

2. The ratio β of the torsional stiffness of the torsional beam to the flexural stiffness of the flexural beam, as given in eq. 2.6.

3. The ratio α of the flexural stiffness of the flexural beam to the flexural stiffness of a half span strip of slab along the flexural beam, as given in eq. 2.8.

4. The ratio of the span of the flexural beam to that of the torsional beam L_1/L_2 (Fig. 2.1).

A total of 46 single-panel floors was analyzed for different combinations of the above four parameters. A wide enough range of d_s/L_1, β, and α was used to establish a pattern of the influence of these parameters on the floor stiffness. The ratios 0.5 and 2.0 were used as limits for L_1/L_2, as it is customary to consider slabs beyond these limits as one-way slabs in the short direction. The following conclusions can be made based on the results given in this chapter:

1. The first term of the stiffness matrix $(K_{11})_S$ increases as d_s/L_1, α, or β are increased, or as L_1/L_2 is decreased.

2. The ratio $(K_{11})_S/(K_{11})_B$, where $(K_{11})_B$ is as defined in eq. 2.5, is primarily dependent on α and L_1/L_2. The influence of d_s/L_1 and β on this ratio for the range of parameters studied is small enough to be neglected. This is a very important relationship since L_1/L_2, α, and $(K_{11})_B$ can be calculated easily for any given floor and this information along with the plots of Fig. 2.11 allow a fairly accurate approximation of $(K_{11})_S$.

3. The ratio $(K_{11})_S/(K_{11})_B$ converges rather rapidly toward its limiting value 1.0 as α increases, and the rate of convergence is faster for lower values of L_1/L_2.

4. The carryover factors CF_{12} through CF_{18}, as defined in eq. 2.10, are all sensitive in varying degrees to changes in the four parameters studied.

5. The carryover factors other than CF_{13} and CF_{15} were generally considered small enough to be neglected. Especially important are the low values of CF_{17} and CF_{18} which show relatively low coupling via the slab between diagonally opposite supports. This reaffirms the usual practice of modeling buildings as a series of planar frames.

6. In floors with ratios of β around those expected in practice, CF_{13} is primarily dependent on the values of α and L_1/L_2, and can be adequately approximated from plots in Fig. 2.13. However, these values can be off by more than 20% in floors with exceptionally stiff torsional beams (high values of β). CF_{13} decreases as β increases.

7. The value of CF_{13} can vary substantially from the carryover factor based on prismatic beams, ψ_{13}, as defined in eq. 2.11. This is especially true in floors with high ratios of L_1/L_2 and low α. Thus the usual practice of estimating $(K_{11})_S$ and then using a CF_{13} value of 0.5 or one based on ψ_{13} can result in substantial errors.

8. CF_{15} was found to depend primarily on L_1/L_2 and β. But α, especially in its upper ranges, also showed a marked influence on CF_{15} so that this parameter could not altogether be neglected. Figure 2.14

shows CF_{15} as a function of α, β, and L_1/L_2.

9. In general, CF_{15} increases with increases in α, β, and L_1/L_2. In floors with L_1/L_2 close to 0.5 or in square panels with very flexible torsional beams, CF_{15} is small enough to be neglected. In buildings with L_1/L_2 close to 2.0, CF_{15} can be as large or larger than CF_{13}. This means that in buildings where adjacent columns do not undergo exactly the same rotations, thus introducing torsion in the cross-beams, the usual practice of modeling the building as a series of independent parallel planar frames is not always adequate. Also buildings with L_1/L_2 ratios close to 2.0, regardless of slab depth, should be modeled as a series of intersecting orthogonal planar frames.

10. The slab contributes relatively more than the beam to the stiffness of the floor for low values of α. This means that as the beams become stiffer, instead of causing comparably larger slab participation, they end up dominating the stiffness of the floor so that the relative slab contribution becomes less.

11. The slab redistributes stresses among the supports by acting as a continuous elastic support for the flexural beam, thus reducing the moments carried by the beam to one support due to a rotation at the other support--an effect which increases with decreases in α. This is reflected in the increased rate of divergence of CF_{13} from ψ_{13} for lower values of α. The slab also redistributes torsional moments along the torsional beams, especially when L_1/L_2 is large (near 2.0).

3. FULL COMPOSITE ACTION IN A TWO-WAY SLAB FLOOR SYSTEM

3.1 Introduction

The analysis of floors with partial composite action (beams symmetric about the slab mid-plane) is useful theoretically because the coincidence of the beam and slab neutral axes simplifies the structure tremendously as in-plane slab stresses can be neglected and thus appreciably reducing the computational effort needed to establish the floor stiffness matrix. These simplifications facilitated parametric studies to establish the main parameters controlling the basic beam-slab interaction and their contribution to terms of the floor stiffness matrix.

Unfortunately, such floors are rarely encountered in practice as usually the top of the slab is flush with the top of the beam, resulting in an eccentricity e between the neutral axes of beam and slab (Fig. 3.1). This eccentricity has a substantial influence on the mechanism determining beam-slab interaction in the floor. The neutral plane of the floor is no longer a plane surface coinciding with the mid-plane of the slab, but rather a curved surface whose location at any point depends on the coordinates of that point within the floor and the relative beam-slab stiffneses. The neutral plane of a single-panel floor (Fig. 3.1) starts at the edges of the floor somewhere between the neutral axes of the beam and slab, then gradually rises to approach the slab neutral axis as it proceeds toward the center of the floor. The location of the neutral plane at the edge and its slope as it proceeds toward the center of the floor depends on the relative stiffnesses of the slab and beams (values of α and β). In floors where α is small (the beams are flexible relative to slab), the vertical intercept at the edge will be close to the neutral axis of the slab, while for higher values of α it will be closer to the beam neutral axis.

The eccentricity e between the neutral axes of floor and slab means that normal stresses within the slab are not symmetrical and that there is a net normal stress within the slab per unit area. Hence, net vertical as well as horizontal shears have to be transferred between slab and beam (full composite action). This is shown in the schematic diagram of Fig. 3.2, where as a moment is introduced along the flexural beam,

part of the slab acts as a flange of a combined beam-slab section producing in-plane slab stresses. The magnitude of these stresses changes in proportion to the distance between the neutral plane of the floor and the slab mid-plane, which is a maximum at the edge of the floor and a minimum at the center.

The structural behavior of the floor along the torsional beams is similar to, but more complex than, that along the flexural beams. When a member with a symmetric section is twisted, it rotates around its shear center which coincides with the intersection of its two orthogonal neutral axes. Hence, in members with symmetric sections, torsional moments are uncoupled from flexure in either direction. In the floors analyzed in this chapter, part of the slab acts as a flange of a combined beam-slab torsional section. This interaction produces a center of shear of the combined beam-slab section which, as shown in Fig. 3.3(a), does not coincide with the shear center of the beam. As the torsional beam rotates about the combined shear center, it also undergoes vertical and lateral translations. The magnitudes of these translations are based on the location of the combined section's shear center and the angle of twist. The location of the shear center is determined by the flange width of the combined section which is dependent on the relative stiffnesses of beam and slab. The angle of twist is dependent on loading, floor stiffness, and boundary conditions.

Given the boundary conditions and loading used in this analysis, the angle of twist will vary along the torsional beam from a maximum at point A to zero at point C (Fig. 3.1). Hence the Δx and Δz translations of the beam geometric center will also vary between these two points producing flexural moments in the x and z direction along beam AC [Fig. 3.3 (a)]. Similarly, flexure in the x and z direction are coupled with torsion along the flexural beam AB.

The interaction between the slab and the torsional beams contributes to the slab in-plane stresses in two ways. First, the flexural moments along the length of the torsional beams will produce in-plane slab stresses in exactly the same manner explained above for the case of flexural beams (Fig. 3.2). Secondly, as the composite beam-slab section twists, there

is a net Δx translation at the slab mid-plane [Fig. 3.3(a)] whose value is determined by the degree of torsion at the section. Consider a slab strip jk [Fig. 3.3(b)] parallel to the flexural beams. The axial displacements, due to torsion, at the two ends of this strip (Δx_j and Δx_k) are not equal since the torsion at point j and k is different. Hence there is a net in-plane stress in the strip due to the torsion in beams AB and CD.

Besides the complex beam-slab interaction, the beam-slab eccentricity adds yet another complication to the floor model to be analyzed, the point of load application. In floors with partial composite action, studied in Chapter 2, the degrees of freedom were located at the neutral plane of the floor which coincided with the mid-plane of the slab. However, in the case of floors with full composite action (eccentric beams), the position of the neutral axis of the combined beam-slab section is not known and there are no convenient analytical methods to locate it. Applying the rotation at any other point, such as the centerline of the slab, will require application of other appropriate forces to compensate for the effect of the eccentricity between the point of load application and the neutral axis of the floor at the supports.

These and other complications are perhaps some of the reasons that experimental rather than analytical methods have predominated the research of the behavior of two-way slab systems. However, the expense of experimental studies and the time they require has limited the extent and scope of those studies. The development of new and efficient computer programs capable of producing acceptable approximations for the solution of these problems is making analytical studies on the behavior of two-way slab systems more feasible.

3.2 Floors and Parameters Considered

All the floors considered in this chapter are of a single-panel with point supports at the corners. The parameters investigated are the same four (d_s/L_1, α, β, and L_1/L_2) that were studied in the previous chapter. Equations 2.6 and 2.8 define the values of β and α.

All floors analyzed (Fig. 3.1) involve beams with a 2:1 depth-to-width ratio, which fixes the ratio of the flexural to torsional stiffness of all beams to be 13.33 $(1 + \nu)$. Different depth-to-width ratios will change the relative flexural to torsional stiffness of the individual beam and this would affect the results of this analysis in that torsion and flexure in the floor beams have been shown to be coupled (section 3.1). Having the top of beams flush with the top of slab fixes the beam-slab eccentricity e to be:

$$e = \frac{1}{2}(D-d_s) \qquad (3.1)$$

3.3 Modeling and Computer Program Used

It is clear from the above discussions that the best analytical model for the problem at hand is a three-dimensional finite element, which would most adequately account for the beam eccentricity and the resulting in-plane slab stresses. Such programs do in fact exist, but the required computational effort and cost would be prohibitive. Hence, a model utilizing planar finite elements and uniaxial prismatic beam elements was developed. Several such models have been suggested and used by analysts with reasonably acceptable accuracy, especially when used in studies of ribbed concrete bridge decks. One such model is that shown in Fig. 3.4 where the slab is represented by a planar finite element along the neutral axis of the slab and the beams are represented by uniaxial prismatic members located a distance of D/2 below the finite elements. Notice that as the finite element mesh extends to the edge of the floor [Fig. 3.4(b) and 3.4(c)], the beam element models only the part of the floor beam extending below the slab. This is necessary so that the overlapping section between slab and beam will not be accounted for twice. The beam ends are connected to the slab by rigid links at the finite element nodes, satisfying compatibility conditions there.

The section of the investigation presented in this chapter was conducted using the computer program SAP-IV [22], a general-use program for the static and dynamic analyses of linear structural systems developed at the University of California over a period of many years. The program contains eight structural elements that can be used separately, or in

combination, to model structures. The Thin Plate and Shell Element, and the Three-Dimensional Beam Element were used for the work of this chapter.

The thin plate element used in the program is a quadrilateral of arbitrary geometry formed from four compatible triangles. The LCCT9 element described in section 2.3.1 is used to represent the bending behavior of the plate. A constant strain triangle, whose plane stress properties are described in reference 23, is used to represent the membrane behavior of the plate. The thin plate quadrilateral element has a total of 24 degrees of freedom in the global coordinate system (i.e., six degrees of freedom per node), after six interior degrees of freedom in the triangular elements are eliminated by static condensation prior to assembly. The stiffness of the quadrilateral element associated with the rotation vector normal to the plate surface is not defined; therefore, the in-plane moments and rotations are neglected in SAP-IV.

The prismatic beam element included in SAP-IV considers torsion, bending about two axes, and axial and shearing deformations. The development of its stiffness properties is standard and is given in reference 24. A unique option is that the end nodes of the beam element (slave nodes) can be geometrically constrained to a master node. Slave degrees of freedom at the end of the beam are eliminated from the formulation and replaced by the transformed degrees of freedom of the master node, based on the geometry of the master and slave joints as defined in Fig. 3.5. The rotations and displacement of the slave node is defined by the following set of equations:

$$
\begin{aligned}
\theta_{xs} &= \theta_{xm} \\
\theta_{ys} &= \theta_{ym} \\
\theta_{zs} &= \theta_{zm} \\
u_{xs} &= u_{xm} + (z_s - z_m)\theta_{ym} - (y_s - y_m)\theta_{zm} \\
u_{ys} &= u_{ym} + (z_s - z_m)\theta_{xm} + (x_s - x_m)\theta_{zm} \\
u_{zs} &= u_{zm} + (y_s - y_m)\theta_{xm} - (x_s - x_m)\theta_{ym}
\end{aligned}
\tag{3.2}
$$

This option in SAP-IV efficiently models rigid links between slave and master nodes.

The method of modeling the floors by a mesh of two-dimensional finite elements connected by rigid links to prismatic uniaxial beam elements, and the specific computer program SAP-IV used, present some limitations to the accuracy of the results. These are summarized below:

1. Beam-slab compatibility is not maintained continuously along the full length of the beams; it is only maintained piecewise at the nodes where the rigid links between the slab and beams are added.

2. In-plane bending of slab is neglected as the stiffness associated with it is not defined in the plate element used. However, it is generally accepted that due to the great slab stiffness associated with in-plane bending, neglecting the rotational degree of freedom normal to the surface of flat plates has a negligible effect on the solution [23].

3. The use of a constant strain element to model the membrane action of the slab results in stepwise, rather than continuous, variation of the membrane stresses across the slab.

4. The three rotational degrees of freedom in the beam element used in SAP-IV are uncoupled. The rigid links connecting the beam ends to the finite element mesh force some coupling between these degrees of freedom. Consder the model shown in Fig. 3.6. The x and y rotations of the finite element nodes B and C are coupled. Hence, as the finite element mesh is subjected to stresses, nodes B and C will undergo x and y rotations. Since the beam nodes b and c are connected to the finite element nodes B and C by rigid links, the beam nodes will also undergo both x and y rotations (see eq. 3.2). Hence, while torsion and flexure are uncoupled in the beam element used, the rigid links to the finite element nodes have the effect of coupling the x and y rotations of the beam nodes. This only approximates the actual beam-slab composite action which has been described in section 3.1.

The overall accuracy of the model suggested above was checked by using it to calculate the stiffness of a 15-ft cantilever T-beam with a moment applied at its free end. The beam section, finite element

mesh, and the boundary conditions used are shown in Fig. 3.7. The model also includes uniaxial prismatic beam elements located 8 in. below the finite element mesh and their end nodes slaved to those of finite elements. The moment was applied to node B and very stiff beams were added between nodes C and B and between nodes A and B, to force equal rotations and displacements of these three nodes.

The results sought are the x-rotation and y-displacement of node B. The moment applied to the beam divided by this rotation yields the beam stiffness, while the y-displacement divided by the tangent of the x-rotation at B gives the position of the neutral axis below the centerline of the slab (Fig. 3.6). Comparison of these results to those from prismatic beam theory were as follows:

	K ($\frac{\text{K-in.}}{\text{rad}}$)	N.A. below Top of Slab
Beam Theory	80987.59	5.857"
Model	80987.40	5.857"

This clearly shows that, for the purpose used, the model is adequate despite the limitations mentioned above. Another calculation for the same beam section but with a span of 4 ft was attempted and the results deviated from the theoretical solution by as much as 17%. Reducing the depth-to-shear span ratio to 1:3 changed the beam from a predominantly flexural to a predominantly shear beam, and the results clearly show that the model is good in flexible beams but fails as shear predominates.

3.4 Stiffness of a Single-Panel Floor with Full Composite Action

The method of analysis followed in this chapter is similar to that used in Chapter 2 for the case of symmetrical beams. A difficulty arises in that the rotation at the first degree of freedom (Fig. 3.1) must be applied at the neutral axis of the floor at support A, whose location, as previously mentioned, is not readily available. Applying the rotation at the floor neutral axis, which lies between the neutral axes of slab and beam, means that the mid-plane of the slab will undergo a Δx translation. This is different from the case of floors with symmetric beams in

Chapter 2 where a rotation at the support is not coupled with a translation of the slab mid-plane. If in the model used in this investigation the moment is applied at the slab mid-plane (Fig. 3.6), and the beam and slab are free to undergo Δx translation at support A, then the floor will rotate about the actual floor's axis of rotation. Furthermore, since only a moment is applied at joint A, then the neutral axis and the axis of rotation at the joint coincide. If the two ends of the rigid link Aa (Fig. 3.6) are free to undergo θ_y rotations and Δx translations, then θ_y will be the same regardless of where the moment is applied along the rigid link. The values of θ_y and u_{xA} are both used as program output and the distance δ between the neutral axis of slab and floor is easily established where:

$$\delta = \frac{u_{xA}}{\tan \theta_y} \tag{3.3}$$

and using eq. 3.1, the distance ξ between the neutral axes of flexural beam and floor is:

$$\xi = \frac{D-d_s}{2.0} - \frac{u_{xA}}{\tan \theta_y} \tag{3.4}$$

Following this procedure, the stiffness of the single-panel floors investigated was established by applying a moment at support A at the level of the slab mid-plane while restraining all degrees of freedom at the support except θ_y rotation and Δx translation at support A.

The material properties used are the same as those given in section 2.3.1. The mesh size is chosen on the basis of adequate convergence of the values of $(K_{11})_S$ and ξ (e.g., Fig. 3.8 for the case $L_1/L_2 = 0.5$). Tables 3.1 to 3.3 give the dimensions of all the floors analyzed and the relationship between the torsional and flexural beams based on the values of β chosen is the same as explained in sections 2.3.3 and 2.3.5.

The results of the analysis are given in Tables 3.4, 3.5, and 3.6. The values of $(K_{11})_B$ are as defined in eq. 2.5 and are independent of the position of the beams relative to the slab. The ratio $(K_{11})_S/(K_{11})_B$ given in the tables follow a similar pattern to those for the symmetrical beams in Chapter 2: they depend primarily on the value of α, but the

variation due to changes in d_s/L_1 and β are more significant than in the case of the symmetrical beams. In the latter case, the ratio $(K_{11})_S/(K_{11})_B$ can be considered a fairly good measure of the slab contribution to the stiffness of the floor, since the value of $(K_{11})_B$, as defined in eq. 2.5, is theoretically the actual stiffness of the beams, and the increase of $(K_{11})_S$ over that is due to the contribution of the slab. This is not true in the case of eccentric beams because, as explained in section 3.1, the neutral axis of the floor does not coincide with that of the beams. Hence, a more accurate measure of the contribution of the beams to the overall stiffness of the floor $(K_{11})_S$ would require that the beam stiffness $(K_{11})_B$ be transformed from the neutral axis of the beams to that of the floor.

If in-plane distortions in a beam are neglected, the torsional stiffness is equal to GJ/L irrespective of the position of the axis of rotation. The flexural stiffness can easily be transformed by transforming the moment of inertia to the new axis of rotation. The axis of rotation at the support is identified in the previous section (Fig. 3.6), but as slab participation varies along the length of the beam, so does the position of the neutral axis. Assuming a shifted beam neutral axis a distance of ξ above the original beam neutral axis (the shifted axis coincides with the floor neutral axis at the supports only), then the transformed bare beam stiffness $(K_{11})_B^r$ is defined as:

$$(K_{11})_B^r = \frac{4E}{L_1} I_{FB}^r + \frac{GJ_{TB}}{L_2} \qquad (3.5)$$

where

$$I_{FB}^r = I_{FB} + A_{FB}\,\xi^2$$

$(K_{11})_B^r$ is not the actual contribution of beams to the total floor stiffness $(K_{11})_S$, but is closer to the actual value than $(K_{11})_B$.

Tables 3.4, 3.5, and 3.6 give the values of $(K_{11})_B^r$ and the ratio $(K_{11})_S/(K_{11})_B^r$ for each floor analyzed. Notice that this ratio follows much more closely the pattern set by $(K_{11})_S/(K_{11})_B$ in the case of symmetrical beams. $(K_{11})_S/(K_{11})_B^r$ primarily varies with α and L_1/L_2 and the effect of β and d_s/L_1 on it are negligible for the range of

parameters used in this investigation. Figure 3.9 plots the values of $(K_{11})_S/(K_{11})_B^r$ vs. α and the three curves follow very closely those of Fig. 2.11 for the case of symmetrical beams. The discussions of sections 2.3.3 and 2.3.5 about the structural significance of α, β, d_s/L_1, and L_1/L_2 on the stiffness of the floor apply also to the case of eccentric beams.

Comparing the results of Tables 3.4 through 3.6 with those of Tables 2.3, 2.8, and 2.9 to identify the effect of the beam eccentricity, it is clear that moving the neutral axis of the beam away from that of the slab significantly increases the stiffness of the floor. This is to be expected since this eccentricity shifts the neutral axis of the floor to somewhere between that of the beam and the slab and hence increases the contribution of both to the stiffness of the floor. The increase in $(K_{11})_S$ is of the order of 20% for $L_1/L_2 = 1.0$ and less for $L_1/L_2 = 2.0$ and 0.5. A very interesting result, however, is that for the cases studied, the ratio of $(K_{11})_S/(K_{11})_B^r$, case for case, is very close to $(K_{11})_S/(K_{11})_B$ for symmetrical beams. Thus it appears that the relative contribution of the slab and beams to the total floor stiffness $(K_{11})_S$ is basically the same whether the beams are symmetric with the slab mid-plane or not.

3.5 Neutral Axis of Floor at Supports

The effect of beam eccentricity on the position of the neutral axis of the floor system is discussed fully in section 3.1. Later discussions have also explained how the results of the computer program can be utilized to establish the position of the neutral axis of the floor at the support, and the importance of this information in determining $(K_{11})_B^r$. Tables 3.4, 3.5, and 3.6 give the distance ξ between the neutral axis of the flexural beam and that of the floor for all cases analyzed. These tables also give the value of γ where:

$$\gamma = \frac{\xi}{e} \tag{3.6}$$

These values of γ vs. α are plotted in Fig. 3.10. It is clear from the definition of γ in eq. 3.6 that as α increases, the influence of the beams in determining the location of the floor neutral axis at the edge increases. Therefore, the value of ξ and γ will decrease so that $\gamma \to 0$

as $\alpha \to \infty$. The results shown in Tables 3.4 through 3.6 confirm this trend and also show that variation in β has only a minor effect on the value of γ for the range of β investigated. Variation in d_s/L_1 has a more pronounced effect on γ than variation in β. However, for the range of d_s/L_1 most prevalent in practice, γ can be considered as being primarily dependent on α and L_1/L_2. Figure 3.10 shows that for any given α there is a significant increase in γ as L_1/L_2 goes from 0.5 to 1.0, but very little change for L_1/L_2 greater than 1.0. It has already been shown (section 2.3.5) that increasing L_1/L_2 also increases the degree of slab participation in the floor stiffness, which should in turn move the floor neutral axis up toward the slab mid-plane (i.e., γ should increase with L_1/L_2). There is a slight deviation from this trend in the results shown in Fig. 3.10. The reason is that a coarser finite element mesh was used for the case of $L_1/L_2 = 1.0$ than for the case of $L_1/L_2 = 2.0$. The coarser mesh results in higher values of γ (Fig. 3.8) which, given how close the values of γ for the two cases are to each other, accounts for the discrepancy.

3.6 Carryover Factors of a Single-Panel Floor with Eccentric Beams

The carryover factors as defined in eq. 2.10 are given in Tables 3.7, 3.8, and 3.9 for the three L_1/L_2 ratios studied. The basic pattern of the carryover factors in these tables is similar to that of the comparable factors for floors with symmetric beams discussed in section 2.3.5b. The values of CF_{17} and CF_{18} in Tables 3.7 through 3.9 are almost identical to those given in section 2.3.5b and confirm once again that, for the range of parameters studied, there is only a small coupling of support moments across the floor's diagonal and, as such, modeling a structure as a series of intersecting orthogonal frames is justified.

The carryover factors given in Tables 3.7 through 3.9 also confirm the conclusions of Chapter 2 that CF_{13} is the largest and the most significant carryover factor in a floor. The others, except for CF_{15} when L_1/L_2 is greater than 1.0, are small enough to be neglected in modeling a two-way slab floor.

a) CF_{13} of a Single-Panel Floor with Eccentric Beams: The values of CF_{13} given in Tables 3.7 through 3.9 clearly show that this factor is

not very sensitive to changes in d_s/L_1 and β for the range or parameters studied. This pattern of CF_{13} is discussed thoroughly in sections 2.3.4a and 2.3.5b. The influence of α and L_1/L_2 on CF_{13} in a single-panel floor with eccentric beams is better shown in Fig. 3.11. Notice that the three curves cross at about α equal to 3.0. This seems to be in conflict with the discussions of section 2.3.4a and 2.3.5b where an asymptotic value ψ_{13} independent of L_1/L_2 and α was established and it was shown that CF_{13} approached that asymptote faster as L_1/L_2 decreased. This argument is still applicable to the results of Fig. 3.11 if the definition of ψ_{13} is modified from that of eq. 2.11 to include the influence of shear in the beams. This is necessary for cases with α larger than 3.0 where the beam's depth-to-shear span ratio increases (especially for low values of L_1/L_2) and shear effects cannot be neglected. The stiffness matrix of a prismatic member with inclusion of shear distortion [25] is:

$$K = \frac{2EI}{L(1+2\tau)}\begin{bmatrix} 2+\tau & 1-\tau \\ 1-\tau & 2+\tau \end{bmatrix} \tag{3.7}$$

where

$$\tau = \frac{6EI}{GA_{eff}L^2} \tag{3.8}$$

Using the above equation, a new relationship for ψ_{13} can be defined which takes into account the shear distortions in the flexural beam. This development is given in Appendix A where ψ_{13} is shown to be not only dependent on β, but also on the size of the flexural beam. Following is a chart which compares the values of CF_{13} from Tables 3.7 through 3.9 with those of ψ_{13}, as defined in Appendix A for three values of α and L_1/L_2, with d_s equal to 6.5 in. and β equal to 0.064.

α	$L_1/L_2 = 2.0$		$L_1/L_2 = 1.0$		$L_1/L_2 = 0.5$	
	ψ_{13}	CF_{13}/ψ_{13}	ψ_{13}	CF_{13}/ψ_{13}	ψ_{13}	CF_{13}/ψ_{13}
0.8	0.467	0.645	0.466	0.725	0.453	0.777
3.0	0.464	0.750	0.462	0.749	0.483	0.789
8.0	0.460	0.780	0.457	0.755	0.419	0.792

Now that shear distortions are taken into account we find that, indeed, the values of CF_{13} do approach ψ_{13} and that they do so at a faster rate as L_1/L_2 decreases. The above table also shows that shear distortion influences ψ_{13} significantly as α increases (i.e. deeper beams), and also as the span of the flexural beams decreases (as a result of lower values of L_1/L_2).

Comparing the results given in Tables 3.7 through 3.9 with those of Chapter 2, we find that CF_{13} is smaller in floors with eccentric beams than in floors with symmetric beams. This is due to the added stiffness of the slab in floors with eccentric beams due to the membrane action. The added slab stiffness results in a higher degree of moment redistribution by the slab, hence lower values of CF_{13}.

b) CF_{15} of a Single-Panel Floor with Eccentric Beams: Similar to those of Chapter 2, the values of CF_{15} given in Tables 3.7 through 3.9 are primarily dependent on β and L_1/L_2. The influence of d_s/L_1 is small enough to be neglected but the influence of α, though less than that of β and L_1/L_2, is substantial for larger values of β. The values of CF_{15} from the tables are plotted in Fig. 3.12. As the figure shows, the pattern established by these curves is similar to that of Fig. 2.14 of floors with symmetric beams, and the reasons for this pattern are presented in sections 2.3.4b and 2.3.5b. Notice that there is some inconsistency in these results (Fig. 3.12) as the values of CF_{15} for β equal 0.2 to 0.4 seem to approach the limit ψ_{15} as α gets smaller. This indicates that the three curves should cross at the same point to be consistent theoretically, and the deviation from this is a function of the approximations inherent in the model. Nevertheless, the relative relationship between the three curves for $L_1/L_2 = 2.0$, outside the area where they cross each other, is consistent with the theoretical considerations of section 2.3.5b.

The influence of beam eccentricity is to reduce the values of CF_{15} from those for symmetric beams, and this is explained by the increased slab capacity to redistribute moments noted in the previous section.

3.7 Summary and Conclusions

This chapter investigates the effect of full composite action (i.e., the neutral axis of the beam does not coincide with that of the slab) on the terms of the stiffness matrix of a single-panel floor. The stiffness matrix of the floor is defined in section 2.3.2. Beam eccentricity produces much more complex stress patterns which increase the difficulty of the analysis and the required computational effort. The difficulty is primarily that of developing an efficient analytical model to represent accurately the compatibility requirements between beam and slab and the in-plane slab stresses which develop.

The slab is modeled as a series of rectangular finite elements, where an LCCT9 element formed from four compatible triangles is used to represent the bending behavior of the slab and a constant strain element with plane stress properties is used to represent its membrane behavior. The beams were modeled as uniaxial, prismatic members, connected at both ends by rigid links to the plate finite element nodes along the beam's centerline. This model's applicability was checked by using it to calculate the stiffness of a T-shaped cantilever beam and the results show that the model is very accurate for flexible beams under predominantly flexural stresses. This accuracy falls off rapidly as the depth-to-shear span ratio increases and shear stresses predominate. The results from the model can also be interpreted in a way that gives a reasonable approximation of the position of neutral axis of the floor at the supports.

Thirty-three single-panel floors are analyzed in this chapter to study the influence of α, β, d_s/L_1, and L_1/L_2 on floors with eccentric beams. In all these floors the beams are considered to be flush with the top of slab and to have a 2:1 depth-to-width ratio. The material properties are the same as those of Chapter 2, allowing a comparison between the results to determine the effect of beam eccentricity.

The results of the analyses show that:

1. The ratio $(K_{11})_S/(K_{11})_B$ is primarily dependent on α and L_1/L_2, but is more sensitive to variations in β and d_s/L_1 than is the case with symmetric beams. However, the ratio $(K_{11})_S/(K_{11})_B^r$, where $(K_{11})_B^r$ is defined by eq. 3.5, is much less sensitive to variations in β and d_s/L_1

and can be approximated on the basis of α and L_1/L_2.

2. Shifting the neutral axis of the floor away from that of the slab increased the stiffness of the floor $(K_{11})_S$. The value of $(K_{11})_S/(K_{11})_B^r$, for a given L_1/L_2 and α was basically the same as the value of $(K_{11})_S/(K_{11})_B$ in a floor with symmetrical beams.

3. The ratio $(K_{11})_S/(K_{11})_B^r$ approached 1.0 as α increased and approached its limiting value at a faster rate as L_1/L_2 decreased. This behavior was identical to that of floors with symmetric beams.

4. The relative position of the neutral axis at the supports as defined by the value of γ (Fig. 3.10) for the range of parameters considered was not found to be very sensitive to variations in β, but was mainly dependent on α and L_1/L_2 with some influence from d_s/L_1.

5. As in the case of floors with symmetric beams, there was very small coupling between the floor supports along a diagonal. CF_{13} was the most significant carryover factor and CF_{15} increased rapidly as L_1/L_2 became greater than one.

6. CF_{13} is primarily dependent on α and L_1/L_2, while CF_{15} is mainly determined by β and L_1/L_2 with some influence by α. This behavior was similar to that of floors with symmetric beams.

7. The carryover factors were smaller in floors with eccentric beams than in symmetric ones. This indicates a higher degree of moment redistribution by the slab in floors with eccentric beams.

4. EFFECT OF BOUNDARY CONDITION ON FLOOR STIFFNESS

4.1 Introduction

The parametric study of single-panel floors with either full or partial composite action has established the relationship between the main floor parameters and stiffness. In a multi-panel floor it is also necessary to consider the different boundary conditions which exist in the floor due to varying slab continuity conditions. In a rectangular floor, such as shown in Fig. 4.1, at least three basic different boundary conditions can be identified: a corner panel, free along two adjoining edges and continuous along the other two; an exterior panel, with one free edge and continuous along the other three; and an interior panel, continuous along all four edges.

In analyzing framed structures by the direct stiffness method, each element stiffness matrix is added directly into the overall structure stiffness matrix. The element stiffness matrix is independent of the position of the element within the structure; i.e., given the beam's properties, its element stiffness matrix will be the same whether the beam is located at the edge or the middle of the frame. Hence, a standard stiffness matrix can be established for prismatic members irrespective of where the member lies within the structure. The boundary conditions of the element are accounted for in the type of support specified for each end of the element, i.e., the stiffness matrix used in the direct stiffness matrix for cantilever and continuous beams is the same and only their support conditions are different. This procedure cannot be used for two-way floor systems. The stiffness of a floor panel as defined in section 2.3.2 depends on the composite action between the slab and beams in the panel. This composite action depends on the relative stiffnesses of slab and beams as well as on the continuity conditions of the slab at the edges. In the interaction between the beams and slab, two aspects are especially relevant to this discussion. First, in the beam-slab composite action, the slab acts as a partial support along the length of the beams, much as an elastic foundation. The degree of restraint offered by the slab is higher when the slab continues across the beams

than when it does not. Hence, an interior panel will be stiffer than a single-panel floor due to the continuity of the slab along the four edges. Second, the shape of the effective beam-slab section produced by the composite action is different depending on whether the slab is continuous or not. Section 3.1 presents a detailed discussion of the interaction between the slab and the flexural and torsional beams in a single-panel floor, where the slab obviously extends along one side of the beams only. It showed the characteristics of the resulting L-shaped composite section (Figs. 3.2, 3.3) in terms of the coupling between torsion and flexure in the x and z directions due to the section's lack of symmetry. This mechanism is totally different when the slab continues across the beam and forms with it a T-shaped composite section. The coupling between torsion and flexure in T-shaped composite sections is much weaker and in cases where the flange extends equally on both sides of the beam, the two are totally uncoupled. Hence in an interior panel such as that shown in Fig. 4.1, if complete symmetry about column lines C and 3 is assumed (i.e., equal number of bays extend on each side of the interior panel as well as having identical support conditions and floor properties on the opposite sides of the lines of symmetry), and a unit rotation corresponding to degree of freedom 5 is imposed then beams C2-C3 and C3-C4 will be in pure torsion and beams B3-C3 and C3-D3 will be in pure flexure due to compatibility requirements. On the other hand, torsion and flexure are always coupled in the edge beams.

The multi-panel floor shown in Fig. 4.1 shows many different combinations of boundary effects in the three different types of panels. The corner panel and the interior panel represent respectively the least and most stiff panels in the floor. A rotation in the sense of the second degree of freedom (Fig. 4.1) tends to induce primarily two torsional L-shaped sections and one flexural T-shaped section, while the third degree of freedom puts the T-shaped section in torsion and the L-shaped sections in flexure.

Another important consideration is the influence of the slab continuity on the carryover factors in the panel. Applying a rotation in the sense of the fourth degree of freedom shown in Fig. 4.1 will transfer different moments to supports A2 and B1 from those transferred to

supports C2 and B3 due to the different slab continuity conditions at the two sets of supports.

This chapter is devoted to determining quantitatively the influence of these boundary conditions on the stiffness matrix of each panel in order to develop a realistic stiffness model for the floor.

4.2 Floor Parameters Considered and Computer Program Used

The same parameters as in the case of single-panel floors (i.e., d_s/L_1, α, β, and L_1/L_2) are considered in this chapter to determine whether changes in boundary conditions change the basic relationships established for single-panel floors, especially the case of the interior panel where the boundary conditions differ most from those of a single-panel floor.

The computer program and modeling techniques utilized in this chapter are the same as those described in section 3.3.

4.3 Corner Panel of a Multi-Panel Floor

In investigating the stiffness of the corner panel shown in Fig. 4.2, two considerations should be taken into account. First, the moment needed to produce a unit rotation at each of the four supports will be different due to the different slab continuity conditions at the edges as discussed in the previous section. The stiffness at support A1 will be closer to that of a single-panel floor and at support B2 to that of an interior panel. Secondly, a single value of α is used to describe the beams in a panel. This is possible in the case of a single-panel floor where the width of slab used to define α (eq. 2.8) is the same for both parallel beams. However, in a corner slab this does not hold true. The slab width defining α for beam B1-B2 in Fig. 4.2 is twice that which defines α for beam A1-A2. Hence, while a constant α in a single-panel floor produces identical parallel beams, in a corner panel it produces interior beams (B1-B2 in Fig. 4.2) with twice the stiffness of edge beams (A1-A2 in Fig. 4.2). Consequently, corner panels with identical parallel beams will have different values of α in the same panel. In practice, the size of the edge beams could vary from a little above half that of parallel interior beams to equalling them. This difference in the size of parallel beams in a corner panel could influence the terms of the panel stiffness matrix.

4.3.1 Scope of Investigation of Corner Panels

The investigation of the corner panel shown in Fig. 4.2 is limited to the following considerations:

1. Establishing the panel stiffness matrix defined by the eight degrees of freedom shown in Fig. 4.3, and the influence of L_1/L_2, d_s/L_1, α, and β on the terms of the matrix.

2. Determining the influence of different-sized edge and interior beams by comparing the results of changing the moment of inertia of the interior beams from equal to, to twice that of the edge beams.

3. Comparing the results of the corner panel with those of a single-panel floor established in Chapter 3. This comparison permits first, to determine the influence of the different boundary conditions along two edges of the panel and, secondly, to decide whether this influence is large enough to require different graphs for determining $(K_{11})_S$, γ, and the carryover factors from those established in Chapter 3.

4.3.2 Modeling of a Corner Panel

The computer program (SAP-IV) and the modeling techniques used are exactly the same as those described in section 3.3. The only outstanding question is the number of panels needed to accurately model the influence of slab continuity along two edges of the corner panel. A four-panel model with 18 degrees of freedom, as shown in Fig. 4.3, is found adequate. This is established by comparing the results of a case where the slab is assumed fixed along edges GI and IC with another case where these edges are free. The results of these two cases are almost identical. The model used for the study of the corner panel considered edges GI and IC free.

The number of finite elements used for each of the three sets of floors (i.e., L_1/L_2 = 1.0, 0.5, and 2.0) was established by convergence studies, similar to those described in section 3.4. It was found that a coarser mesh in the three panels adjacent to the corner panel gave adequate results. Figure 4.3 shows the finite element mesh pattern used for the case L_1/L_2 = 1.0.

The corner panels analyzed fall into two basic categories. First are those which have interior beams (e.g., beams B1-B2 and C1-C2 in Fig. 4.2) with twice the flexural stiffness of the edge beams parallel to them (i.e., beam A1-A2 in Fig. 4.2), meaning that the value of α is constant for all parallel beams in the floor. The reason for choosing this relationship between the interior and edge beams in this section of the analysis is that it defines corner panels with the largest expected differences from the single-panel floors of Chapter 3, thus establishing the higher limits of variance in the stiffness values and carryover factors in the two cases. These corner panels are referred to in this chapter as floors with "consistent values of α." The term "consistent" is used since one value of α is sufficient to define both parallel flexural beams (i.e., beams AD and BE in Fig. 4.3). The physical dimensions of the panels analyzed are given in Table 4.1.

The second set of corner panels has identical parallel beams (e.g., beams A1-A2, B1-B2 and C1-C2). Comparing the results of this set of floors with those described above will establish the influence of varying the size of the interior beams on the stiffness and carryover factors of corner panels. This comparison is only carried out for the case of $L_1/L_2 = 2.0$ inasmuch as Chapter 3 established that the influence of the slab is most significant for that value. Furthermore, the influence of the interior beams on the stiffness at the corner support is dependent on the influence of the slab in interrelating all these beams. Hence, the higher the slab participation (i.e., larger L_1/L_2) the more the change in the interior beams will affect the stiffness at the corner support. Corner panels with equal parallel beams analyzed in this section are referred to in this chapter as "floors with nonconsistent α," and their physical dimensions are given in Table 4.2.

4.3.3 Stiffness, Carryover Factors and Neutral Axis Location of a Corner Panel

The results given in this section correspond to the degrees of freedom shown in Fig. 4.3 and are evaluated in exactly the same fashion as described in sections 3.4, 3.5 and 3.6 of Chapter 3.

The stiffness $(K_{11})_S$ of a corner support and the position of the neutral axis ξ for floors with a consistent value of α are given in Tables 4.3, 4.4, and 4.5, and those for floors with nonconsistent values

of α are given in Table 4.6. These results agree with the basic patterns established in Chapter 3.

Comparing the results of Tables 4.5 and 4.6 shows the influence of changing the cross section of the interior beams to be negligible. Reducing the stiffness of the interior beams by one-half resulted in a maximum variation of 0.64% in the value of $(K_{11})_S/(K_{11})_B^r$ and 0.36% in the values of γ. These small variations become even smaller as the α of the edge beams increases, thus reducing the relative contribution of the slab.

The carryover factors for floors with consistent values of α are given in Table 4.7 and those for floors with nonconsistent values in Table 4.8, using degrees of freedom shown in Fig. 4.3. Again the results agree with the basic patterns established in Chapter 3.

Comparing the results of Tables 4.7 and 4.8 again shows the influence of varying interior beam size to be small. The maximum variation in CF_{13} is 2.15% while that in CF_{15} is 8.17%. Notice that the variation in CF_{15} is far less significant than the percentage variations make it appear. The maximum difference occurs when $\alpha = 0.4$ and CF_{15} in the two types of floors is -0.225 vs. -0.208. The variation in carryover values falls off quickly so that for edge beams with α equal to 8.0 the maximum variation in CF_{13} is only 0.85% and for CF_{15}, 1.19%. This larger influence on the carryover factors than on $(K_{11})_S$ and γ is to be expected since doubling the stiffness of the interior beams will have its maximum effect around the support into which these beams frame.

It can be concluded from this that the stiffness, the position of the floor neutral axis, CF_{13} and CF_{15} at a corner support can be adequately evaluated from the slab thickness and structural properties of the edge beams framing into the support, whether or not identical parallel beams are used in the floor.

Tables 4.7 and 4.8 also show values of CF_{19}, $CF_{1\ 13}$, and $CF_{1\ 17}$. These reflect the coupling between supports more than one panel apart resulting from continuity of the floor slab. The very small amount of coupling reflected by these three carryover factors confirms the established practice of neglecting such coupling and modeling the building as a series of intersecting orthogonal planar frames.

4.3.4 Influence of Boundary Conditions on $(K_{11})_S$, γ, and Carryover Factors of a Corner Panel

Table 4.9 presents a comparative summary of the stiffness $(K_{11})_S$, position of the neutral axis γ, CF_{13} and CF_{15} of a corner panel and a single-panel floor. The percentage differences (Diff. %) reflect the influence that changing the boundary conditions along the two edges of a panel farthest from where the moment is applied has on these terms. A careful study of Table 4.9 shows the following:

1. Slab continuity makes the corner panel stiffness $(K_{11})_S$ higher than that of a single-panel floor, but the increase is small (the maximum difference in these floors is 4.5%) with the increase being larger for lower values of α and for higher values of L_1/L_2. This is consistent since decreasing α and increasing L_1/L_2 both have the effect of increasing the relative contribution of the slab to the total stiffness of the floor $(K_{11})_S$. Hence, changing the boundary conditions along the edges of the slab is expected to have its maximum effect in floors with lower values of α and with higher values of L_1/L_2.

2. The percentage difference in γ is higher than that for $(K_{11})_S$, but is not substantial. In the cases L_1/L_2 = 1.0 and 0.5, this difference falls off as α increases (e.g., goes from 7.87% for α = 0.8 to 0.5% for α = 8.0 when L_1/L_2 = 0.5). Notice that γ, as defined in eq. 3.6, defines the position of the neutral axis somewhere between that of the slab and the beam. Hence, for shallow beams (i.e., low α), the eccentricity e is already small and even larger differences in percentage than those registered in Table 4.9 for the value of γ will translate into only small shifts of the position of the neutral axis. This trend is reversed for L_1/L_2 = 2.0 where the difference increases as α is increased. Furthermore, the change of boundary conditions results in moving the floor's neutral axis in a different direction for L_1/L_2 = 2.0 than for L_1/L_2 = 1.0 or 0.5. Hence, while the slab continuity moves the floor neutral axis closer to that of the beam for L_1/L_2 = 1.0 and 0.5, it moves the floor neutral axis up toward the neutral axis of the slab for L_1/L_2 = 2.0 (i.e., γ for a corner panel decreases for L_1/L_2 = 1.0 and 0.5, and increases for L_1/L_2 = 2.0). This indicates that the influence

of slab continuity of a corner panel depends on the value of L_1/L_2. In the case of short flexural beams ($L_1/L_2 = 0.5$), the primary effect of slab continuity is to increase the restraint at the top of the beam, thus increasing its stiffness and sending the neutral axis of the floor closer to that of the beam. In floors with long flexural beams ($L_1/L_2 = 2.0$) the primary influence of the slab continuity is to increase the effective slab width acting as a flange of the composite beam-slab section. This larger "flange" of the combined effective section brings the floor's neutral axis closer to that of the slab (i.e., larger γ).

3. The influence of slab continuity on CF_{13} and CF_{15} is extremely small for $L_1/L_2 = 1.0$ and 0.5. The Diff. % for $L_1/L_2 = 2.0$, however, can be substantial as it reaches 38% for CF_{15} when $\alpha = 0.4$. These differences fall off as α and β are increased. It should also be noted that as large as the Diff. % are, the differences in absolute values are not as dramatic. The largest difference between a corner panel and a single-panel floor was $CF_{15} = -0.16$ vs. -0.23 when $\alpha = 0.4$ and $\beta = 0.064$.

4.3.5 Summary and Conclusions

The influence of continuing the slab across two edges of a corner panel as compared with a single-panel floor is a small increase in $(K_{11})_S$ at the corner support, a small shift in the position of the floor's neutral axis, and for $L_1/L_2 > 1.0$ some effect on the carryover factors CF_{13} and CF_{15}. These variations are primarily determined by the panels, aspect ratio, slab thickness, and size of beams framing into the corner support. Varying the size of the other beams in the floor has a negligible influence on the results.

Given the small change due to the difference in boundary conditions, the graphs and tables developed for single-panel floors in Chapter 3 adequately model the stiffness of a corner panel.

4.4 Interior Panel of a Multi-Panel Floor

It is the accepted practice in analyzing interior panels of a floor to assume an unlimited number of panels extending in all directions. Beside this condition, the interior panels analyzed here are assumed to be within floors with a constant slab thickness d_s, identical beam

cross sections for all parallel interior beams, and identical span lengths for all the panels in the floor. It should also be noted here that in an interior panel such as that shown in Fig. 4.1, it is assumed that a unit rotation at a support is resisted by four surrounding panels and the term $(K_{11})_B^r$ is twice that defined by eq. 3.5, since two identical sets of flexural and torsional beams frame into the support. Hence, in the section dealing with interior panels:

$$(K_{11})_B^r = 2\left[\frac{4EI_{FB}^r}{L_1} + \frac{GJ_{TB}}{L_2}\right] \qquad (4.1)$$

Furthermore, there are now eight supports one panel length away from an applied rotation as compared with only three in previously considered cases, and hence more carryover factors become relevant in the case of an interior panel.

4.4.1 Modeling of an Interior Panel

The computational effort for analyzing an interior panel can be greatly reduced by utilizing symmetry conditions in the floor. Given the conditions of a uniform slab thickness, identical parallel beams, and identical panel spans, the floor shown in Fig. 4.4 has two axes of symmetry. Compatibility conditions along these two axes require that when a rotation θ_{yy} is applied at support C3 while all other supports are fixed, the floor is in pure torsion along column line C and in pure flexure along column line 3. Hence, the analysis could be carried out using only a quarter of the number of panels (cutting the floor along the axes of symmetry, and using only half of the stiffness of the beams along column lines C and 3). In this case only θ_{yy} rotations are allowed along column line C, and only Δ_z displacements and θ_{yy} rotations are allowed along column line 3. These boundary conditions along column lines C and 3 apply at the neutral axis of the floor. However, the analytical model used (Figs. 3.4 and 3.7) applies all boundary conditions and loads at the finite element nodes situated along the slab mid-plane. Translating the above boundary conditions from the floor neutral axis produces the following boundary conditions at the finite element nodes (Fig. 4.4):

Col. Line	Δ_x	Δ_y	Δ_z	θ_{xx}	θ_{yy}	θ_{zz}
3	0	1	0	1	0	1
C	0	1	1	1	0	1

0 = Free
1 = Fixed

The discussion of the use of symmetry presented above is theoretically sound. However, there remains a question of whether the inherent inaccuracies of the modeling and computer program used (see section 3.3) will not be exaggerated by the use of symmetry to the point of introducing unacceptable errors into the results. To check for this, a sample case was run starting with a four-panel floor and comparing the results with those using only one panel with appropriate boundary conditions. The floors used and the finite element mesh utilized are shown in Fig. 4.5. The structural properties of beams EH and EF used in the quarter model were only half those of the actual floor. The results of the two analyses are:

	$(K_{11})_S \frac{K\text{-in}}{rad}$	γ	CF_{12}	CF_{13}	CF_{14}	CF_{15}	CF_{16}	CF_{17}	CF_{18}
Full Floor	3755.88	0.66	0	.1585	.001	.0212	0	.0127	.0084
1/4 Floor	3756.60	0.66	0	.1588	0	.0212	0	.0127	.0083
Diff. %	-.02	-	-	.19	-	-	-	-	.12

Notice that in the quarter floor model, the applied moment is a quarter of that in the actual floor. The rotation at support E will be the same for the full floor and quarter floor model used. A correct interpretation of the quarter floor model would be as follows:

$$(M_{11})_M = 0.25\ (M_{11})_F \tag{4.2}$$

$$[(K_{11})_S]_F = 4.0\ \frac{(M_{11})_M}{(\theta_{11})_M} \tag{4.3}$$

$$[CF_{1j}]_F = 2.0 \frac{(M_{1j})_M}{(M_{11})_M} \quad \text{for } j = 3,4,5,6 \tag{4.4}$$

$$[CF_{1j}]_F = \frac{(M_{1j})_M}{(M_{11})_M} \quad \text{for } j = 2,7,8 \tag{4.5}$$

These results clearly show that the finite element model and the computer program used maintain accuracy when structural symmetry is utilized, provided that correct boundary conditions are used and the results adequately interpreted.

While symmetry reduces tremendously the computational effort required to analyze an interior panel, it is necessary to determine the number of panels to be included in the analysis to determine the influence of the floor continuity along all four edges. The 16-panel floor shown in Fig. 4.4 was analyzed for the stiffness $(K_{11})_S$ at support C3 and the carryover factors to adjacent supports with the outer edges of the floor either fixed or free. The 16 panels were all square with d_s = 10.0 in., α = 0.8, β = 0.065, and L_1 = 240.0 in. The results of these two analyses were:

	$(K_{11})_S \frac{\text{K-in}}{\text{rad}}$	γ	CF_{13}	CF_{15}
Free Outside Edges	3543510.77	0.438	0.314	-0.050
Fixed Outside Edges	3544628.65	0.436	0.316	-0.050
Diff. %	-0.03	0.46	-0.64	-

The number of finite elements needed for each set of interior panels (i.e., L_1/L_2 = 1.0, 0.5, and 2.0) was established through convergence studies such as those described in section 3.4. The convergence studies showed that the outside panels required a coarser mesh than the interior panels where the rotations are applied.

The physical dimensions of the interior panels analyzed are given in Tables 4.10, 4.11 and 4.12. The significance of the chosen values of α and β is similar to that described in Table 2.2a with the primary consideration being to include the bounds of values most commonly expected in practice.

4.4.2 Stiffness, Carryover Factors and Position of Neutral Axis of an Interior Panel

Considering a support in an interior panel of a floor, such as support E in Fig. 4.6, $(K_{11})_S$ is the moment necessary to produce a unit rotation in the sense of the first degree of freedom shown in the figure while all other rotational degrees of freedom at the floor's supports are fully restrained. Following the procedures of previous chapters, Fig. 4.6 clearly shows that 16 carryover factors should be considered. However, due to the symmetry of the floors described in section 4.4.1, the following relationship between these carryover factors exists:

$$|CF_{13}| = |CF_{19}| \tag{4.6}$$

$$|CF_{14}| \quad |CF_{1\ 10}| \tag{4.7}$$

$$|CF_{15}| \quad |CF_{1\ 13}| \tag{4.8}$$

$$|CF_{16}| \quad |CF_{1\ 14}| \tag{4.9}$$

$$|CF_{17}| \quad |CF_{1\ 11}| = |CF_{1\ 15}| = |CF_{1\ 17}| \tag{4.10}$$

$$|CF_{18}| \quad |CF_{1\ 12}| = |CF_{1\ 16}| = |CF_{1\ 18}| \tag{4.11}$$

Hence the first eight carryover factors are sufficient to establish all sixteen.

The floor stiffness at an interior support $(K_{11})_S$ and the position of the neutral axis γ are given in Tables 4.13, 4.14, and 4.15. The results in these tables confirm the general conclusions of Chapter 3 as to the influence of the four structural parameters α, β, d_s/L_1, and L_1/L_2 on $(K_{11})_S$ and γ, and establish the fact that these relationships are practically independent of the boundary conditions.

The influence of slab continuity on the stiffness of an interior panel can best be displayed by the plots shown in Figs. 4.7, 4.8, and 4.9 where values of $(K_{11})_S/(K_{11})_B^r$ for a single-panel and an interior panel are presented together for the three L_1/L_2 ratios investigated. As expected, the interior panels are consistently stiffer as the slab continuity adds a partial restraint along the edges of the panel. There is a discrepancy in the case of $L_1/L_2 = 0.5$ (Fig. 4.8) and $\alpha > 3.0$ where the interior panel has a lower value of $(K_{11})_S/(K_{11})_B^r$ than the single-panel floors. This is due to the error introduced into the model of the interior panel from using flexural beams with short shear spans and large moments of inertia where shear dominates the behavior. As an example, for $L_1/L_2 = 0.5$, $L_1 = 120$ in., and $\alpha = 4.0$, Table 4.11 shows the flexural beams to have a depth of 31.5 in. resulting in a depth-to-shear span ratio of larger than 1:4. As shown in section 3.3, the beam-slab model used in this investigation is accurate for slender beams, but degrades as the beam depth-to-shear span ratio increases. Notice that shear effects become predominant in an interior panel for smaller values of α than in a single-panel floor. The reason is that the width of slab used to define α (eq. 2.8) is larger in an interior panel, as the slab extends on both sides of the beam and, hence, the same value of α produces deeper beams (i.e., larger depth-to-shear span ratio) in an interior panel than in a single-panel floor.

Figures 4.7, 4.8, and 4.9 also show that the increase in the floor stiffness due to slab continuity in an interior panel over the stiffness of a single-panel floor is small for low values of L_1/L_2 (e.g., an increase of 6.1% in the value of $(K_{11})_S/(K_{11})_B^r$ for $L_1/L_2 = 0.5$ and $\alpha = 0.4$). The increase in stiffness becomes sizable as L_1/L_2 increases (e.g., an increase of 15.9% in $(K_{11})_S/(K_{11})_B^r$ for $L_1/L_2 = 2.0$ and $\alpha = 0.4$). This trend is consistent theoretically as it has already been shown that the relative contribution of the slab to the overall stiffness of the floor gets higher as L_1/L_2 increases and consequently the effect of changing the slab boundary conditions from a single-panel floor to an interior panel will also be higher as L_1/L_2 increases. Hence, while the boundary conditions of a corner panel did not produce a significant increase in the stiffness over that of a single-panel floor,

the increase due to slab continuity on all four sides as in an interior panel cannot always be neglected. This is especially true when α is low and $L_1/L_2 > 1.0$.

Figures 4.10, 4.11, and 4.12 show plots of γ for a single-panel floor and for an interior panel. Here, the influence of the boundary conditions is not as easily discernible. As explained in section 3.5 above, the value of γ is primarily dependent on α and L_1/L_2, but can be significantly influenced by varying d_s/L_1 and to a lesser extent by varying β. In the case of $L_1/L_2 \leq 1.0$ (Fig. 4.10 and 4.11) the difference in the values of γ for a single-panel floor and an interior panel are close enough that a single curve can be used for both cases. Comparing the values of I^r_{FB} (eq. 3.5) based on the values of γ from the analysis with those based on values of γ from the curve in Fig. 4.11 gives a maximum variation of 5.0% which occurs for the case where $L_1/L_2 = 0.5$ and $\alpha = 0.8$.

The difference in γ for the case of $L_1/L_2 = 2.0$ (Fig. 4.12) is more significant with γ being larger in interior panels reflecting the influence of slab continuity along the edges of the interior panel. Notice that the values of γ (Fig. 4.12) diverge as α increases. The reason is that as α gets smaller, the beams become shallow and the eccentricity e between the neutral axes of slab and beam is small so that a larger slab participation in the overall stiffness has a small effect on shifting the floor neutral axis. An analogy with a T-beam could be drawn here where if the flanges of the beam are very wide relative to the web, an increase in the flange width will increase the stiffness more appreciably than it will move the location of the neutral axis which is already close to the flange centerline. Conversely, a T-beam with a relatively narrow flange will undergo a more significant shift in the location of its neutral axis away from the web's centerline as the flange width increases. Thus the results of Figs. 4.9 and 4.12 show that the increased "flange width" of the effective section in an interior panel has its higher influence on γ for higher values of α (i.e., deep web) and higher influence on $(K_{11})_S$ for lower values of α (i.e., shallow beams).

The carryover factors, as defined by the degrees of freedom shown in Fig. 4.6, are given in Tables 4.16, 4.17, and 4.18. These carryover factors are as defined by eq. 2.10 where CF_{ij} is the ratio of the moment needed to restrain support j to the moment necessary to produce a unit rotation at support i. However, a rotation at an interior support such as rotation θ_{11} at support E (Fig. 4.6) is resisted by four adjacent interior panels and the contribution of each interior panel to the support stiffness $(K_{11})_{IP}$ is equal to 1/4 $(K_{11})_S$. On the other hand, the number of interior panels contributing to the moments at the other supports is less than four (i.e., imposing a unit rotation in sense of the first degree of freedom, two panels contribute to moments at supports B, D, F, and H, while only one panel contributes to moments at supports A, C, G, and I in Fig. 4.6). If each of the interior panels considered were to be isolated along the column centerlines, splitting the beams equally between adjacent panels, then the interior panel contribution to the carryover factors $(CF_{ij})_{IP}$ would be as follows:

$$(CF_{ij})_{IP} = \frac{(K_{ij})_{IP}}{(K_{11})_{IP}} \tag{4.14}$$

$$(CF_{ij})_{IP} = \frac{(K_{ij})_{IP}}{0.25(K_{11})_S} \tag{4.15}$$

$$\therefore \quad (CF_{13})_{IP} = \frac{0.5(K_{13})_S}{0.25(K_{11})_S} = 2.0\ (CF_{13}) \tag{4.16}$$

similarly:

$$(CF_{15})_{IP} = 2.0\ (CF_{15}) \tag{4.17}$$

These panel carryover factors can now be compared to the single-panel floor carryover factors to identify the influence of slab continuity along the four edges of a panel. Figures 4.13, 4.14 and 4.15 give comparative plots of CF_{13} for a single-panel floor and $(CF_{13})_{IP}$ of an interior panel. Figure 4.16 gives a similar plot for CF_{15}. These figures show that the increased stiffness of an interior panel slab, due to its continuity at

the edges, results in a higher capacity to redistribute the moments away from the flexural beams (i.e., lower values of CF_{13}) and toward the torsional beam (i.e., higher values of CF_{15}). This influence is most significant for $L_1/L_2 = 2.0$ as the slab participation increases with the panel aspect ratio.

The values of CF_{17} and CF_{18} shown in Tables 4.16, 4.17, and 4.18 confirm earlier findings that coupling between diagonal supports in a floor panel is very weak. Notice that $CF_{12} = CF_{14} = CF_{16} = 0.0$ and are not given in the tables.

The values of $(K_{11})_S/(K_{11})_B^r$ given in Tables 4.13, 4.14, and 4.15 are also for an interior support and include the contribution of the four panels sharing that support. Unlike the carryover factors, however, this ratio remains the same when the contribution of only one interior panel is considered since both $(K_{11})_S$ and $(K_{11})_B^r$ would have to be divided by 4.0.

4.4.3 Summary and Conclusions

The boundary conditions created by slab continuity along the four edges of an interior panel markedly influenced the stiffness when compared with a single-panel floor. The restraint along the edges increased the stiffness of the panel which was more pronounced as L_1/L_2 increased and α decreased.

The position of the neutral axis was not affected substantially except for floors with $L_1/L_2 > 1.0$. The influence of the boundary restraint was to shift the neutral axis closer to the slab centerline reflecting a wider slab participation along the beam span.

Carryover factors CF_{12}, CF_{14}, and CF_{16} are equal to zero in an interior panel. The interior panel carryover factor CF_{13} was lower than that of a single-panel floor with the largest drop being for $L_1/L_2 = 2.0$ and for lower values of α. On the other hand, CF_{15} was higher in an interior panel which reflected an increased role of the slab in redistributing the moments.

The variations in the values of $(K_{11})_S/(K_{11})_B^r$ and the carryover factors due to the boundary conditions of an interior panel were large enough to make desirable an independent set of curves for these values

rather than use those established for a single-panel floor. In the case of γ, this was only true for $L_1/L_2 > 1.0$.

4.5 Exterior Panel of a Multi-Panel Floor

The single-panel floor and an interior panel represent the two extremes in boundary conditions that are encountered when dealing with floor stiffnesses. A single-panel floor, discontinuous along all four edges, is the most flexible while an interior panel continuous along all four edges, represents the stiffest panel. These two limiting cases have been presented above and divergence between them illustrated in Figs. 4.7 through 4.16. However, in the multi-panel floor shown in Fig. 4.1 there are other panels with boundary conditions that would place their stiffness matrix somewhere between these two bounds. The stiffness at supports B1 and B2 and the carryover factors associated with them are good examples of this.

The divergence between the two limiting cases (Figs. 4.7 through 4.16) is distinguishable but not very large. This raises the question of whether developing three more intermediate sets of curves for exterior panels is necessary. Increasing the number of different panels to be considered when analyzing a floor substantially increases the complexity of modeling without necessarily enhancing the accuracy of the final results. Furthermore, the computational effort required to analyze an exterior panel far exceeds that for others. The symmetry conditions of an interior panel make it possible to analyze only a quarter of the floor and thus reduce the computational effort required. This is not so with the exterior panels where a larger number of panels must be included in the analysis. Nevertheless, one of these intermediate cases is analyzed below to illustrate the validity of the above arguments. Figure 4.17 gives the case analyzed and the degrees of freedom studied. The floor had the following structural properties:

$$L_1 = L_2 = 240 \text{ in.}$$
$$d_s = 6.5 \text{ in.}$$
$$\alpha = 0.8$$
$$\beta = 0.064$$
$$D_{FB} = D_{TB} = 18.021 \text{ in.}$$
$$(K_{11})_B = 517534.84 \text{ K-in/rad.}$$

Notice that bays EFJI, FGKJ, IJNM, and JKPN all require fine grids of finite elements to give adequate results as all four frame into support J where the rotation is applied. In this particular case, 672 finite elements, 232 beam elements, and a total of 967 nodes were used to model the floor. This was not arrived at through convergence studies but was rather based on experience from previous analyses in the thesis. This was necessary due to the prohibitive cost of a convergence study. The slab-beam model and computer program used are the same as those described in Chapter 3.

4.5.1 Stiffness, Position of Neutral Axis, and Carryover Factors of an Exterior Panel

The stiffness of the exterior panel and the position of the neutral axis resulting from the analysis are:

γ	$(K_{11})_S$ $\frac{K\text{-in}}{rad}$	$(K_{11})^r_B$ $\frac{K\text{-in}}{rad}$	$(K_{11})_S/(K_{11})_B$	$(K_{11})_S/(K_{11})^r_B$
0.536	10066662.11	689196.57	2.061	1.548

The carryover factors corresponding to the degrees of freedom shown in Fig. 4.17 are:

CF_{12}	CF_{13}	CF_{14}	CF_{15}	CF_{16}	CF_{17}	CF_{18}	CF_{19}	$CF_{1\ 10}$	$CF_{1\ 11}$	$CF_{1\ 12}$
-	.164	-	-.027	.001	.008	.007	.162	-	.009	.002

These are support carryover factors, as distinguished from panel carryover factors, of an exterior panel. The distinction is explained in section 4.4.2. It should be noted that, despite the fact that the slab was continuous across column line GK and was discontinuous along IE, the carryover factors CF_{13} and CF_{19} were very close as were CF_{17} and $CF_{1\ 11}$. This shows that the change of boundary conditions one panel length away from where the rotation is applied, does not appreciably change the carryover factors. The carryover factors at supports M, N, and P (Fig. 4.17) are the same as those at supports E, F, and G, respectively.

The following table compares the stiffness and CF_{13} for a single-panel floor with an exterior and an interior panel. Notice that the CF_{13} used is for a panel and not a support.

Panel	$(K_{11})_S/(K_{11})_B^r$	CF_{13}
Single	1.476	.338
Exterior	1.548	.328
Interior	1.578	.328

The values in the table confirm that the exterior panel has stiffness and carryover factors intermediate between the two limiting cases of a single-panel floor and an interior panel. However, the values of the main terms of the stiffness matrix of an exterior panel are shown here to be closer to those of an interior panel.

4.6 Summary and Conclusions for the Influence of Boundary Conditions on the Stiffness Matrix of a Floor Panel

The influence of boundary conditions on $(K_{11})_S$, position of the neutral axis γ, and the carryover factors of a floor panel is determined by analyzing corner, exterior, and interior panels. The results are compared with those of a single-panel floor. The slab-beam model and the computer program used in the analysis are the same as those described in Chapter 3. The findings of the investigation carried out in this chapter can be summarized as follows:

1. Slab continuity along any of a panel's edges produced an increase in the rotational stiffness $(K_{11})_S$, and consequently a higher value of the ratio $(K_{11})_S/(K_{11})_B^r$, due to the stiffening of the slab as it is partially restrained along the continuous edges and thus increases its contribution to the overall stiffness of the panel.

2. The carryover factor CF_{13} decreased and CF_{15} increased as the number of continuous edges in a panel increased. The higher slab stiffness due to the partial restraint at the edges increased the slab's capacity to redistribute floor moments.

3. In general, the influence of slab continuity across the panel edges was to shift the floor neutral axis higher toward the slab mid-plane and therefore to increase γ. The increase in γ was proportional to the number of continuous edges in the panel. Nevertheless, the change in γ was small and was significantly different from that of a single-panel floor only in the case of an interior panel with $L_1/L_2 = 2.0$.

4. It was necessary in interior and exterior panels to distinguish between "support" and "panel" stiffness and carryover factors. The distinction is between the total support stiffness and the contribution of each panel framing into the support. The "support stiffness matrix" terms are defined as the moments necessary to impose a unit rotation at a support while restraining all other supports. The "panel stiffness matrix" is the contribution of a panel to the support stiffness (e.g., at an interior support, four interior panels contribute to the stiffness at the support).

5. The panel stiffness increased with the number of continuous edges. Thus, interior panels and single-panel floors set the upper and lower bounds of a panel stiffness. All the terms of the stiffness matrix of a single-panel floor and a corner panel were close enough that they could be used interchangeably for analytical models.

6. The terms for the stiffness of an exterior panel fell between those of corner and interior panels. The stiffness of edge supports of an exterior panel is closer to that of a corner support and the stiffness of an interior support of an exterior panel is closer to the stiffness of an interior panel support. Hence, the values for the stiffness matrix of corner and interior panels can be used to approximate the stiffness of an exterior panel.

5. "STIFFNESS MATRIX METHOD" OF MODELING ROTATIONAL STIFFNESS OF TWO-WAY SLAB FLOORS

5.1 Introduction

The previous three chapters present a detailed investigation of the rotational stiffness of a two-way floor slab as determined by the panel's main structural parameters (i.e., d_s/L_1, α, β, L_1/L_2) and the possible different boundary conditions of a panel according to its position within a multi-panel continuous floor system. The objective of this investigation, as already stated in Chapter 1, is to develop a practical and accurate model of the rotational stiffness of a floor slab for use in analyzing multistory moment-resisting frame structures having as a floor system two-way slabs (Fig. 5.1).

Presently used models, which are described in section 1.2, seek to establish the physical properties of an equivalent structure that will accurately model the rotational and translational stiffness of the column-floor moment-resisting frame. In general this is accomplished by establishing a certain "effective slab width" to be considered as a flange of an equivalent beam. This L- or T-shaped beam is then considered to define the approximate contribution of the floor to the overall stiffness of the structure. The ACI 318-71 equivalent frame method, which is described in section 1.2, goes further in also modifying the rotational stiffness of the column in an attempt to upgrade model representation of the floor's structural behavior.

In the elastic analysis of a structure using the direct stiffness method, the stiffness matrix of equivalent members, which models the floor contribution, is alone sufficient. Defining an actual physical shape for these elements is not only unnecessary but can add restrictions on the versatility of the model as described in section 1.2. The Stiffness Matrix Method (SMM) is developed in this chapter from the results of this investigation. In this method, the elastic stiffness of a floor panel is modeled by a set of uniaxial members, each with three degrees of freedom. The SMM does not identify a physical shape for these members; rather, it establishes a procedure by which the position of the neutral axis of the equivalent member in relation to the top

of slab and its member stiffness matrix can be computed directly from a set of graphs based on the boundary conditions and the main physical parameters (d_s, α, β, and L_1/L_2) of the panel under consideration.

The rest of the chapter is devoted to applying the stiffness matrix method in analyzing lateral stiffness of some structures. The results are then compared with those derived from other currently used models and with those based on a finite element model whenever this is possible. This comparison allows an objective evaluation of the accuracy and practicability of the various models.

5.2 Stiffness Matrix Method for Modeling Rotational Stiffness of a Two-Way Slab Floor

The results obtained in the studies of individual panels and the evaluation and discussion of these results presented in the previous chapters have allowed the determination of the main parameters controlling the rotational stiffness of a two-way slab floor which is the basis for the SMM. The results clearly show that coupling between supports along a diagonal and supports more than one span length from each other is very weak. Hence, it is concluded that the currently used method of replacing the floor by equivalent members which only couple adjacent supports is adequate in an elastic analysis.

The investigation also shows that while coupling between supports is higher along a flexural beam, the coupling along a torsional beam cannot always be ignored. Hence the equivalent members in the SMM are defined with three degrees of freedom [Fig. 5.2(b)], one torsional and two flexural (one flexural degree of freedom at each end of the member). The torsional degree of freedom is uncoupled from the flexural one, and the stiffness matrix of the equivalent member, [k] (equivalent member), has the form:

$$[k]_{\substack{\text{(equivalent)}\\ \text{member}}} = (K)_{em} \begin{bmatrix} S_{11} & 0 & 0 \\ 0 & S_{22} & k_{23} \\ 0 & k_{32} & S_{33} \end{bmatrix} \qquad (5.1)$$

where $(K)_{em}$ is a scalar, $S_{22} = S_{33}$ and $k_{23} = k_{32}$

The symmetry conditions (i.e., $S_{22} = S_{33}$ and $k_{23} = k_{32}$) given in eq. 5.1 are theoretically correct in interior panels (as defined in section 4.4) only. In other panels there is some difference in the value of these terms. As an example, the contribution of the corner panel (Fig. 5.1) to resisting a θ_{yy} rotation at support B is a little higher than at support A due to the different slab continuity conditions along column lines AE and BF. Hence S_{22} and S_{33} in equivalent member AB [Fig. 5.2(a)] should be different. However, the results presented in Chapter 4 show that this difference is very small and does not justify the complication resulting in the model if these differences were to be included. A compromise between accuracy and simplicity is necessary for practical applications.

The investigation of the floor stiffness presented in previous chapters was based on support degrees of freedom and the stiffness terms reflected the contribution of the flexural and torsional beams of all the panels that framed into a support. Hence, it is necessary that the stiffness matrix of the equivalent members be such that as they are added together they will produce the same support stiffnesses as those found in the investigation.

The SMM identifies two types of equivalent members: edge members [e.g., members BC and AE in Fig. 5.2(a)] and interior members [e.g., members BF and FJ in Fig. 5.2(a)]. Both have a 3 x 3 stiffness matrix (eq. 5.1) and differ only in the equations and graphs used to determine the matrix elements. Again it can be shown that the stiffness of the exterior panel (Fig. 5.1) along beam BC is higher than that of the corner panel along beam AB as well as that along beam BF being different from the stiffness of the interior panel along beam FJ. However, these differences were found to be small (see Chapter 4) and using one set of equations and graphs for all edge members and another for all interior members is justified.

Figures 5.3(a), 5.3(b), 5.3(c), and 5.3(d) give all the graphs necessary to locate the neutral axis and calculate the stiffness matrix of equivalent edge members; and Figs. 5.4(a), 5.4(b), 5.4(c), and 5.4(d) are sufficient for calculating equivalent interior members. These figures

are derived from the results of the investigation presented in the previous three chapters as follows:

1. Figures 5.3(a) and 5.4(a) define the position of the neutral axis of equivalent edge and interior members respectively. Figure 5.3(a) is derived from the results for a single-panel floor (Fig. 3.10) after the curves for $L_1/L_2 = 1.0$ and 2.0 were merged due to the very small variation between them. Figure 5.4(a) is an exact reproduction of the results of an interior panel (Figs. 4.10, 4.11, and 4.12).

2. Figures 5.3(b) and 5.4(b) define the stiffness matrix term $(K)_{em}$ for equivalent edge and interior members respectively. Figure 5.3(b) is derived from the results of a single-panel floor (Fig. 3.9) and Fig. 5.4(b) from the results of an interior panel (Figs. 4.7, 4.8, and 4.9). In the SMM, the value of $(K_{11})_S$ of a floor panel as defined in previous chapters is proportioned between orthogonal equivalent members such that the flexural stiffness of one equivalent member plus the torsional stiffness of the orthogonal equivalent member will equal the $(K_{11})_S$ of the panel. As an example, if the single-panel floor shown in Fig. 3.1 is modeled by four equivalent members between the supports, then:

$$[(K_{11})_S] = [(K)_{em}\ (S_{22})]_{AB} + [(K)_{em}\ (S_{11})]_{AC}$$

where $(K_{11})_S$ = single panel floor stiffness as defined in Chapter 3

$[(K)_{em}\ (S_{22})]_{AB}$ = terms of stiffness matrix of equivalent member AB as defined by eq. 5.1.

$[(K)_{em}\ (S_{11})]_{AC}$ = terms of stiffness matrix of equivalent member AC as defined by eq. 5.2.

3. Figures 5.3(c) and 5.4(c) define the off-diagonal matrix terms k_{23} and are identical to the graphs for CF_{13} vs. α of a single-panel floor (Fig. 3.11) and those of an interior panel (Figs. 4.13, 4.14, and 4.15). CF_{13} in the actual floor panel and k_{23} in the equivalent member both define the moment necessary to restrain a floor support when a unit rotation is applied to the adjacent support (the rotation vector being orthogonal to the column line connecting the two supports).

4. Figures 5.3(d) and 5.4(d) define a factor S which is to be used in computing the value of S_{11} of the equivalent member stiffness matrix. The product S_{11} $(K)_{em}$ in eq. 5.1 defines the torsional stiffness of the equivalent member, and can be derived from the results of the analysis reported in previous chapters.

Consider the single-panel floor shown in Fig. 3.1. The product (CF_{15}) $(K_{11})_S$ is the torsion carried by the floor along beam AC due to a unit rotation at A in the sense of the first degree of freedom. This is analogous to the torsional stiffness of the equivalent member AC to be used in modeling the floor. Hence, the values of CF_{15} given in Figs. 3.12, 4.16 and Tables 4.16 through 4.18 can be used to determine S_{11} as follows:

a) In the figures and tables of CF_{15} mentioned above, the values of L_1/L_2 are based on L_1 being the span of the flexural beam (Fig. 3.1). In the SMM it is found more convenient to work with a value L_{em} which is the span of the equivalent member being considered and L_{cm} as the orthogonal span (cross member). This means that L_m/L_{cm} used in Figs. 5.3(d) and 5.4(d) are the reciprocals of L_1/L_2 used in Figs. 3.12 and 4.16 and in Tables 4.16 through 4.18. Notice that this is only necessary in dealing with the torsional stiffness of the equivalent member since in computing the flexural stiffness terms (i.e., $(K)_{em}$, S_{22}, S_{33}, k_{23} and k_{32} in eq. 5.1) the equivalent member and the flexural beam in the panel coincide. Changing the values of L_1/L_2 in Figs. 3.12 and 4.16, and Tables 4.16 through 4.18 to their reciprocals gives the curves shown in Figs. 5.3(d) and 5.4(d) for the term S.

b) The torsional moment at C due to a unit rotation at A (Fig. 3.1) was defined above as $CF_{15}(K_{11})_S$. Notice that $(K_{11})_S$ is the panel stiffness term which has been assigned to equivalent member AB in the SMM (see point 2 above). Hence the torsional stiffness of equivalent member AC in this floor is equal to $S[(K)_{em}]_{AB}$. Thus, given the definition of S_{11} in eq. 5.1, it is clear that

$$(S_{11})_{AC} = \frac{[(K)_{em}]_{AB}}{[(K)_{em}]_{AC}} (S)_{AC} \qquad (5.1a)$$

5. In the computations of the stiffness matrix of edge members, a parameter ϕ is defined such that $\phi = 1.0$ for all equivalent members framing into a corner support (AB, AE in Fig. 5.2) and $\phi = 0.5$ for all other equivalent edge members (BC, EI in Fig. 5.2). This is based on assuming that when computing the stiffness of an equivalent edge member such as CD (Fig. 5.1), only half of floor beam CG acts with it as part of exterior panel CGHD while the other half of beam CG acts with the adjacent panel. Similarly, in the case of computing the stiffness of an interior equivalent member (e.g., GK in Fig. 5.2) only half of the orthogonal floor beams are considered to contribute; i.e., only half of floor beams GH and GF of Fig. 5.1 contributes to the stiffness of equivalent member GK and the other half contributes to equivalent member GC.

5.2.1 Equations for Calculating Member Stiffnesses for the Stiffness Matrix Method

This section describes in detail the step-by-step procedure to locate the neutral axes and to compute the value of the terms of the stiffness matrix of equivalent edge and interior members.

a) Procedure to Calculate Stiffness of an Equivalent Edge Member*

1. Calculate panel parameters ϕ, α, β, e, and L_{em}/L_{cm} where:

ϕ = member parameter equal to 1.0 for members framing into a corner support and assumed equal to 0.5 for all other edge members.

α = ratio of flexural stiffness of floor beam in the direction of edge member being considered to the slab stiffness as given by eq. 2.8.

β = $\dfrac{\text{torsional stiffness of floor beam in direction of member}}{\phi\ [\text{flexural stiffness of orthogonal floor beam}]}$

e = eccentricity between slab mid-plane and the neutral axis of the floor beam in the direction of member being considered (Fig. 5.3).

L_{em}/L_{cm} = panel aspect ratio with L_{em} being the span of the equivalent member being considered.

* A detailed application of this procedure to model a 3 x 3 panel two-way slab floor is given in Appendix D.

2. Enter Fig. 5.3(a) with α and L_{em}/L_{cm} and determine γ. Then calculate the position of the member neutral axis ξ where:

$$\xi = \gamma e$$

3. Calculate $(K_{11})_B^r$ at support where:

$$(K_{11})_B^r = \frac{4EI'_{FB}}{L_{em}} + \phi \frac{GJ_{TB}}{L_{cm}}$$

and

$$I'_{FB} = I_{FB} + (A\xi^2)_{FB}$$

A = area of floor beam cross section

Notice that flexural beam (FB) here refers to the floor beam in the direction of the equivalent member and the torsional beam (TB) is the orthogonal floor beam.

4. Enter Fig. 5.3(b) with α and L_{em}/L_{cm} and determine $(K)_{em}/(K_{11})_B^r$. Given $(K_{11})_B^r$ from step 3, compute $(K)_{em}$.

5. Enter Fig. 5.3(c) with α and L_{em}/L_{cm} and determine k_{23}. From eq. 5.1, $k_{32} = k_{23}$.

6. Enter Fig. 5.3(d) with β, α, and L_{em}/L_{cm} (as computed in step 1) and determine S. Then compute S_{11} where:

$$S_{11} = \frac{\phi\ [(K)_{em}]\ \text{orthogonal member}}{[(K)_{em}]\ \text{member being considered}}\ (S)$$

7. Compute S_{22} where:

$$S_{22} = 1.0 - \frac{\phi\ [(K)_{em}\ S_{11}]\ \text{orthogonal member}}{[(K)_{em}]\ \text{member being considered}}$$

(Notice that for $L_{em}/L_{cm} > 1.0$, the fraction is very small and S_{22} could be taken to be 1.0. However for small panel aspect ratios and high values of β of the orthogonal member, the fraction should not be neglected.)

From eq. 5.1, $S_{33} = S_{22}$.

b) Procedure to Calculate Stiffness of an Equivalent Interior Member*

1. Calculate panel parameters α, β, e, and L_{em}/L_{cm} where α, e, and L_{em}/L_{cm} are computed the same as for an edge member, and

$$\beta = \frac{\text{torsional stiffness of floor beam in direction of member}}{0.5\ \Sigma\ \text{flexural stiffness of orthogonal beams}}$$

2. Enter Fig. 5.4(a) with α and L_{em}/L_{cm} and determine γ. Then calculate the position of the member neutral axis where:

$$\xi = \gamma e$$

3. Calculate $(K_{11})^r_B$ at support where:

$$(K_{11})^r_B = \frac{4EI'_{FB}}{L_{em}} + 0.5\ [\Sigma\ \frac{GJ_{TB}}{L_{cm}}]\ \text{orthogonal members}$$

$$I'_{FB} = I_{FB} + (A\xi^2)_{FB}$$

A = area of floor beam cross section.

[Notice that the flexural beam (FB) and torsional beam (TB) are the same as defined for an equivalent edge member.]

4. Enter Fig. 5.4(b) with α and L_{em}/L_{cm} and determine $(K)_{em}/(K_{11})^r_B$. Given $(K_{11})^r_B$ from step 3, compute $(K)_{em}$.

5. Enter Fig. 5.4(c) with α and L_{em}/L_{cm} and determine k_{23}. From eq. 5.1, $k_{32} = k_{23}$.

6. Enter Fig. 5.4(d) with β, α, and L_{em}/L_{cm} (as computed in step 1) and determine S. Then compute S_{11} where:

$$S_{11} = \frac{0.5\ \Sigma\ L(K)_{em}]\ \text{orthogonal member}}{[(K)_{em}]\ \text{member being considered}}\ (S)$$

---

* A detailed application of this procedure to model a 3 x 3 panel two-way slab floor is given in Appendix D.

7. Compute S_{22} where:

$$S_{22} = 1.0 - \frac{0.5\ \Sigma\ [(K)_{em}\ S_{11}]\ \text{orthogonal member}}{[(K)_{em}\ \text{member being considered}}$$

From eq. 5.1, $S_{33} = S_{22}$. Similar to the case of edge members, S_{22} can be assumed to be 1.0 for $L_{em}/L_{cm} > 1.0$.

Once the stiffness matrix and position of the neutral axis of each member are determined, the structure can be analyzed as a three-dimensional frame. The effects of shear on the floor stiffness are already included in the terms of eq. 5.1; hence, no other terms to model shear effects are necessary. Furthermore, if the floor is considered rigid in its own plane, as is usual in such analyses, then the axial areas of the equivalent members are not necessary and the 3 x 3 element stiffness matrix is sufficient.

5.3 Application of Different Models to Compute Lateral Stiffness of Single-Panel, Single-Story Structures

The SMM as well as other currently used methods (see section 1.2) is applicable for modeling a floor under combined loading conditions. This section, however, is limited only to investigating structures under lateral loads and is intended to evaluate the accuracy and practicability of the different models for use in analysis of structures under lateral forces (wind or due to seismic excitations).

Four different models are used to evaluate the lateral stiffness of a set of single-panel, single-story structures shown in Fig. 5.5 and described in Tables 5.1 through 5.4. These structures are monolithic, with material properties as those given in section 2.3.1, and have rectangular floors of uniform slab thickness d_s, parallel floor beams of identical cross section and four square columns with identical column depth C.

The lateral stiffness of the structure K_L is defined as:

$$K_L = \frac{P}{\Delta_T} \qquad (5.2)$$

where P = static lateral laod applied at the floor level, P/2 at each column top and Δ_T = lateral displacement of top of slab.

5.3.1 Finite Element Method

In this method, the floor slab is modeled as two-dimensional finite elements and the floor beams and columns as uniaxial prismatic members. The beams are connected to the finite element mesh with rigid links as described in section 3.3. The column members are placed at the column centerline and extend from the building's base to the bottoms of floor beams AB and CD. The top of the column is connected to the finite element mesh with a rigid link (assuming the beam-column joint to be infinitely stiff). Figure 5.6 shows the finite element model described above. Notice that the lateral load is applied at the slab's centerline which is customary in such analyses and is based on the assumption that the floor slab accounts for the major share of the floor mass and, hence, also shares the largest part of the inertial forces in seismic loading.

Computer program SAP-IV, which is described in section 3.3, is used to analyze the finite element model, and the results from the program include the displacements and rotations of the finite element nodes. Assuming plane sections in the slab remain plane, the displacement at the top of slab is easily calculated where:

$$\Delta_{\text{Top of Slab}} = \Delta_{\text{Center of Slab}} + \frac{d_s}{2.0} [\tan \theta_{yy}] \qquad (5.3)$$

and θ_{yy} = rotation of finite element node at which lateral displacement is calculated.

Notice that in a finite element model of the structure shown in Fig. 5.5, the lateral displacements at points A and C are equal as are those of points B and D. Since the model includes membrane stresses and strains, however, there will be some axial strain in the plane of the slab and the lateral displacement of point A will be slightly greater than that at point B. The lateral displacement used to calculate the

lateral stiffness of the structure is the average of the two, so that Δ_T used in eq. 5.2 becomes:

$$\Delta_T = \frac{1}{2} [\Delta_A + \Delta_B]_{\text{Top of Slab}} \qquad (5.4)$$

5.3.2 Equivalent Frame Method

The equivalent frame method recommended in the 1971 ACI Building Code [3] is described fully in section 1.2, which also describes the difficulties of applying it for analyzing structures subjected to lateral loads. Figure 5.7 shows the equivalent frame model used to represent the single-panel, single-story structure shown in Fig. 5.5. Due to the symmetry of the structure, only one frame need be analyzed to determine the lateral stiffness. Notice that the lateral load is applied at the top of the slab to simplify the analysis and approximates loading at the centerline of the slab as was done in the finite element method. This difference has a negligible influence on the final results. A closed-form solution for the lateral stiffness of the equivalent frame shown in Fig. 5.7 is given in Appendix B. The physical and structural properties of the equivalent frame shown in Fig. 5.7 are given in Tables 5.5(a) through 5.5(d).

5.3.3 Model Based on Strength Requirements of ACI 318-71, Section 8.7.

This method is described in section 1.2. Figure 5.8 shows the model based on this method for the single-panel, single-story structure shown in Fig. 5.5, and the member structural properties are given in Tables 5.6(a) through 5.6(d). The columns are assumed rigid across the depths of beams AB and CD, and the lateral loads are applied at the neutral axes of the equivalent beams. Due to the symmetry of the structure and the loading, only one frame need be analyzed for the lateral stiffness of the model.

The frame shown in Fig. 5.8 is analyzed with the use of computer program ETABS [26]. This is a general-use program for the linear structural analysis of frame and shear wall buildings subjected to both

static and earthquake loadings, in which

> The building is idealized by a system of independent frame and shear wall elements interconnected by floor diaphragms which are rigid in their own plane. Within each column, bending, axial, and shearing deformations are included. Beams and girders may be nonprismatic and bending and shearing deformations are included.

Nonprismatic beams are defined by using their stiffness matrix with the building data as input for the program. This particular program, rather than SAP-IV, was used for its high efficiency in analyzing framed structures.

The equivalent beam of the frame shown in Fig. 5.8 will not have any torsional moments when analyzed for the lateral load P/2.0 shown in Fig. 5.5. Hence, a stiffness matrix for the two flexural degrees of freedom in the floor beams is sufficient for the analysis. The stiffness matrix used for the beams in this model is of the form:

$$[K]_{AB} = \frac{EI_{AB}}{L_1} \begin{matrix} 4.0 & 2.0 \\ 2.0 & 4.0 \end{matrix} \qquad (5.5)$$

where I_{AB} = moment of inertia of equivalent beam AB

The results from the computer program include the lateral displacement of the equivalent beam ($\Delta_{N.A.}$), the moment at the column base (M_{BC}), and the moment at the column top (M_{TC}) where the rigid section meets the column. Assuming plane sections in the beam remain plane, the lateral displacement at the top of slab (Δ_T) can be calculated as:

$$\Delta_T = \Delta_{N.A.} + \lambda \, (\tan \theta_{TC}) \qquad (5.6)$$

where λ = distance from top of slab to neutral axis of equivalent beam.

$$\theta_{TC} = \frac{H-D}{2EI_C} [M_{BC}-M_{TC}] \qquad (5.7)$$

5.3.4 Stiffness Matrix Method

This method is described in section 5.2. Since the structure shown in Fig. 5.5 has only exterior members, the equivalent member stiffness matrices can be determined by following the procedure described in section 5.2.1a. The model for the structure shown in Fig. 5.5, based on this method, is shown in Fig. 5.9 and the member structural properties are

given in Tables 5.7(a) through 5.7(d). The lateral load is applied at the neutral axis of the equivalent members AB and CD which is defined by the term ξ.

Due to the symmetry of the model and of the loading, equivalent members AB and CD are in pure flexure while equivalent members AC and BD are free to stress in the analysis. Hence, the lateral stiffness of the whole frame can be determined by analyzing only one frame, such as frame EABF.

The frame is analyzed using computer program ETABS [26], which is described above, and the lateral displacement of the structure at the top of the slab is calculated according to eq. 5.6.

5.4 Evaluation of Different Models Used to Compute Lateral Stiffness of Single-Panel, Single-Story Structures

The accuracy of the results is necessarily the single most important characteristic of an analytical model. However, a good model must also be relatively simple to use, adaptable to different analytical methods (e.g., computer programs, moment distribution, etc.) and different loading conditions (e.g., gravity and lateral loads), and efficient in its requirement of computational effort.

The four models used in this investigation each have some particular properties based on the assumptions used in developing the model and these different properties must be considered when evaluating the results. Following are some of these aspects:

1. The equivalent frame method is the only one with a provision for the influence of the column depth on the stiffness of the structure. This provision modifies the moment of inertia of the equivalent beam across the depth of the column. The other three methods neglect this effect and consider the columns as uniaxial prismatic members along the column centerlines. Neglecting the increased stiffness of the floor across the column depth has the effect of underestimating the floor stiffness. The influence of the column on the floor stiffness increases as the ratio of the floor span to the column depth decreases. The increase of the lateral stiffness of the structure in the equivalent frame method due to accounting for the increased floor stiffness at the columns

will be evaluated in the discussion of the results.

2. The finite element model is the only one which accounts for in-plane axial strains in the slab. The other three models assume the slab to be rigid in its own plane. Neglecting in-plane strains overestimates the lateral stiffness of the structure.

3. The lateral load is applied at different points in each model: at the slab's centerline in model one, at the top of slab in model two, and at the neutral axis of the equivalent beams in models three and four. This has little effect in floors with thick slabs and shallow beams, but the effect increases with beam depth. If the lateral load is consistently applied at the slab's centerline, the net effect would be to increase the lateral stiffness of model two and decrease that of models three and four. The change, however, would be slight.

4. Model three is the only one that totally neglects the torsional effects of the slab and beams AC and BD. Including the torsional effects would increase the lateral stiffness of the model, especially for the case where $L_1/L_2 = 2.0$.

5. Tables 5.5a through 5.5d point out that in the equivalent frame method, the influence of the torsional beam decreases as α increases, reflecting the diminished capacity of the slab to distribute the floor stresses as it becomes more flexible in relation to the beams (e.g., for $L_1/L_2 = 1.0$, $d_s = 6.5$ in., and C = 15 in., $K_{ec}/K_c = 0.62$ for $\alpha = 0.8$ while $K_{ec}/K_c = 0.93$ for $\alpha = 3.0$). For the same reason, changing the size of the torsional beam has a greater influence on K_{ec} for lower values of α (e.g., for $L_1/L_2 = 1.0$, $d_s = 6.5$ in., and C = 15 in., increasing β from 0.064 to 0.160 increases K_{ec} by 28.3% when $\alpha = 0.80$ while the increase is only 0.8% when $\alpha = 8.0$).

6. Tables 5.6a through 5.6d point out that the model based on ACI-71 Section 8.7 neglects the influence of the torsional beam on the effective slab width b_f, and that b_f is fairly insensitive to α. For the range of values used in this section, Tables 5.6a through 5.6d show that b_f is determined by L_1 only (i.e., $b_f = L_1/12$). Accordingly, the effective width of slab remains at 20 in. when $L_1/L_2 = 1.0$ and $L_1 = 240$ in. even when the moment of inertia of the flexural beam is increased

10 times (i.e., from α = 0.80 to α = 8.0). The same is true when L_1/L_2 is changed and when the size of the torsional beam is changed. This further emphasizes the point made in section 1.2 that this method lacks any systematic theoretical basis for use in modeling the floor stiffness.

7. Tables 5.6 and 5.7 point out that the method based on provisions of ACI-71 Section 8.7 and the SMM, both give floor models independent of column size. This is clearly different from the models based on the equivalent frame method.

The lateral stiffness determined by the four different models is given in Tables 5.8a, 5.8b, 5.8c, and 5.8d. The calculation for transforming the lateral displacements from the point of load application to the top of slab for the finite element model, the ACI-71, Section 8.7 model, and the SMM model are given in Appendix C. Table 5.8 also gives the Diff % where:

$$\text{Diff. \%} = \frac{(P/\Delta_T)\ \text{model} - (P/\Delta_T)\ \text{finite element}}{(P/\Delta_T)\ \ \text{finite element}} \times 100 \quad (5.8)$$

In this equation the finite element model is considered the most accurate representation of the actual structure and hence is used as the basis for evaluating the other models.

The results of Tables 5.8a through 5.8d point out some very important characteristics of the three frame models when compared with the results of the finite element model.

5.4.1 Equivalent Frame Model

The most important trend shown in the results of Table 5.8 is the very poor correlation of the lateral stiffness based on the equivalent frame with that of the finite element method. This is the only method expressly recommended for use by the ACI 318-71 Code, yet it produced the largest Diff. %, reaching as high as 169.4%. Beyond this general statement, two other more specific observations about this method are in order. First, the method gives inconsistent results as the floor-to-column stiffnesses are changed. While the method generally overestimates the lateral stiffness of the structure, the trend is reversed as the floor

stiffness, relative to the columns, is increased. This can be seen in Table 5.8a for the case where 15-in. columns and a 9-in. slab are used. The lateral stiffness is overestimated by 10.5% for α = 0.8 and underestimated by 11.4% for α = 8.0. The second trend observed in Tables 5.8a through 5.8d is that the results of the equivalent frame method have the largest Diff. % in cases with stiff columns and flexible floors. This trend holds whether the floors are kept the same and the columns increased in stiffness or vice versa. An example of the influence of increasing the column stiffness on the performance of the equivalent frame method is seen in Table 5.8b where, for α = 0.40, the method overestimates the lateral stiffness by 56.0% when 15-in. columns are used, and by 169.4% when 25-in. columns are used. On the other hand, the floor stiffness can be decreased in any of four different ways: by decreasing slab depth, decreasing α, decreasing β, or by increasing L_1/L_2. Hence in Table 5.8a, for α = 0.8 and C = 15 in., the equivalent frame method overestimates the alteral stiffness by 10.5% for a 9-in. slab and by 31.5% for a 6.5-in. slab. In Table 5.8d for C = 15 in., it overestimates the lateral stiffness by 4.8% for α = 8.0 and by 63.1% for α = 0.80. In Table 5.8a, for C = 15 in. and α = 0.80, it overestimates the lateral stiffness by 22.0% for β = 0.160 and by 31.5% for β = 0.064. Finally in Tables 5.8b and 5.8d, for C = 15 in. and α = 8.0, it underestimates the lateral stiffness by 7.4% for L_1/L_2 = 0.5 and overestimates it by 4.8% for L_1/L_2 = 2.0. As stated in section 5.4, some difference between the results of a finite element analysis and the equivalent frame method is due to the fact that the latter takes into account the influence of column size while the finite element method does not. To evaluate the significance of this difference in the two models, the increase in the beam-slab moment of inertia across the depth of the column was neglected in the equivalent frame analysis of the structure where L_1/L_2 = 0.5, α = 0.4, and C = 25 in. This has the effect of assuming a zero column depth as is done in the finite element model. This change reduced the lateral stiffness of the structure from 1512.8 k/in. to 1474.0 k/in. (i.e., a reduction of only 2.6%). This shows that accounting for the influence of the column depth in the equivalent frame analysis is not the source of the high variance from the results of the finite element analysis shown in Tables 5.8a through 5.8d.

5.4.2 ACI 318-71 Method

The results based on this method show good correlation with those of the finite element method, especially when compared with the equivalent frame method. The maximum Diff. % in the structures analyzed is 13.8% compared with 169% in the equivalent frame. The results shown in Tables 5.8a, 5.8b, 5.8c, and 5.8d point out several problems with the use of this method. First, it neglects the contribution of the torsional beam to the overall floor stiffness. This is shown in Table 5.8a where changing β from 0.064 to 0.160, while all other factors are held constant, does not have any influence on the lateral stiffness of the structure. The results shown in Table 5.8a seem to indicate better correlation between this and the finite element method as β increases. A closer inspection, however, gives a different interpretation of the results. Tables 5.8a through 5.8d show that this method generally overestimates the lateral stiffness of structures. As the size of the torsional beam increases, so does the lateral stiffness of the structure as reflected by the finite element method. Since this method ignores the influence of the torsional beam, the lateral stiffness remains unchanged giving the illusion that this method gives better results for higher values of β. However, if β continues to increase, so will the lateral stiffness of the structure and this method will then underestimate the stiffness. This is seen in Table 5.8a where for C = 15 in. and α = 0.80, this method overestimates (P/Δ_T) by 1.0% for β = 0.064 and underestimates it by 1.1% for β = 0.160.

Second, the method underestimates the rotational stiffness of floors with shallow beams by ignoring the slab's two-way action and assuming the slab to act only in the direction of the flexural beams. This is seen in Table 5.8b where this method underestimates (P/Δ_T) by 3.4% for the case where C = 15 in. and α = 0.4. This margin of error decreases as the column size is increased due to the fact that the column stiffness begins to dominate the (P/Δ_T) of the whole structure.

Third, the method is inconsistent as α is increased. In Table 5.8a, with C = 15 in., d_s = 6.5 in., and β = 0.064, the Diff. % increases from 1.0% to 5.5% and then decreases to 4.5% as α goes from 0.80 to 3.0 to 8.0. This inconsistency repeats itself in Table 5.8b for the case of

C = 15.0 in. It is difficult to attribute this erratic behavior to a specific cause. There is no sound theoretical reason to use the provisions of ACI 318-71 to model floor stiffness. The net result of doing so is to neglect the torsional effects and to use a model which defines the effective slab width to be $L_1/12$ for all the cases analyzed herein, irrespective of slab depth, beam size, or L_1/L_2 ratio. Hence, it is not surprising that the results do not fit into a set pattern.

5.4.3 Stiffness Matrix Method

The results in Tables 5.8a, 5.8b, 5.8c, and 5.8d show that this method gives the best correlation with the results from the finite element method. The SMM generally overestimates the lateral stiffness of the structure, with the maximum Diff. % registered for the cases analyzed being 6.1%. This method performs best for flexible structures, with the Diff. % increasing as the structure becomes stiffer. This trend holds whether the structure is stiffened by increasing the slab thickness, increasing α, increasing the column size, or by a combination of these factors. The trend is also consistent for the different values of L_1/L_2 used. Taking the results of Table 5.8d as an example, for C = 15 in. and d_s = 6.5 in., the Diff. % increases from 0.20% to 3.8% as α goes from 0.8 to 8.0. Keeping α equal to 0.80, the Diff. % increases from 0.2% to 1.5% as C increases from 15 in. to 20 in. In Table 5.8a, with C = 20 in. and α = 8.0, the Diff. % increases from 2.2% to 3.5% as d_s increases from 6.5 in. to 9.0 in. Also in Table 5.8a, increasing C from 15 in. to 20 in., α from 3.0 to 8.0, and d_s from 6.5 in. to 9.0 in. increases the Diff. % from 0.3% to 3.5%. The results in Table 5.8 also show that the Diff. % for this method is smallest for L_1/L_2 = 1.0, increasing as this ratio increases or decreases. Finally, Table 5.8c shows that in the case L_1/L_2 = .75, where interpolation between the graphs of Figs. 5.3(a), 5.3(b), 5.3(c), and 5.3(d) is necessary, the Diff % is basically the same as for the other L_1/L_2 ratios used. Hence, straight line interpolation between the graphs does not impair the accuracy of the SMM.

5.5 Effective Slab Width

The widespread use of an effective slab width to model a floor system makes it useful to consider whether the results of this investigation confirm the validity of this approach. In a seismic analysis of a structure, the effective slab width is required to be such that the lateral stiffness of the resulting plane frame is the same as that of the column-floor moment resisting frame. In the single-panel, single-story structures analyzed above (Fig. 5.5) the lateral load P produces equal clockwise rotations at the four floor supports. To match the lateral stiffness of these structures, it is sufficient that the stiffness of the two equivalent beams based on a unit clockwise rotation at each end $6EI/L_1$, be equal to the moment necessary to produce a unit clockwise rotation at each floor support. This floor stiffness can be adequately estimated from the graphs of Figs. 5.3(a) through 5.3(d). Appendix E gives the equations and procedure to compute an effective slab width according to the criteria discussed above and the results are shown in Table 5.9.

The results of Table 5.9 show the difficulty of seeking an effective slab width to model the floor stiffness. There is no definite pattern for the ratio of the effective slab width to the half-span $b_f/0.5L_2$. This ratio is found to vary with each floor parameter (i.e., α, β, L_1/L_2 and d_s/L_1). The effective slab width seems to be most sensitive to the aspect ratio L_1/L_2 where in the cases investigated $b_f/0.5L_2$ varied from 0.13 for $L_1/L_2 = 0.5$ and $\alpha = 3.0$ to 0.49 for $L_1/L_2 = 2.0$ and $\alpha = 0.80$. The variation of $b_f/0.5L_2$ with α, β, and d_s/L_1 is inconsistent and depends on each combination of these values in a specific floor.

5.6 Lateral Stiffness of a Multi-Panel, Single-Story Structure

The single-panel structures analyzed above give important insight into the adequacy of the different methods used to model two-way slab floors. Limiting the structures to one panel only made it possible to use finite element analyses for a large number of structures with moderate computational costs. Due to symmetry, the equivalent members AC and BD (Figs. 5.8 and 5.9) in the models using the SMM and the ACI-71,

8.7 method have no torsional moments. Hence, there remains the question of how well these models perform when there is torsion in the equivalent cross beams. Thus it would be ideal to conduct similar analyses of structures having a multi-panel floor system to evaluate the different methods when there are interior panels and when there is torsion involved in the equivalent cross beams.

The multi-panel, single-story structure, shown in Fig. 5.10, is selected as an example to evaluate the different cases discussed above. It was necessary to limit this effort to one structure due to the high cost of a finite element analysis of a multibay structure. As shown in Fig. 5.10, the structure analyzed consists of a 3 x 3 panel floor, each panel being 16 ft x 20 ft. The floor slab is 8 in. thick, each beam is 15 in. x 30 in.; the single-story structure has 16 columns, each 26 in. x 26 in. in cross section; and story height from top of slab to column base is 12 ft. The structural properties of the floor beam are:

$$A_b = 450.0 \text{ in}^2$$
$$I_B = 33750.0 \text{ in}^4$$
$$J_B = 20250.0 \text{ in}^4$$

The column structural properties are:

$$A_c = 676.0 \text{ in}^2$$
$$(A_{sh})_c = 563.3 \text{ in}^2$$
$$I_c = 38081.33 \text{ in}^4$$
$$J_c = 91395.20 \text{ in}^4$$

As shown in Fig. 5.10, lateral forces in only the y-direction are applied to the structure at the floor level. The 3 x 3 panel floor includes corner, exterior, and interior panels and thus will enable evaluation of the effect of different boundary conditions along panel edges within the floor on the performance of each method used for the modeling. Also, since all the columns will not have the same rotation at their tops, torsion in the floor equivalent members must be included.

Five different methods are used to evaluate the lateral stiffness of the multi-panel structure.

5.6.1 Finite Element Method

The application of this method is similar to the procedure described in section 5.3.1 for the single-panel structure and the model shown in Fig. 5.6. The lateral displacements at the top of slab are evaluated according to eq. 5.3. Due to the symmetry of the structure and the loading, the model will give four different lateral displacements at the top of slab at the supports if in-plane axial strains are included. These are:

1. Displacements at corner supports A, D, M, and R.
2. Displacements at exterior supports B, C, N, and Q.
3. Displacements at exterior supports E, H, I, and L.
4. Displacements at interior supports F, G, J, and K.

The lateral stiffness of the structure (P/Δ_T) is defined as the average of these four values of Δ_T. The results of the finite element analysis are given in Table 5.14.

5.6.2 Equivalent Frame Method

Application of this method is similar to that described for the single-panel structure in section 5.3.2 and the model shown in Fig. 5.7. The structure is modeled by four equivalent frames: two exterior frames along column lines AM and DR, and two interior frames along column lines BN and CQ. The equivalent columns used in this method depend on the "equivalent torsional beams" framing into the column. Four different types of equivalent columns can be identified in the structure shown in Fig. 5.10: corner columns A, D, M, and R; exterior columns B, C, N, and Q; exterior columns E, I, H, and L; and interior columns F, G, J, and K. The structural properties of the two types of frames are given in Table 5.10.

As the equivalent frame method does not lend itself easily to available computer programs, it was found easier to develop a closed form solution for the case of a single-panel structure. However, a closed form solution cannot be readily developed for a multi-panel structure

and it was necessary to modify the program ETABS [26] (described in section 5.3.3) by changing the diagonal terms of the column stiffness matrix and replacing the rotational terms by the equivalent column stiffness (K_{ec}). The program modification was checked against the closed form solution for a single-panel structure and found to be exact. Notice that ETABS forces the lateral displacements at each floor level to be the same throughout the floor. Hence the different frames all have the same lateral translations, and since the model (Fig. 5.7) places the equivalent beams at the level of the top of slab, no translation of lateral displacements is necessary. The top of slab lateral displacement of the structure according to this method was:

$$\Delta_T = 0.0117 \text{ in.}$$

5.6.3 ACI 318-71 Section 8.7 Method

Application of this method is similar to the procedure described for the single-panel structure in section 5.3.3, and the model shown in Fig. 5.8. The multi-panel structure is modeled as a three-dimensional frame with equivalent beams defined according to ACI 318-71, Section 8.7. Two types of equivalent beams are identified in the structure: L-shaped exterior beams and T-shaped interior beams. Structural properties of these equivalent beams are given in Table 5.11. Notice that these beams have their neutral axes at different distances (λ) below the top of slab. However, the computer program used, ETABS, requires that all floor beams be along the same level. Hence, an average value of λ is used to define the position of the neutral axis of all beams in the floor.

The program gives the same lateral displacement throughout the floor (the floor is rigid in its own plane), but since the column top rotations are different, displacements at the top of slab will also be different. Due to symmetry of the structure and the loading, four different column rotations can be identified at the corner columns A, D, M, and R; exterior columns B, C, N, and Q; exterior columns E, H, I, and L; and interior columns F, G, J, and K. This is the same as in the case of the finite element method. The lateral displacements at the top of slab are given in Table 5.15 and are calculated according to eqs. C.5 and C.6 in Appendix C. The lateral stiffness of the structure (P/Δ_T) is based on the average of these four displacements.

5.6.4 ACI 318-71, Sections 8.7 and 11.7 Method

This method is exactly the same as that above with the exception that the equivalent beams in the x-x direction are defined according to the provisions of ACI 318-71, Section 11.7.2. This section of the ACI defines the maximum allowable flange width for torsional shear requirements and states that for "flanged sections ... the overhanging flange width used in design shall not exceed three times the thickness of the flange" [3], thus:

$$b_f \leq 3\, d_s \tag{5.9}$$

This provision is used for the beams in the x-x direction because, due to the symmetry of the model and the loading, these beams are in pure torsion while those in the y-y direction are in pure flexure. Table 5.12 gives the structural properties of the equivalent beams of the model based on this method, and Table 5.16 gives the lateral displacements of the model.

5.6.5 Stiffness Matrix Method

Application of this method is similar to the procedure described in section 5.3.4 for the single-panel structure and the model shown in Fig. 5.9, except that the procedure of section 5.3.1b and Figs. 5.4(a) through 5.4(d) must be used for the computation of equivalent interior members. For the multi-panel floor of Fig. 5.10, six different floor members can be identified.

1. Corner Member AB, CD, MN, and QR.
2. Corner Member AE, DH, IM, and LR.
3. Exterior Member BC and NQ.
4. Exterior Member EI and HL.
5. Interior Member EF, FG, GH, IJ, JK, and KL.
6. Interior Member BF, FJ, JN, CG, GK, and KQ.

The calculations for the structural properties of these members are given in Appendix D and the results of these calculations are summarized in Table 5.13.

Similarly to the above methods, four lateral displacements at the top of slab based on eqs. C.5 and C.6 in Appendix C are identified in Table 5.17 and the lateral stiffness of the structure (P/Δ_T) is based on the average of these displacements.

5.7 Evaluation of Different Models Used to Compute Lateral Stiffness of a Multi-Panel, Single-Story Structure

The lateral stiffness (P/Δ_T) of the multi-panel structure shown in Fig. 5.10 is given in Table 5.18. The Diff. % in each model is based on comparing the results with those of the finite element method and is computed according to eq. 5.8.

The two methods based on allowable widths of beam flange (i.e., the ACI 318-71, 8.7 and the ACI 318-71, 8.7 and 11.7 methods) gave basically identical results for this structure. However, one case is not sufficient to show that the two provisions used to define effective slab widths will always give nearly equal results. The provisions of ACI 318-71, 8.7 were used in both cases to define the equivalent beams in the y-y direction which are primarily in flexure for the loading shown in Fig. 5.10, and the provisions of ACI 318-71, 8.7 and 11.7 were used to define the equivalent members in the x-x direction which are primarily in torsion. Had there been substantial torsional moments generated in the equivalent beams in the x-x direction, the difference in using the two code provisions would have been reflected in the lateral displacements of the structure as given by the two models. However, the results of the analysis show that the torsion, generated by the lateral loads used, is small (e.g., torsion in equivalent beam IJ is 1.2 k-in. while flexure in equivalent beam JF is 236.2 k-in.) and the contribution of the floor model was determined primarily by the flexural stiffness of the equivalent beams in the y-y direction which were identical in both cases. The Diff. % given in Table 5.18 for the different models, are in general agreement with those of comparable single-panel structures, indicating that the different models perform with approximately the same accuracy for interior

and exterior panels and that they also maintain their level of accuracy whether the equivalent cross beams undergo torsion or not.

Finally, notice that the floor properties used were such that all the terms needed for the SMM had to be interpolated from the curves in Figs. 5.3 and 5.4. The fact that the Diff. % for this method remains within a range of 1% to 5% again confirms the fact that the method maintains accuracy when interpolation between the curves is necessary.

5.8 Dynamic Response of a Multistory Building

The dynamic response of a 12-story building with a two-way slab floor system (Fig. 5.11) is also analyzed, using the SMM, the effective slab width method (ACI 318-71, 8.7), and the equivalent frame method. A finite element analysis could not be attempted due to prohibitive computational effort required. The building was adapted from that presented in reference 11. The beams were modified to have a 2:1 depth-to-width ratio while maintaining the same moment of inertia as the beams given in reference 11. The dynamic response of the building is evaluated for 8-in. and 12-in. thick floor slabs to assess the different models used as the values of α and d_s/L_1 are varied. Computer program ETABS is used for this part of the investigation.

Tables 5.19 through 5.23b give the structural properties of the equivalent members to model this building as defined by the three methods used. The distributed masses at each story are assumed to be lumped at the center of mass of each floor. The mass used in the analysis of the building with an 8-in. floor slab is identical to that given in reference 11. The mass for the 12-in. slab floor is equal to the above mass plus the increase in the mass of the slab only. This assumes that all other elements contributing to the mass (partition walls, fixtures, etc.) are the same for both cases. The value of the mass per floor used in the analysis is:

Floor Level	Mass for 8 in. Slab $[K \frac{(sec)^2}{in}]$	Mass for 12 in. Slab $[K \frac{(sec)^2}{in}]$
Roof	5.43	6.74
All other Floors	5.69	7.00

Table 5.24 gives the natural periods of vibration for the first four mode shapes in the longitudinal (x-x) direction. The table also includes the period of the building when the bare beams are used for the floor stiffness, i.e., the mass of the system remains the same but the slab is neglected when formulating the stiffness of the building. Comparison of the periods based on each method with those of the bare beams structure helps to give an idea of each method's estimate of the contribution of the slab to the building's periods of vibration.

The results in Table 5.24 show that for both the 8-in. and the 12-in. slab floors, the SMM gives the highest natural periods of vibration and the equivalent frame method the lowest. This is consistent with previous results in this chapter establishing both the equivalent frame method and the effective slab width method as generally overestimating the lateral stiffness of the structure. The Diff. % between the SMM and each of the other two methods remains basically the same for the different mode shapes, and is higher for the equivalent frame method than the effective slab width method. The Diff. % between the SMM and each of the other two methods also decreases as the slab thickness increases.

Notice that the periods of vibration based on all three methods increase as the slab thickness increases from 8 in. to 12 in. This means that the effect of the increase in stiffness of the building is less than the effect of the increase in mass. However, the increase in the period is smallest in SMM, which shows that this method gives a higher increase in building stiffness (per same increase in mass) as the slab thickness goes from 8 in. to 12 in.

Table 5.25 gives the terms of the building's first mode shape vector $< \phi_1 >$ in the longitudinal direction based on the four different models used.

These mode shape vectors are scaled such that the generalized mass in the first mode shape M_1^*, where:

$$M_1^* = \langle \phi_1 \rangle^T [M] \langle \phi_1 \rangle \tag{5.10}$$

and $[M]$ = a diagonal 12 x 12 mass matrix

is equal to 0.12 for the building with an 8-in. slab floor and to 0.15 for the building with a 12-in. slab floor for each of the four methods used. Given the first natural period of vibration T_1 and having computed M_1^*, the building's generalized stiffness in the first mode K_1^*, where:

$$K_1^* = \langle \phi_1 \rangle^T [K] \langle \phi_1 \rangle \tag{5.11}$$

and $[K]$ = 12 x 12 building lateral stiffness matrix

and be shown to be:

$$K_1^* = \frac{(2\pi)^2 (M_1^*)}{(T_1)^2} \tag{5.12}$$

The values of K_1^* are given in Table 5.26. Since the mass matrix used in the analysis is the same for all four methods used, the increase in K_1^* over that of the bare beams method reflects the contribution of the slab to the lateral stiffness of the building as estimated by each of these methods. The results of Table 5.26 show that for the building with an 8-in. slab, the effective slab width method estimates the contribution of the slab to K_1^* as twice that estimated by the SMM and the equivalent frame method is more than three times that of the SMM. However, as the slab thickness is increased from 8 in. to 12 in., a different pattern emerges. The SMM estimates the increase in K_1^* due to the increased slab thickness as 16.7% while the effective slab width method and the equivalent frame method estimate the increase as 0.7% and 9.2% respectively. The performance of the effective slab width method (based on ACI 318-71, 8.7) is unrealistic as it implies that the lateral stiffness of the building as reflected by K_1^* remains basically the same even when the floor slab thickness is increased by 50%. The results of the equivalent frame

method show that the method highly overestimates the contribution of two-way slab floor systems to the lateral stiffness of moment-resisting frames and that this overestimation is higher for the more flexible floors.

The dynamic response of a building to seismic motion depends on the dynamic properties of the building (natural periods, mode shapes, etc.) as well as on the characteristics of the particular earthquake considered (peak accelerations, frequency content, duration of severe pulses, etc.). Hence the difference in the dynamic properties of the building based on the different models is not sufficient to evaluate the difference in response (lateral displacements, story shears, etc.) due to using these models. As an illustration, the building of Fig. 5.11 was analyzed for the N-S recorded component of El Centro earthquake of 1940 [27] acting in the longitudinal direction (x-x only) and the analysis is based on the earthquake's elastic response spectrum with 5% damping. Figure 5.12 gives the envelope of maximum lateral displacements [based on modal superposition using square root of the sum of the squares (SRSS) values] as estimated by three methods (SMM, effective slab width, and equivalent frame). Table 5.27 gives these displacements for the roof only and shows that the Diff. % between the SMM and the effective slab width method and the equivalent frame method is 13.10% and 24.17%, respectively, for an 8-in. floor slab and 3.44% and 23.73%, respectively, for a 12-in. floor slab.

5.9 Summary and Conclusions

This chapter develops the SMM to model the stiffness of two-way slab floors, a method based on the research presented and discussed in Chapters 2 through 4. It consists of replacing the floor by a set of equivalent members connecting the vertical floor supports. The SMM does not define a physical shape (cross section) for these members, but rather a 3 x 3 stiffness matrix and the position of the member neutral axis in relation to the top of slab. The 3 x 3 member stiffness matrix is based on one torsional and two flexural degrees of freedom [Fig. 5.2(b)]. Two sets of tables and graphs are presented to describe a step-by-step procedure to calculate the stiffness matrix of equivalent edge and interior members, and the position of their neutral axis.

The rest of the chapter is devoted to evaluating the accuracy and practicability of the SMM for modeling two-way slab floors and comparing its performance to that of other models currently used. The lateral stiffnesses of 27 single-panel, single-story structures with different floor and column stiffnesses are calculated, each according to four models: the equivalent frame method, ACI 318-71, 8.7 method, SMM, and the finite element method. Results are compared with the latter method which, from the analytical point of view, is generally considered the most accurate. The lateral stiffness of the structure (P/Δ_T) is based on the lateral deflection of the top of slab when a lateral load P is applied at the floor level. The lateral stiffness of one 3 x 3 panel floor, single-story structure is also calculated according to five different models in order to evaluate the performance of each model when interior panels are added to the floor and also when there is torsion in some floor beams. In addition to the four models used in the single-panel floors, another model is added in which the flexural and torsional properties of the equivalent beams are defined by effective slab widths based on the provisions of ACI 318-71, 8.7 and ACI 318-71, 11.7, respectively. The lateral stiffness of the structure (Δ_T) is defined the same way as for the single-panel structures.

The results from using the different models to evaluate the lateral stiffnesses of the 27 single-panel and one multi-panel structure show that:

1. The equivalent frame method, besides being very complicated to use, is fairly inaccurate when compared with results of a finite element analysis, with the Diff. % reaching as high as 169%. The method is also inconsistent in that it overestimates the lateral stiffness of some structures and underestimates it for others. The error in the lateral stiffness based on the equivalent frame method increases as the floor becomes more flexible relative to the columns. These results point out the need to reassess the ACI 318-71 Code recommendations of using the equivalent frame method to analyze structures with two-way slab floors. As described in section 1.2, the research and development for this method was done for flat slabs, and its application to two-way slabs needs to be investigated further as the analytical results of this study do not justify such application.

2. The method based on the ACI 318-71 provisions for beam strength (i.e., ACI 318-71, sections 8.7 and 11.7) seems to perform better than the equivalent frame method with the maximum registered Diff. % being 13.8%. However the results are erratic and a clear trend in the results is not evident. This, coupled with the fact that there is no sound theoretical basis for using these provisions to model two-way slab stiffness, leaves open the possibility that much higher margins of error could result for certain structures and loading conditions.

3. The results of the SMM were consistently closer to those of a finite element method than were those of other methods, with the maximum registered Diff. % being 6.1%. The method maintained its level of accuracy when interpolation was used between the curves given in Figs. 5.3 and 5.4. The SMM gave the best results in flexible structures and also improved as the floor became more flexible relative to the columns.

4. The results of this investigation also show that the effective width approach does not adequately model the stiffness of a two-way slab floor, the composite beam-slab action is much too complex for this approach.

5. The results of analyzing a 12-story building with a two-way slab floor system show that appreciable differences in the estimate of the dynamic characteristics of a building and its response to a particular earthquake can result from using different analytical models for the stiffness of the floor system.

6. SUMMARY, CONCLUSIONS AND RECOMMENDATIONS

6.1 Summary

Studies have shown that the seismic analysis of buildings whose floor slab is part of a moment-resisting frame is sensitive to the assumed slab participation in the overall stiffness. Although some methods have been suggested for modeling the contribution of the slab to the stiffness of the floor system, at present their accuracy and reliability are highly questionable. Finite element models can be very accurate but their use requires computational effort that is prohibitive in practical applications. Currently used models based on some form of effective width of slab do not have a consistent theoretical basis, and they have not been rigorously studied to determine their accuracy for use in seismic analyses of buildings.

In the study reported herein, the elastic stiffness of composite beam-slab reinforced concrete floor systems has been thoroughly studied. The floor rotational stiffness is defined by a stiffness matrix based on two rotational degrees of freedom in the plane of the slab at each of the floor's supports. The moments needed to produce a unit rotation at one degree of freedom, and restraining all others, make up the elements of one row of the matrix.

Point supports are assumed, thus neglecting the increase in the floor stiffness across the column size. The effect of this assumption is to underestimate the floor stiffness, especially in buildings with short floor spans and wide columns. All floor beams have a 2:1 depth-to-width ratio, thus maintaining a $\frac{40}{3}(1+\nu)$ (see section 2.3.1) ratio between the flexural and torsional stiffnesses of each beam. Floors are assumed to have rectangular panels of identical span lengths and a slab of uniform thickness supported on beams between supports. The floors are also assumed to be of monolithic construction with homogeneous, elastic, and isotropic material properties.

The floors are modeled as a mesh of two-dimensional linear curvature compatible triangular finite elements with cubic transverse displacement expansion and piecewise continuous derivatives, and uniaxial beam elements.

In the case of partial composite beam-slab action (i.e., beams symmetrical about mid-plane of slab), the beam elements are embedded in the slab. In the case of complete composite beam-slab action (i.e., beam and slab neutral axes not at the same level), a constant strain element is added to model the in-plane (membrane) slab stresses, and the uniaxial beams are connected to the finite element nodes by rigid links which maintain the condition that plane sections at the nodes remain plane. Several mesh sizes for each type of floor were attempted to establish the finite element mesh size needed for adequate convergence of the results.

Single-panel floors with partial and full composite beam-slab action are analyzed to determine the influence of beam eccentricity of floor stiffness. An analysis of the many different parameters that can affect the stiffness of a two-way slab floor led to the identification of the following four main parameters:

1. The ratio d_s/L_1 of slab thickness to panel span in the direction of the flexural beam.

2. The ratio α of the flexural stiffness of the flexural beam to that of the half-width of slab.

$$\alpha = \frac{4EI_{FB}/L_1}{4EI_S/L_1} \tag{6.1}$$

3. The ratio β of the torsional stiffness of the torsional beam (beam orthogonal to flexural beam) to the flexural stiffness of the flexural beam.

$$\beta = \frac{GJ_{TB}/L_2}{4EI_{FB}/L_1} \tag{6.2}$$

4. The aspect ratio of the panel L_1/L_2.

Parametric studies are conducted to determine the influence of these four parameters on floor stiffness.

Varying boundary conditions along panel edges, as represented by interior, exterior, and corner panels, also are investigated for floors with full composite beam-slab action.

A SMM to model the stiffness of a two-way slab floor is developed from the results of this investigation. In this method, the elastic stiffness of a beam-slab floor is estimated as the stiffness of equivalent uniaxial members between supports, each with three degrees of freedom: one torsional and two flexural (one flexural degree of freedom at each end of the member). The SMM does not identify a physical cross section for these members; rather, it establishes a procedure by which the position of the neutral axis of the equivalent member in relation to the top of slab and its member stiffness matrix can be computed from a set of graphs. Each member stiffness matrix is added directly to obtain the structure's stiffness matrix which can then be used to analyze the building properties and response. The effect of shear on the floor stiffness is included in the terms of the equivalent member's stiffness matrix, hence no other terms to model shear effect are necessary.

The SMM is evaluated by applying it to calculate the lateral stiffnesses of 27 single-panel structures and one multi-panel single-story structure, as well as the dynamic response of a multi-story building. Lateral stiffness for the single-story structures is defined as the force necessary to produce a unit lateral displacement of the top of slab. The structures analyzed include cases with floors of varying slab thickness and beam and column sizes. The lateral stiffness of each single-story structure is evaluated on the basis of four different methods: a finite element method, an equivalent frame method, an effective slab width method based on provisions of the ACI 318-71, 8.7, and the SMM. The results from the last three methods are compared with those from a finite element analysis, and the Diff. % in the results is used as the basis to evaluate the accuracy of the method.

6.2 Conclusions

Detailed conclusions are presented at the end of each chapter. The most important of these, and some general overall conclusions, are presented here.

1. The elastic rotational stiffness of a floor panel is a function of d_s/L_1, α, β, L_1/L_2, the boundary conditions along the panel edges, and the degree of beam-slab composite action which is determined by the

extent of eccentricity between beam and slab neutral axes.

The transition from partial to full composite action between beams and slab produces a marked increase in the rotational stiffness of the floor. This is caused by the shift of the floor neutral axis away from the neutral axis of the slab. The proportional increase in stiffness due to full composite action is more pronounced for larger values of α because of the accompanying increase in the eccentricity e. The increase in the contribution of the beams to the floor stiffness (due to the eccentricity introduced by the slab) can be approximated by $(K_{11})_B^r$ which is the beam stiffness computed about an axis defined by ξ. This axis coincides with the composite neutral axis of the floor only at the supports. Since e is equal to zero in floors with partial beam-slab composite action (i.e., symmetric beams), $(K_{11})_B^r$ in such floors is equal to the prismatic bare beam stiffness $(K_{11})_B$.

The contribution of the slab to the overall panel stiffness can be defined by the ratio $(K_{11})_S/(K_{11})_B^r$. Over the range of the different parameters investigated, it was found that $(K_{11})_S/(K_{11})_B^r$ is primarily a function of α, L_1/L_2, and the boundary conditions along the panel edges. $(K_{11})_S/(K_{11})_B^r$ approaches an asymptotic value of 1.0 as α increases, which shows that the relative slab contribution to the panel stiffness is higher in floors with shallow beams. This ratio approaches the 1.0 asymptote faster as the number of continuous edges in a panel increases and L_1/L_2 decreases. Given the same d_s/L_1, α, β, L_1/L_2, and panel boundary conditions, the ratio $(K_{11})_S/(K_{11})_B^r$ is very close in floors with partial or full composite action. Hence the graphs in Figs. 5.3(b) and 5.4(b) can be used interchangeably for both types of floors.

2. The two-way action of the floor theoretically couples the rotations of all the supports in a floor. However, the degree of coupling between diagonally placed panel supports and supports more than one panel away from each other was found to be very small. Hence, the usual practice of modeling the floor by uniaxial equivalent members, which only couple adjacent supports, can give adequate results.

3. The carryover factors (CF_{13} and CF_{15}) in a floor panel were found to be a function of α, β, L_1/L_2, and the boundary conditions. The two-way action of the slab redistributes the stresses in the panel so that the moments carried by beams to orthogonal supports are more evenly distributed than would be the case in a floor with only bare beams. The effect of the slab in floors with very stiff torsional beams relative to the flexural beams (i.e., high values of L_1/L_2 and β) is to reduce the values of CF_{15} from that of the bare beams. This signifies that the slab redistributes moments away from the torsional beams to the flexural beams. The slab has the opposite influence in floors with stiff flexural beams relative to the torsional beams. The difference between the panel carryover factors CF_{13} and CF_{15} from those of the prismatic bare beams ψ_{13} and ψ_{15} increases as the contribution of the slab to the overall panel stiffness increases. Thus this difference increases as α decreases, and L_1/L_2 and the number of continuous edges in the panel increases. This aspect of the behavior of two-way slabs has hitherto been neglected by researchers. Currently available models seek equivalent members that will match the diagonal terms of the panel's stiffness matrix and assume that carryover factors equal to those of prismatic beams can be used for these equivalent members. This investigation refutes that assumption and points out the need for models that will adequately approximate off-diagonal as well as diagonal terms of the floor panel's stiffness matrix.

There was some difference in the values of CF_{13} and CF_{15} in floors with symmetric or eccentric floor beams. Eccentric beams produced smaller values of CF_{13} and larger values of CF_{15} reflecting a higher degree of slab participation in the floor's stiffness. Hence using the graphs in Figs. 5.3(c), 5.3(d) and 5.4(c), 5.4(d) for modeling floors with symmetric beams will introduce a small error into the results of the analysis. CF_{15} was found to be a function of β, L_1/L_2, and the boundary conditions except for floors with L_1/L_2 (panel aspect ratio) close to 2.0 where the influence of α should also be accounted for.

4. Changing the boundary condition of a floor panel from being completely free (single-panel floor) to continuous on all four sides (an interior panel) has an appreciable effect on its stiffness. A continuous panel is stiffer and the influence of the boundary conditions

increases as L_1/L_2 is increased and α is decreased. The stiffness of floors with other boundary conditions falls between these two bounds. However, for practical purposes the graphs for an interior panel and those for a single-panel are sufficient to estimate adequately the stiffness of the different panels in a floor.

5. The accuracy and practicability of currently used methods to estimate the lateral stiffness of moment-resisting frames was investigated by analyzing a large number of single-story structures. The equivalent frame method, which is the only one suggested by the ACI 318-71 Code, was found to be complicated to use and gave poor results with a Diff. % as high as 169% when compared with analytical results obtained using a finite element model. This corresponds to a Diff. % of 39% in the structure's period which can lead to substantially different estimates of the structure's dynamic responses. The error in the results from using this method increases as the relative column-to-floor stiffness increases. The equivalent frame method was also found to be inconsistent in that it overestimated or underestimated the lateral stiffness, depending on the individual case considered.

The effective slab width method based on ACI 318-71, section 8.7 fared better than the equivalent frame, with a 13.8% maximum Diff. %. However, this method is not based on reliable experimental or analytical studies, and the correlation of results from the effective slab width method with the finite element analysis was inconsistent and did not establish well-defined trends. This suggests that the effective slab width method could lead to much higher error in estimating the lateral stiffness than the 13.8% Diff. % registered in this investigation.

A trial-and error procedure, used to compute an effective slab width that would yield the same lateral stiffness of the structure as from a finite element analysis, gave a wide range of values of the effective slab width. This width varied with each of the floor parameters considered. This points out the difficulty of attempting to model the stiffness of a two-way floor system with just an effective slab width method.

The analysis of a twelve-story building confirmed the conclusions based on analyzing the single-story structures. The equivalent frame method overestimated the floor stiffness, especially for relatively thin slabs. This led to lower natural periods of vibration with a Diff. % in the first period between this method and the SMM of 17.2% for the case of an 8-in. floor slab. The effective slab width method also overestimated the floor stiffness, although to a lesser degree than the equivalent frame method. However, the effective slab width method, based on the provisions of ACI 318-71, 8.7 proved inadequate in estimating the increase in floor stiffness as the slab thickness was increased from 8 in. to 12 in. (the generalized stiffness in the first mode K_1^* increased by less than 1%). The envelope of the expected maximum lateral displacements (based on SRSS) also showed marked differences as different models for the floor stiffness were used. Applying the N-S component of the 1940 El Centro earthquake to the longitudinal (x-x) direction of the building resulted in maximum expected roof displacement of 8.4 in. and 6.4 in. for the SMM and the equivalent frame method, respectively (Diff. % of 24.2%).

6. The analytical results of this investigation indicate the need for a careful study of the soundness of using the equivalent frame method to model buildings with two-way slab floors and subjected to lateral loads, as is suggested in present codes. Theoretically, the SMM seems to be a more accurate and consistent model. The SMM was found to be practical for use in that it does not require complex, time-consuming computations to calculate the structural properties of the equivalent members used to model the floor stiffness, and can be used directly in existing computer programs for frame analysis or for hand calculations (e.g. moment distribution procedures). The SMM not only proved accurate when compared with results of a finite element model but also the cost of the computations was a small fraction of the computer costs required to carry out a finite element analysis.

6.3 Recommendations for Future Studies

A large number of investigations and proper interpretation of their results are still necessary to reach the point where engineers will be able to ascertain, consistnetly, rationally and economically, the contribution of the floors to the stiffness, strength, and stability of

buildings. Following are some topics that need further attention:

1. The influence of the column width on the floor stiffness should be studied to evaluate the error introduced by assuming point supports. The results of this investigation can then be used to modify the SMM to account for the influence of the column size on the elastic stiffness of a two-way slab floor system.

2. The studies reported herein should be repeated for floor beams having a depth-to-width ratio different than the 2:1 ratio considered in this investigation. Bounds of the values of this ratio should be considered to evaluate the influence of this ratio on the floor stiffness.

3. The procedure developed in this investigation can be extended to the analysis of the elastic stiffness of other slab systems (e.g., flat and waffle slabs). Such a study must identify the primary parameters affecting the stiffness of each type of floor system, and evaluate the existing models to determine whether they can be improved or whether completely new models need be developed. An integrated SMM for all the main floor systems encountered in the field would be a powerful tool for analysts and designers.

4. Elastic analysis is no longer sufficient. It is well known that cracks in reinforced concrete develop during construction and then under excitations at service load levels. The knowledge of the floor behavior in the inelastic range, including yielding of the steel is an indispensible part of an aseismic design. Thus, the present investigation should be extended to the inelastic behavior of two-way slab systems as well as other floor systems.

Such inelastic studies are much more involved in that the behavior of the slab system must be analyzed stepwise from the initial appearance of first cracks to the formation of slab yield lines and proceed until a full mechanism develops. Such investigations must model degradations of stiffness and strength due to both increasing load levels and to stress reversals, as well as the composite action of reinforcing steel and concrete in the floor. The first step would be to consider the effect of cracking under working load. To solve this problem, integrated analytical and experimental studies are necessary.

5. In parametric studies, computer programs based on finite element methods are the most powerful tools available. They require less time and are far cheaper than experimental studies. At present, the inelastic behavior of reinforced concrete structures subjected to combined states of stress and/or strain are not well understood. Thus present analytical studies are based on a number of assumptions and simplifications which necessarily introduce a margin of error into the final results. Hence experimental studies remain the only conclusive method to study the elastic and inelastic behavior of a floor system.

REFERENCES

1. Mahin, S. A., et al., "Response of the Olive View Hospital Building During the San Fernando Earthquake," Earthquake Engineering Research Center Report No. EERC 76-22, University of California, Berkeley, 1976.

2. International Conference of Building Officials, Uniform Building Code, Whittier, California, 1973.

3. ACI Committee 318, Building Code Requirements for Reinforced Concrete (ACI 318-71), ACI, Detroit, Michigan, 1971.

4. Seismology Committee, Recommended Lateral Force Requirements and Commentary, Structural Engineers Association of California, San Francisco, California, 1973.

5. Bertero, V. V., et al., "Seismic Analysis of the Charaima Building, Caraballeda, Venezuela," Earthquake Engineering Research Center Report No. EERC 70-4, University of California, Berkeley, 1970.

6. Mahin, S. A. and Bertero, V. V., "An Evaluation of Some Methods for Predicting Seismic Behavior of Reinforced Concrete Buildings," Earthquake Engineering Research Center Report No. EERC 75-5, University of California, Berkeley, 1975.

7. Corley, W. G., Sozen, M. A. and Siess, C. P., "The Equivalent-Frame Analysis for Reinforced Concrete Slabs," Civil Engineering Studies, Structural Research Series No. 218, University of Illinois, Urbana, June 1961.

8. Jirsa, J. O., Sozen, M. A., and Siess, C. P., "The Effect of Pattern Loadings on Reinforced Concrete Floor Slabs," Civil Engineering Studies, Structural Research Series No. 269, University of Illinois, Urbana, July 1963.

9. Corley, W. G. and Jirsa, J. O., "Equivalent Frame Analysis for Slab Design," ACI Journal, Proceedings, V. 67, No. 11, Nov. 1970, pp. 875-884.

10. ACI Committee 318, Commentary of Building Code Requirements for Reinforced Concrete (ACI 318-71), ACI, Detroit, Michigan, 1971.

11. Fintel, M., Handbook of Concrete Engineering, Van Nostrand Reinhold Col, New York, 1974.

12. Khan, F. R., Sharounis, J. A., "Interaction of Shear Walls and Frames," Journal of the Structural Division, ASCE, Vol. 90, No. ST3, June 1964.

13. Jofriet, J. C., McNeice, G. M., "Finite Element Analysis of Reinforced Concrete Slabs," Journal of the Structural Division, Proceedings of the ASCE, March 1971.

14. Khan, M. A. and Kemp, K. O., "Elastic Full Composite Action in a Slab and Beam System," Structural Engineer, Vol. 48, September 1970.

15. Khan, M. A., "Elastic Composite Action in a Slab and Frame System," Structural Engineer, Vol. 49, June 1971.

16. Wood, R. H., "Studies in Composite Construction," Part II, National Building Studies, Research Paper No. 22, London, 1955.

17. ACI Committee 318, Commentary on Building Code Requirements for Reinforced Concrete (ACI 318-63), ACI, Detroit, Michigan, 1963.

18. Winter, G., et al., Design of Concrete Structures, Seventh Edition, McGraw-Hill Book Company, New York, 1964.

19. Felippa, C. A., "PLATE," CE Computer Programs Library, Department of Civil Engineering, University of California, Berkeley, 1967.

20. Clough, R. W. and Felippa, C. A., "A Refined Quadrilateral Element for Analysis of Plate Bending," Proceedings of the 2nd Conference on Matrix Methods in Structural Mechanics, Wright Patterson AFB, Fairfield, Ohio, 1968.

21. Timoshenko, S., Theory of Elasticity, John Wiley and Sons, New York, 1951.

22. Bathe, K. J., Wilson, E. L., and Peterson, F. E., "SAP-IV, A Structural Analysis Program for Static and Dynamic Response of Linear Systems," Earthquake Engineering Research Center Report No. EERC 73-11, University of California, Berkeley, April 1974.

23. Felippa, C. A., "Refined Finite Element Analysis of Linear and Non-linear Two-Dimensional Structures," SESM Report 66-2, Department of Civil Engineering, University of California, Berkeley, 1966.

24. Prezemieniecki, S., Theory of Matrix Structural Analysis, McGraw-Hill, New York, 1968.

25. Meek, J. L., Matrix Structural Analysis, McGraw-Hill, New York, 1971.

26. Wilson, E. L., Hollings, J. P. and Dovey, H. H., "Three-Dimensional Analysis of Building Systems (Extended Version) - ETABS," Earthquake Engineering Research Center Report No. EERC 75-13, April 1975.

27. "Strong-Motion Earthquake Accelerograms, Digitized and Plotted," Vol. 1A, Earthquake Engineering Research Laboratory Report No. 70-20, California Institute of Technology, Pasadena, California.

TABLE 2.1: STIFFNESS OF SINGLE-PANEL FLOOR SLAB WITH BEAMS SYMMETRIC AROUND MID-PLANE OF SLAB*

d_s (in.)	e_s/L	Group "A"			Group "B"		
		$(K_{11})_S$ $\left(\frac{\text{K-in.}}{\text{rad}}\right)$	$(K_{11})_B$ $\left(\frac{\text{K-in.}}{\text{rad}}\right)$	$\frac{(K_{11})_S}{(K_{11})_B}$	$(K_{11})_S$ $\left(\frac{\text{K-in.}}{\text{rad}}\right)$	$(K_{11})_B$ $\left(\frac{\text{K-in.}}{\text{rad}}\right)$	$\frac{(K_{11})_S}{(K_{11})_B}$
1.5	1/160, .006	140528.39	139659.57	1.01	315346.82	315346.82	1.00
6.5	1/37 , .027	218531.47	139659.57	1.57	397772.47	315346.82	1.26
7.0	1/34 , .029	233644.86	139659.57	1.67	-	-	-
8.0	1/30 , .033	267379.68	139659.57	1.92	-	-	-
9.0	1/27 , .038	304878.05	139659.57	2.18	494559.84	315346.82	1.57
10.0	1/24 , .042	349650.35	139659.57	2.50	-	-	-

* For floor properties and degrees of freedom, see Fig. 2.5.

TABLE 2.2: STRUCTURAL PROPERTIES OF SQUARE SINGLE-PANEL FLOOR SLABS

α	β	d_s (in.)	Flexural Beam	Torsional Beam
0.8	0.064	6.5	7.53" x 15.15"	7.53" x 15.15"
		7.5	8.44" x 16.87"	8.44" x 16.87"
		9.0	9.67" x 19.34"	9.67" x 19.34"
	0.107	6.5	7.53" x 15.15"	8.61" x 17.22"
	0.160	6.5	7.53" x 15.15"	9.53" x 19.05"
1.2	0.064	6.5	8.39" x 16.77"	8.39" x 16.77"
		7.5	9.34" x 18.67"	9.34" x 18.67"
		9.0	10.71" x 21.41"	10.71" x 21.41"
	0.107	6.5	8.39" x 16.77"	9.53" x 19.05"
	0.160	6.5	8.39" x 16.77"	10.55" x 21.09"
2.0	0.064	6.5	9.53" x 19.05"	9.53" x 19.05"
		7.5	10.61" x 21.21"	10.61" x 21.21"
		9.0	12.16" x 24.32"	12.16" x 24.32"
	0.107	6.5	9.53" x 19.05"	10.83" x 21.65"
	0.160	6.5	9.53" x 19.05"	11.98" x 23.96"
3.0	0.064	6.5	10.55" x 21.09"	10.55" x 21.09"
		7.5	11.74" x 23.48"	11.74" x 23.48"
		9.0	13.46" x 26.92"	13.46" x 26.92"
	0.107	6.5	10.55" x 21.09"	11.98" x 23.96"
		9.0	13.46" x 26.92"	15.29" x 30.58"
	0.160	6.5	10.55" x 21.09"	13.26" x 26.52"

TABLE 2.3: SQUARE SINGLE-PANEL FLOOR SYSTEMS

α	β	d_s (in.)	$(K_{11})_S$ $\frac{K\text{-in}}{rad}$	$(K_{11})_B$ $\frac{K\text{-in}}{rad}$	$(K_{11})_S/(K_{11})_B$
0.8	0.064	6.5	199521.15	129383.71	1.54
		7.5	305250.31	198757.41	1.54
		9.0	524658.97	343452.80	1.53
	0.107	6.5	209467.95	134579.98	1.56
	0.160	6.5	220458.55	141075.32	1.56
1.2	0.064	6.5	269541.78	194075.57	1.39
		7.5	412541.25	298136.11	1.38
		9.0	709219.86	515179.20	1.38
	0.107	6.5	282645.56	201869.97	1.40
	0.160	6.5	297265.16	211612.98	1.40
2.0	0.064	6.5	405515.00	323459.28	1.25
		7.5	621118.01	496893.52	1.25
		9.0	1068376.07	858632.00	1.24
	0.107	6.5	424448.22	336449.95	1.26
	0.160	6.5	445632.80	352688.30	1.26
3.0	0.064	6.5	571428.57	485188.91	1.18
		7.5	875656.74	745340.27	1.17
		9.0	1501501.50	1287947.99	1.17
	0.107	6.5	597157.53	504674.93	1.18
		9.0	1571832.76	1339674.19	1.17
	0.160	6.5	626409.42	529032.45	1.18

TABLE 2.4: INFLUENCE OF d_s, α, AND β ON STIFFNESS OF A SQUARE SINGLE-PANEL FLOOR SYSTEM*

	d_s (in.)	α	β	$(K_{11})_S$ $\frac{K\text{-in}}{rad}$	$(K_{11})_B$ $\frac{K\text{-in}}{rad}$	$(K_{11})_S/(K_{11})_B$
Group "A"	1.5	66.67	0.122	140528.39	139659.57	1.01
	6.5	0.819	0.122	218531.47	139659.57	1.57
	7.0	0.656	0.122	233644.86	139659.57	1.67
	8.0	0.439	0.122	267379.68	139659.57	1.92
	9.0	0.309	0.122	304878.05	139659.57	2.18
	10.0	0.225	0.122	349650.35	139659.57	2.50
Group "B"	1.5	158.025	0.068	315346.82	315346.82	1.00
	6.5	1.942	0.068	397772.47	315346.82	1.26
	9.0	0.732	0.068	494559.84	315346.82	1.57

* For structural properties of the floors, see Fig. 2.5.

TABLE 2.5: INFLUENCE OF d_s, α, AND β ON CARRYOVER FACTORS OF A SQUARE SINGLE-PANEL FLOOR SYSTEM

α	β	d_s (in)	CF_{12}	CF_{13}	CF_{14}	CF_{15}	CF_{16}	CF_{17}	CF_{18}	ψ_{13}
0.8	0.064	6.5	-.035	.376	.019	-.037	-.017	.028	-.013	.470
		7.5	-.036	.375	.019	-.037	-.018	.028	-.013	
		9.0	-.038	.374	.020	-.036	-.019	.028	-.014	
	0.107	6.5	-.046	.372	.025	-.049	-.014	.033	-.016	.452
	0.160	6.5	-.056	.366	.031	-.064	-.009	.038	-.018	.431
1.2	0.064	6.5	-.040	.397	.016	-.038	-.015	.027	-.013	.470
		7.5	-.041	.396	.017	-.038	-.016	.027	-.013	
		9.0	-.043	.394	.017	-.037	-.016	.027	-.013	
	0.107	6.5	-.050	.390	.022	-.053	-.011	.032	-.016	.452
	0.160	6.5	-.058	.381	.028	-.073	-.006	.036	-.019	.431
2.0	0.064	6.5	-.042	.417	.013	-.041	-.012	.024	-.013	.470
		7.5	-.043	.416	.013	-.040	-.013	.024	-.013	
		9.0	-.044	.414	.014	-.040	-.013	.024	-.013	
	0.107	6.5	-.049	.408	.018	-.060	-.008	.029	-.016	.452
	0.160	6.5	-.054	.396	.022	-.086	-.004	.033	-.018	.431
3.0	0.064	6.5	-.039	.428	.010	-.043	-.010	.022	-.013	.470
		7.5	-.040	.427	.011	-.043	-.010	.022	-.013	
		9.0	-.041	.425	.011	-.042	-.010	.022	-.013	
	0.107	6.5	-.044	.417	.014	-.066	-.006	.026	-.015	.452
		9.0	-.046	.413	.015	-.066	-.006	.026	-.016	
	0.160	6.5	-.047	.403	.017	-.096	-.003	.029	-.017	.431

TABLE 2.6: STRUCTURAL PROPERTIES OF SINGLE-PANEL FLOOR WHERE $L_1/L_2 = 0.5$, $d_s = 6.5$ in., AND $L_1 = 120$ in.

α	β	Flexural Beam	Torsional Beam
0.4	.032	6.37" x 12.74"	6.37" x 12.74"
	.064	6.37" x 12.74"	7.58" x 15.15"
0.8	.064	7.58" x 15.15"	9.01" x 18.02"
3.0	.032	10.54" x 21.09"	10.54" x 21.09"
	.064	10.54" x 21.09"	12.54" x 25.08"
	.128	10.54" x 21.09"	14.91" x 29.82"

TABLE 2.7: STRUCTURAL PROPERTIES OF SINGLE-PANEL FLOOR WHERE $L_1/L_2 = 2.0$, $d_s = 6.5$ in., AND $L_1 = 240$ in.

α	β	Flexural Beam	Torsional Beam
0.8	.064	6.37" x 12.74"	5.36" x 10.72"
	.128	6.37" x 12.74"	6.37" x 12.74"
	.600	6.37" x 12.74"	9.37" x 18.74"
1.2	.064	7.05" x 14.01"	5.93" x 11.86"
	.600	7.05" x 14.01"	10.37" x 20.74"
2.0	.064	8.01" x 16.02"	6.74" x 13.47"
	.600	8.01" x 16.02"	11.79" x 23.57"
3.0	.064	8.87" x 17.73"	7.46" x 14.91"
	.128	8.87" x 17.73"	8.87" x 17.73"
	.600	8.87" x 17.73"	13.04" x 26.08"

TABLE 2.8: STIFFNESS OF A SINGLE-PANEL FLOOR WHERE $L_1/L_2 = 0.5$, $d_s = 6.5$ in., AND $L_1 = 120$ in.

α	β	$(K_{11})_S \left(\frac{\text{K-in.}}{\text{rad}}\right)$	$(K_{11})_B \left(\frac{\text{K-in.}}{\text{rad}}\right)$	$\frac{(K_{11})_S}{(K_{11})_B}$
0.4	.032	194704.05	125480.16	1.55
	.064	208942.75	129371.02	1.62
0.8	.064	351370.34	258742.04	1.36
3.0	.032	1015228.43	941101.21	1.08
	.064	1065416.58	970282.64	1.10
	.128	1146000.46	1028645.51	1.11

TABLE 2.9: STIFFNESS OF A SINGLE-PANEL FLOOR WHERE $L_1/L_2 = 2.0$, $d_s = 6.5$ in., AND $L_1 = 240$ in.

α	β	$(K_{11})_S \left(\frac{\text{K-in.}}{\text{rad}}\right)$	$(K_{11})_B \left(\frac{\text{K-in.}}{\text{rad}}\right)$	$\frac{(K_{11})_S}{(K_{11})_B}$
0.8	.064	122518.99	64685.51	1.89
	.128	128700.13	68589.06	1.88
	.600	164652.42	97271.44	1.69
1.2	.064	159591.45	97028.26	1.64
	.600	218092.99	145907.16	1.50
2.0	.064	230840.26	230840.26	1.43
	.600	321564.09	243178.61	1.32
3.0	.064	317258.88	242570.66	1.31
	.128	334672.02	257161.38	1.30
	.600	448149.14	364767.91	1.23

TABLE 2.10: DISTRIBUTION FACTORS FOR SINGLE-PANEL FLOOR WHERE $L_1/L_2 = 0.50$, $d_s = 6.5$ in., AND $L_1 = 120$ in.

α	β	CF_{12}	CF_{13}	CF_{14}	CF_{15}	CF_{16}	CF_{17}	CF_{18}	ψ_{13}
0.4	.032	-.031	.375	.034	-.003	-.004	.004	-.006	.484
	.064	-.052	.372	.048	-.006	-.000	.006	-.011	.470
0.8	.064	-.059	.401	.046	-.009	.004	.008	-.014	.470
3.0	.032	-.035	.437	.023	-.009	.004	.006	-.010	.484
	.064	-.047	.428	.034	-.024	.011	.012	-.017	.470
	.128	-.058	.410	.045	-.060	.020	.019	-.025	.443

TABLE 2.11: DISTRIBUTION FACTORS FOR SINGLE-PANEL FLOOR WHERE $L_1/L_2 = 2.00$, $d_s = 6.5$ in., AND $L_1 = 240$ in.

α	β	CF_{12}	CF_{13}	CF_{14}	CF_{15}	CF_{16}	CF_{17}	CF_{18}	ψ_{13}
0.8	,064	-.040	.311	.005	-.133	-.053	.069	-.015	.470
	.128	-.047	.306	.008	-.151	-.051	.071	-.016	.443
	.600	-.072	.268	.020	-.270	-.035	.072	-.017	.313
1.2	.064	-.050	.334	.003	-.129	-.053	.062	-.015	.470
	.600	-.072	.274	.017	-.294	-.032	.063	-.017	.313
2.0	.064	-.059	.360	.000	-.121	-.051	.052	-.015	.470
	.600	-.067	.279	.011	-.322	-.030	.051	-.016	.313
3.0	.064	-.062	.377	-.003	-.114	-.049	.046	-.016	.470
	.128	-.065	.363	.000	-.147	-.044	.047	-.017	.443
	.600	-.061	.281	.006	-.340	-.029	.043	-.015	.313

TABLE 3.1: STRUCTURAL PROPERTIES OF SINGLE-PANEL FLOORS WHERE $L_1/L_2 = 1.0$, $L_1 = 240$ in.

α	β	d_s (in.)	Flexural Beam	Torsional Beam
0.4	.064	6.5	6.37" x 12.74"	6.37" x 12.74"
0.8	.064	6.5	7.58" x 15.15"	7.58" x 15.15"
		9.0	9.67" x 19.34"	9.67" x 19.34"
	.107	6.5	7.58" x 15.15"	8.61" x 17.22"
	.160	6.5	7.58" x 15.15"	9.53" x 19.05"
1.2	.064	6.5	8.39" x 16.77"	8.39" x 16.77"
2.0	.064	6.5	9.53" x 19.05"	9.53" x 19.05"
3.0	.064	6.5	10.55" x 21.09"	10.55" x 21.09"
		9.0	13.46" x 26.92"	13.46" x 26.92"
	.107	6.5	10.55" x 21.09"	11.98" x 23.96"
	.160	6.5	10.55" x 21.09"	13.26" x 26.52"
8.0	.064	6.5	13.48" x 26.95"	13.48" x 26.95"

TABLE 3.2: STRUCTURAL PROPERTIES OF SINGLE-PANEL FLOORS
WHERE $L_1/L_2 = 2.0$, $L_1 = 240$ in.

α	β	d_s (in.)	Flexural Beam	Torsional Beam
0.4	.064	6.5	5.36" x 10.72"	4.51" x 9.01"
0.8	.064	6.5	6.37" x 12.74"	5.36" x 10.72"
		9.0	8.13" x 16.27"	6.84" x 13.68"
	.256	6.5	6.37" x 12.74"	7.58" x 15.15"
1.2	.128	6.5	7.05" x 14.10"	7.05" x 14.10"
2.0	.128	6.5	8.01" x 16.02"	8.01" x 16.02"
3.0	.064	6.5	8.87" x 17.73"	7.46" x 14.91"
		9.0	11.32" x 22.64"	9.52" x 19.03"
	.128	6.5	8.87" x 17.73"	8.87" x 17.73"
	.256	6.5	8.87" x 17.73	10.54" x 21.09"
8.0	.064	6.5	11.33" x 22.66"	9.53" x 19.05"

TABLE 3.3: STRUCTURAL PROPERTIES OF SINGLE-PANEL FLOORS
WHERE $L_1/L_2 = 0.5$, $L_1 = 120$ in.

α	β	d_s (in.)	Flexural Beam	Torsional Beam
0.4	.032	6.5	6.37" x 12.74"	6.37" x 12.74"
		9.0	8.13" x 16.27"	8.13" x 16.27"
	.128	6.5	6.37" x 12.74"	9.01" x 18.01"
0.8	.064	6.5	7.58" x 15.15"	9.01" x 18.01"
1.5	.064	6.5	8.87" x 17.73"	10.54" x 21.09"
3.0	.032	6.5	10.54" x 21.09"	10.54" x 21.09"
		9.0	13.46" x 26.92"	13.46" x 26.92"
	.064	6.5	10.54" x 21.09"	12.53" x 25.07"
	.128	6.5	10.54" x 21.09"	14.91" x 29.81"
8.0	.064	6.5	13.48" x 26.95"	16.02" x 32.03"

TABLE 3.4: STIFFNESS OF A SINGLE-PANEL FLOOR WHERE L_1/L_2 = 1.0, L_1 = 240 in.

α	β	d_s (in.)	E (in.)	γ	$(K_{11})_S$ $\left(\frac{\text{K-in.}}{\text{rad}}\right)$	$(K_{11})_B$ $\left(\frac{\text{K-in.}}{\text{rad}}\right)$	$(K_{11})_B^r$ $\left(\frac{\text{K-in.}}{\text{rad}}\right)$	$(K_{11})_S/(K_{11})_B$	$(K_{11})_S/(K_{11})_B^r$
0.4	.064	6.5	1.752	.561	146426.18	64685.51	78475.97	2.264	1.866
0.8	.064	6.5	2.201	.509	236418.92	129383.71	160151.31	1.827	1.476
		9.0	2.381	.460	598131.20	343452.80	402108.13	1.742	1.487
	.107	6.5	2.197	.508	244496.39	134599.36	165267.87	1.816	1.479
	.160	6.5	2.193	.507	253655.17	141043.59	171600.53	1.798	1.478
1.2	.064	6.5	2.439	.475	321820.73	194056.53	240350.56	1.658	1.339
2.0	.064	6.5	2.700	.430	485951.15	323427.55	396665.33	1.503	1.225
3.0	.064	6.5	2.869	.393	684714.84	485141.32	586421.86	1.411	1.168
		9.0	3.148	.351	1709489.38	1287821.66	1486488.69	1.327	1.150
	.107	6.5	2.893	.397	709097.15	504747.60	607729.70	1.405	1.167
	.160	6.5	2.911	.399	736791.54	528913.47	633181.06	1.393	1.164
8.0	.064	6.5	3.136	.307	1625482.36	1293710.19	1491319.89	1.256	1.090

TABLE 3.5: STIFFNESS OF A SINGLE-PANEL SLAB WHERE $L_1/L_2 = 2.0$

α	β	d_s	ξ (in.)	γ	$(K_{11})_B \left(\frac{\text{K-in.}}{\text{rad}}\right)$	$(K_{11})_B \left(\frac{\text{K-in.}}{\text{rad}}\right)$	$(K_{11})_B^r \left(\frac{\text{K-in.}}{\text{rad}}\right)$	$(K_{11})_S/(K_{11})_B$	$(K_{11})_S/(K_{11})_B^r$
0.4	.064	6.5	1.151	.546	94270.43	32345.93	36552.82	2.914	2.579
0.8	.064	6.5	1.540	.493	142665.56	64691.86	75347.11	2.205	1.893
		9.0	1.602	.441	362973.77	171726.40	190524.36	2.114	1.905
	.256	6.5	1.509	.483	156909.02	76383.47	86617.36	2.054	1.812
1.2	.128	6.5	1.743	.459	196297.82	102864.55	119582.83	1.908	1.642
2.0	.128	6.5	1.981	.416	288595.29	171473.26	199367.25	1.683	1.448
3.0	.064	6.5	2.136	.380	385406.95	242595.34	282290.82	1.589	1.365
		9.0	2.287	.335	967505.36	643974.00	718120.77	1.502	1.347
	.128	6.5	2.139	.380	400246.55	257209.91	297026.58	1.556	1.348
	.256	6.5	2.125	.378	428735.57	286439.06	325723.59	1.497	1.316
8.0	.064	6.5	2.397	.297	887191.79	646918.55	728561.44	1.371	1.218

TABLE 3.6: STIFFNESS OF A SINGLE-PANEL SLAB WHERE $L_1/L_2 = 0.5$

α	β	d_s	ξ	γ	$(K_{11})_S$ $\left(\frac{K\text{-in.}}{rad}\right)$	$(K_{11})_B$ $\left(\frac{K\text{-in.}}{rad}\right)$	$(K_{11})_B^r$ $\left(\frac{K\text{-in.}}{rad}\right)$	$\frac{(K_{11})_S}{(K_{11})_B}$	$\frac{(K_{11})_S}{(K_{11})_B}$
0.4	.032	6.5	1.384	.443	216885.87	125480.27	142691.49	1.728	1.520
		9.0	1.402	.386	550790.00	333107.98	361882.02	1.653	1.522
	.128	6.5	1.316	.422	230864.77	137153.18	152719.63	1.683	1.512
0.8	.064	6.5	1.604	.371	368658.16	258742.48	291430.02	1.425	1.265
1.5	.064	6.5	1.821	.324	644928.28	485188.57	542891.87	1.329	1.188
3.0	.032	6.5	1.889	.259	1111135.80	941147.90	1028914.46	1.181	1.080
		9.0	1.952	.218	2735873.32	2498303.49	2651021.07	1.095	1.032
	.064	6.5	1.961	.269	1164212.12	970281.30	1064933.58	1.200	1.093
	.128	6.5	2.045	.280	1248667.05	1028648.81	1131514.17	1.214	1.104
8.0	.064	6.5	2.056	.201	2750199.94	2587424.75	2757393.49	1.063	0.997

TABLE 3.7: CARRYOVER FACTORS FOR A SINGLE-PANEL FLOOR WHERE $L_1/L_2 = 1.0$, $L_1 = 240$ in.

α	β	d_s	CF_{12}	CF_{13}	CF_{14}	CF_{15}	CF_{16}	CF_{17}	CF_{18}
0.4	.064	6.5	-.057	.318	.023	-.030	-.034	.037	-.012
0.8	.064	6.5	-.063	.338	.020	-.029	-.037	.031	-.008
		9.0	-.064	.335	.021	-.033	-.035	.032	-.010
	.107	6.5	-.077	.337	.027	-.039	-.041	.034	-.008
	.160	6.5	-.091	.335	.033	-.050	-.045	.038	-.009
1.2	.064	6.5	-.065	.344	.018	-.029	-.038	.028	-.007
2.0	.064	6.5	-.063	.346	.016	-.028	-.037	.024	-.006
3.0	.064	6.5	-.060	.346	.013	-.029	-.036	.022	-.005
		9.0	-.057	.339	.012	-.031	-.032	.023	-.007
	.107	6.5	-.069	.342	.018	-.045	-.040	.025	-.005
	.160	6.5	-.077	.336	.021	-.067	-.043	.027	-.005
8.0	.064	6.5	-.045	.345	.008	-.030	-.029	.018	-.004

TABLE 3.8: CARRYOVER FACTORS FOR A SINGLE-PANEL FLOOR WHERE $L_1/L_2 = 2.00$, $L_1 = 240$ in.

α	β	d_s	CF_{12}	CF_{13}	CF_{14}	CF_{15}	CF_{16}	CF_{17}	CF_{18}
0.4	.064	6.5	-.053	.264	.009	-.163	-.057	.076	-.007
0.8	.064	6.5	-.065	.301	.009	-.146	-.062	.066	-.005
		9.0	-.065	.296	.008	-.153	-.060	.067	-.006
	.256	6.5	-.092	.291	.020	-.187	-.072	.069	-.002
1.2	.064	6.5	-.080	.315	.014	-.149	-.067	.060	-.002
2.0	.064	6.5	-.080	.332	.013	-.133	-.064	.052	-.0001
3.0	.064	6.5	-.070	.348	.007	-.100	-.058	.044	-.002
		9.0	-.071	.340	.005	-.107	-.056	.047	-.005
	.128	6.5	-.076	.341	.012	-.122	-.060	.046	-.0004
	.256	6.5	-.082	.325	.016	-.166	-.060	.048	-.002
8.0	.064	6.5	-.057	.359	.002	-.073	-.046	.036	-.003

TABLE 3.9: CARRYOVER FACTORS FOR A SINGLE-PANEL FLOOR WHERE $L_1/L_2 = 0.5$, $L_1 = 120$ in.

α	β	d_s (in.)	CF_{12}	CF_{13}	CF_{14}	CF_{15}	CF_{16}	CF_{17}	CF_{18}
0.4	.032	6.5	-.054	.340	.033	.0001	-.016	.004	-.009
		9.0	-.056	.339	.034	-.001	-.015	.004	-.009
	.128	6.5	-.093	.344	.050	-.004	-.029	.005	-.013
0.8	.064	6.5	-.067	.354	.028	-.002	-.026	.004	-.011
1.5	.064	6.5	-.074	.353	.029	-.009	-.019	.009	-.018
3.0	.032	6.5	-.047	.348	.012	-.004	-.015	.007	-.014
		9.0	-.045	.335	.013	-.005	-.011	.007	-.016
	.064	6.5	-.062	.346	.020	-.014	-.015	.011	-.021
	.128	6.5	-.076	.339	.028	-.041	-.012	.019	-.030
8.0	.064	6.5	-.040	.332	.008	-.024	-.007	.013	-.023

TABLE 4.1: PHYSICAL PROPERTIES OF CORNER PANELS WITH CONSISTENT α AND β WHERE d_s = 6.5 in., β = .064

L_1/L_2	α	Beam AC	Beam AG	Beams DF & GI	Beams BH & CI
1.0 L_1=240 in	0.8	7.58" x 15.15"	7.58" x 15.15"	9.01" x 18.02"	9.01" x 18.02"
	2.0	9.53" x 19.05"	7.59" x 15.15"	9.97" x 19.94"	9.97" x 19.94"
	8.0	13.48" x 26.95"	13.48" x 26.95"	16.02" x 32.05"	16.02" x 32.05"
0.5 L_1=120 in	0.8	7.58" x 15.15"	9.01" x 18.01"	9.01" x 18.02"	10.71" x 21.42"
	3.0	10.54" x 21.09"	12.53" x 25.07"	9.97" x 19.94"	14.90" x 29.81"
	8.0	13.48" x 26.95"	16.02" x 32.03"	16.02" x 32.05"	19.05" x 38.09"
2.0 L_1=240 in	0.4	5.36" x 10.72"	4.51" x 9.01"	6.37" x 12.74"	5.36" x 10.72"
	3.0	8.87" x 17.73"	7.46" x 14.91"	10.54" x 21.09"	8.87" x 17.73"
	3.0 β=.256	8.87" x 17.73"	10.54" x 21.09"	10.54" x 21.09"	12.54" x 25.08"
	8.0	11.33" x 22.66"	9.53" x 19.05"	13.47" x 26.95"	11.33" x 22.66"

TABLE 4.2: PHYSICAL PROPERTIES OF CORNER PANELS WITH NONCONSISTENT α WHERE d_s = 6.5 in., L_1/L_2 = 2.0, L_1 = 240 in.

α Edge Beams	β	Beams AC, DF, GI	Beams AG, BH, CI
0.4	.064	5.36" x 10.72"	4.51" x 9.01"
3.0	.064	8.87" x 17.73"	7.46" x 14.91"
3.0	.256	8.87" x 17.73"	10.54" x 21.09"
8.0	.064	11.33" x 22.66"	9.53" x 19.05"

TABLE 4.3: STIFFNESS OF A CORNER PANEL WITH CONSISTENT α WHERE $L_1/L_2 = 1.0$, $d_s = 6.5$ in., $\beta = .064$, $L_1 = 240$ in.

α	ξ (in.)	γ	$(K_{11})_S$ $\left(\frac{\text{K-in.}}{\text{rad}}\right)$	$(K_{11})_B$ $\left(\frac{\text{K-in.}}{\text{rad}}\right)$	$(K_{11})_B^r$ $\left(\frac{\text{K-in.}}{\text{rad}}\right)$	$(K_{11})_S/(K_{11})_B$	$(K_{11})_S/(K_{11})_B^r$
0.8	2.066	.478	239808.15	129383.71	156490.83	1.853	1.532
2.0	2.545	.406	491443.96	323459.28	388225.64	1.519	1.266
8.0	3.004	.294	1636280.93	1293710.19	1475821.71	1.265	1.109

TABLE 4.4: STIFFNESS OF A CORNER PANEL WITH CONSISTENT α WHERE $L_1/L_2 = 0.5$, $d_s = 6.5$ in., $\beta = .064$, $L_1 = 120$ in.

α	ξ (in.)	γ	$(K_{11})_S$ $\left(\frac{\text{K-in.}}{\text{rad}}\right)$	$(K_{11})_B$ $\left(\frac{\text{K-in.}}{\text{rad}}\right)$	$(K_{11})_B^r$ $\left(\frac{\text{K-in.}}{\text{rad}}\right)$	$(K_{11})_S/(K_{11})_B$	$(K_{11})_S/(K_{11})_B^r$
0.8	1.511	.349	391453.78	258742.48	287730.76	1.513	1.360
3.0	1.862	.255	1176777.94	970284.29	1055206.03	1.213	1.115
8.0	2.041	.200	2765303.19	2587424.79	2754864.46	1.069	1.004

TABLE 4.5: STIFFNESS OF A CORNER PANEL WITH CONSISTENT α
WHERE $L_1/L_2 = 2.0$, $d_s = 6.5$ in., $L_1 = 240$ in.

α	β	ξ (in.)	γ	$(K_{11})_S \left(\frac{K\text{-in.}}{rad}\right)$	$(K_{11})_B \left(\frac{K\text{-in.}}{rad}\right)$	$(K_{11})_B^r \left(\frac{K\text{-in.}}{rad}\right)$	$(K_{11})_S/(K_{11})_B$	$(K_{11})_S/(K_{11})_B^r$
0.4	.064	1.155	.548	98512.07	32342.81	36578.95	3.046	2.693
3.0	.064	2.179	.388	397184.76	242571.07	283893.79	1.637	1.399
3.0	.256	2.189	.389	440369.56	286344.46	327936.84	1.538	1.343
8.0	.064	2.478	.307	909962.82	646856.20	734174.74	1.407	1.239

TABLE 4.6: STIFFNESS OF A CORNER PANEL WITH NON-CONSISTENT α
WHERE $L_1/L_2 = 2.0$, $d_s = 6.5$ in., $L_1 = 240$ in.

α Edge Beam	β	ξ (in.)	γ	$(K_{11})_S \left(\frac{K\text{-in.}}{rad}\right)$	$(K_{11})_B \left(\frac{K\text{-in.}}{rad}\right)$	$(K_{11})_B^r \left(\frac{K\text{-in.}}{rad}\right)$	$(K_{11})_S/(K_{11})_B$	$(K_{11})_S/(K_{11})_B^r$
0.4	.064	1.159	.550	97966.99	32342.81	36610.85	3.029	2.676
3.0	.064	2.182	.389	395544.59	242571.07	284003.93	1.631	1.393
3.0	.256	2.190	.390	438388.83	286344.46	328076.51	1.531	1.336
8.0	.064	2.479	.307	906981.76	646856.20	734229.23	1.402	1.235

TABLE 4.9: COMPARISON OF STIFFNESS PROPERTIES OF A SINGLE-PANEL FLOOR AND A CORNER PANEL OF A MULTI-PANEL FLOOR WHERE d_s = 6.5 in., β = .064

L_1/L_2	α	$(K_{11})_s$ $\frac{k\text{-in}}{rad}$			γ			CF_{13}			CF_{15}		
		SB	CB	Δ%	SB	CB	Δ%	SB	CB	Δ%	SB	CB	Δ%
1.0 L_1=240 in	0.8	236418.92	239808.15	-1.41	.509	.478	6.49	.338	.335	.89	-.031	-.036	-
	2.0	485951.15	491443.96	-1.12	.430	.406	5.91	.345	.347	-.58	-.030	-.033	-
	8.0	1625482.36	1636280.93	- .66	.307	.294	4.42	.343	.344	-.29	-.031	-.032	-
0.5 L_1=120 in	0.8	385561.49	391453.78	-1.53	.379	.349	7.87	.352	.356	1.14	-.005	-.004	-
	3.0	1111135.80	1176777.94	-1.08	.259	.255	1.54	.346	.350	1.16	-.004	-.013	-
	8.0	2750199.94	2765303.19	- .55	.201	.200	.50	.327	.326	.31	-.024	-.024	-
2.0 L_1=240 in	0.4	94270.43	98512.07	-4.50	.546	.548	-.37	.264	.228	13.64	-.163	-.225	38.04
	3.0	385406.95	397184.76	-3.06	.380	.388	-2.10	.348	.332	4.60	-.100	-.129	29.00
	3.0 β=.256	428735.57	440369.56	-2.71	.378	.389	-2.91	.325	.309	4.92	-.166	-.192	15.66
	8.0	887191.79	909962.82	-2.57	.297	.307	-3.37	.359	.349	2.79	-.073	-.085	16.44

SB = Single-Panel Floor

CB = Corner Panel of a Multi-Panel Floor with a Consistent Value of α

$$\Delta\% = \frac{SB - CB}{CB} \times 100$$

TABLE 4.10: PHYSICAL PROPERTIES OF INTERIOR PANELS WHERE $L_1/L_2 = 1.0$, $L_1 = 240$ in.

α	β	d_s (in.)	Flexural Beams	Torsional Beams
0.4	.064	8.0	8.85" x 17.71"	8.85" x 17.71"
0.8	.064	6.5	9.01" x 18.02"	9.01" x 18.02"
		10.0	12.45" x 24.89"	12.45" x 24.89"
	.192	10.0	12.45" x 24.89"	16.37" x 32.75"
2.0	.064	8.0	13.24" x 26.48"	13.24" x 26.48"
6.0	.064	6.5	14.91" x 29.82"	14.91" x 29.82"
		10.0	20.60" x 41.20"	20.60" x 41.20"
	.096	10.0	20.60" x 41.20"	22.79" x 45.57"
	.192	10.0	20.60" x 41.20"	27.10" x 54.19"
16.0	.064	8.0	22.27" x 44.53"	22.27" x 44.53"

TABLE 4.11: PHYSICAL PROPERTIES OF INTERIOR PANELS WHERE $L_1/L_2 = 0.5$, $L_1 = 120$ in.

α	β	d_s (in.)	Flexural Beams	Torsional Beams
0.4	.064	8.0	8.85" x 17.71"	10.52" x 21.05"
0.8	.032	10.0	12.45" x 24.89"	12.45" x 24.89"
	.064	6.5	9.01" x 18.02"	10.71" x 21.42"
		10.0	12.45" x 24.89"	14.80" x 29.59"
	.128	10.0	12.45" x 24.89"	17.60" x 35.19"
2.0	.064	8.0	13.24" x 26.48"	15.74" x 31.48"
4.0	.064	8.0	15.74" x 31.49"	18.72" x 37.43"

TABLE 4.12: PHYSICAL PROPERTIES OF INTERIOR PANEL WHERE $L_1/L_2 = 2.0$

α	β	d_s (in.)	Flexural Beams	Torsional Beams
0.4	.064	8.0	7.45 x 14.89	6.26 x 12.52
0.8	.064	6.5	7.58 x 15.15	6.37 x 12.74
		10.0	10.47 x 20.93	8.80 x 17.60
	.256	10.0	10.47 x 20.93	12.44 x 24.88
2.0	.064	8.0	11.13 x 22.27	9.36 x 18.72
4.0	.064	8.0	13.24 x 26.48	11.13 x 22.26
6.0	.064	6.5	12.54 x 25.08	10.54 x 21.08
		10.0	17.32 x 34.64	14.56 x 29.12
	.128	10.0	17.32 x 34.64	17.31 x 34.63
	.256	10.0	17.32 x 34.64	20.59 x 41.18
16.0	.064	8.0	18.72 x 37.45	15.74 x 31.48

TABLE 4.13: STIFFNESS AND POSITION OF THE NEUTRAL AXIS OF AN INTERIOR PANEL WHERE $L_1/L_2 = 1.0$, $L_1 = 240$ in.

α	β	d_s (in.)	ξ (in.)	γ	$(K_{11})_S$ $\left(\frac{\text{K-in.}}{\text{rad}}\right)$	$(K_{11})_B$ $\left(\frac{\text{K-in.}}{\text{rad}}\right)$	$(K_{11})^r_B$ $\left(\frac{\text{K-in.}}{\text{rad}}\right)$	$\frac{(K_{11})_S}{(K_{11})_B}$	$\frac{(K_{11})_S}{(K_{11})^r_B}$
0.4	.064	8.0	2.560	.527	1202269.89	482435.76	596173.84	2.492	2.017
0.8	.064	6.5	3.014	.523	1074188.85	517534.84	680762.71	2.076	1.578
		10.0	3.261	.438	3543510.77	1884514.67	2249252.66	1.880	1.575
	.192	10.0	3.292	.442	3864816.45	2111025.73	2482744.80	1.831	1.557
2.0	.064	8.0	3.842	.416	3873881.90	2412178.77	2984835.54	1.606	1.298
6.0	.064	6.5	4.186	.359	5562910.96	3881511.30	4744084.08	1.433	1.173
		10.0	4.664	.299	17856505.12	14133860.00	16176762.74	1.263	1.104
	.096	10.0	4.745	.304	18393341.61	14557546.50	16671865.50	1.263	1.103
	.192	10.0	4.867	.312	19884273.53	15832692.99	18057377.43	1.256	1.101
16.0	.064	8.0	4.766	.261	22972715.31	19297430.19	21790292.47	1.190	1.054

TABLE 4.14: STIFFNESS AND POSITION OF THE NEUTRAL AXIS AT AN INTERIOR PANEL WHERE $L_1/L_2 = 0.5$, $L_1 = 120$ in.

α	β	d_s (in.)	ξ (in.)	γ	$(K_{11})_S \left(\frac{\text{K-in.}}{\text{rad}}\right)$	$(K_{11})_B \left(\frac{\text{K-in.}}{\text{rad}}\right)$	$(K_{11})_B^r \left(\frac{\text{K-in.}}{\text{rad}}\right)$	$\frac{(K_{11})_S}{(K_{11})_B}$	$\frac{(K_{11})_S}{(K_{11})_B^r}$
0.40	.064	8.0	1.957	.403	1771134.06	964778.51	1097699.94	1.836	1.613
0.80	.032	10.0	2.225	.299	5118296.63	3655319.69	3994913.06	1.400	1.281
	.064	6.5	2.283	.396	1663755.10	1034969.91	1222377.53	1.608	1.361
		10.0	2.228	.299	5389644.34	3768666.04	4109016.21	1.430	1.321
	.128	10.0	2.243	.301	5857921.96	3995358.75	4340454.99	1.466	1.350
2.0	.064	8.0	2.653	.287	6041985.76	4823892.54	5370000.15	1.253	1.125
4.0	.064	8.0	2.873	.245	10676688.52	9647785.07	10553909.39	1.107	1.012

TABLE 4.15: STIFFNESS AND POSITION OF THE NEUTRAL AXIS OF AN INTERIOR PANEL WHERE $L_1/L_2 = 2.0$, $L_1 = 240$ in.

α	β	d_s (in.)	ξ (in.)	γ	$(K_{11})_S \left(\frac{\text{K-in.}}{\text{rad}}\right)$	$(K_{11})_B \left(\frac{\text{K-in.}}{\text{rad}}\right)$	$(K_{11})_B^r \left(\frac{\text{K-in.}}{\text{rad}}\right)$	$\frac{(K_{11})_S}{(K_{11})_B}$	$\frac{(K_{11})_S}{(K_{11})_B^r}$
0.4	.064	8.0	1.849	.537	846639.69	241194.63	283138.84	3.510	2.990
0.8	.064	6.5	2.332	.539	703237.35	258742.48	327838.11	2.718	2.145
		10.0	2.418	.442	2329245.90	942166.51	1083972.16	2.472	2.149
	.256	10.0	2.367	.433	2514745.84	1112186.04	1248008.88	2.261	2.015
2.0	.064	8.0	3.116	.437	2328098.99	1205973.13	1472332.78	1.930	1.581
4.0	.064	8.0	3.581	.388	3955797.91	2411946.27	2909626.43	1.640	1.360
6.0	.064	6.5	3.637	.392	3116128.77	1940568.59	2400850.44	1.606	1.298
		10.0	3.949	.321	10056113.11	7066248.83	8101962.46	1.423	1.241
	.128	10.0	3.963	.322	10490097.35	7491297.66	8534425.29	1.400	1.229
	.256	10.0	3.896	.316	11385501.70	8341395.33	9349374.89	1.365	1.218
16.0	.064	8.0	4.244	.288	12519248.34	9647785.07	11045659.46	1.298	1.133

TABLE 4.16: CARRYOVER FACTORS FOR AN INTERIOR PANEL WHERE $L_1/L_2 = 1.0$, $L_1 = 240$ in.

α	β	d_s (in.)	CF_{13}	CF_{15}	CF_{17}	CF_{18}
0.4	.064	8.0	.141	-.028	.012	-.010
0.8	.064	6.5	.164	-.024	.009	-.008
		10.0	.157	-.025	.009	-.008
	.192	10.0	.157	-.037	.012	-.008
2.0	.064	8.0	.157	-.019	.005	-.004
6.0	.064	6.5	.177	-.016	.003	-.001
		10.0	.163	-.017	.004	-.002
	.096	10.0	.162	-.024	.005	-.001
	.192	10.0	.154	-.049	.006	-.001
16.0	.064	8.0	.160	-.016	.003	-

TABLE 4.17: CARRYOVER FACTORS FOR AN INTERIOR PANEL WHERE $L_1/L_2 = 0.5$, $L_1 = 120$ in.

α	β	d_s (in.)	CF_{13}	CF_{15}	CF_{17}	CF_{18}
0.4	.064	8.0	.159	-.003	.001	-.006
0.8	.032	10.0	.159	-.002	-	-.004
	.064	6.5	.170	-.004	.001	-.006
		10.0	.162	-.004	.001	-.004
	.128	10.0	.163	-.008	.003	-.009
2.0	.064	8.0	.160	-.006	.002	-.005
4.0	.064	8.0	.147	-.009	.003	-.005

TABLE 4.18: CARRYOVER FACTORS FOR AN INTERIOR PANEL WHERE $L_1/L_2 = 2.0$, $L_1 = 240$ in.

α	β	d_s (in.)	CF_{13}	CF_{15}	CF_{17}	CF_{18}
0.4	.064	8.0	.085	-.124	.034	-.005
0.8	.064	6.5	.106	-.116	.032	-.005
		10.0	.102	-.116	.033	-.005
	.256	10.0	.100	-.132	.033	-.006
2.0	.064	8.0	.131	-.089	.025	-.005
4.0	.064	8.0	.146	-.066	.018	-.004
6.0	.064	6.5	.158	-.054	.014	-.003
		10.0	.145	-.056	.016	-.004
	.128	10.0	.142	-.069	.016	-.003
	.256	10.0	.134	-.098	.016	-.002
16.0	.064	8.0	.156	-.034	.009	-.002

TABLE 5.1: PHYSICAL PROPERTIES OF FLOORS ANALYZED
WHERE L_1/L_2 = 1.0, L_1 = 240 in., H = 180 in.

C (in.)	α_{AB}	β_{AC}	d_s (in.)	D_{AB} (in.)	D_{AC} (in.)
15	0.8	.064	6.5	15.15	15.15
			9.0	19.34	19.34
		.160	6.5	15.15	19.05
15	3.0	.064	6.5	21.09	21.09
21	3.0	.064	6.5	21.09	21.09
15	8.0	.064	6.5	26.95	26.95
			9.0	34.40	34.40
		.160	6.5	26.95	33.87
20	8.0	.064	6.5	26.95	26.95
			9.0	34.40	34.40
		.160	6.5	26.95	33.87
27	8.0	.064	6.5	26.95	26.95

TABLE 5.2a: PHYSICAL PROPERTIES OF STRUCTURES ANALYZED WITH $L_1/L_2 = 0.5$, $L_1 = 120$ in., H = 144 in.

C (in.)	α_{AB}	β_{AC}	d_s (in.)	D_{AB} (in.)	D_{AC} (in.)
15	0.4	.064	6.5	12.74	15.15
	3.0	.064	6.5	21.09	25.07
	8.0	.064	6.5	26.95	32.03
25	0.4	.064	6.5	12.74	15.15
	3.0	.064	6.5	21.09	25.07
	8.0	.064	6.5	26.95	32.03

TABLE 5.2b: PHYSICAL PROPERTIES OF STRUCTURES ANALYZED WHERE $L_1/L_2 = 0.75$, $L_1 = 180$ in., H = 144 in.

C (in.)	α_{AB}	β_{AC}	d_s (in.)	D_{AB} (in.)	D_{AC} (in.)
25	0.8	.064	8.0	17.71	19.02
25	3.0	.064	8.0	24.64	26.47
25	8.0	.064	8.0	31.49	33.82

TABLE 5.3: PHYSICAL PROPERTIES OF STRUCTURES ANALYZED WITH $L_1/L_2 = 2.0$, $L_1 = 240$ in., H = 144 in.

C (in.)	α_{AB}	β_{AC}	d_s (in.)	D_{AB} (in.)	D_{AC} (in.)
15	0.8	.064	6.5	12.74	10.72
	3.0	.064	6.5	17.73	14.91
	8.0	.064	6.5	22.66	19.05
20	0.8	.064	6.5	12.74	10.72
	3.0	.064	6.5	17.73	14.91
	8.0	.064	6.5	22.66	19.05

TABLE 5.4: STRUCTURAL PROPERTIES OF COLUMNS

C (in.)	A $(in.)^2$	A_{SH} $(in.)^2$	I_C $(in.)^4$
15	225.0	187.5	4218.8
20	400.0	333.3	13333.3
21	441.0	367.5	16206.8
25	625.0	520.8	32552.1
27	729.0	607.5	44286.8

TABLE 5.5a: MEMBER STRUCTURAL PROPERTIES FOR EQUIVALENT FRAME METHOD
WHERE $L_1/L_2 = 1.0$, $L_1 = 240$ in., H = 180 in.

C (in.)	α_{AB}	β_{AC}	d_s (in.)	I_B (in.)^4	I_{BT} (in.)^4	K_c $\left(\frac{K\text{-in.}}{rad}\right)$	K_{ta} $\left(\frac{K\text{-in.}}{rad}\right)$	K_{ec} $\left(\frac{K\text{-in.}}{rad}\right)$
15	0.8	.064	6.5	6721.81	7647.93	442277.14	710951.95	272658.57
			9.0	17065.00	19416.18	489924.60	1814806.85	385779.66
		.160	6.5	6721.81	7647.93	442277.14	1675715.84	349921.28
15	3.0	.064	6.5	19974.79	22726.87	511612.73	7258913.47	477928.06
21	3.0	.064	6.5	19974.79	23989.23	1965411.46	7872031.60	1572744.16
15	8.0	.064	6.5	49976.71	56862.39	593541.23	45505497.85	585899.18
			9.0	125075.21	142307.80	722010.76	116011699.63	717545.06
		.160	6.5	49976.71	56862.39	593541.23	108815051.38	590321.27
20	8.0	.064	6.5	49976.71	59476.41	1875883.40	48679194.35	1806277.37
			9.0	125075.21	148849.84	2281910.60	124102720.33	2240710.06
		.160	6.5	49976.21	59476.41	1875883.40	116404155.21	1846132.50
27	8.0	.064	6.5	49976.71	63449.90	6230758.45	53638004.71	5582300.91

TABLE 5.5b: MEMBER STRUCTURAL PROPERTIES FOR EQUIVALENT FRAME METHOD
WHERE $L_1/L_2 = 0.5$, $L_1 = 120$ in., H = 144 in.

C (in.)	α_{AB}	β_{AC}	d_s (in.)	I_B $(in.)^4$	I_{BT} $(in.)^4$	K_c $\frac{K\text{-in.}}{rad}$	K_{ta} $\frac{K\text{-in.}}{rad}$	K_{ec} $\frac{K\text{-in.}}{rad}$
15	0.4	.064	6.5	4486.06	5104.14	563305.12	474481.02	257545.92
	3.0	.064	6.5	19974.79	22726.87	730786.69	13843170.71	694142.62
	8.0	.064	6.5	49976.71	56862.39	885446.46	88044966.55	876630.40
25	0.4	.064	6.5	4486.06	5589.98	4346490.09	543814.80	483341.16
	3.0	.064	6.5	19974.79	24890.16	5638786.20	15866010.93	4160236.57
	8.0	.064	6.5	49976.71	62274.93	6832148.59	100910581.17	6398910.50

TABLE 5.5c: MEMBER STRUCTURAL PROPERTIES FOR EQUIVALENT FRAME METHOD
WHERE $L_1/L_2 = 0.75$, $L_1 = 180$ in., H = 144 in.

C (in.)	α_{AB}	β_{AC}	d_s (in.)	I_B $(in.)^4$	I_{BT} $(in.)^4$	K_c $\left(\frac{K\text{-in.}}{rad}\right)$	K_{ta} $\left(\frac{K\text{-in.}}{rad}\right)$	K_{ec} $\left(\frac{K\text{-in.}}{rad}\right)$
15	0.8	.064	8.0	12184.75	15183.16	5065443.43	1960383.77	1413387.04
	3.0	.064	8.0	35981.32	44835.57	6329080.20	19837263.01	4798210.72
	8.0	.064	8.0	89781.87	111875.30	7972783.59	124211334.14	7491457.70

TABLE 5.5d: MEMBER STRUCTURAL PROPERTIES FOR EQUIVALENT FRAME METHOD WHERE $L_1/L_2 = 2.0$, $L_1 = 240$ in., H = 144 in.

C (in.)	α_{AB}	β_{AC}	d_s (in.)	I_B (in.)^4	I_{BT} (in.)^4	K_c $\left(\frac{K\text{-in.}}{rad}\right)$	K_{ta} $\left(\frac{K\text{-in.}}{rad}\right)$	K_{ec} $\left(\frac{K\text{-in.}}{rad}\right)$
15	0.8	.064	6.5	3046.81	3979.51	563305.12	319400.70	203827.87
	3.0	.064	6.5	8845.61	11553.45	656996.34	4325095.73	570357.20
	8.0	.064	6.5	21935.10	28649.93	768840.51	26939787.49	747507.23
20	0.8	.064	6.5	3046.81	4387.41	1780322.34	369746.24	306161.16
	3.0	.064	6.5	8845.61	12737.68	2076432.89	5006838.94	1467734.87
	8.0	.064	6.5	21935.10	31586.55	2429915.68	31186171.50	2254270.90

TABLE 5.6a: MEMBER STRUCTURAL PROPERTIES FOR ACI-71, 8.7 METHOD WHERE L_1/L_2 = 1.0, L_1 = 240 in., H = 180 in.

α_{AB}	β_{AC}	d_s (in.)	b_f (in.)	λ (in.)	I_B $(in.)^4$
0.8	.064	6.5	20.0	5.28	3795.67
		9.0	20.0	7.14	9499.48
	.160	6.5	20.0	5.28	3795.67
3.0	.064	6.5	20.0	7.85	13060.00
8.0	.064	6.5	20.0	10.78	32432.90
		9.0	20.0	14.24	81787.41
	.160	6.5	20.0	10.78	32432.90

TABLE 5.6b: MEMBER STRUCTURAL PROPERTIES FOR ACI-71, 8.7 METHOD WHERE L_1/L_2 = 0.5, L_1 = 120 in., H = 144 in.

α_{AB}	β_{AC}	d_s (in.)	b_f (in.)	λ (in.)	I_B $(in.)^4$
0.4	.064	6.5	10.0	4.98	1678.81
3.0	.064	6.5	10.0	8.89	11142.84
8.0	.064	6.5	10.0	11.92	27961.07

TABLE 5.6c: MEMBER STRUCTURAL PROPERTIES FOR ACI-71, 8.7 METHOD WHERE L_1/L_2 = 0.75, L_1 = 130 in., H - 144 in.

α_{AB}	β_{AC}	d_s (in.)	b_f (in.)	λ (in.)	I_B $(in.)^4$
0.8	.064	8.0	15.0	6.75	6337.24
3.0	.064	8.0	15.0	9.96	21955.27
8.0	.064	8.0	15.0	13.46	54925.98

TABLE 5.6d: MEMBER STRUCTURAL PROPERTIES FOR ACI-71, 8.7 METHOD WHERE L_1/L_2 = 2.0, L_1 = 240 in., H = 144 in.

α_{AB}	β_{AC}	d_s (in.)	b_f (in.)	λ (in.)	I_B $(in.)^4$
0.8	.064	6.5	20.0	4.45	2042.83
3.0	.064	6.5	20.0	6.32	6821.27
8.0	.064	6.5	20.0	8.61	17077.72

TABLE 5.7a: MEMBER STRUCTURAL PROPERTIES FOR STIFFNESS MATRIX METHOD
WHERE $L_1/L_2 = 1.0$, $L_1 = 240$ in., H = 180 in.

α_{AB}	β_{AC}	d_s (in.)	γ	λ (in.)	$(K_{11})^r_B$ $\left(\frac{K\text{-in.}}{rad}\right)$	$\frac{K_{em}}{(K_{11})^r_B}$	$(K_{em})_{AB}$ $\left(\frac{K\text{-in.}}{rad}\right)$	$(S_{22})_{AB}$	$(k_{23})_{AB}$
0.8	.064	6.5	0.48	5.50	156772.16	1.48	232022.79	0.97	.336
		9.0		7.19	407212.23		602674.10	0.97	
	.160	6.5		5.50	168434.35		249282.84	0.95	
3.0	.064	6.5	0.36	7.92	570002.49	1.16	661202.89	0.97	.340
8.0	.064	6.5	0.30	10.41	1482853.97	1.09	1616310.83	0.97	.340
		9.0		13.39	4007766.81		4368465.82	0.97	
	.160	6.5		10.41	1599446.98		1743397.21	0.90	

TABLE 5.7b: MEMBER STRUCTURAL PROPERTIES FOR STIFFNESS MATRIX METHOD WHERE $L_1/L_2 = 0.5$, $L_1 = 120$ in., H = 144 in.

α_{AB}	β_{AC}	d (in	γ	λ (in)	$(K_{11})_B^r$ $\frac{K\text{-in}}{rad}$	$K_{em}/(K_{11})_B^r$	$(K_{em})_{AB}$ $\frac{K\text{-in}}{rad}$	$(S_{22})_{AB}$	$(k_{23})_{AB}$
0.4	.064	6.5	0.42	5.06	144822.14	1.51	218681.43	.99	.34
3.0	.064	6.5	0.25	8.72	1052101.93	1.06	1115228.04	.99	.34
8.0	.064	6.5	0.20	11.43	2755434.33	1.00	2755434.33	.99	.33

TABLE 5.7c: MEMBER STRUCTURAL PROPERTIES FOR STIFFNESS MATRIX METHOD WHERE $L_1/L_2 = 0.75$, $L_1 = 180$ in., H = 144 in.

α_{AB}	β_{AC}	ds (in	γ	X (in)	$(K_{11})_B^r$ $\frac{K\text{-in}}{rad}$	$K_{em}/(K_{11})_B^r$	$(K_{em})_{AB}$ $\frac{K\text{-in}}{rad}$	$(S_{22})_{AB}$	$(k_{23})_{AB}$
0.8	.064	8.0	0.43	6.77	371978.42	1.39	517050.01	.98	.34
3.0	.064	8.0	0.31	10.37	1355014.55	1.11	1504066.15	.98	.34
8.0	.064	8.0	0.25	12.81	3531260.88	1.05	3707823.93	.98	.33

TABLE 5.7d: MEMBER STRUCTURAL PROPERTIES FOR STIFFNESS MATRIX METHOD
WHERE $L_1/L_2 = 2.0$, $L_1 = 240$ in., $H = 144$ in.

α_{AB}	β_{AC}	d_s (in.)	γ	λ (in.)	$(K_{11})^r_B$ $\frac{K\text{-in.}}{rad}$	$K_{em}/(K_{11})^r_B$	$(K_{em})_{AB}$ $\left(\frac{K\text{-in.}}{rad}\right)$	$(S_{22})_{AB}$	$(k_{23})_{AB}$
0.8	.064	6.5	.48	4.87	74774.65	1.86	139080.85	0.85	0.29
3.0	.064	6.5	.36	6.84	278159.29	1.34	372733.45	0.90	0.34
8.0	.064	6.5	.29	8.99	724932.78	1.21	877168.67	0.92	0.36

TABLE 5.8a: COMPARATIVE LISTING OF LATERAL STIFFNESS OF SINGLE-PANEL, SINGLE-STORY STRUCTURES BASED ON FOUR DIFFERENT MODELS, WHERE $L_1/L_2 = 1.0$, $L_1 = 240$ in., H = 180 in.

c (in.)	α_{AB}	β_{AC}	d_s (in.)	$\frac{P}{\Delta_T}\frac{K}{in.}$ [Finite El.]	Equivalent Frame		ACI-71, 8.7		SMM	
					$P/\Delta_T \frac{K}{in.}$	Diff. %	$P/\Delta_T \frac{K}{in.}$	Diff. %	$P/\Delta_T \frac{K}{in.}$	Diff. %
15	0.8	.064	6.5	79.16	104.12	31.53	79.93	0.98	79.07	-0.11
			9.0	110.36	121.89	10.45	110.86	0.45	111.12	0.69
		.160	6.5	80.83	98.26	21.57	79.93	-1.11	80.66	-0.20
15	3.0	.064	6.5	115.92	123.52	6.56	122.27	5.48	116.20	0.25
21	3.0	.064	6.5	276.81	365.18	31.92	302.41	9.25	279.04	0.81
15	8.0	.064	6.5	149.59	144.95	-3.10	156.33	4.50	151.13	1.03
			9.0	189.34	167.82	-11.36	194.25	2.60	192.01	1.41
		.160	6.5	150.31	144.85	-3.63	156.33	4.01	151.60	0.86
20	8.0	.064	6.5	349.55	393.32	12.52	382.36	9.39	357.27	2.21
			9.0	488.78	485.02	-0.77	520.49	6.49	505.77	3.48
		.160	6.5	352.96	390.59	10.66	382.36	8.33	359.49	1.85
27	8.0	.064	6.5	715.81	974.19	36.10	811.09	13.31	741.29	3.56

TABLE 5.8b: COMPARATIVE LISTING OF LATERAL STIFFNESS OF SINGEL-PANEL, SINGLE-STORY STRUCTURES BASED ON FOUR DIFFERENT MODELS, WHERE L_1/L_2 = 0.5, L_1 = 120 in., H = 144 in.

C (in.)	α_{AB}	β_{AC}	d_s (in.)	$\frac{P}{\Delta_{TS}}$ [Fi.El.] $\left(\frac{K}{in.}\right)$	Equivalent Frame $\frac{P}{\Delta_{TS}}$ $\left(\frac{K}{in.}\right)$	Diff. %	ACI-71, 8.7 $\frac{P}{\Delta_{TS}}$ $\left(\frac{K}{in.}\right)$	Diff. %	SMM $\frac{P}{\Delta_{TS}}$ $\left(\frac{K}{in.}\right)$	Diff. %
15	0.4	.064	6.5	141.23	220.37	55.99	136.43	-3.40	140.06	- .83
	3.0	.064	6.5	254.59	270.30	6.17	264.40	3.85	256.83	.88
	8.0	.064	6.5	328.73	317.27	-7.39	340.85	3.69	335.24	1.98
25	0.4	.064	6.5	561.50	1512.82	169.4	556.76	-0.84	564.39	.51
	3.0	.064	6.5	923.89	1436.15	55.45	997.68	7.99	947.73	2.58
	8.0	.064	6.5	1324.15	1821.04	20.87	1474.17	11.33	1404.55	6.07

TABLE 5.8c: COMPARATIVE LISTING OF LATERAL STIFFNESS OF SINGEL-PANEL, SINGLE-STORY STRUCTURES BASED ON FOUR DIFFERENT MODELS, WHERE L_1/L_2 = 0.75, L_1 = 180 in., H = 144 in.

C (in.)	α_{AB}	β_{AC}	d_s (in.)	$\frac{P}{\Delta_{TS}}$ [Fi.El.] $\left(\frac{K}{in.}\right)$	Equivalent Frame $\frac{P}{\Delta_{TS}}$ $\left(\frac{K}{in.}\right)$	Diff. %	ACI-71, 8.7 $\frac{P}{\Delta_{TS}}$ $\left(\frac{K}{in.}\right)$	Diff. %	SMM $\frac{P}{\Delta_{TS}}$ $\left(\frac{K}{in.}\right)$	Diff. %
25	0.8	.064	8.0	697.61	1423.40	104.04	710.68	1.87	710.95	1.91
	3.0	.064	8.0	1060.49	1527.51	44.04	1157.48	9.15	1094.74	3.23
	8.0	.064	8.0	1571.19	1967.25	25.21	1748.41	11.28	1656.03	5.40

TABLE 5.8d: COMPARATIVE LISTING OF LATERAL STIFFNESS OF SINGLE-PANEL, SINGLE-STORY STRUCTURES BASED ON FOUR DIFFERENT MODELS, WHERE $L_1/L_2 = 2.0$, $L_1 = 240$ in., $H = 144$ in.

c (in.)	α_{AB}	β_{AC}	d_s (in.)	$\frac{P}{\Delta_{TS}}$[Fi.El.] $\left(\frac{K}{in.}\right)$	Equivalent Frame		ACI-71, 8.7		SMM	
					$\frac{P}{\Delta_{TS}}\left(\frac{K}{in.}\right)$	Diff. %	$\frac{P}{\Delta_{TS}}\left(\frac{K}{in.}\right)$	Diff. %	$\frac{P}{\Delta_{TS}}\left(\frac{K}{in.}\right)$	Diff. %
15	0.8	.064	6.5	111.86	182.44	63.09	114.24	2.13	112.06	.17
	3.0	.064	6.5	170.74	199.12	16.62	186.04	8.96	174.28	2.07
	8.0	.064	6.5	238.43	249.98	4.84	261.46	9.66	247.59	3.84
20	0.8	.064	6.5	243.81	516.42	111.81	250.12	2.59	247.52	1.52
	3.0	.064	6.5	340.26	474.28	39.39	373.86	9.88	349.64	2.76
	8.0	.064	6.5	487.98	600.08	10.54	555.25	13.79	512.07	4.94

TABLE 5.9: EFFECTIVE SLAB WIDTH, b_f, OF SINGLE-PANEL FLOORS

L_1/L_2	α_{AB}	β_{AC}	d_s (in.)	b_f (in.)	$\frac{b_f}{0.5\ L_2}$
1.0 L_1=240 in	0.8	.064	6.5	25.02	.21
			9.0	29.79	.25
		.160	6.5	29.25	.24
	3.0	.064	6.5	17.62	.15
	8.0	.064	6.5	18.97	.16
			9.0	24.99	.21
		.160	6.5	19.90	.17
0.5 L_1=120 in	0.4	.064	6.5	18.18	.15
	3.0	.064	6.5	12.52	.10
	8.0	.064	6.5	13.49	.11
0.75 L_1=180 in	0.8	.064	8.0	22.20	.19
	3.0	.064	8.0	17.15	.14
	8.0	.064	8.0	18.71	.16
2.0 L_1=240 in	0.8	.064	6.5	22.46	.37
	3.0	.064	6.5	17.11	.29
	8.0	.064	6.5	17.90	.30

TABLE 5.10: STRUCTURAL PROPERTIES OF EQUIVALENT FRAME FOR THE MULTI-PANEL, SINGLE-STORY STRUCTURE

Col.	I_B (in.)^4	I_{BT} (in.)^4	K_c $\frac{\text{K-in.}}{\text{rad}}$	K_{ta} $\frac{\text{K-in.}}{\text{rad}}$	K_{ec} $\frac{\text{K-in.}}{\text{rad}}$
A	70816.67	94737.47	8861595.30	108319729.66	8191455.48
B	70816.67	94737.47	8861595.30	60186257.14	7724298.94
E	82620.97	110529.08	8861595.30	252750681.38	8561426.39
F	82620.97	110529.08	8861595.30	140437181.19	8335617.30

TABLE 5.11: STRUCTURAL PROPERTIES FOR ACI 318-71, 8.7 MODEL OF THE MULTI-PANEL, SINGLE-STORY STRUCTURE

Beam	b_f (in.)	λ (in.)	I (in.)^4	J (in.)^4
AB	16.0	12.56	46490.80	21888.40
AE	20.0	12.12	48885.30	22298.00
EF	48.0	10.93	55290.77	23629.20
BF	60.0	10.11	59870.00	24858.00

TABLE 5.12: STRUCTURAL PROPERTIES OF MEMBERS OF THE MODEL, BASED ON PROVISION OF ACI-71, SECTIONS 8.7 AND 11.7, FOR THE MULTI-PANEL, SINGLE-STORY STRUCTURE

	X-X Direction				Y-Y Direction			
	b_f (in.)	λ (in.)	I $(in.)^4$	J $(in.)^4$	b_f (in.)	λ (in.)	I $(in.)^4$	J $(in.)^4$
Exterior Fr. Beams	24.0	11.71	51058.11	22707.60	20.0	12.12	48885.30	22298.00
Interior Fr. Beams	63.0	9.93	60868.50	25165.20	60.0	10.11	59870.00	24858.00

TABLE 5.13: STRUCTURAL PROPERTIES OF MEMBERS OF THE SMM FOR THE MULTI-PANEL, SINGLE-STORY STRUCTURE

Member	λ (in.)	K_{em} $\frac{K\text{-in.}}{rad}$	S_{11}	S_{22}	k_{23}
AB, CD, MN, QR	12.03	2903798.12	.06	.98	.34
AE, DH, IM, LR	11.75	2531423.80	.02	.93	.35
BC, NQ	12.03	2829421.57	.03	.98	.34
EI, HL	11.75	2448356.87	.01	.95	.35
EF, FG, GH, IJ, JK, KL	11.49	3207014.41	.07	.97	.33
BF, FJ, JN CG, GK, KQ	11.11	2897475.46	.03	.92	.33

TABLE 5.14: LATERAL DISPLACEMENTS OF MULTI-BAY SINGLE-STORY STRUCTURE BASED ON FINITE ELEMENT METHOD

	d_s (in.)	Δ_{CS} (in.)	θ_{YY} (rad)	Δ_T (in.)
Corner Col.	8.0	.0144	.000105	.0148
Ext. Col. (X-X)	8.0	.0141	.000096	.0144
Ext. Col. (Y-Y)	8.0	.0140	.000074	.0143
Int. Col.	8.0	.0139	.000067	.0139
			$\frac{1}{4}\Sigma\Delta_T$	.0144

TABLE 5.15: LATERAL DISPLACEMENTS OF MULTI-BAY SINGLE-STORY STRUCTURE BASED ON THE ACI-71, SECTION 8.7 METHOD

	Δ_{NA} (in.)	X (in.)	M_{TC} (K-in.)	M_{BC} (K-in)	Δ_T (in.)
Corner Col.	.0121	11.43	195.46	382.92	.0130
Ext. Col. (X-X)	.0121	11.43	223.57	398.42	.0130
Ext. Col. (Y-Y)	.0121	11.43	337.58	461.30	.0127
Int. Col.	.0121	11.43	371.01	479.73	.0126
				$\frac{1}{4}\Sigma\Delta_T$	.0128

TABLE 5.16: LATERAL DISPLACEMENTS OF MULTI-PANEL SINGLE-STORY STRUCTURE BASED ON THE ACI-71, SECTIONS 8.7 AND 11.7 METHOD

Column	Δ_{NA} (in.)	λ (in.)	M_{TC} (K-in.)	M_{BC} (K-in.)	Δ_T (in.)
A	.01215	10.97	194.71	382.98	.0131
B	.01215	10.97	222.89	398.58	.0130
E	.01215	10.97	337.35	461.94	.0128
F	.01215	10.97	370.99	480.56	.0127
				$\frac{1}{4}\Sigma\Delta_T$	.0129

TABLE 5.17: LATERAL DISPLACEMENTS OF MULTI-PANEL, SINGLE-STORY STRUCTURE BASED ON THE SMM

Column	Δ_{NA} (in.)	λ (in.)	M_{TC} (k-in.)	M_{BC} (K-in.)	Δ_T (in.)
A	.01303	11.59	188.79	401.26	.0141
B	.01303	11.59	205.06	410.22	.0141
E	.01303	11.59	328.24	478.06	.0138
F	.01303	11.59	348.93	489.45	.0138
				$\frac{1}{4}\Sigma\Delta_T$	.0140

TABLE 5.18: COMPARATIVE LISTING OF THE LATERAL STIFFNESS OF MULTI-PANEL, SINGLE-STORY STRUCTURE

Model	$\frac{P}{\Delta_T}$ $\left(\frac{K}{in.}\right)$	Diff. %
Finite Element	6950.67	-
Equiv. Frame	8335.83	19.93
ACI-71, 8.7	7783.70	11.99
ACI-71, 8.7 + 11.7	7763.79	11.70
SMM	7164.98	3.08

TABLE 5.19: STRUCTURAL PROPERTIES OF COLUMNS AND FLOOR BEAMS OF MULTISTORY BUILDING

Member	A $(in.)^2$	A_{sh} $(in.)^2$	I $(in.)^4$	J $(in.)^4$
Ext. Col.	400.0	333.3	13333.3	32000.0
Int. Col.	676.0	563.3	38081.3	91395.2
Ext. Bm.	338.0	281.7	19040.7	11424.4
Int. Bm.	392.0	326.7	25610.7	15366.4

TABLE 5.20: VALUES OF PARAMETERS NEEDED TO DEFINE THE SMM EQUIVALENT MEMBERS FOR THE MULTISTORY BUILDING

Equivalent Member	L_{em}/L_{cm}	ϕ	d_s (in.)	e (in.)	α	β
d1-d2	1.18	1.0	8.0	9.0	3.38	0.05
			12.0	7.0	1.00	0.05
d1-c1	0.85	1.0	8.0	9.0	2.86	0.08
			12.0	7.0	0.85	0.08
d2-d3	1.18	0.5	8.0	9.0	3.38	0.08
			12.0	7.0	1.00	0.08
c1-b1	0.85	0.5	8.0	9.0	2.86	0.11
			12.0	7.0	0.85	0.11
c2-c3	1.18	-	8.0	10.0	2.27	0.05
			12.0	8.0	0.67	0.05
c2-b2	0.85	-	8.0	10.0	1.92	0.08
			12.0	8.0	0.57	0.08

TABLE 5.21: MULTISTORY BUILDING EQUIVALENT MEMBER PROPERTIES FOR SMM

Equiv. Member	d_s (in.)	γ	$\frac{K_{em}}{(K_{11})^r_B}$	k_{23}	S	ξ (in.)	$(K_{11})^r_B$ $\left(\frac{K\text{-in.}}{rad}\right)$	K_{em} $\left(\frac{K\text{-in.}}{rad}\right)$	S_{11}	S_{22}
d1-d2	8.0	0.36	1.18	0.34	.022	3.24	1023058.8	1207209.4	0.02	0.96
	12.0	0.47	1.45	0.34	.022	3.29	1027757.0	1490247.7	0.02	0.93
d1-c1	8.0	0.34	1.13	0.34	.048	3.06	1169172.0	1321164.4	0.04	0.98
	12.0	0.45	1.40	0.33	.069	3.15	1178676.5	1650147.1	0.06	0.98
d2-d3	8.0	0.36	1.18	0.34	.034	3.24	1002948.4	1183479.2	0.03	0.93
	12.0	0.47	1.45	0.34	.034	3.29	1007646.7	1461087.6	0.03	0.93
c1-b1	8.0	0.34	1.13	0.34	.065	3.06	1152155.6	1301935.8	0.05	0.97
	12.0	0.45	1.40	0.33	.079	3.15	1161660.0	1626324.1	0.06	0.97
c2-c3	8.0	0.41	1.31	0.34	.038	4.10	1453420.1	1903980.3	0.04	0.91
	12.0	0.49	1.77	0.29	.038	3.92	1429329.2	2529912.6	0.04	0.92
c2-b2	8.0	0.37	1.26	0.32	.086	3.70	1628418.6	2051807.5	0.08	0.96
	12.0	0.46	1.65	0.31	.086	3.68	1625507.6	2682087.5	0.08	0.96

TABLE 5.22: EQUIVALENT MEMBER PROPERTIES FOR THE MULTISTORY BUILDING USING THE EFFECTIVE SLAB WIDTH (ACI-71, 8.7) METHOD

Equiv. Member	d_s (in.)	b_f (in.)	λ (in.)	A $(in.)^2$	I $(in.)^4$	J $(in.)^4$
d1-d2	8.0	26.0	9.58	546.0	30602.9	14086.8
	12.0	26.0	9.64	650.0	30734.4	20410.0
d1-c1	8.0	22.0	9.92	514.0	29353.9	13677.2
	12.0	22.0	9.64	602.0	29471.7	19027.6
c2-c3	8.0	78.0	8.34	904.0	50543.1	21920.0
	12.0	78.0	8.70	1160.0	51436.7	37484.8
c2-b2	8.0	66.0	8.85	808.0	48011.5	20691.2
	12.0	66.0	9.09	1016.0	48507.1	33337.6

TABLE 5.23a: EQUIVALENT BEAM PROPERTIES FOR MULTISTORY BUILDING USING THE EQUIVALENT FRAME METHOD

Equiv. Member	d_s (in.)	A $(in.)^2$	I $(in.)^4$	J $(in.)^4$
Ext. Frame Beam	8.0	1342.0	44877.8	24275.6
	12.0	1844.0	50638.9	54797.2
Int. Frame Beam	8.0	2392.0	69053.3	28166.4
	12.0	3392.0	83799.4	101766.4

TABLE 5.23b: EQUIVALENT COLUMN PROPERTIES FOR THE MULTISTORY BUILDING USING THE EQUIVALENT FRAME METHOD

Story	Col.	Col. End	8 in. Slab		12 in. Slab	
			K_c $\left(\frac{K\text{-in.}}{rad}\right)$	K_{ec} $\left(\frac{K\text{-in.}}{rad}\right)$	K_c $\left(\frac{K\text{-in.}}{rad}\right)$	K_{ec} $\left(\frac{K\text{-in.}}{rad}\right)$
1st.	Cor	Top	1498543.8	1268720.0	1452692.1	969011.1
	d2	Top	1498543.8	1138352.8	1452692.1	799359.5
	c1	Top	1570481.4	1480480.9	1522524.3	1317360.4
	Int.	Top	4485451.9	3685528.5	4348481.7	2885067.5
2nd thru 11th	Cor.	Top	2496794.7	2016110.1	2393318.5	1453895.2
		Bott.	1658637.4	1404260.8	1741418.3	1161604.5
	d2	Top	2496794.7	1762701.1	2393318.5	1162928.0
		Bott.	1658637.4	1259966.1	1741418.3	958234.3
	c1	Top	2670385.6	2469610.3	2560102.9	2125043.6
		Bott.	1690094.5	1593239.3	1775870.0	1536567.0
	Int.	Top	7626888.3	5911120.8	7311909.8	4386796.1
		Bott.	4827078.9	3966230.7	5072062.2	3365138.1
12th	Cor.	Top	2496794.7	2183933.3	2393318.5	1741851.9
		Bott.	1658637.4	1339315.4	1741418.3	1057878.3
	d2	Top	2496794.7	1997068.3	2393318.5	1484310.8
		Bott.	1658637.4	1170974.1	1741418.3	846165.8
	c1	Top	2670385.6	2543738.9	2560102.9	2284013.3
		Bott.	1690094.5	1563023.3	1775870.0	1474081.9
	Int.	Top	7626888.3	6475770.6	7311909.8	5246399.0
		Bott.	4827078.9	3741164.8	5072062.2	3042994.7

TABLE 5.24: NATURAL PERIODS OF VIBRATION FOR FRAMED STRUCTURES OF FIG. 5.11

d_s (in.)	Method	1st Mode		2nd Mode		3rd Mode		4th Mode	
		T_1 (sec)	Diff. %	T_2	Diff. %	T_3	Diff. %	T_4	Diff. %
8.0	Bare Beams	2.19	-	0.71	-	0.41	-	0.28	-
	SMM	1.95	-	0.64	-	0.37	-	0.25	-
	Eff. Slab Width	1.79	8.12	0.59	7.84	0.34	7.59	0.24	7.09
	Equiv. Fr.	1.61	17.21	0.53	16.77	0.31	16.26	0.22	15.35
12.0	Bare Beams	2.43	-	0.79	-	0.46	-	0.31	-
	SMM	2.00	-	0.66	-	0.38	-	0.26	-
	Eff. Slab Width	1.97	1.45	0.65	1.37	0.38	0.0	0.26	0.0
	Equiv. Fr.	1.71	14.88	0.56	14.44	0.33	14.14	0.23	13.26

TABLE 5.25: FIRST MODE SHAPE - LONGITUDINAL DIRECTION - OF MULTISTORY BUILDING

Level	8 in. Slab				12 in. Slab			
	Bare Beams	SMM	Eff. Slab Width	Equiv. Frame	Bare Beams	SMM	Eff. Slab Width	Equiv. Frame
1	.007	.008	.009	.010	.007	.009	.009	.010
2	.015	.015	.016	.017	.015	.016	.016	.017
3	.021	.022	.023	.023	.021	.022	.023	.023
4	.028	.029	.029	.029	.028	.029	.029	.029
5	.034	.035	.035	.035	.034	.035	.035	.035
6	.040	.040	.040	.040	.040	.040	.040	.040
7	.045	.045	.045	.045	.045	.045	.045	.045
8	.049	.049	.049	.049	.049	.049	.049	.049
9	.053	.053	.053	.052	.053	.053	.053	.052
10	.056	.056	.055	.055	.056	.055	.055	.055
11	.058	.057	.057	.057	.058	.057	.057	.057
12	.059	.059	.058	.058	.059	.058	.058	.058

TABLE 5.26: STIFFNESS PARTICIPATION IN THE FIRST MODE SHAPE (K_1^*)

Method	Slab Thickness, d_s		% Increase in K_1^* due to increase in d_s
	8.0 in.	12.0 in.	
Bare Beams	1.00	1.00	-
SMM	1.26	1.47	16.7
Eff. Slab Width	1.50	1.51	0.7
Equiv. Fr.	1.84	2.01	9.2

TABLE 5.27: MAXIMUM (SRSS) LATERAL ROOF DISPLACEMENT OF THE BUILDING OF FIG. 5.11

Method	8 in Slab		12 in Slab	
	Δ_Y (in.)	Diff. %	Δ_Y (in.)	Diff. %
SMM	8.40	-	9.02	-
Eff. Slab Width	7.30	-13.10	8.71	-3.44
Equiv. Fr.	6.37	-24.17	6.88	-23.73

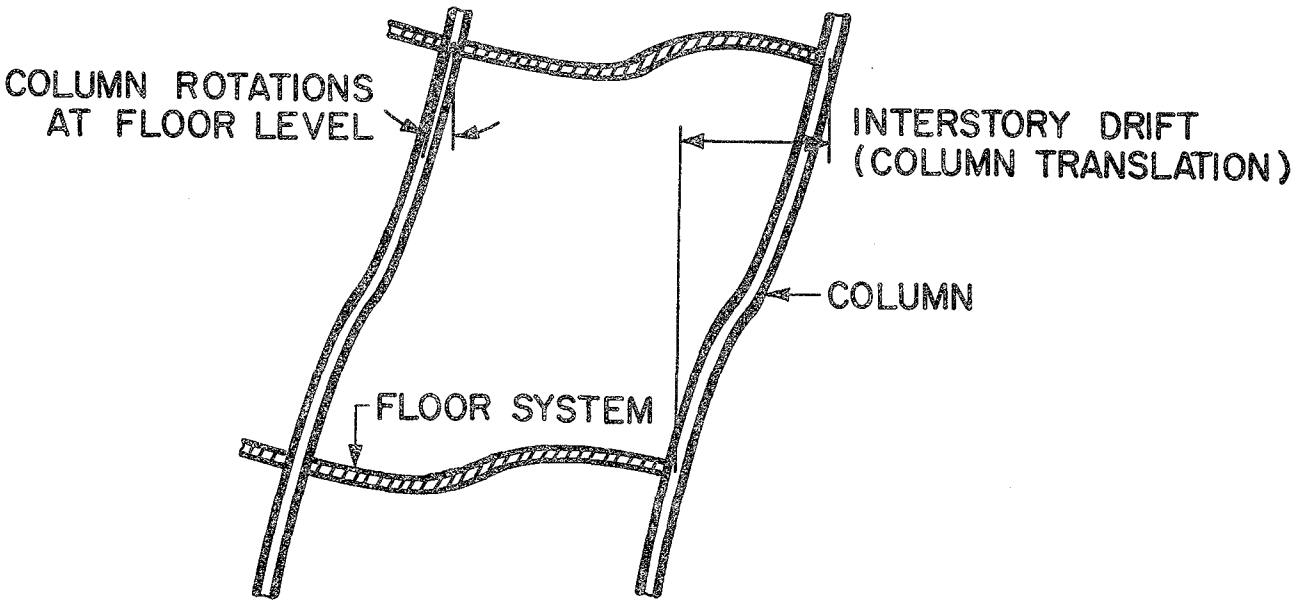

Fig. 1.1 Deformations of Moment-Resisting Frame Subjected to Lateral Loads

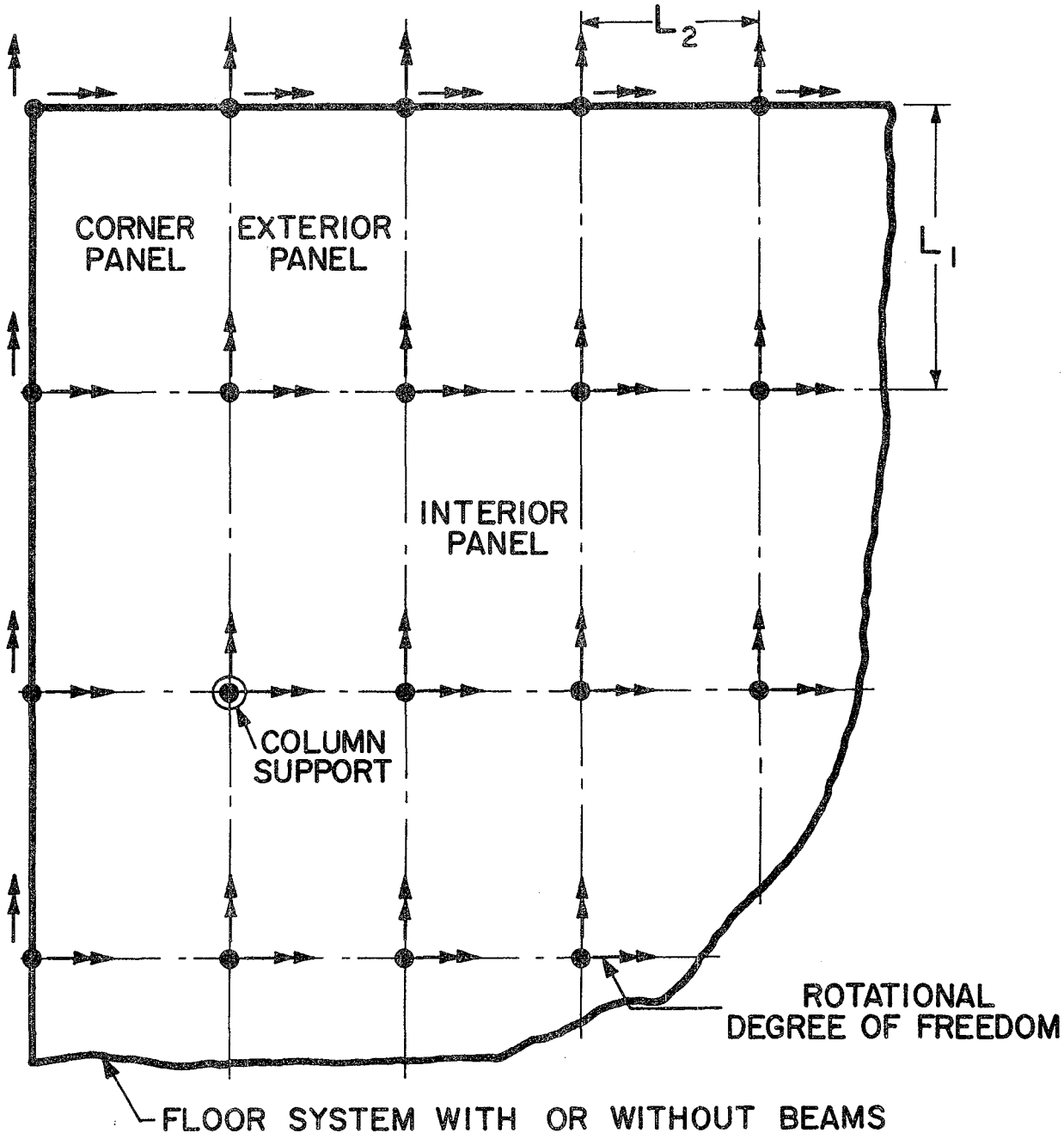

Fig. 1.2 Degrees of Freedom in Floor System

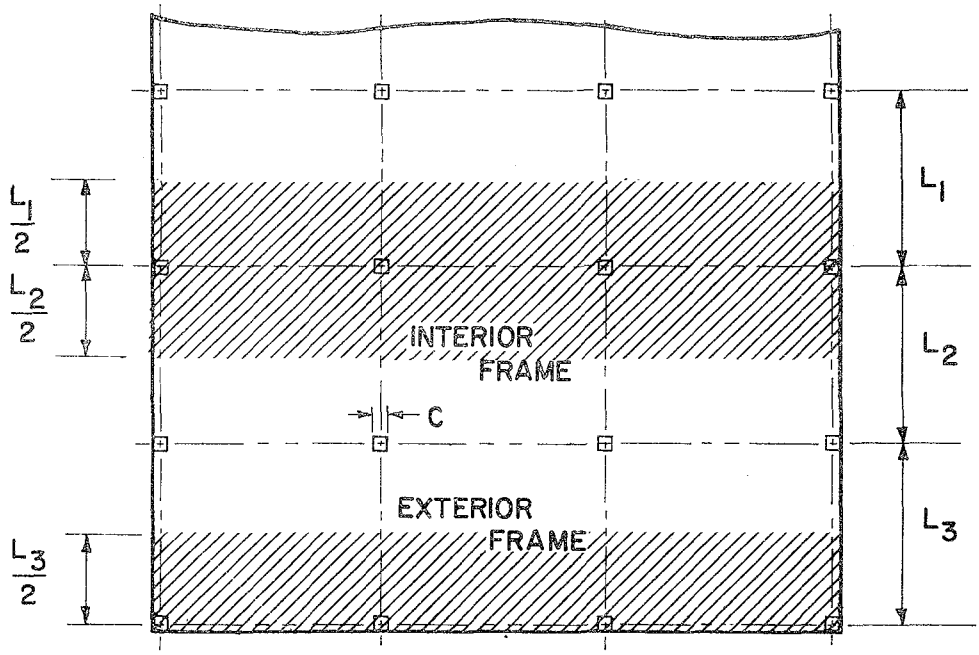

(a) Area to be considered as equivalent frame

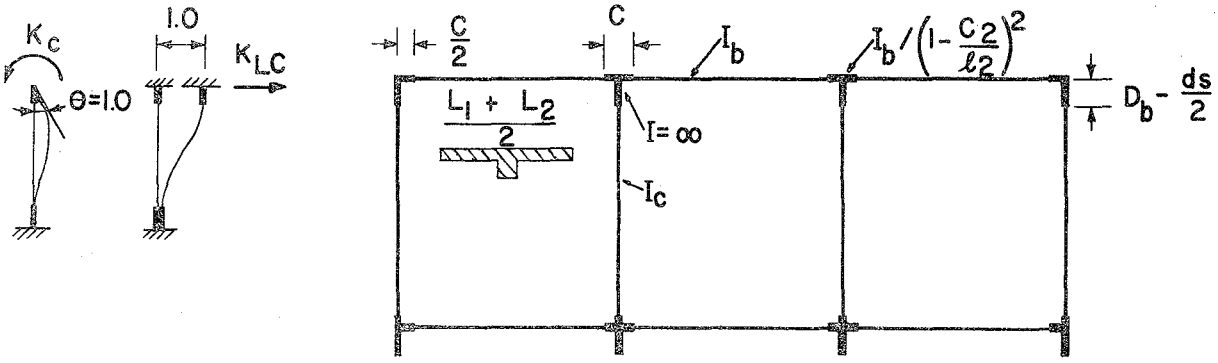

(b) Equivalent interior frame

Fig. 1.3 Illustration of Equivalent Frame as Defined in ACI 318-71 Code, Section 13.4

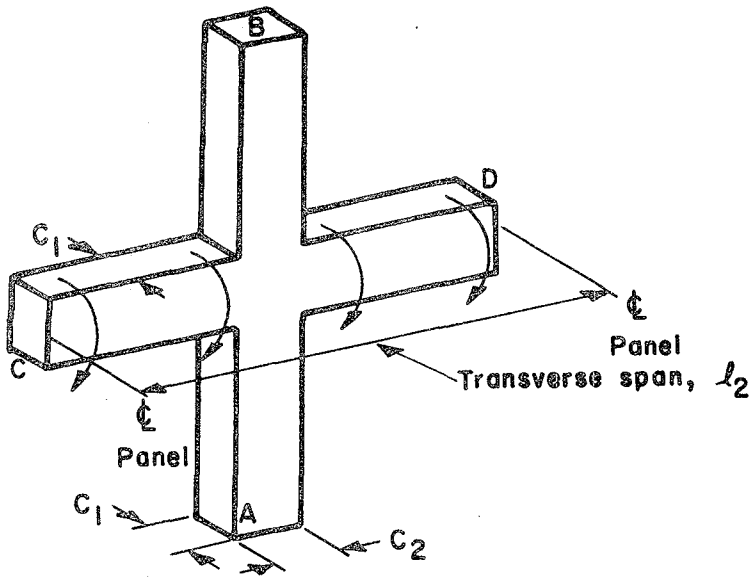

Fig. 1.4 Simplified Physical Model

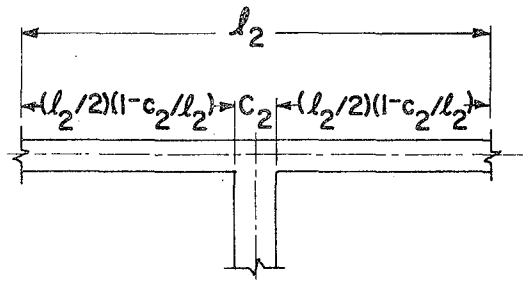

(a) Beam-column combination

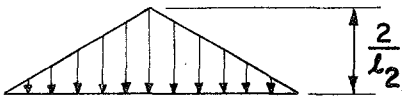

(b) Distribution of unit twisting moment along column centerline

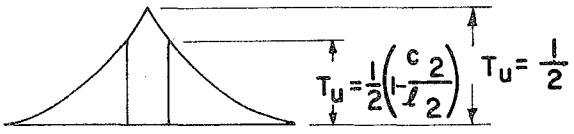

(c) Twisting moment diagram

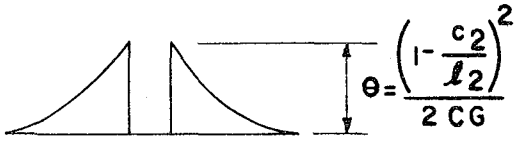

Where G = modulus of elasticity or rigidity

(d) Unit rotation diagram

Fig. 1.5 Assumed Distribution of Unit Twisting Moment Applied Along Column Centerline, Twisting Moment Diagram, and Unit Rotation Diagram [10]

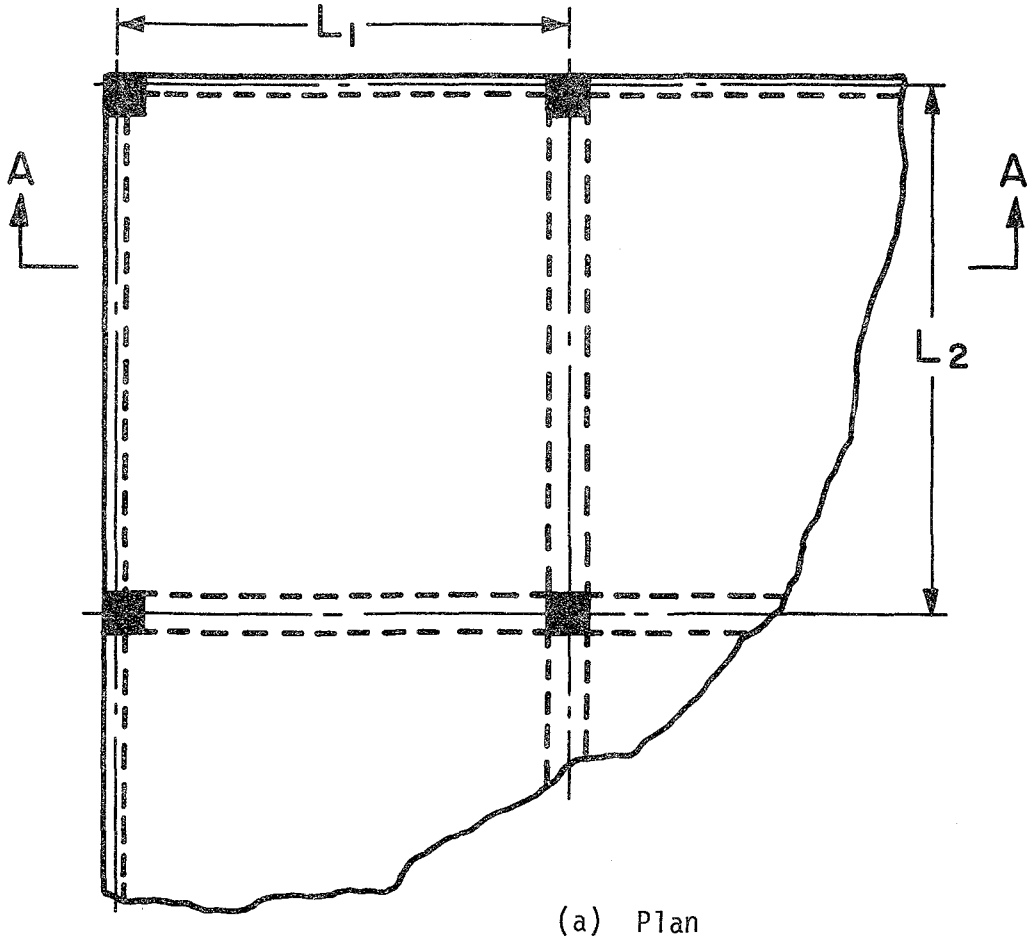

(a) Plan

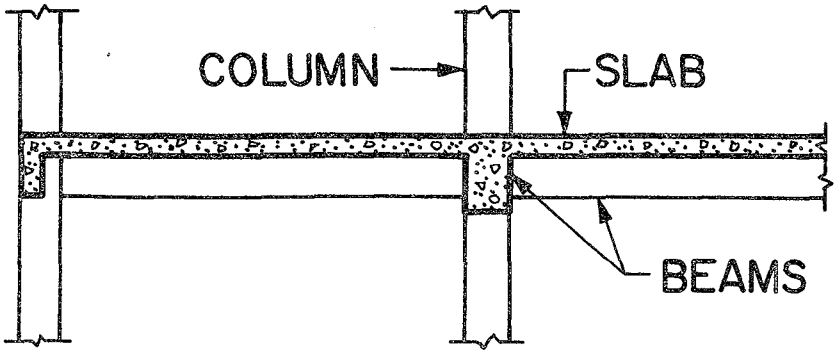

(b) Section A-A

Fig. 1.6 Floor System with Two-Way Slab Supported on Beams Between Columns

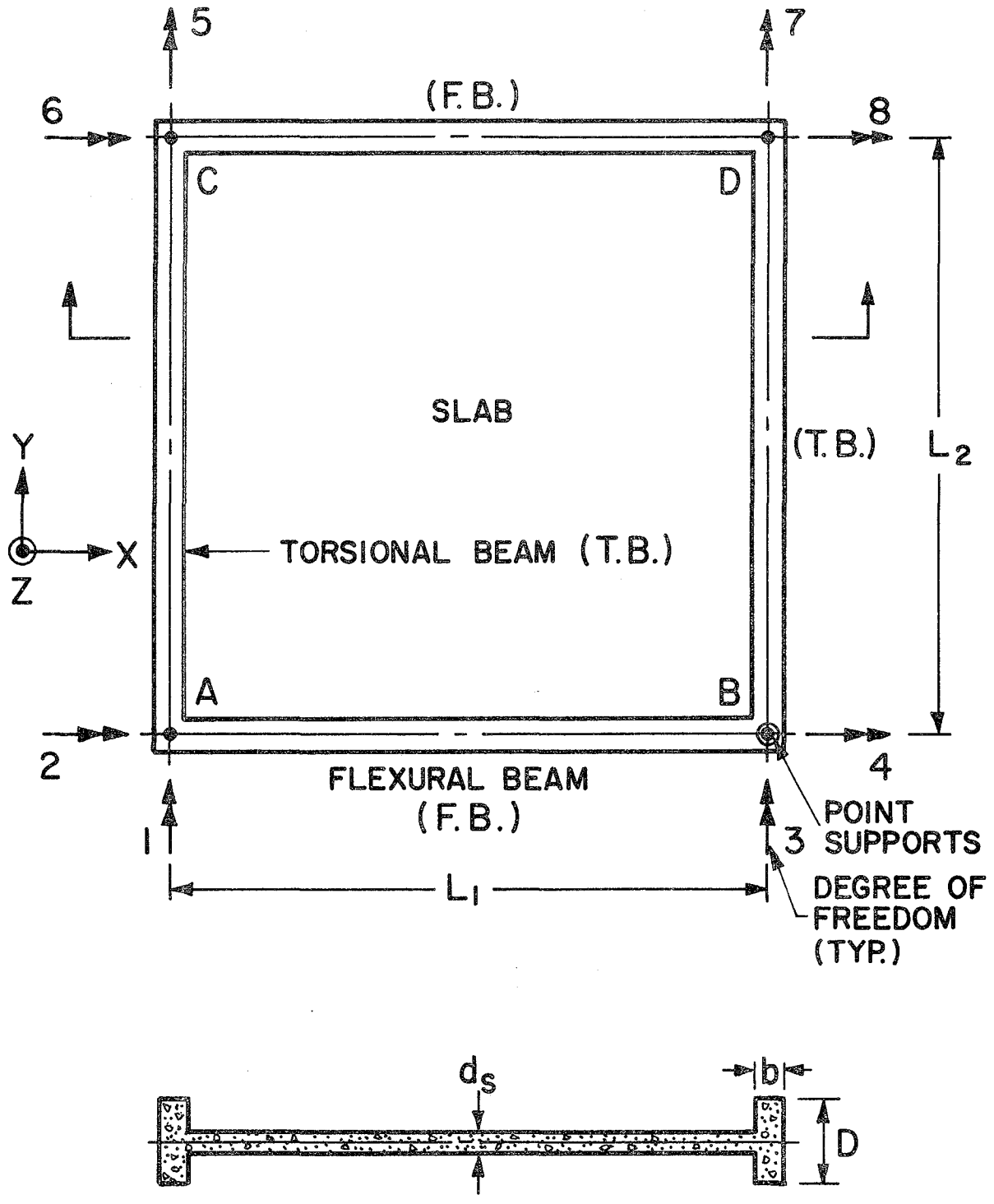

Section A-A

Fig. 2.1 Typical Single-Panel Floor with Beams Symmetric around Slab Neutral Surface

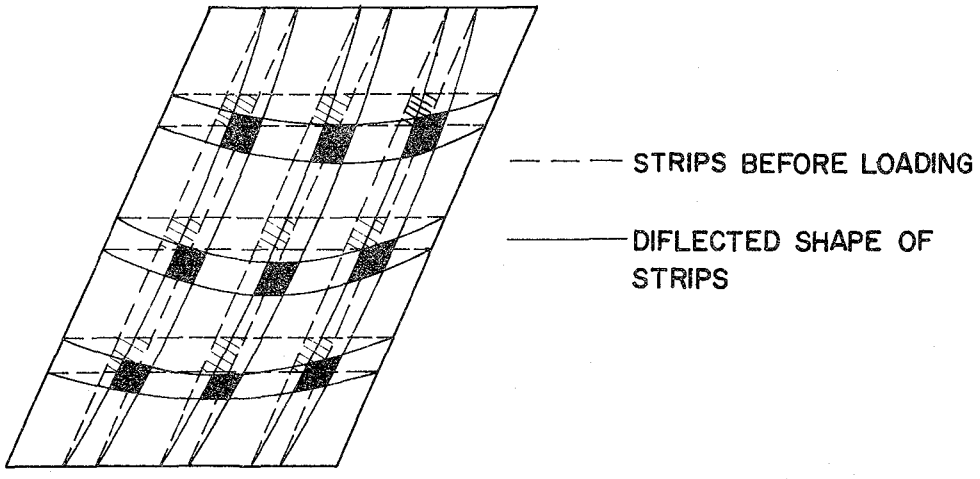

(a) Schematic Diagram of a Simply Supported Slab with Uniform Gravity Load [18]

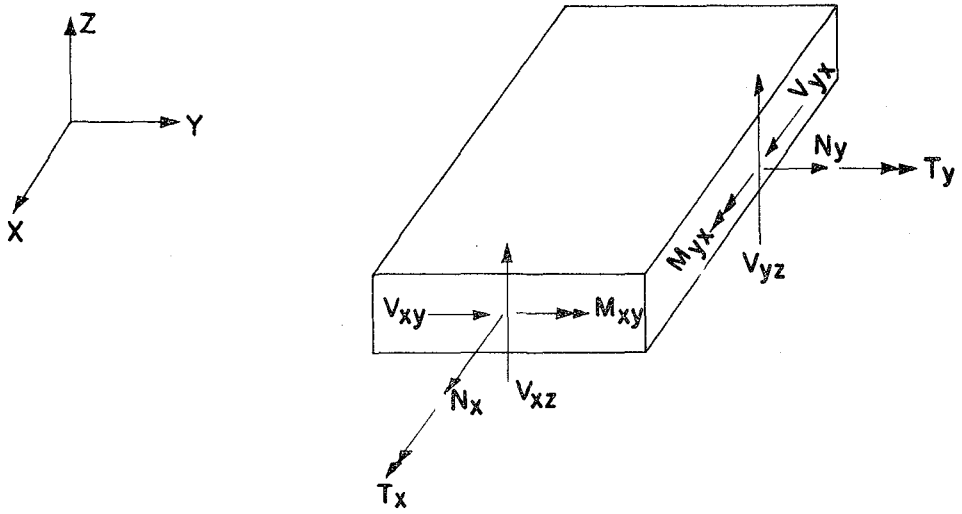

(b) Moments, shears, and in-plane (membrane) forces in slab element

Fig. 2.2 Load Carrying Mechanism in a Two-Way Reinforced Concrete Slab

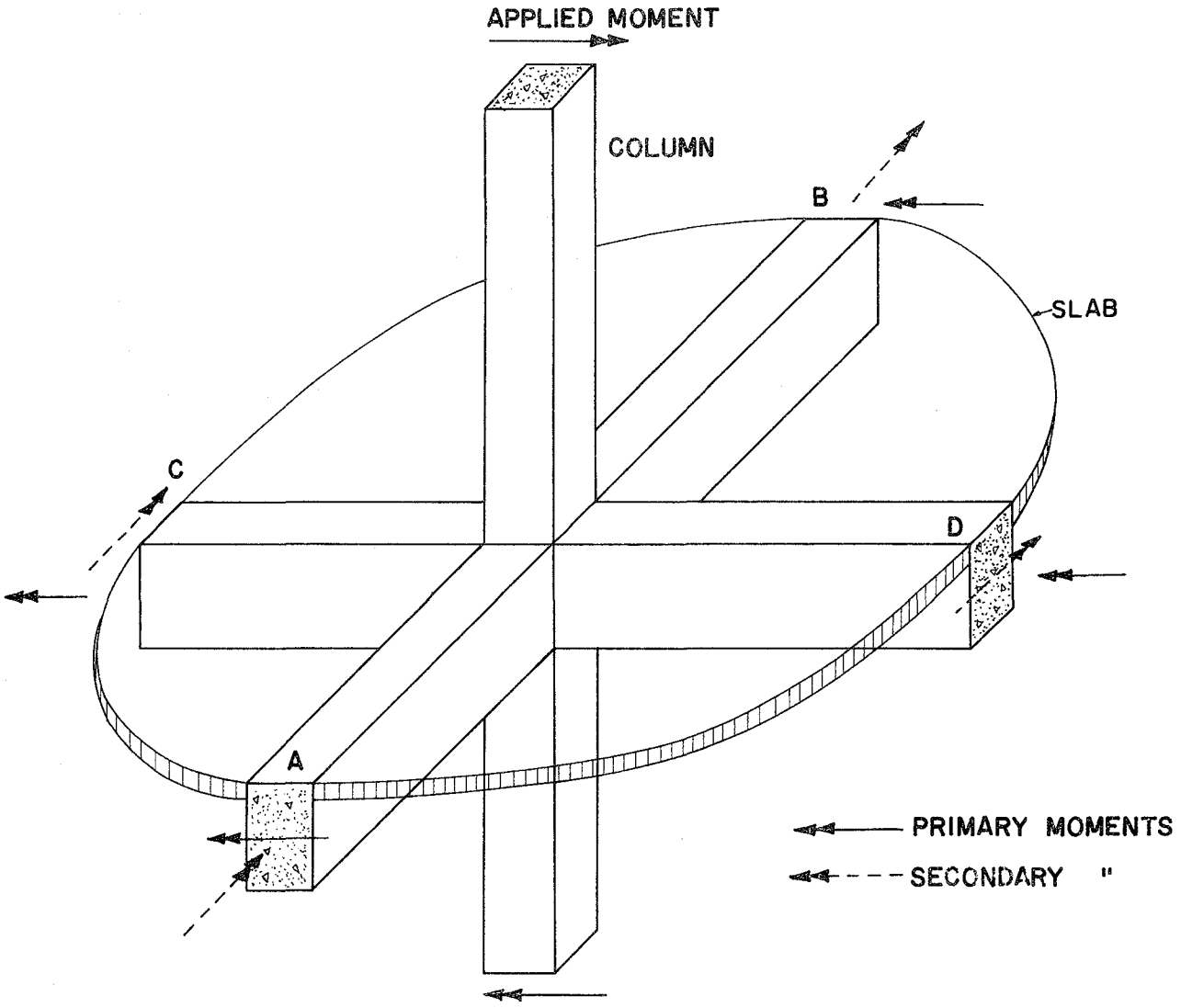

Fig. 2.3 Schematic Illustration of Beam Internal Moments Due to Applied Column Moment

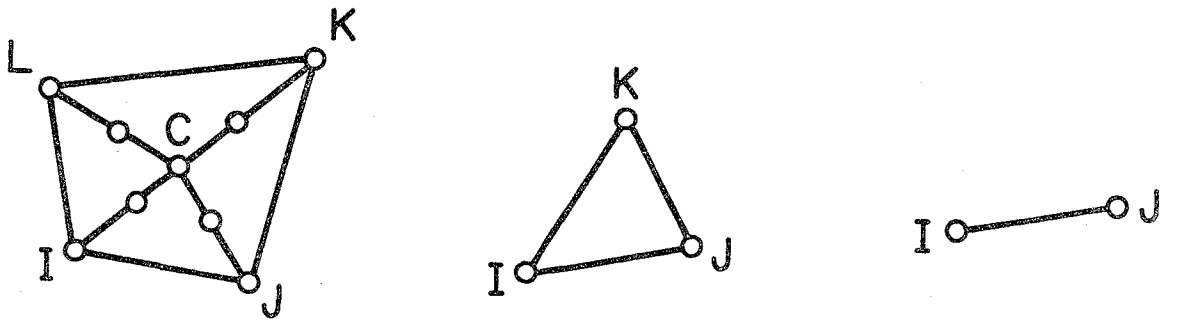

(a) Quadrilateral (b) Single Triangle (c) Prismatic Beam

Fig. 2.4 Finite Elements Used in Program PLATE

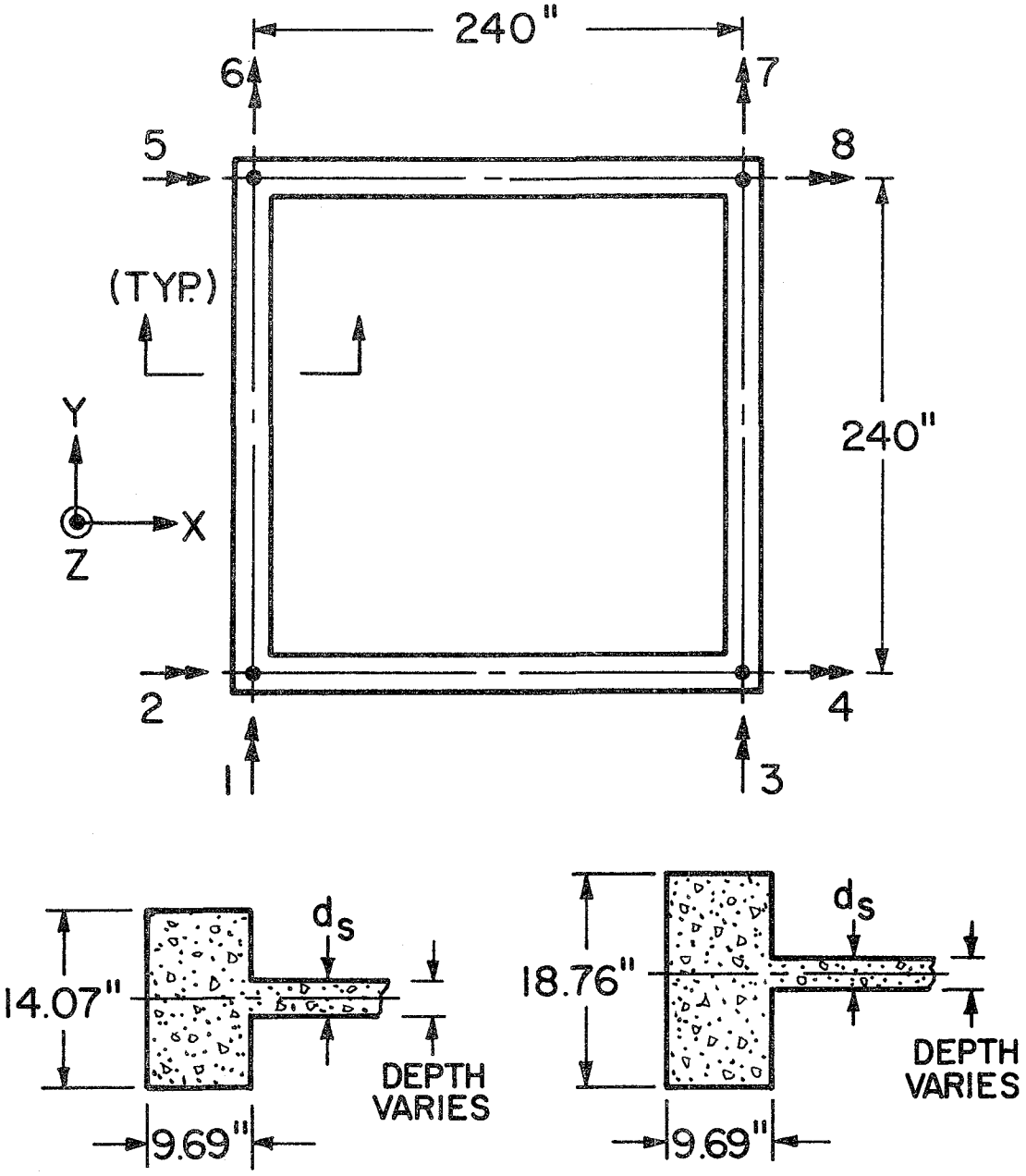

(a) Group "A"

(b) Group "B"

Fig. 2.5 Effect of d_s/L_1 on Stiffness of Single-Panel Floor System

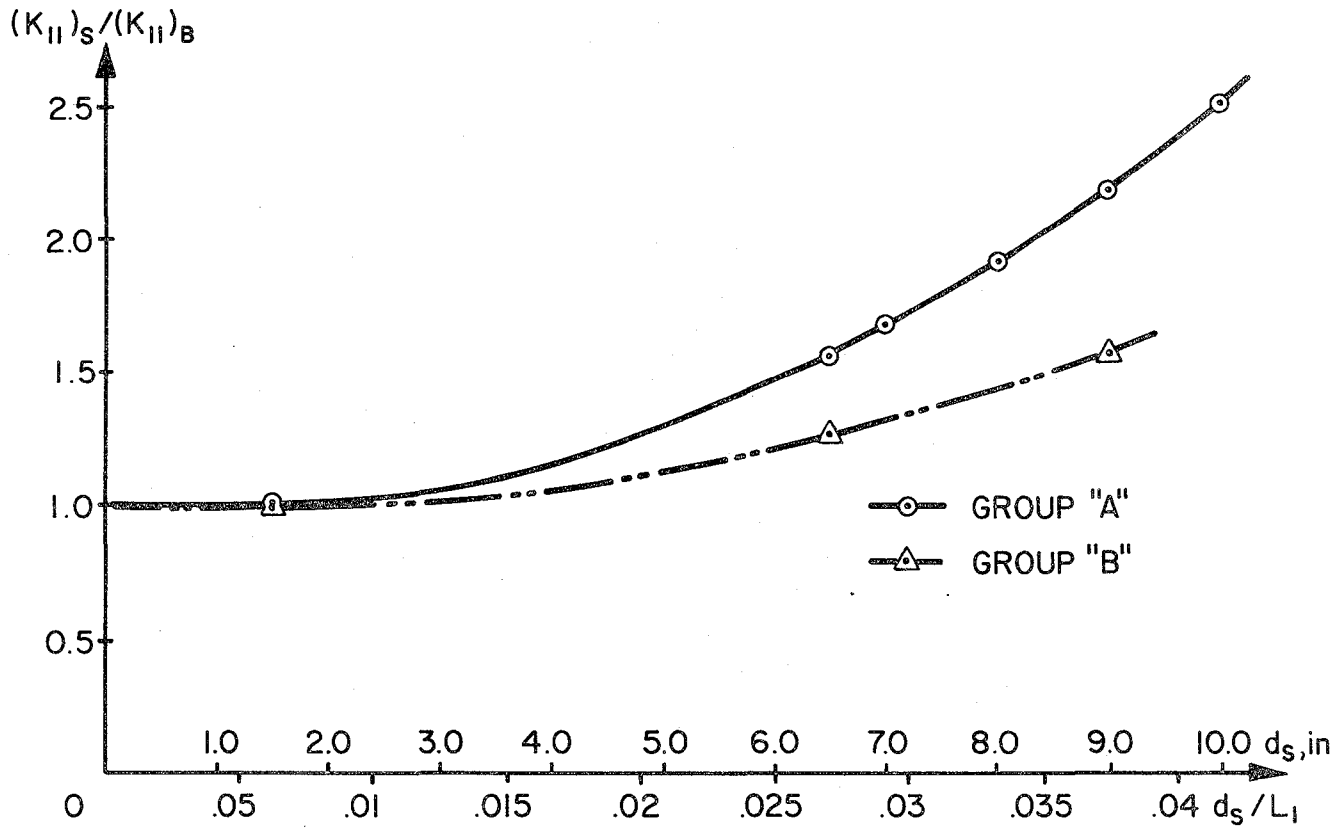

Fig. 2.6 Effect of Slab Thickness on Stiffness of Single-Panel Floor with Beams Symmetric around Mid-Plane of Slab

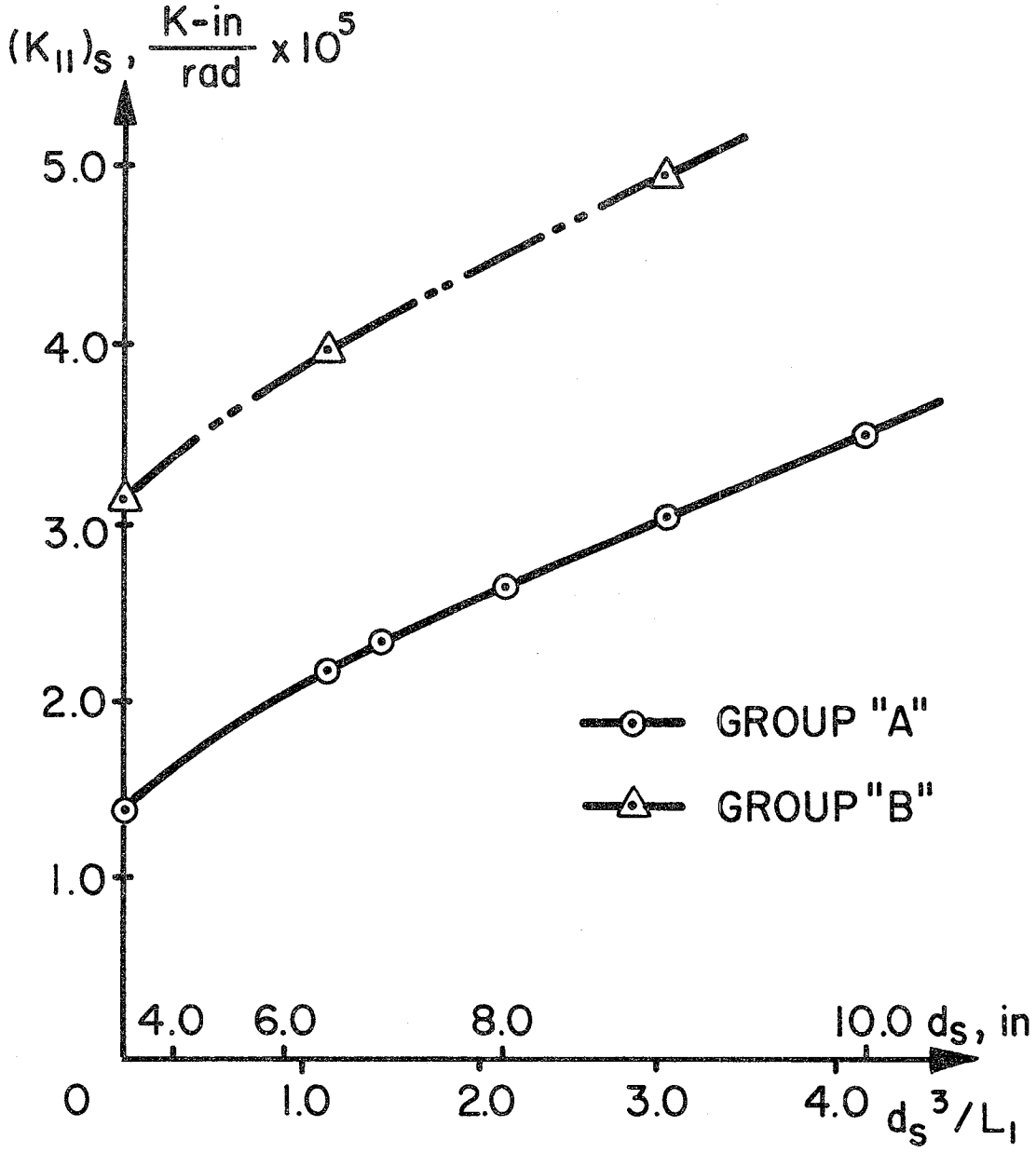

Fig. 2.7 Effect of d_s^3/L_1 on Stiffness of Single-Panel Floor with Beams Symmetric around Mid-Plane of Slab

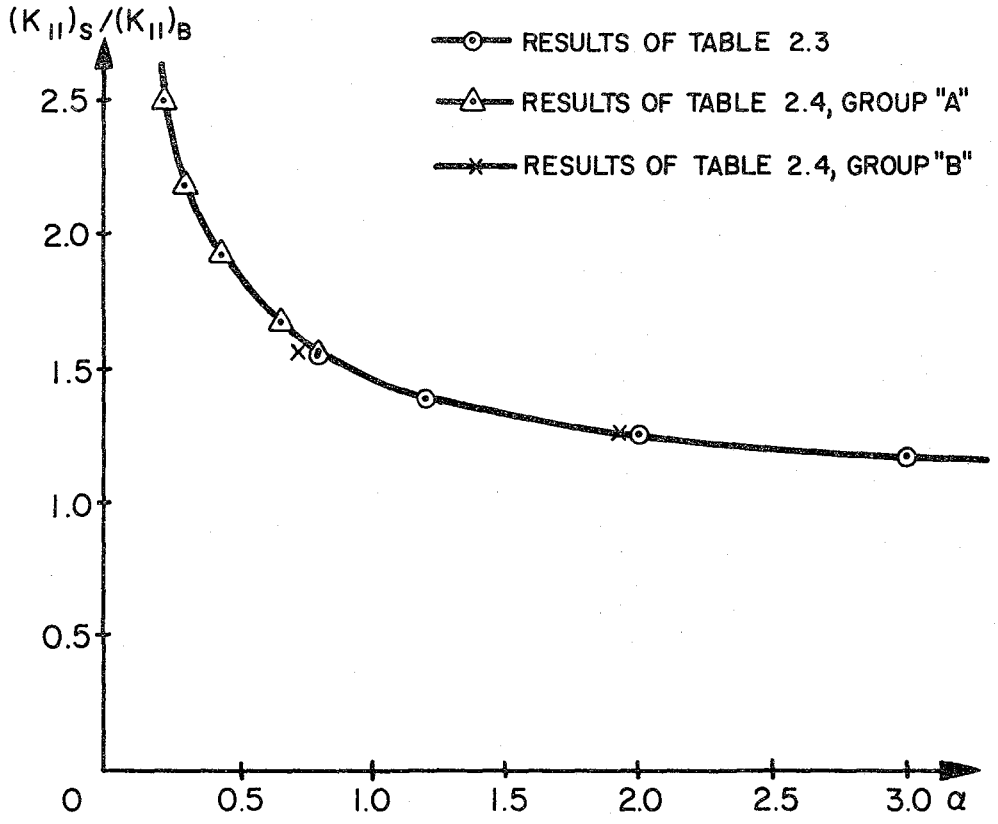

Fig. 2.8 Contribution of Slab to Stiffness of a Square, Single-Panel Floor System as Function of α

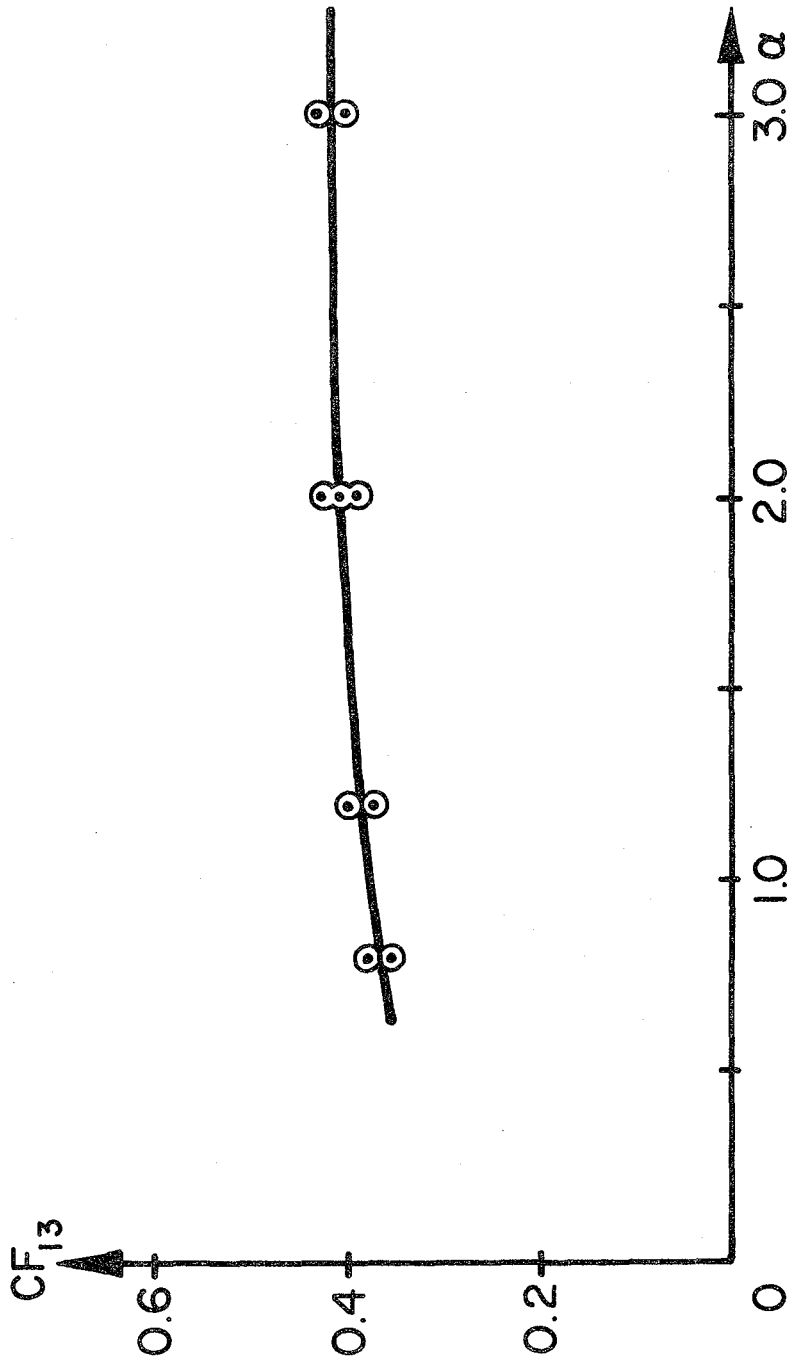

Fig. 2.9 Carryover Factor CF_{13} in a Square, Single-Panel Floor

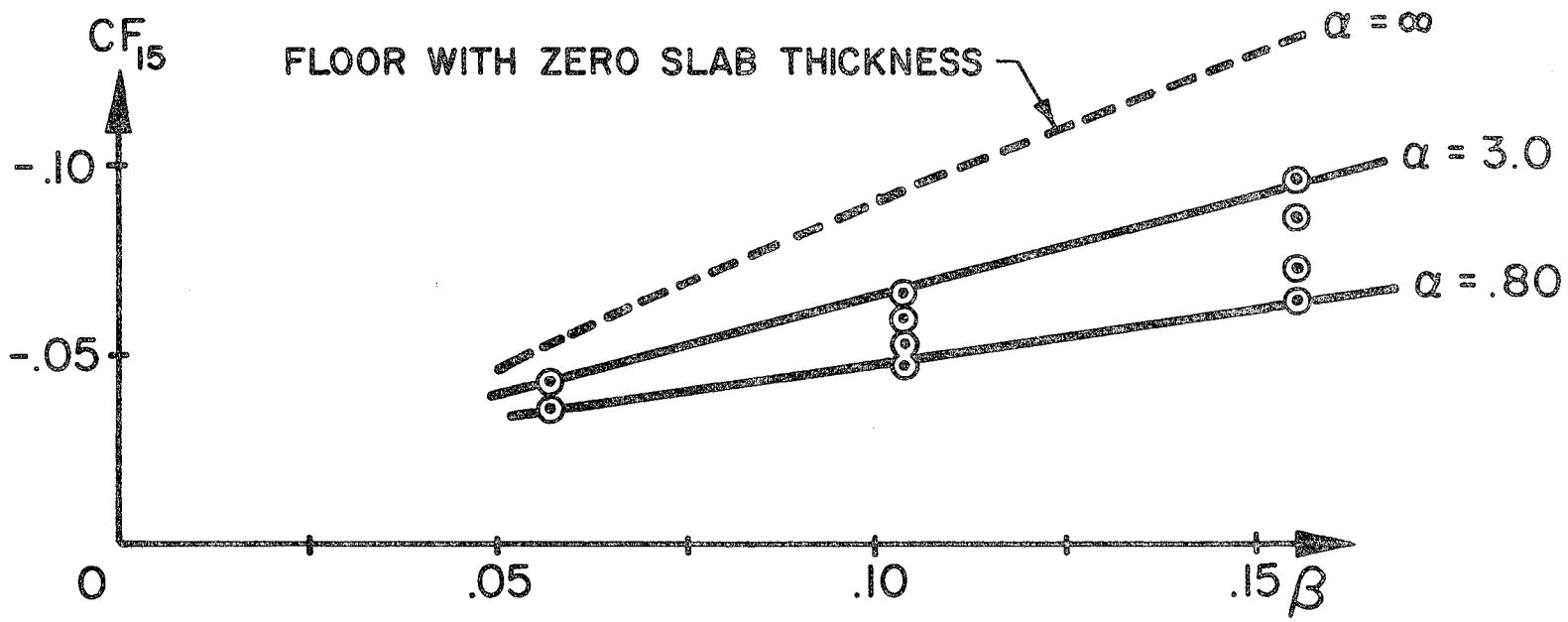

Fig. 2.10 Carryover Factor CF_{15} in a Square Single-Panel Floor

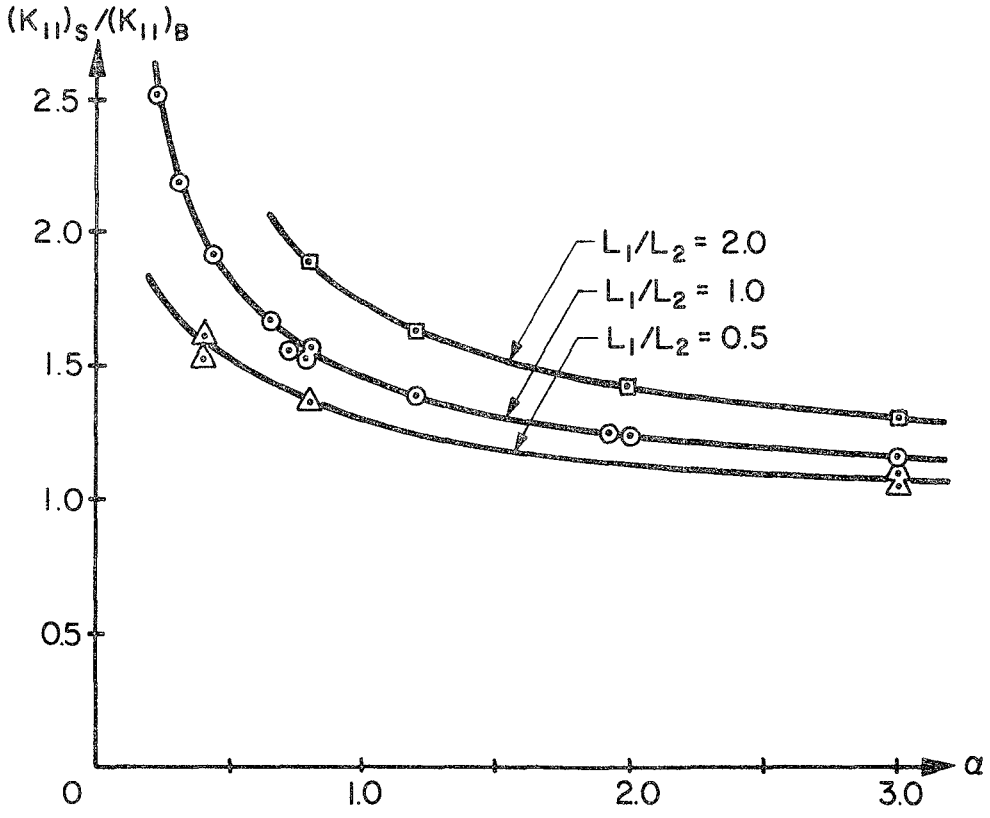

Fig. 2.11 $(K_{11})_S/(K_{11})_B$ vs. α for a Single-Panel Floor with Beams Symmetric around Slab Neutral Axis

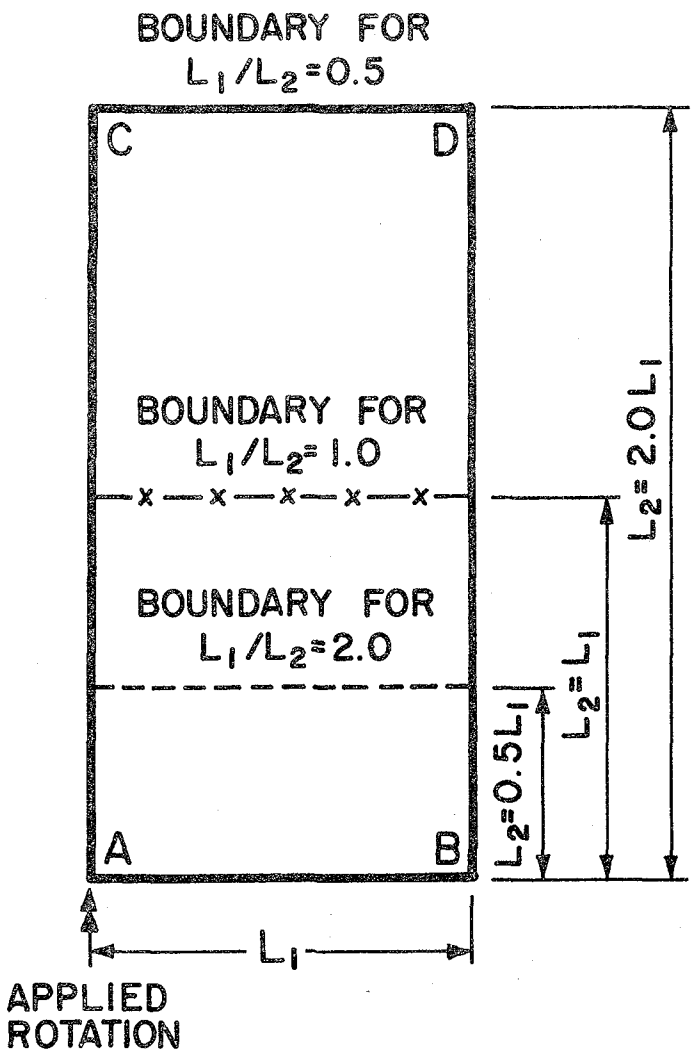

Fig. 2.12 Schematic Diagram of Physical Layout of Floor as L_1/L_2 Varies

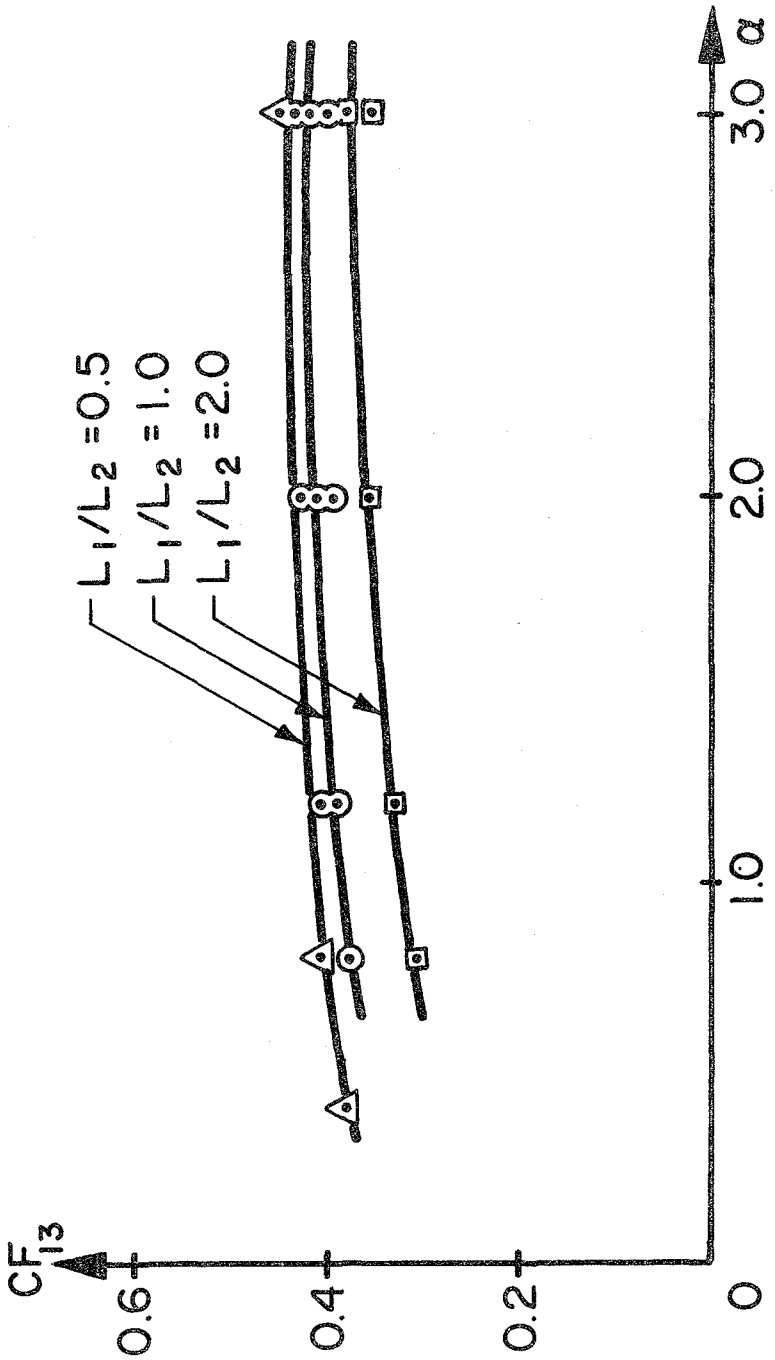

Fig. 2.13 Carryover Factor CF_{13} vs. α in a Single-Panel Floor

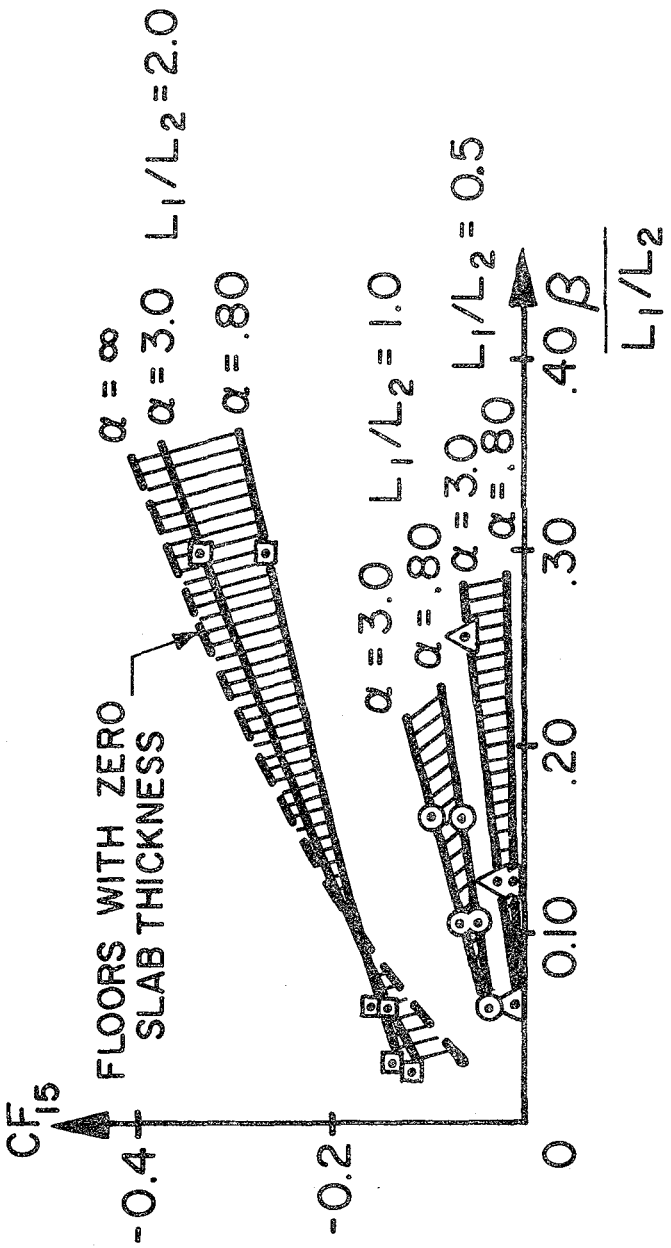

Fig. 2.14 Carryover Factor CF_{15} vs. $\frac{\beta}{L_1/L_2}$ for a Single-Panel Floor

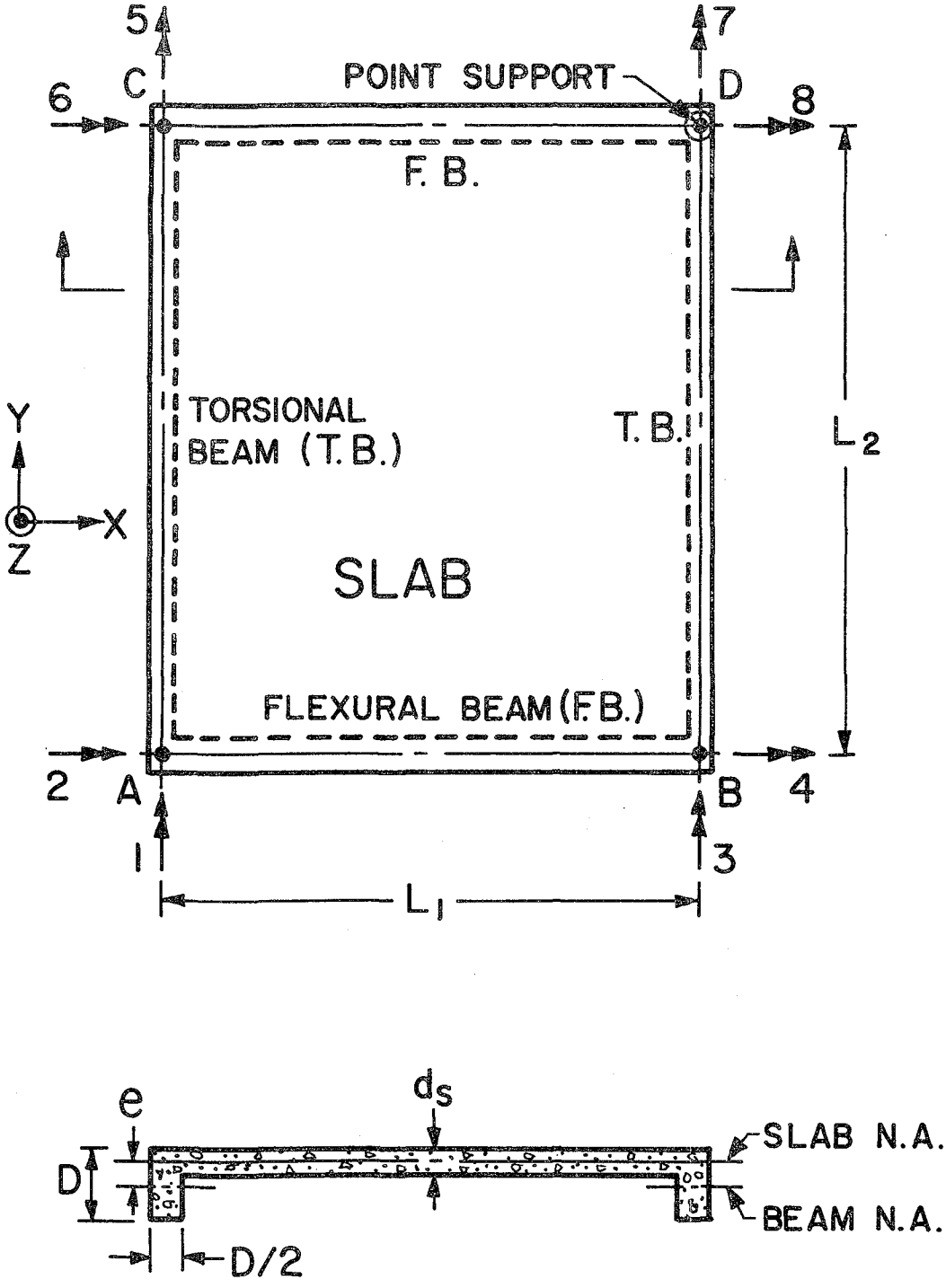

Fig. 3.1 Single-Panel Floor with Eccentric Beams

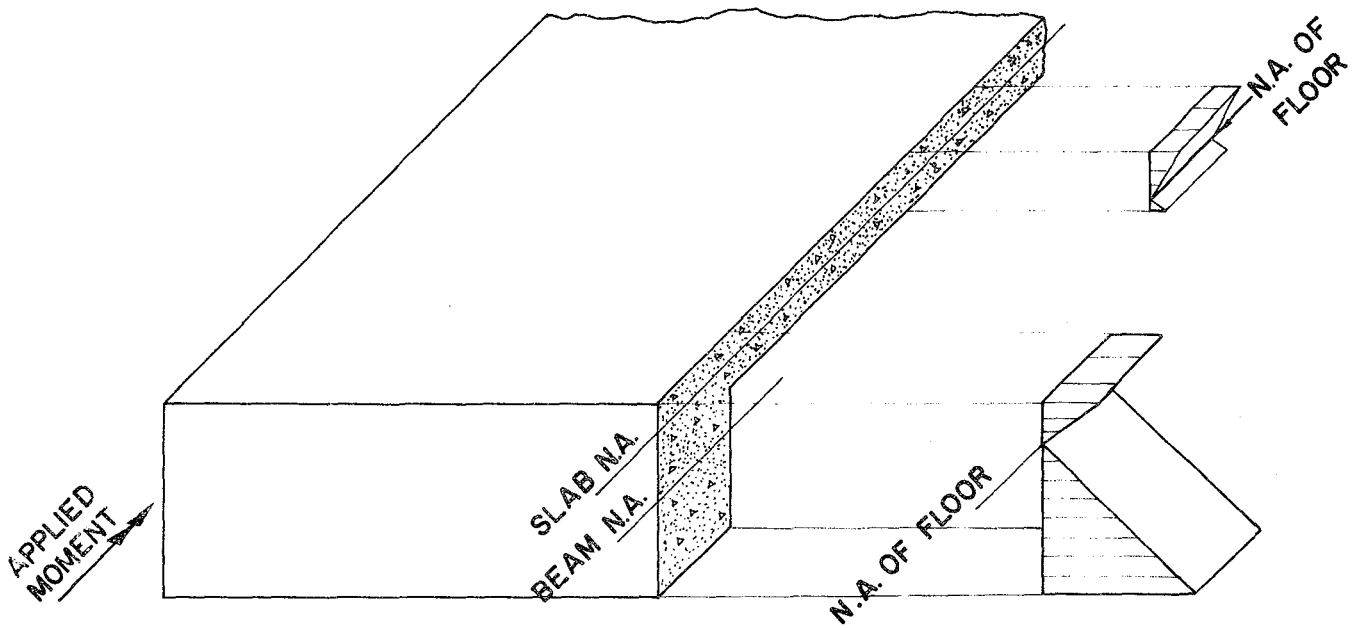

Fig. 3.2 Schematic Illustration of Stresses along Flexural Beam

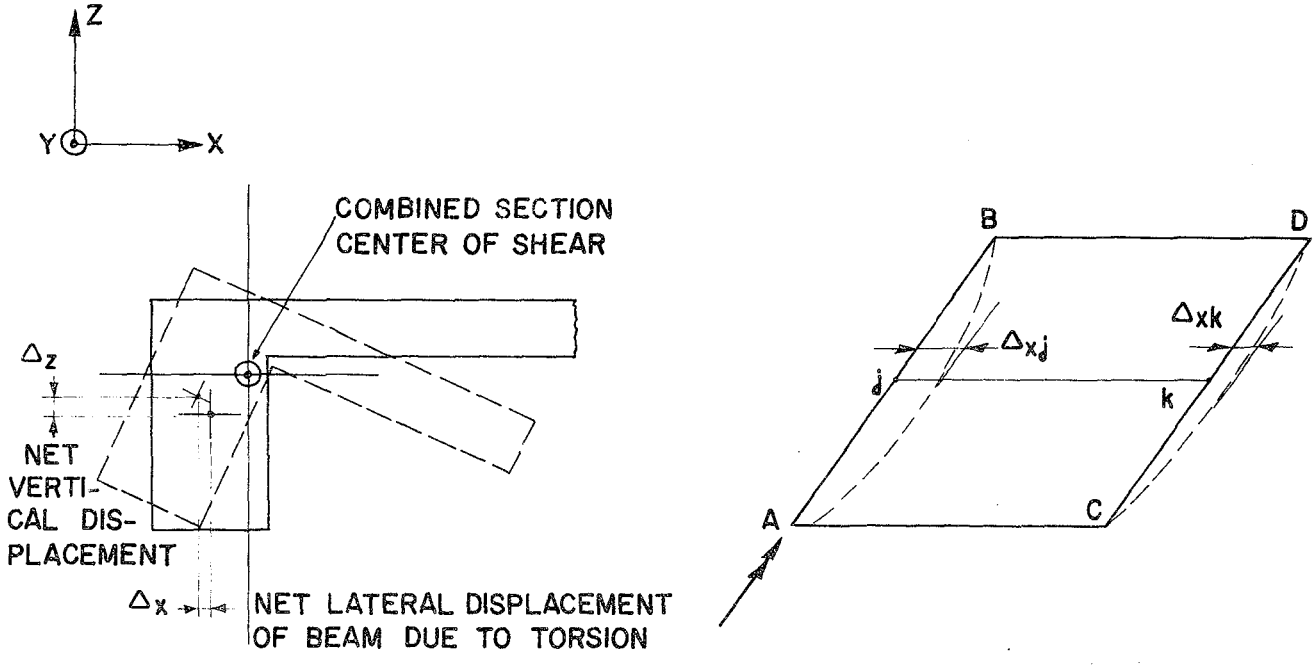

(a) Cross Section through Torsional Beam

(b) Plan View through Slab Mid-Plane

Fig. 3.3 Schematic Illustration of Rotation of Torsional Beam and Slab

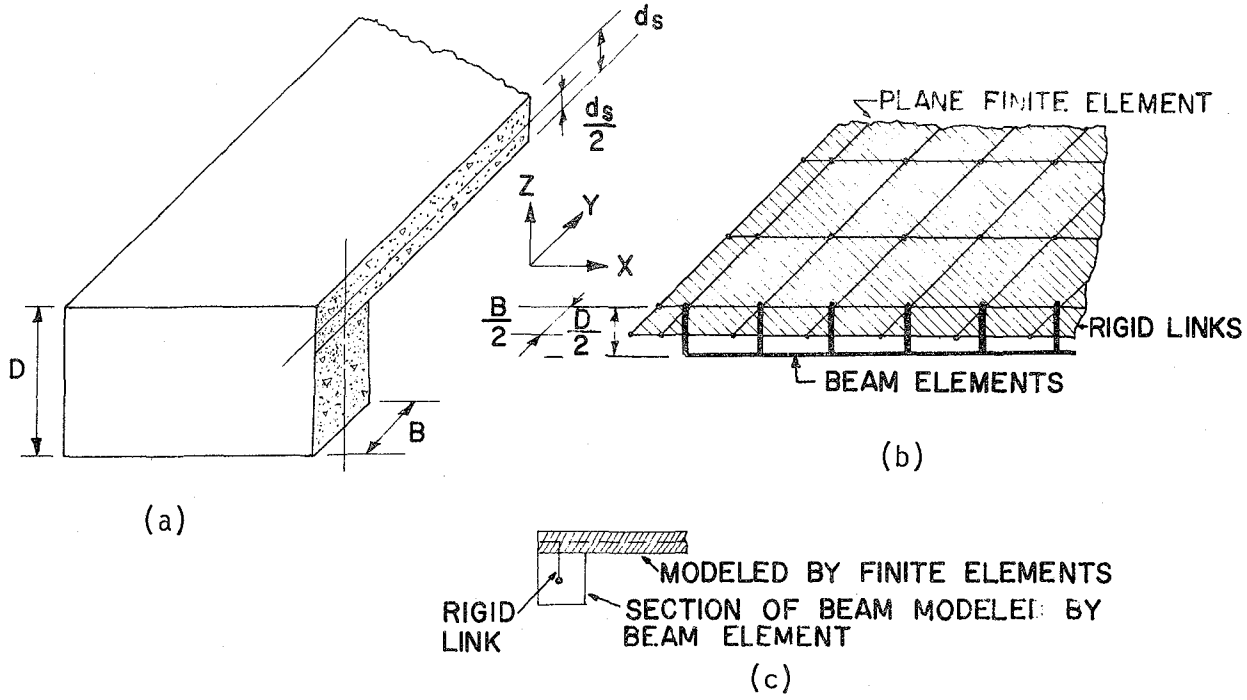

Fig. 3.4 Modeling of Floors with Eccentric Beams

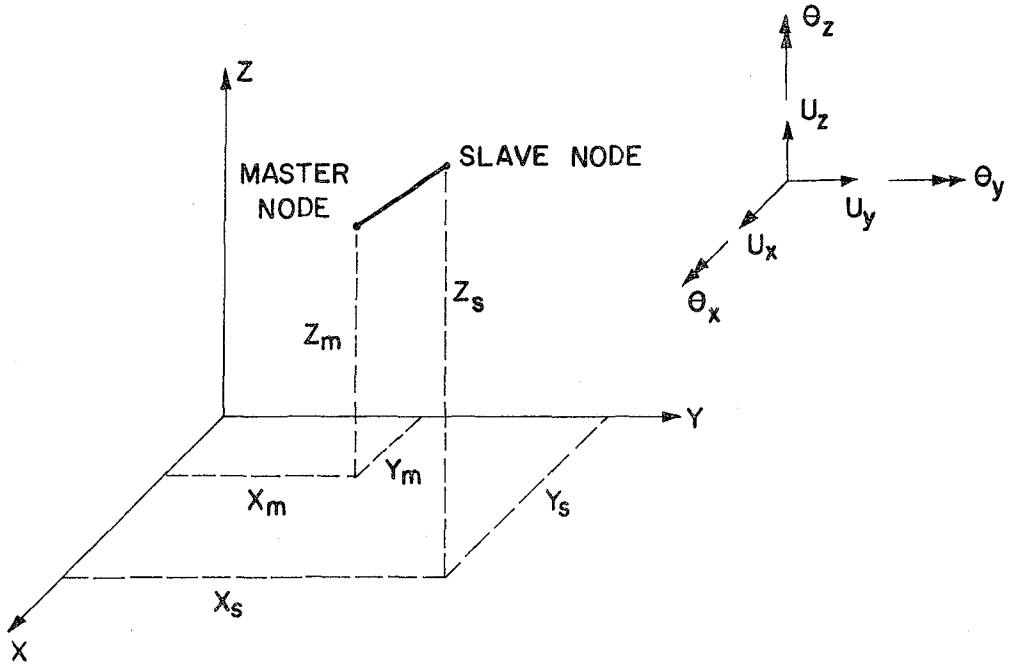

Fig. 3.5 Geometry of Slave and Master Nodes

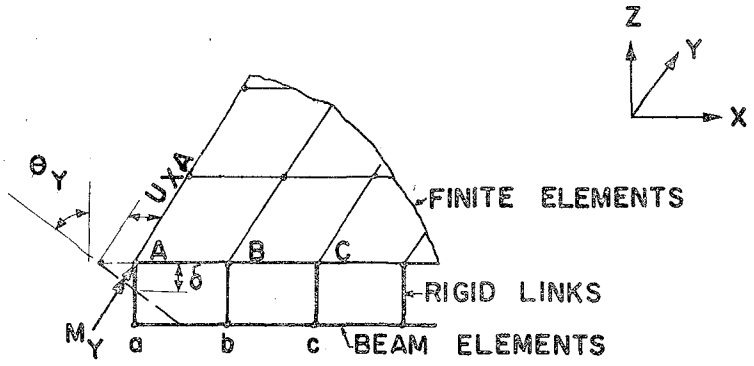

Fig. 3.6 Rotations and Displacements at Support A

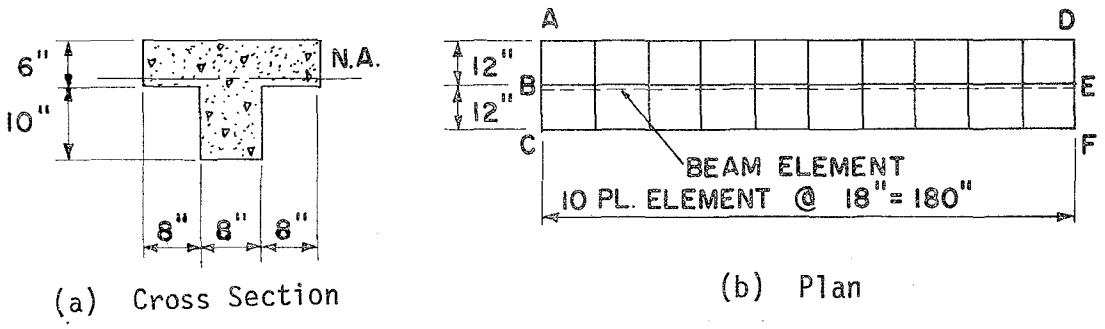

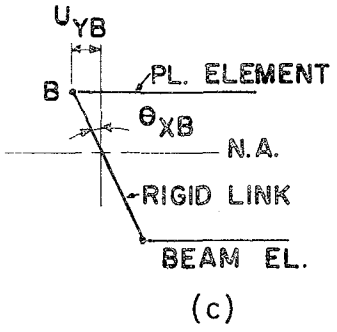

BOUNDARY CONDITIONS

NODE	Δ_x	Δ_y	Δ_z	θ_{xx}	θ_{yy}	θ_{zz}
A	0	0	0	0	1	1
B	0	0	0	0	1	1
C	0	0	0	0	1	1
D	0	1	0	1	0	0
E	1	1	1	1	1	1
F	0	1	0	1	0	0

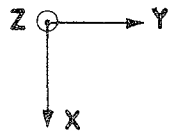

0 = FREE
1 = FIXED

Fig. 3.7 Cantilever T-Beam Model

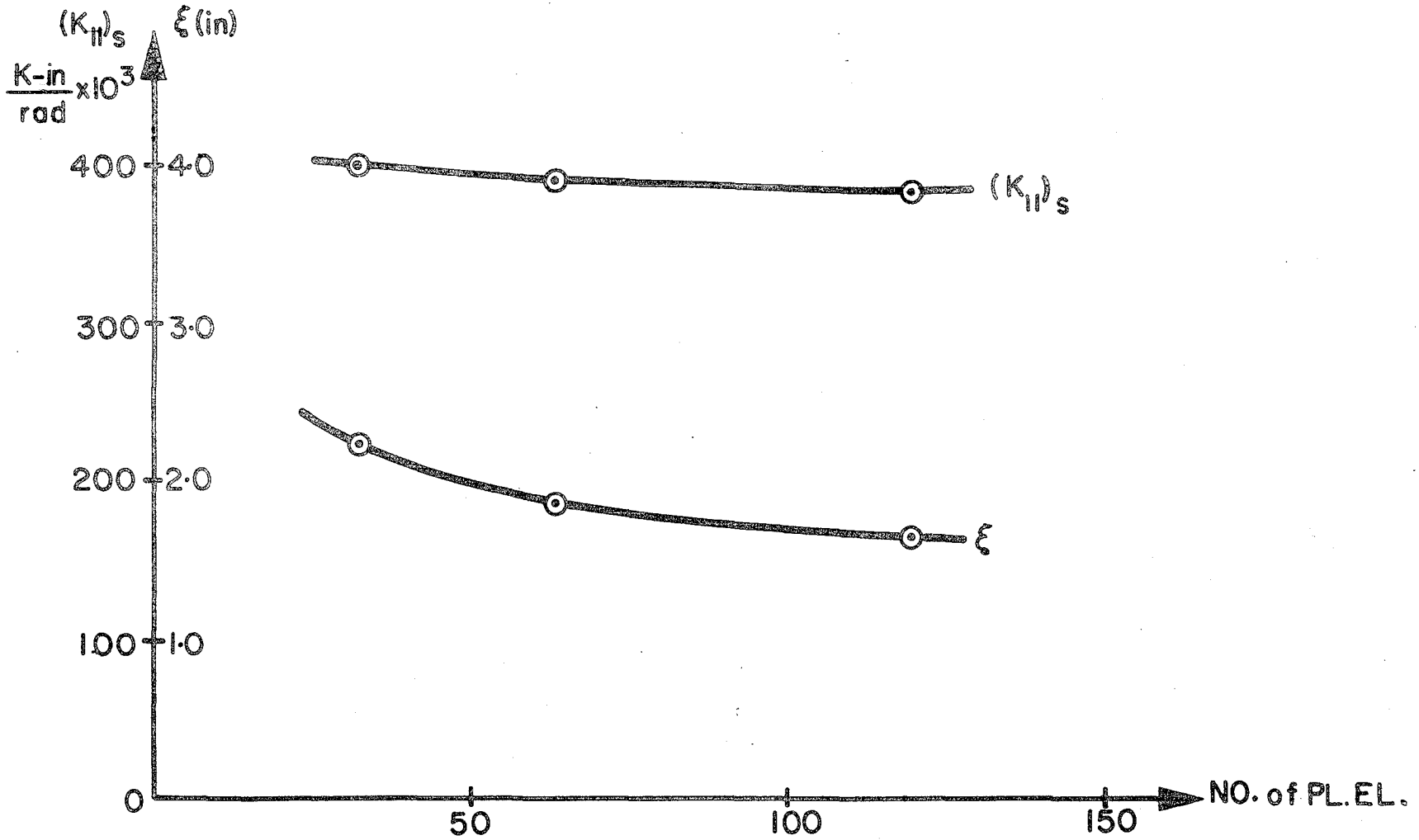

Fig. 3.8 Mesh Convergence of a Single-Panel Floor where $L_1/L_2 = 0.5$, $\alpha = 0.8$, $d_s = 6.5$ in., $L_1 = 120$ in.

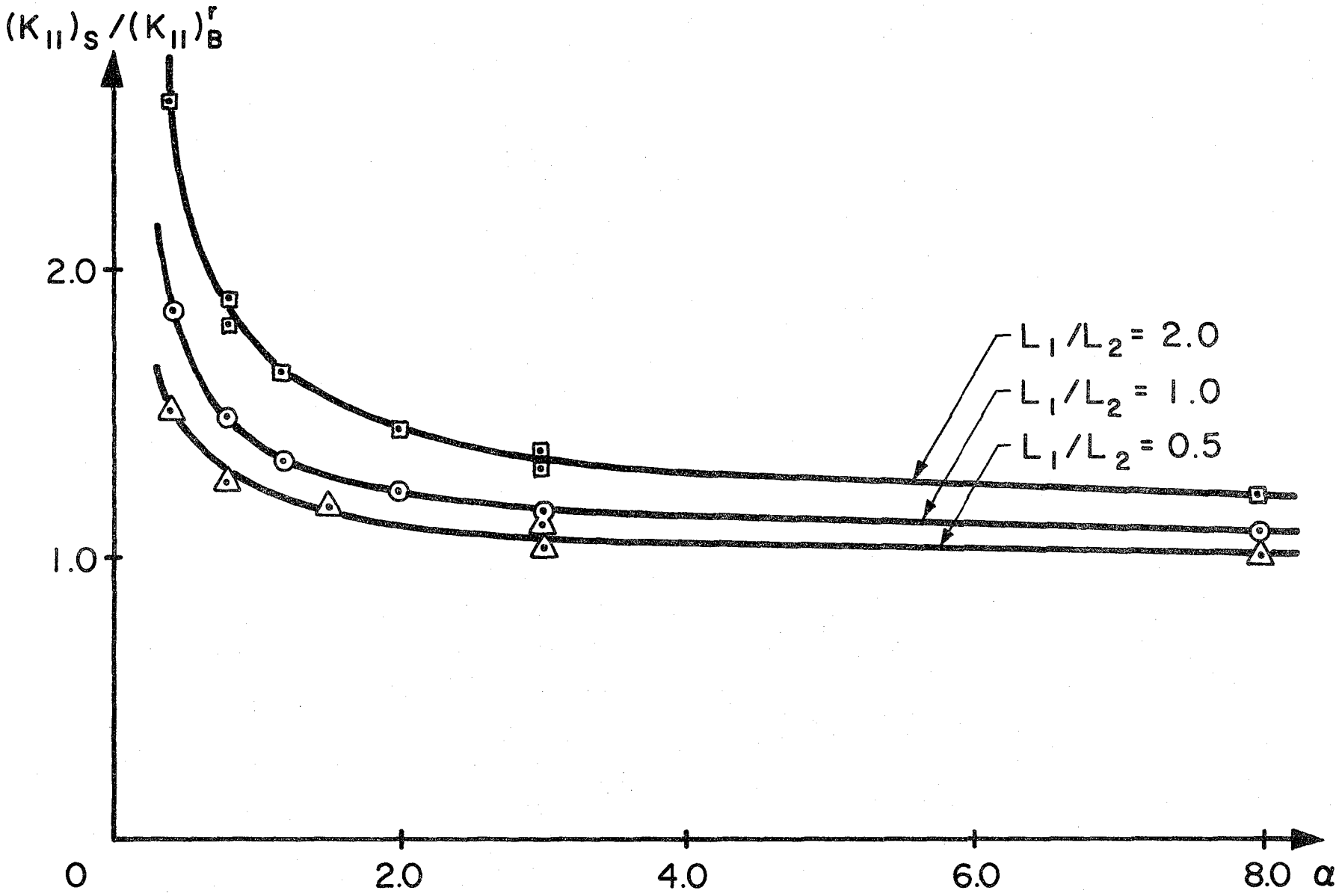

Fig. 3.9 Contribution of Slab to Stiffness of a Single-Panel Floor

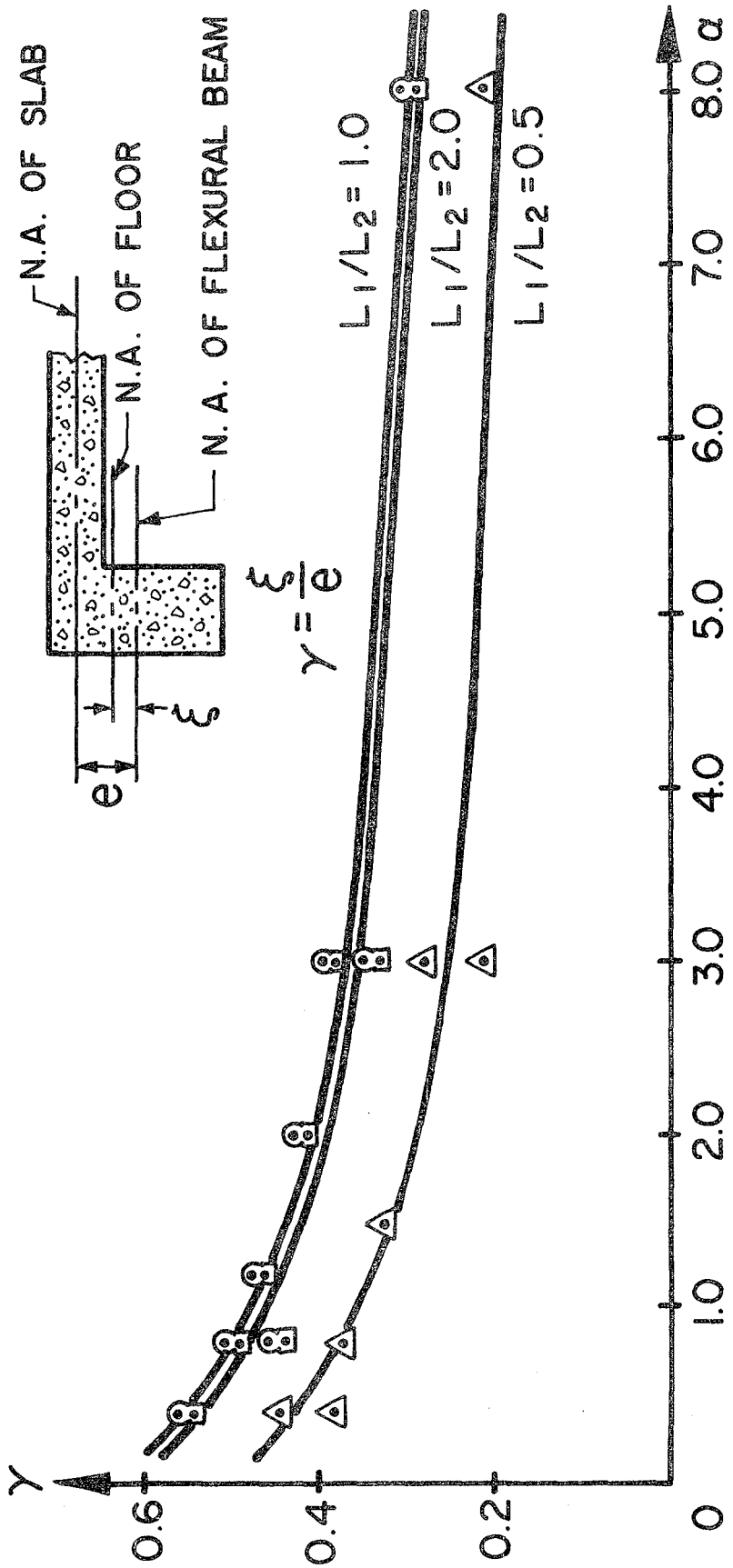

Fig. 3.10 Neutral Axis of a Single-Panel Floor at Supports

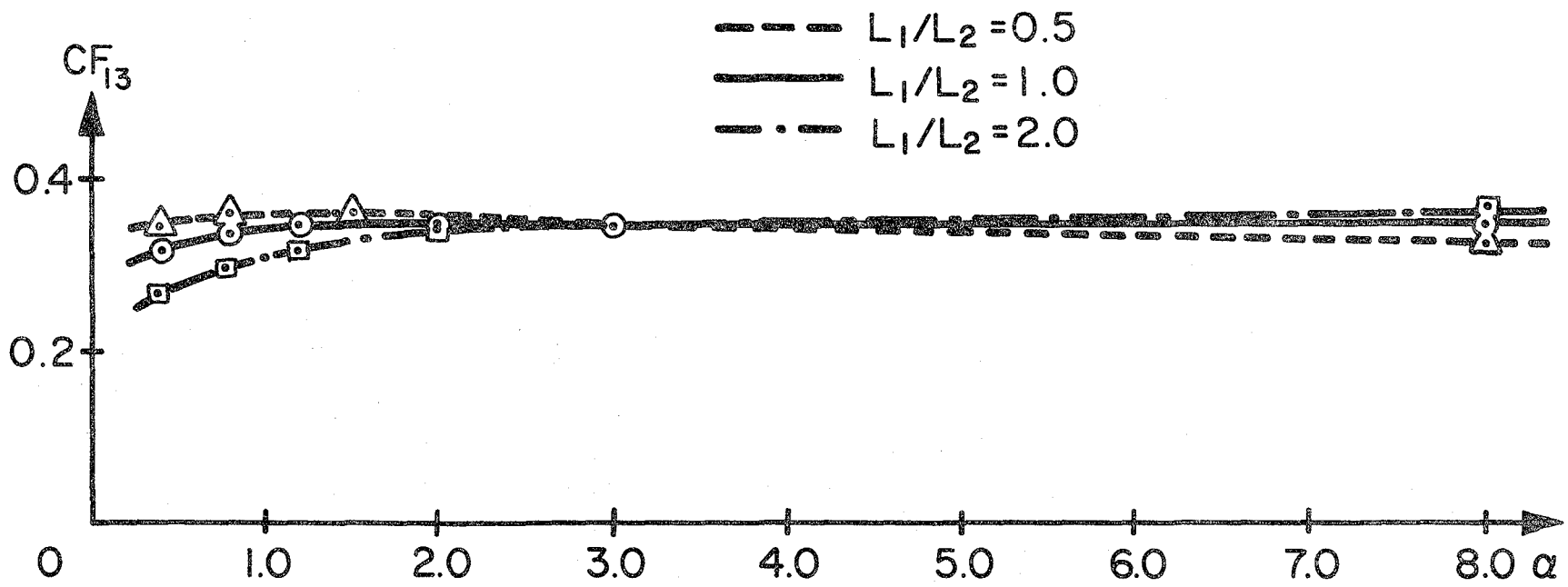

Fig. 3.11 Carryover Factor CF_{13} in a Single-Panel Floor with Eccentric Beams

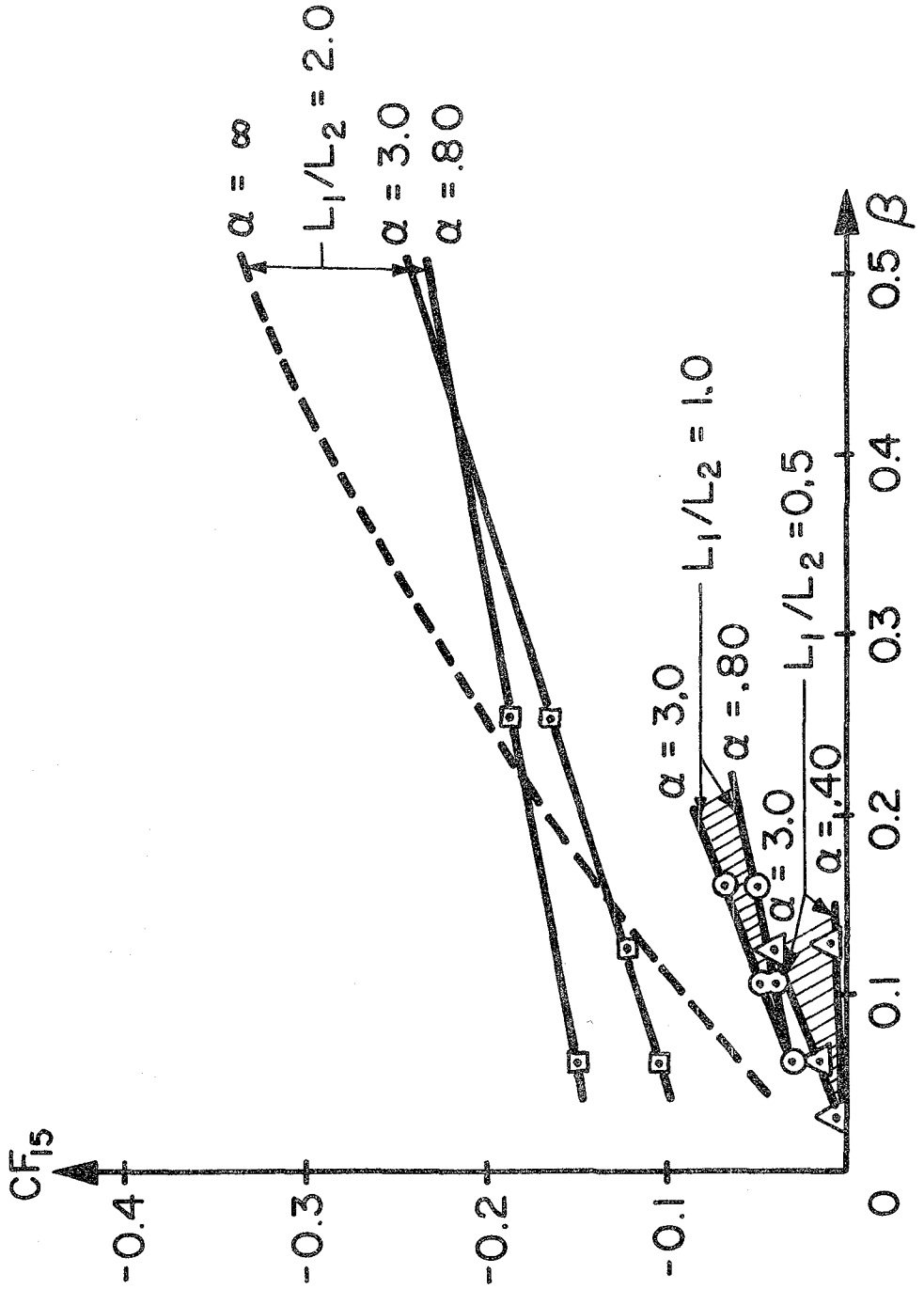

Fig. 3.12 Carryover Factor CF_{15} of a Single-Panel Floor with Eccentric Beams

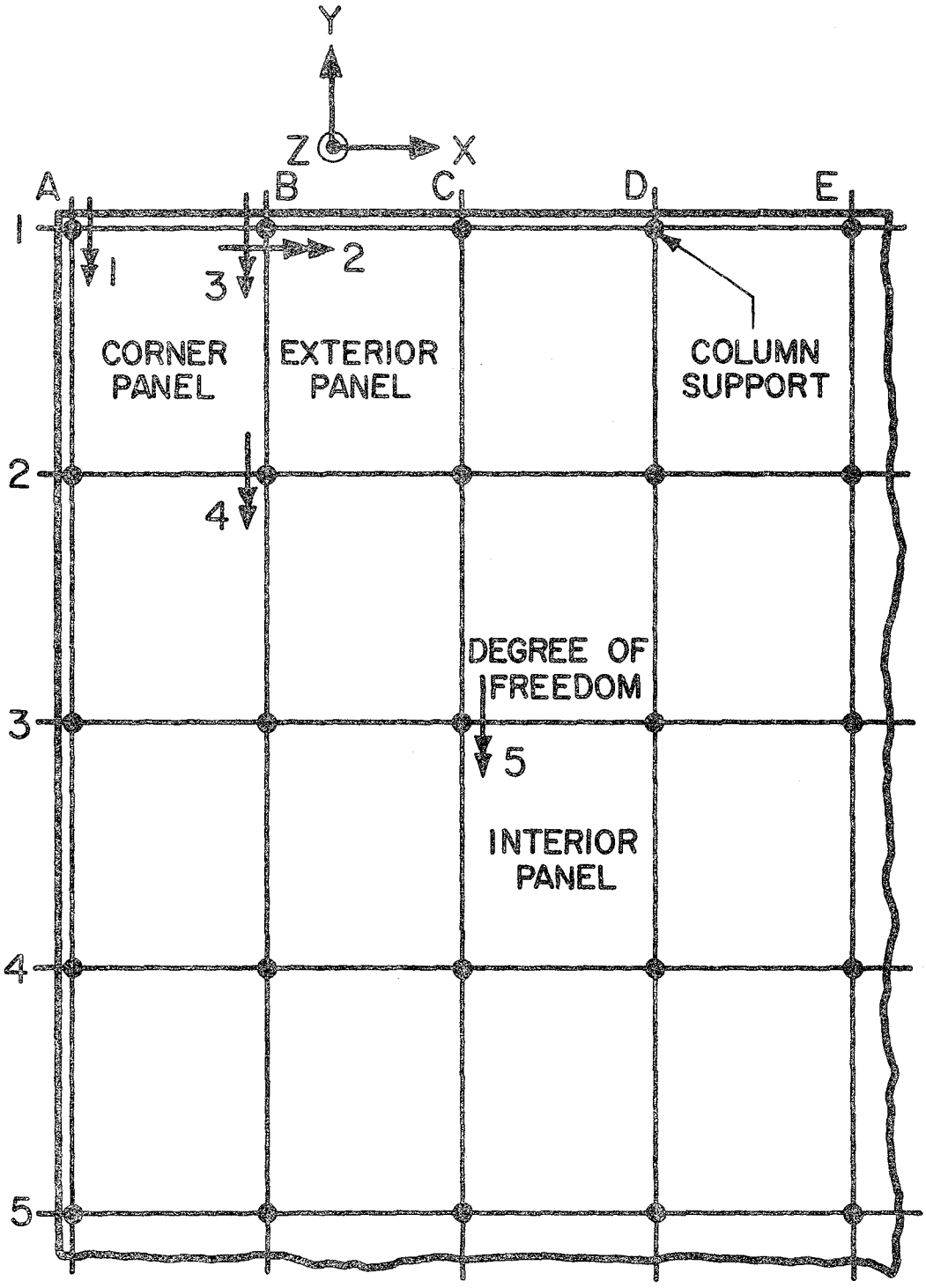

Fig. 4.1 Schematic of Multi-Panel Floor

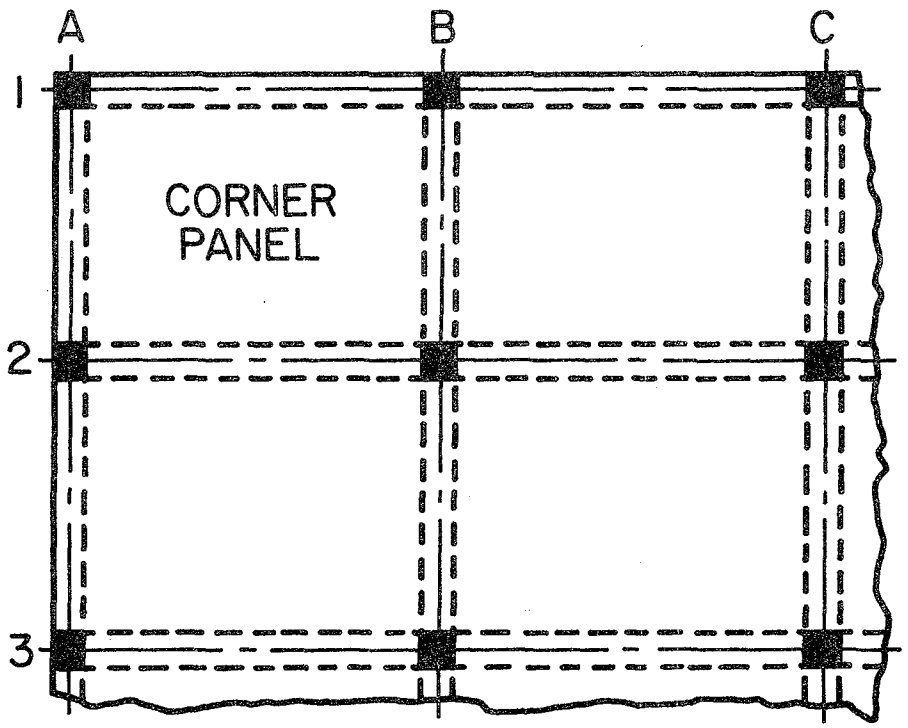

Fig. 4.2 Corner Panel

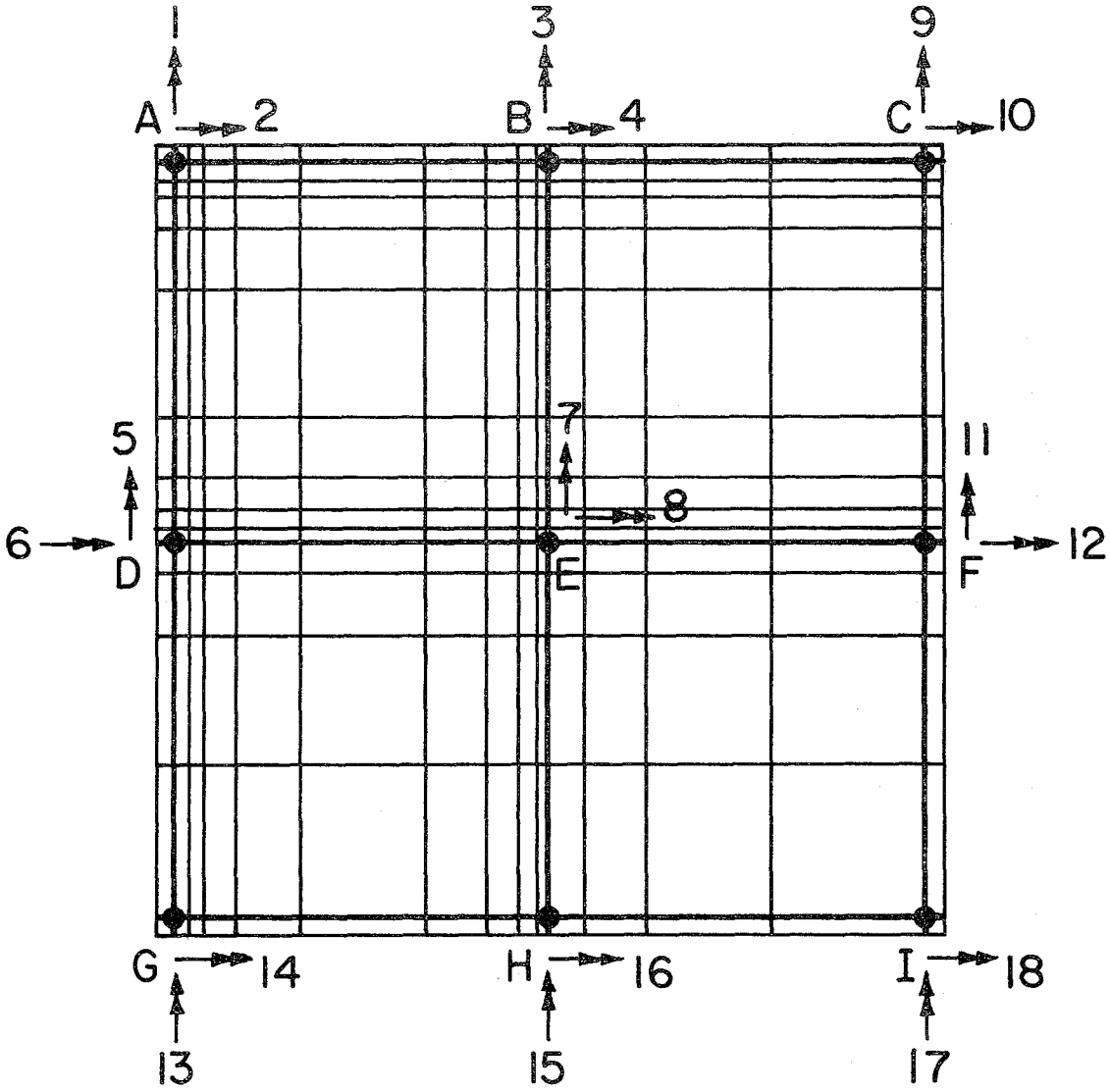

Fig. 4.3 Modeling of Corner Panel

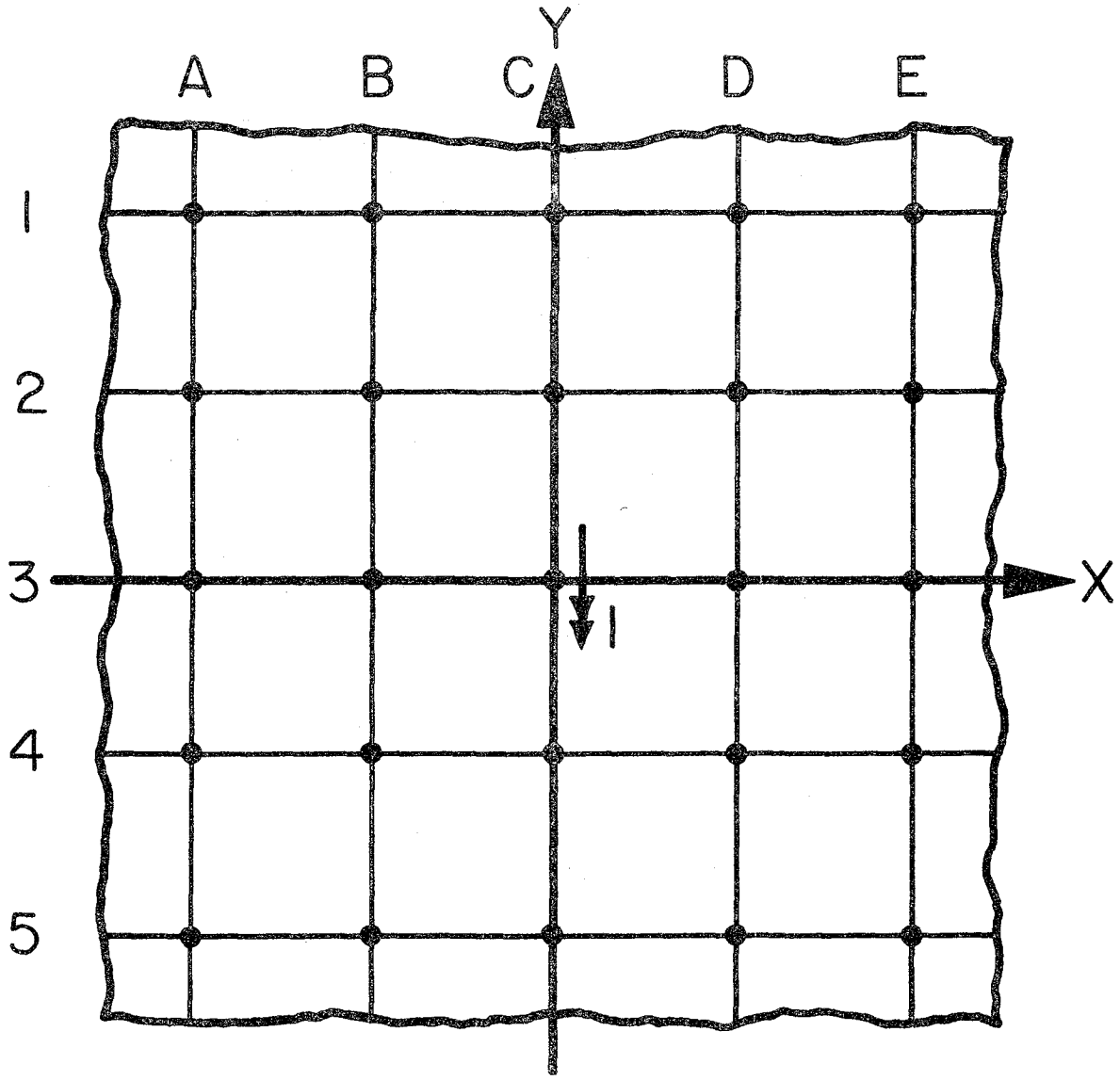

Fig. 4.4 Schematic Plan of a Multi-Panel Floor

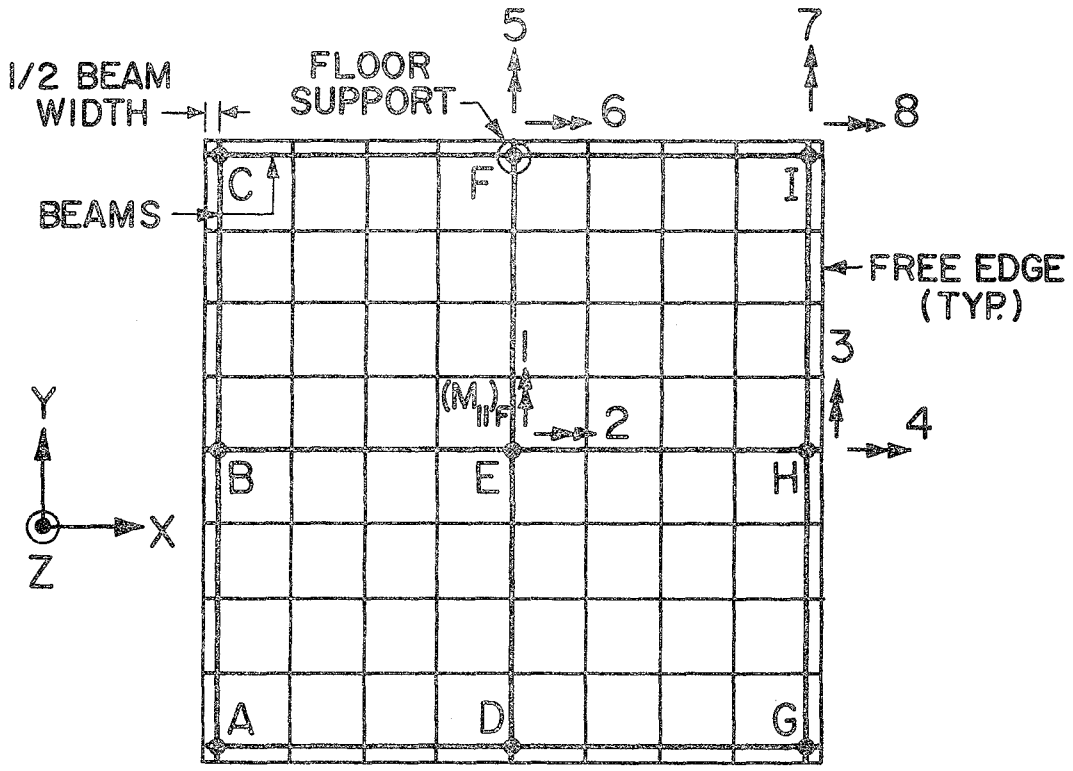

(a) Full floor and finite element mesh used

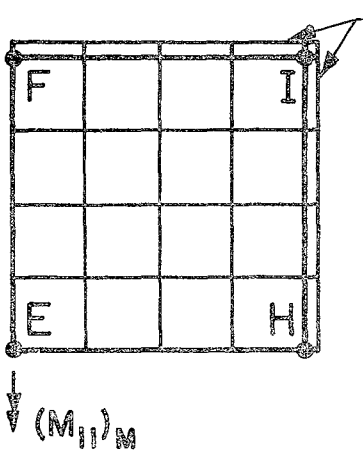

COL. LINE \ DOF	Δ_x	Δ_y	Δ_z	θ_{xx}	θ_{yy}	θ_{zz}
EH	0	1	0	1	0	1
EF	0	1	1	1	0	1

(b) Quarter of floor with imposed boundary conditions

Fig. 4.5 Example of Structural Symmetry

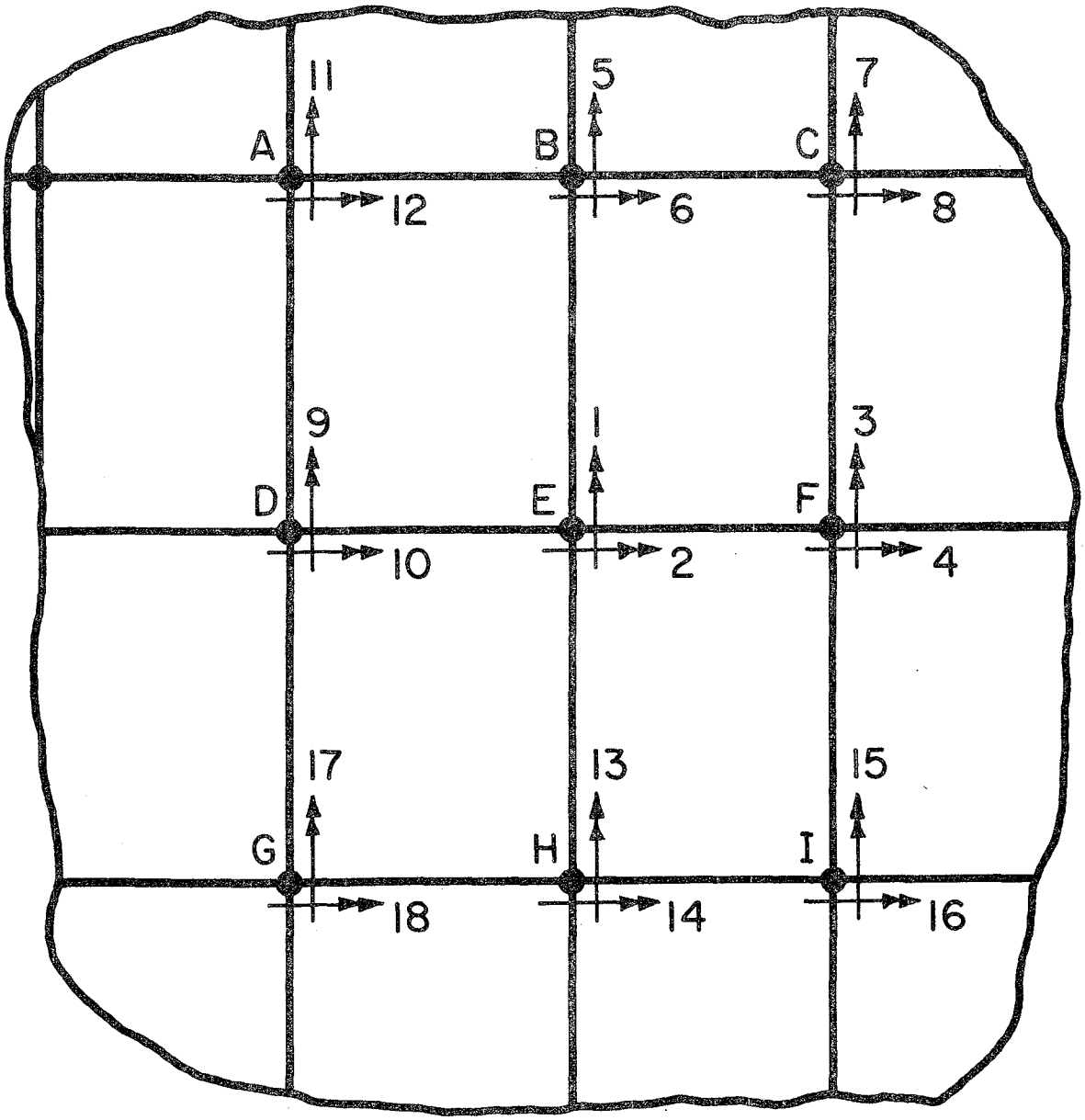

Fig. 4.6 Degrees of Freedom at Interior Panel Supports

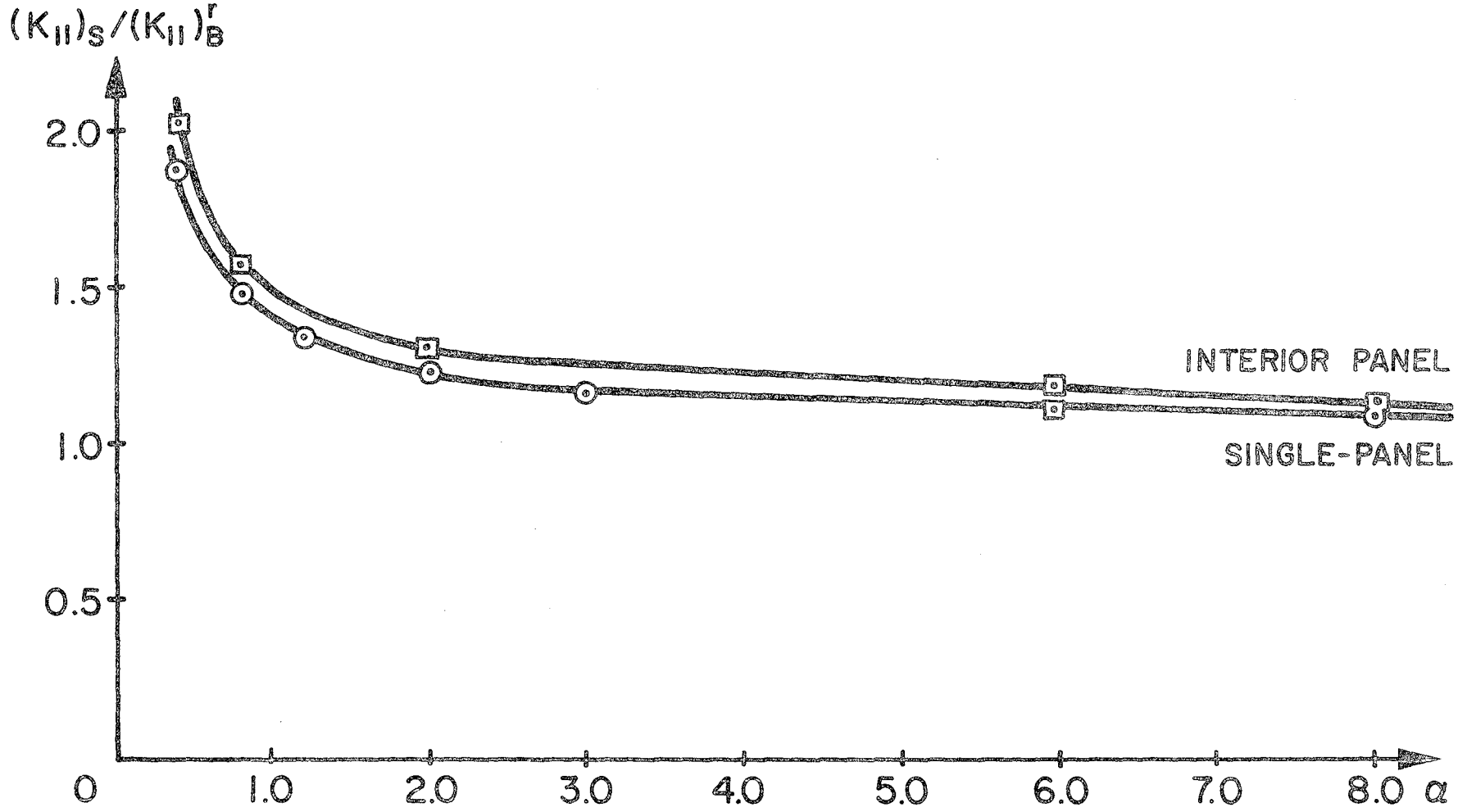

Fig. 4.7 $(K_{11})_S/(K_{11})^r_B$ vs. α for a Single-Panel Floor and an Interior Panel of Floor where $L_1/L_2 = 1.0$

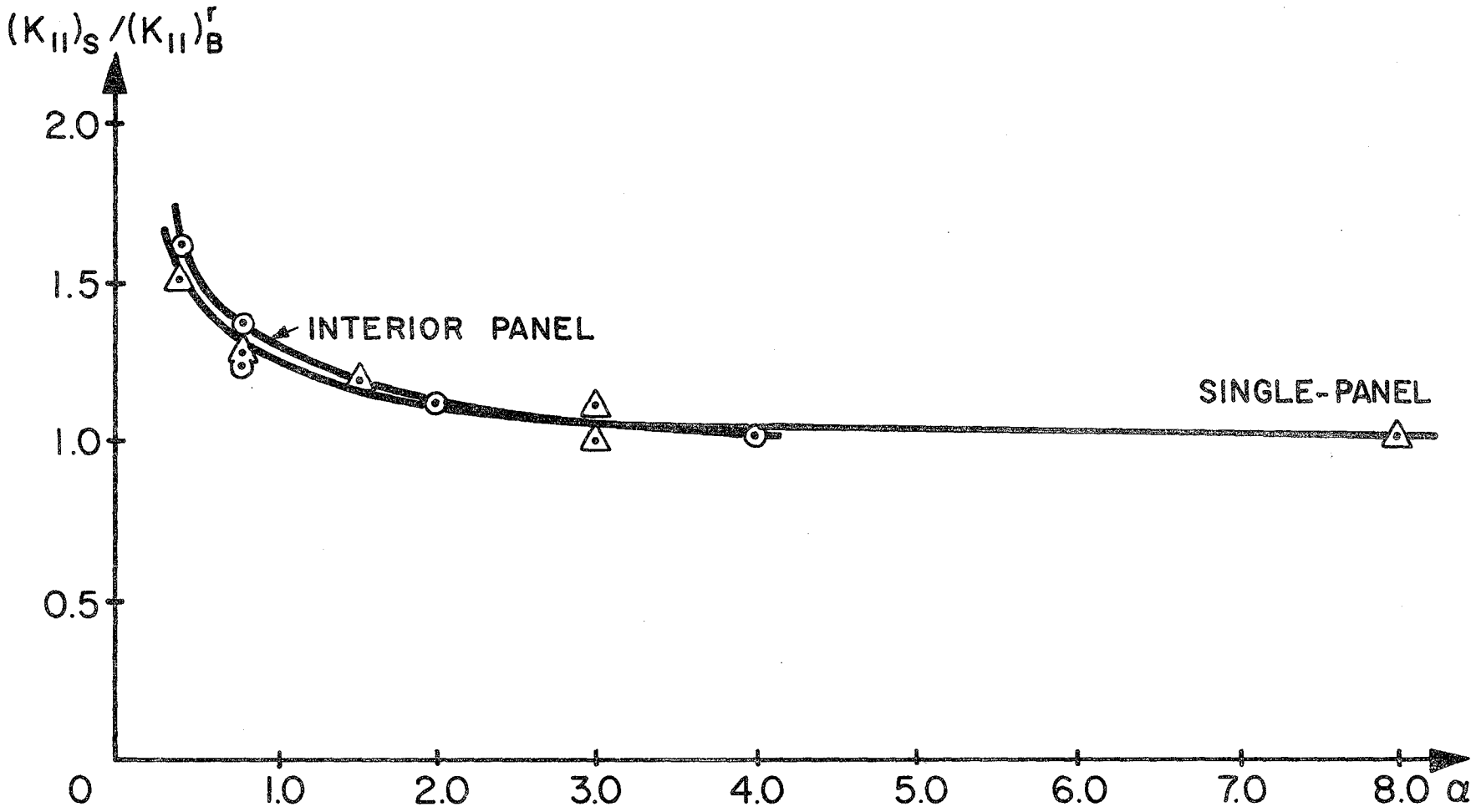

Fig. 4.8 $(K_{11})_S/(K_{11})^r_B$ vs. α for a Single-Panel Floor and an Interior Panel of Floor where $L_1/L_2 = 0.5$

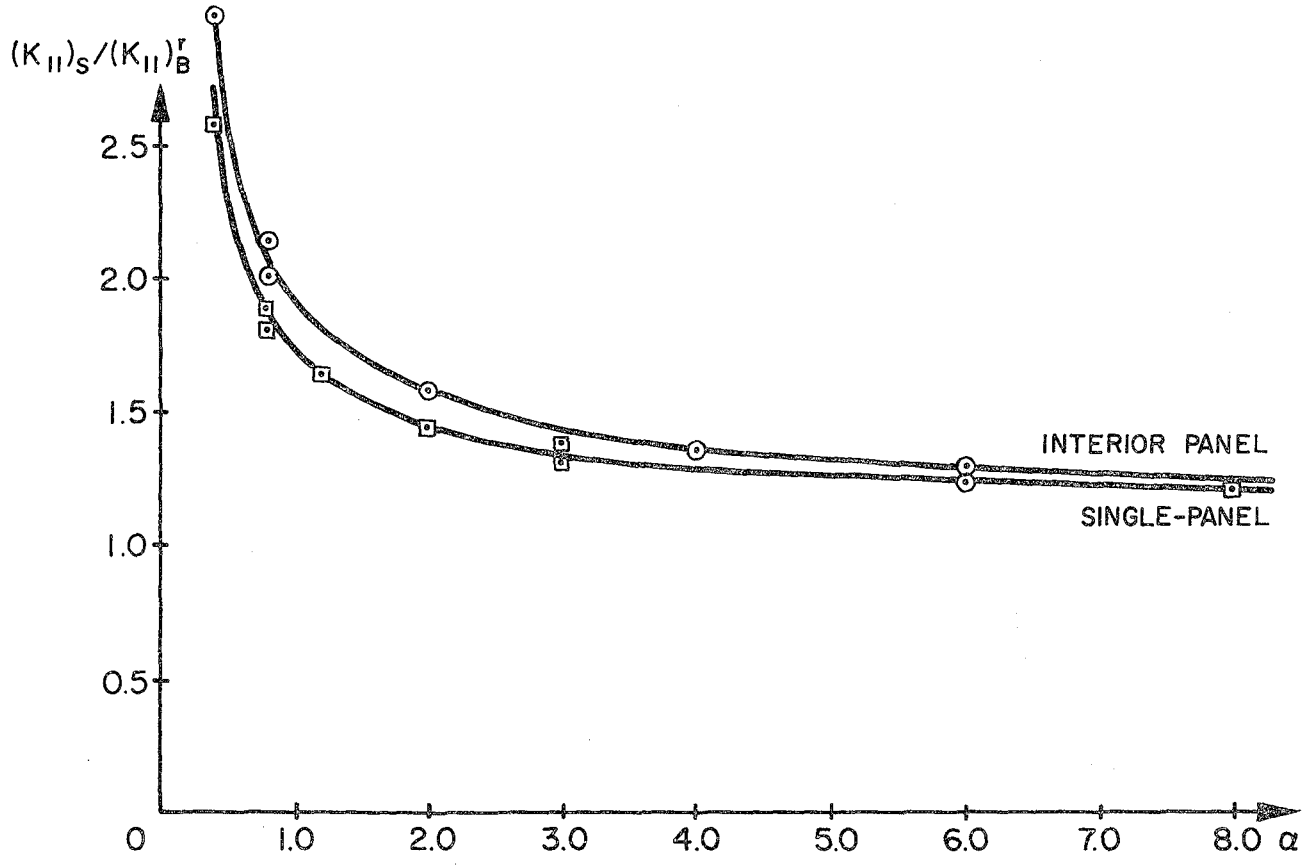

Fig. 4.9 $(K_{11})_S/(K_{11})^r_B$ vs. α for a Single-Panel Floor and an Interior Panel of Floor where $L_1/L_2 = 2.0$

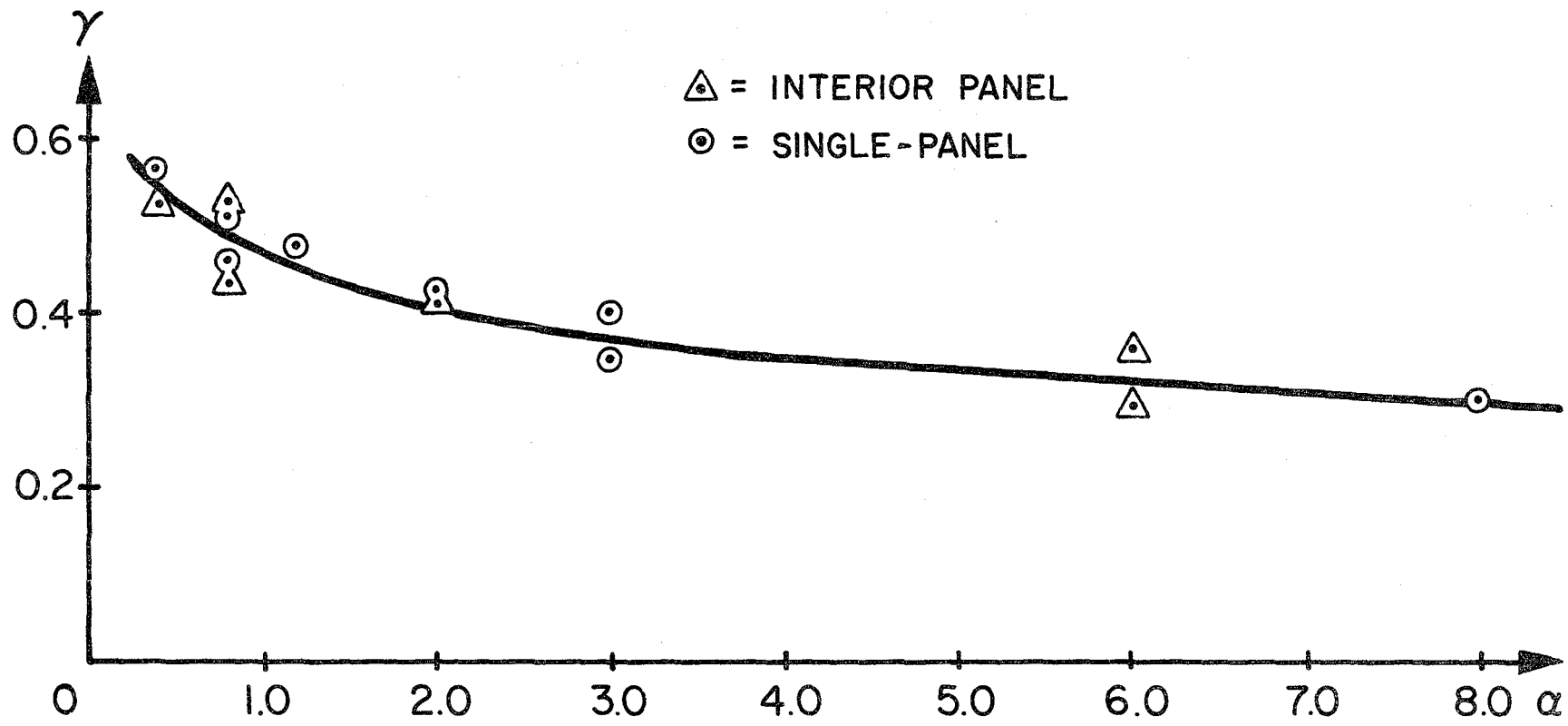

Fig. 4.10 γ vs. α for a Single-Panel Floor and an Interior Panel of Floor where $L_1/L_2 = 1.0$

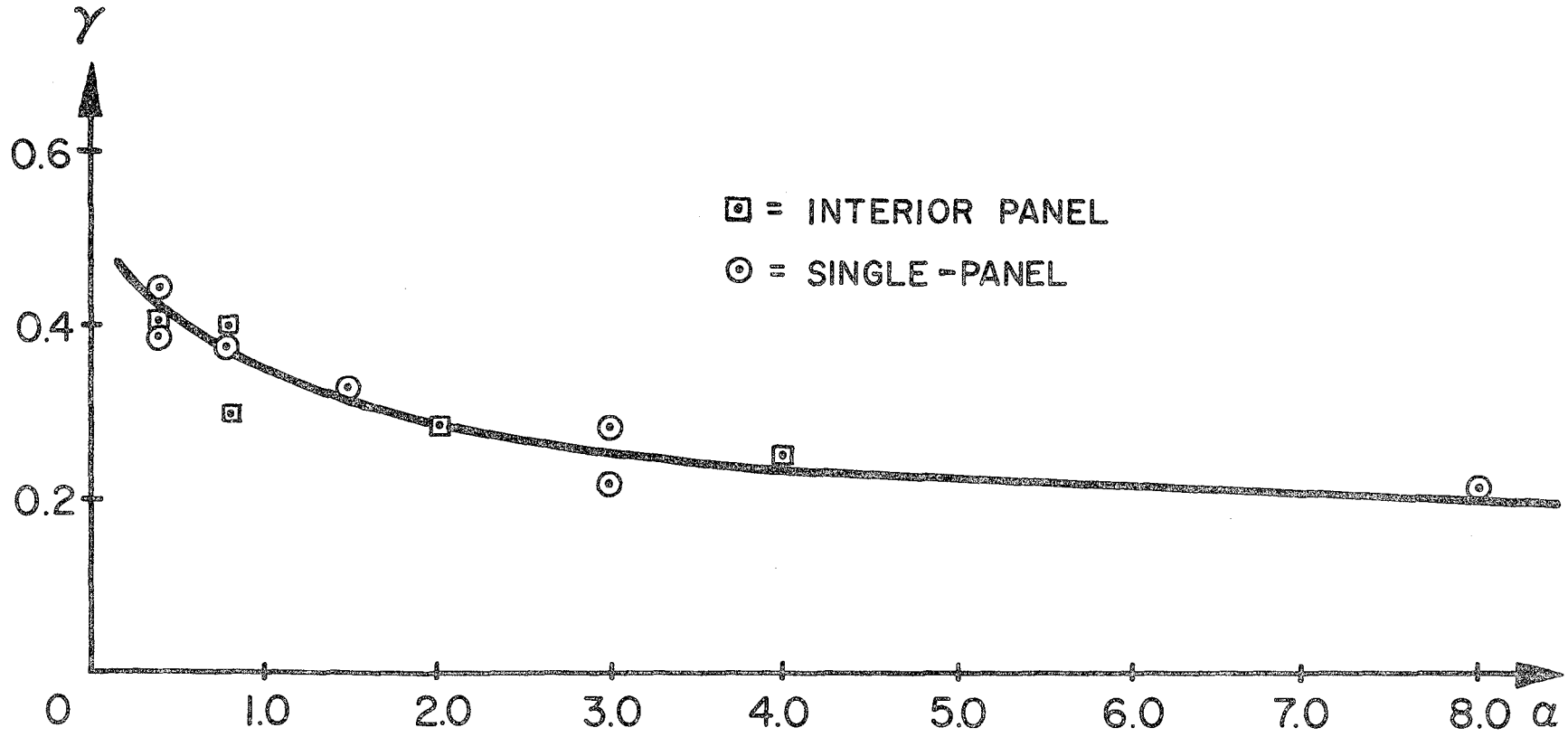

Fig. 4.11 γ vs. α for a Single-Panel Floor and an Interior Panel of Floor where $L_1/L_2 = 0.5$

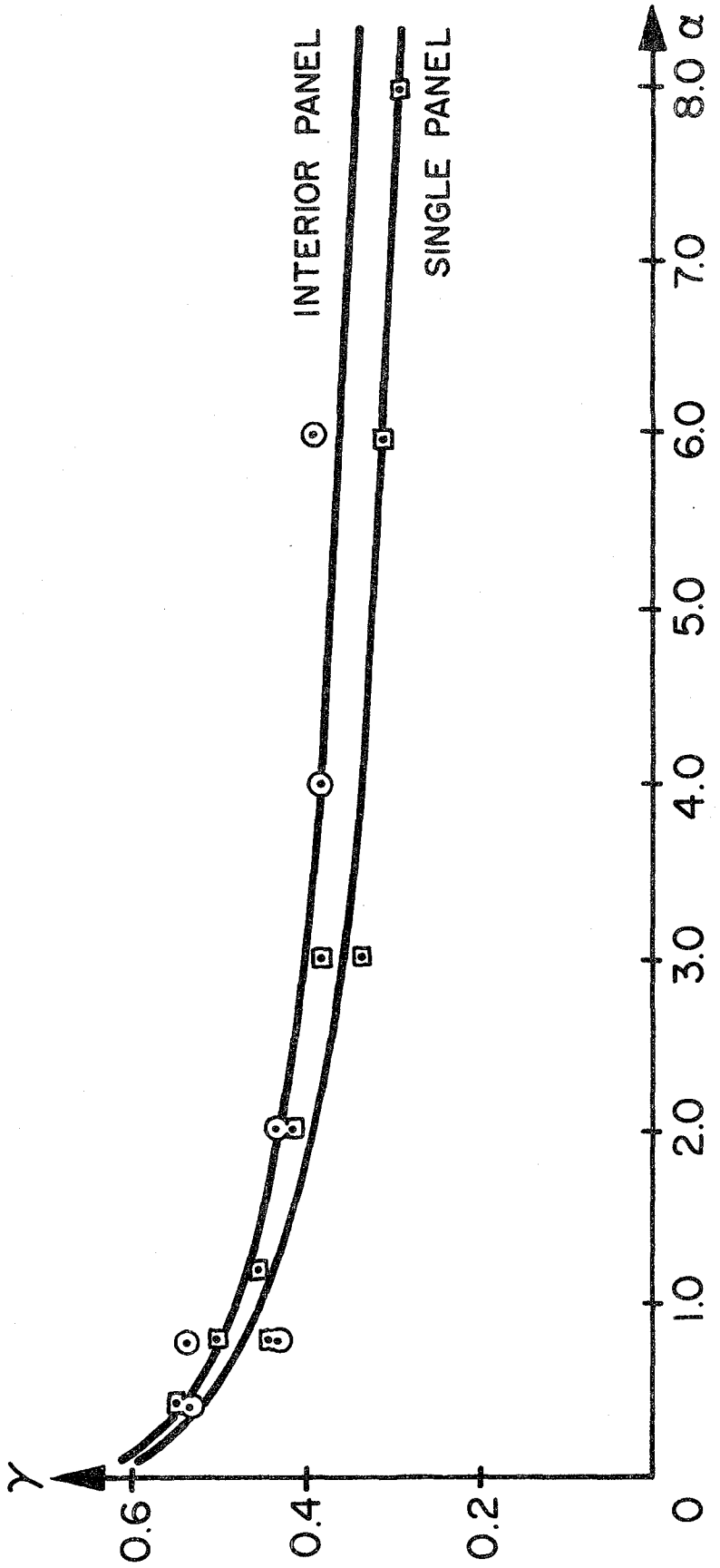

Fig. 4.12 γ vs. α for a Single-Panel Floor and an Interior Panel of Floor where $L_1/L_2 = 2.0$

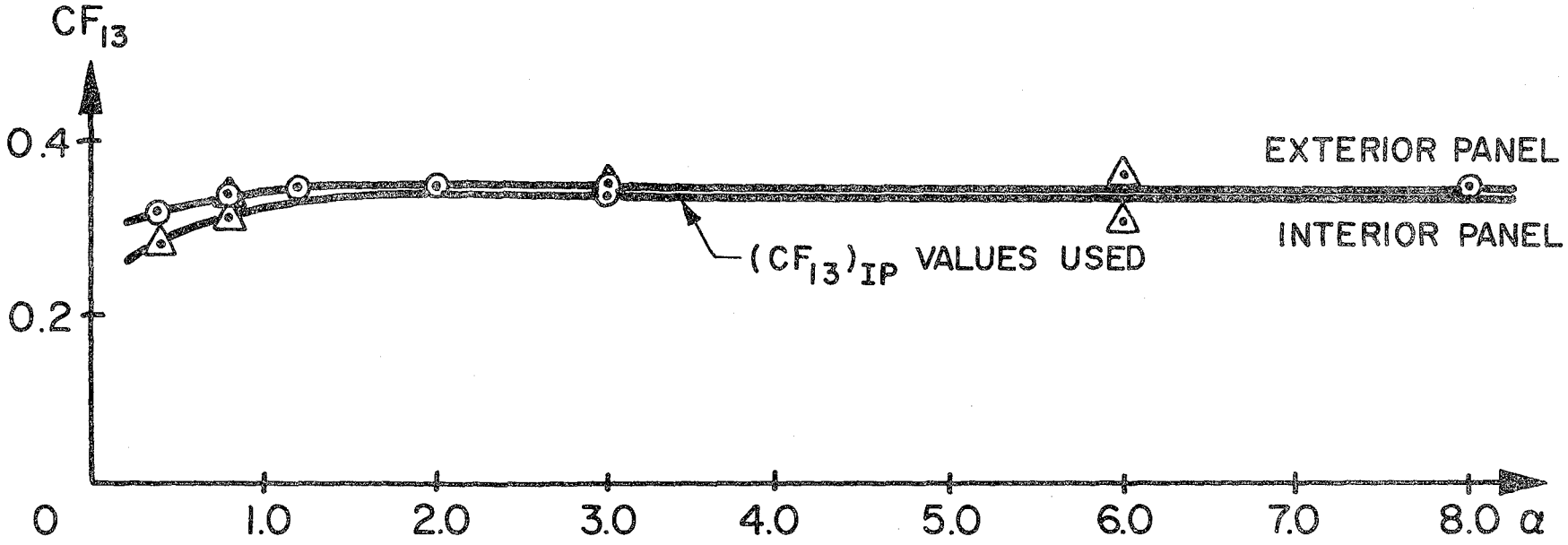

Fig. 4.13 Plot of CF_{13} vs. α for a Single-Panel Floor and an Interior Panel of Floor where $L_1/L_2 = 1.0$, $L_1 = 240$ in.

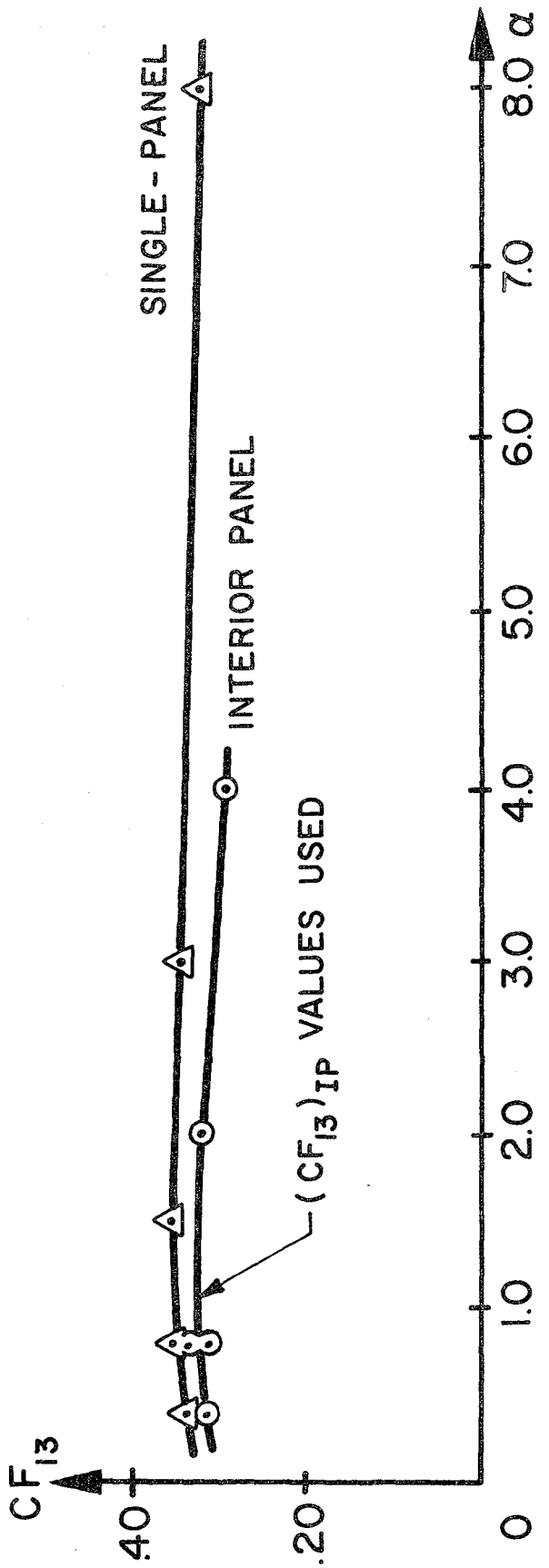

Fig. 4.14 Plot of CF_{13} vs. α for a Single-Panel Floor and an Interior Panel of Floor where $L_1/L_2 = 0.5$

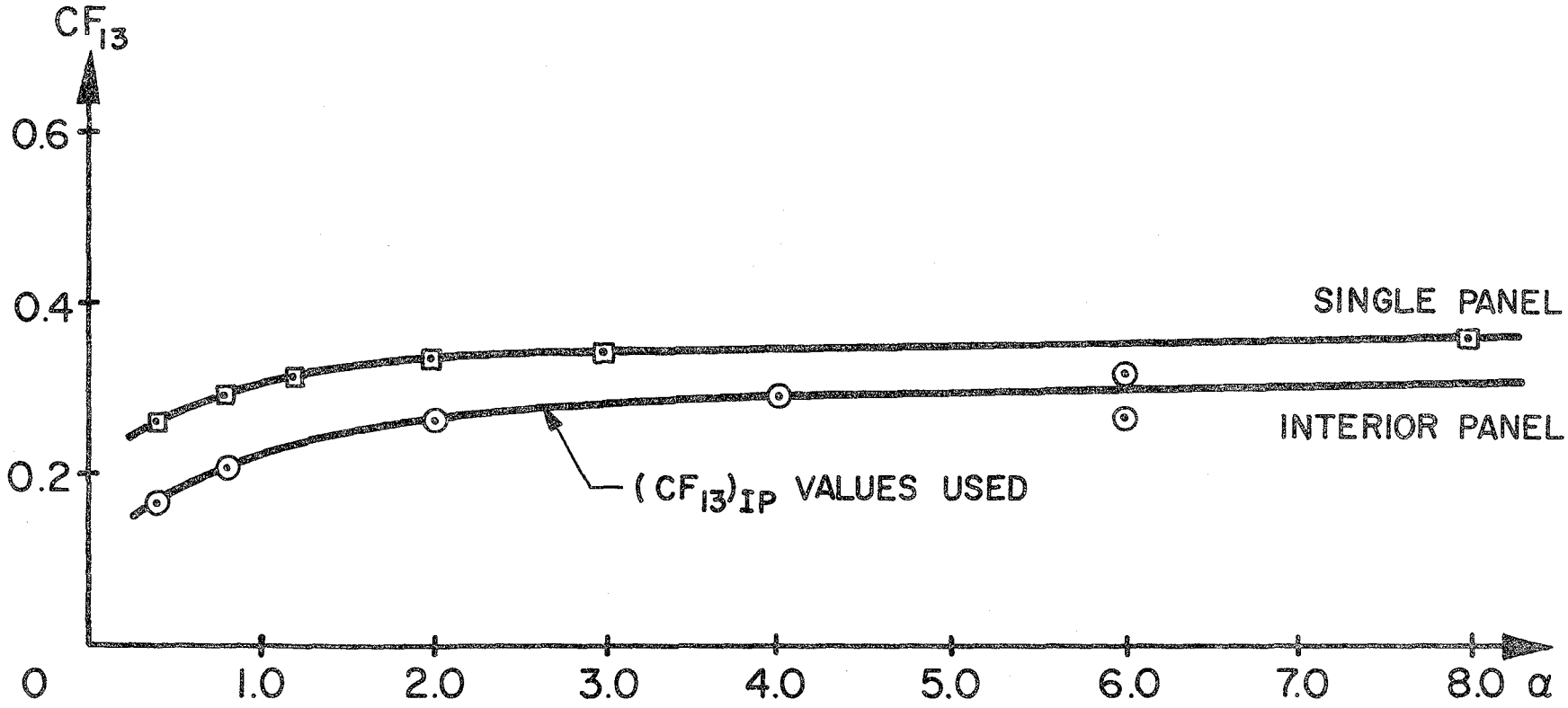

Fig. 4.15 Plot of CF_{13} vs. α for a Single-Panel Floor and an Interior Panel of Floor where $L_1/L_2 = 2.0$, L_1 - 240 in.

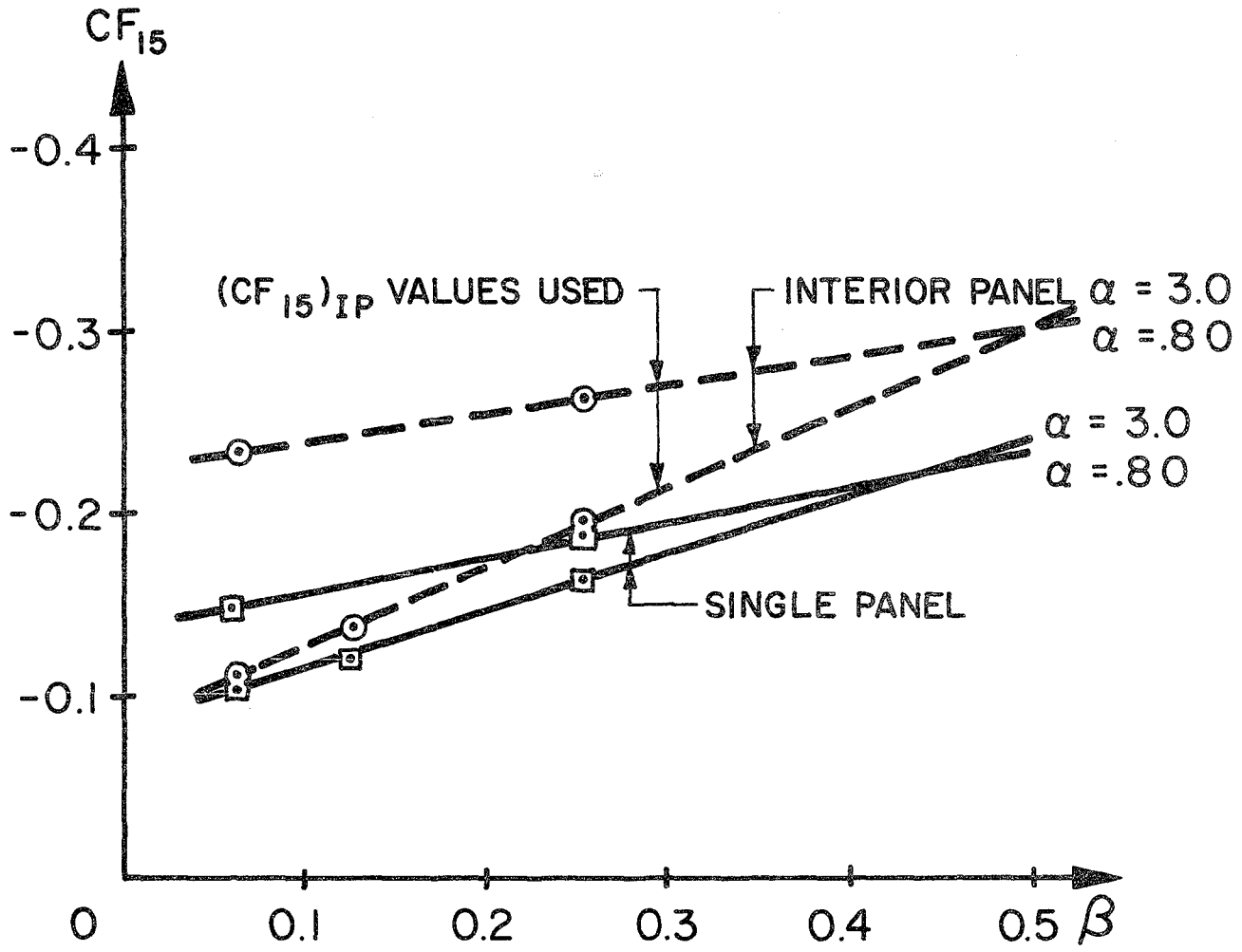

Fig. 4.16 CF_{15} vs. β for a Single-Panel Floor and an Interior Panel of Floor where L_1/L_2 = 2.0, L_1 = 240 in.

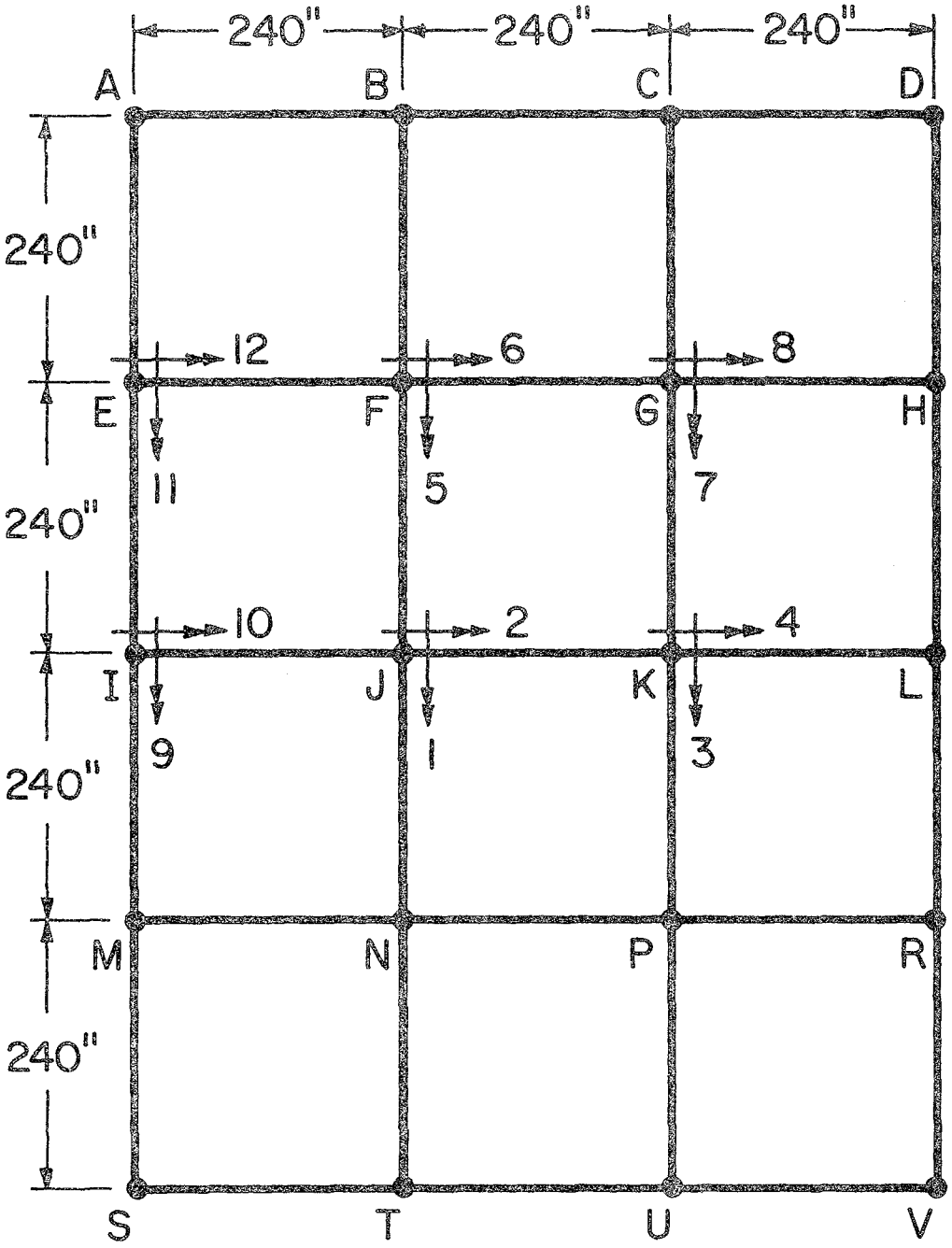

Fig. 4.17 Exterior Panel and Degrees of Freedom

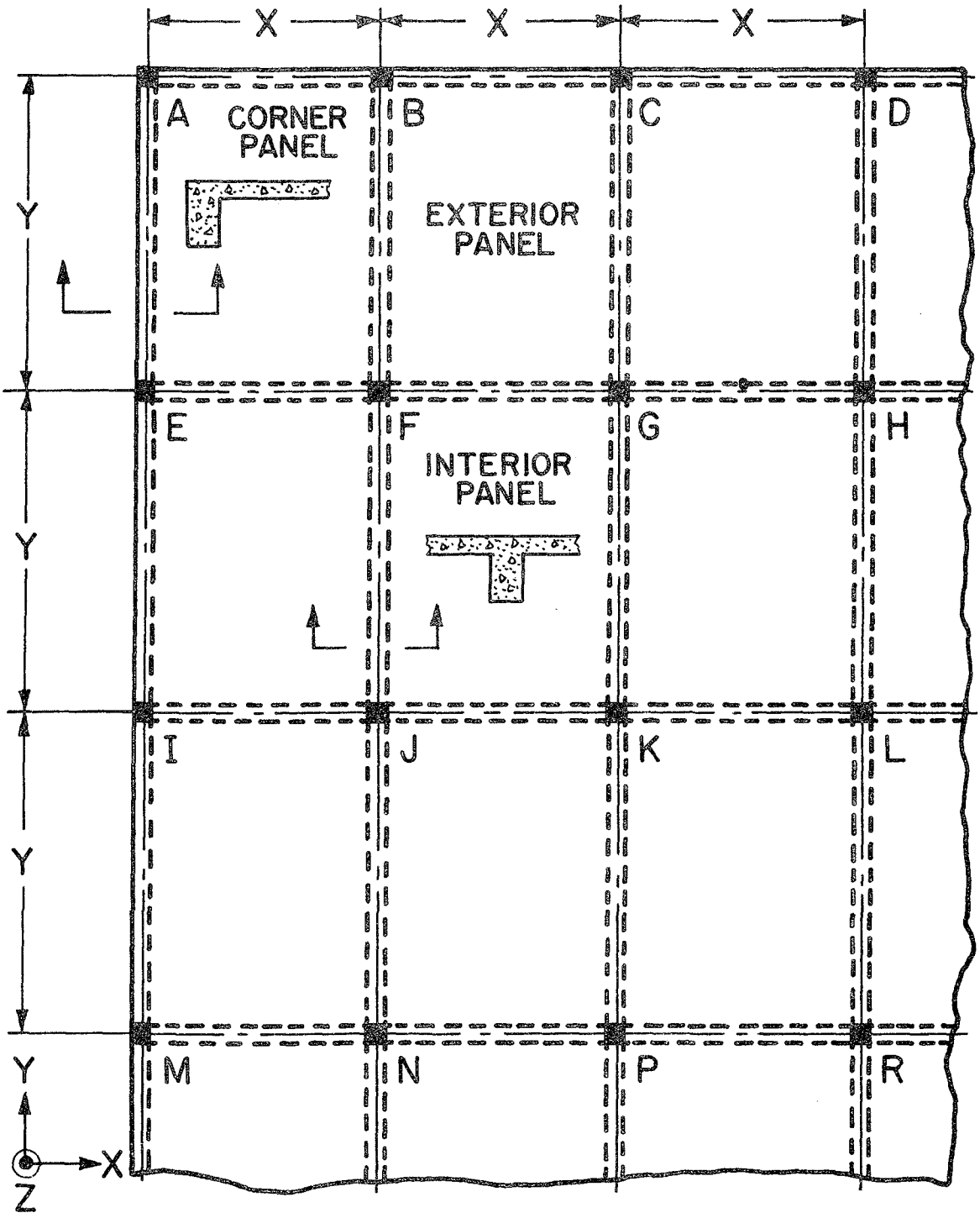

Fig. 5.1 Typical Multi-Panel Two-Way Slab Floor

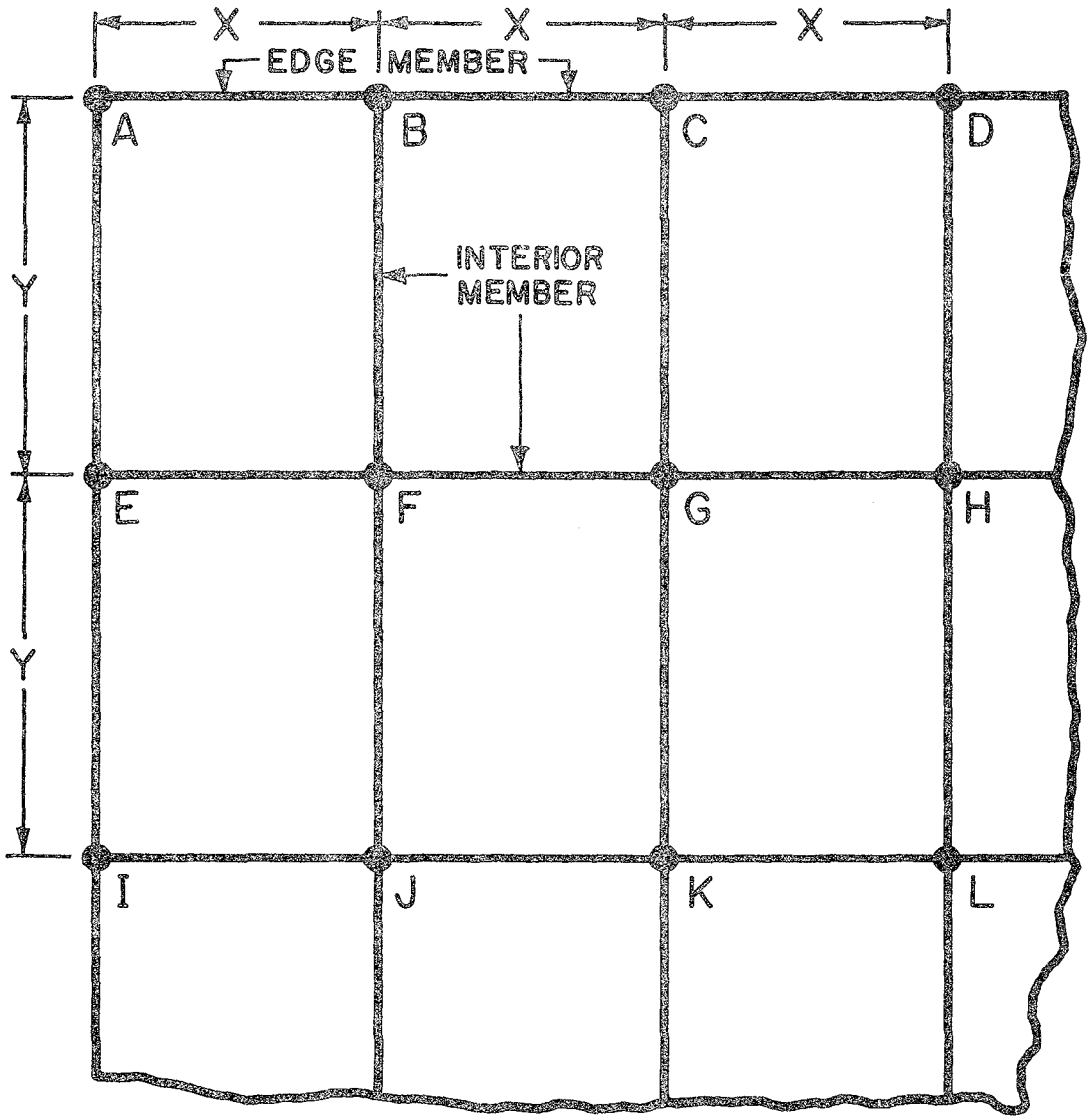

(a) Stiffness matrix method model

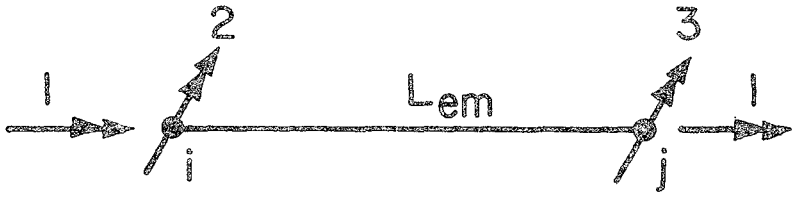

(b) Equivalent member degrees of freedom

Fig. 5.2 Stiffness Matrix Method Floor Model

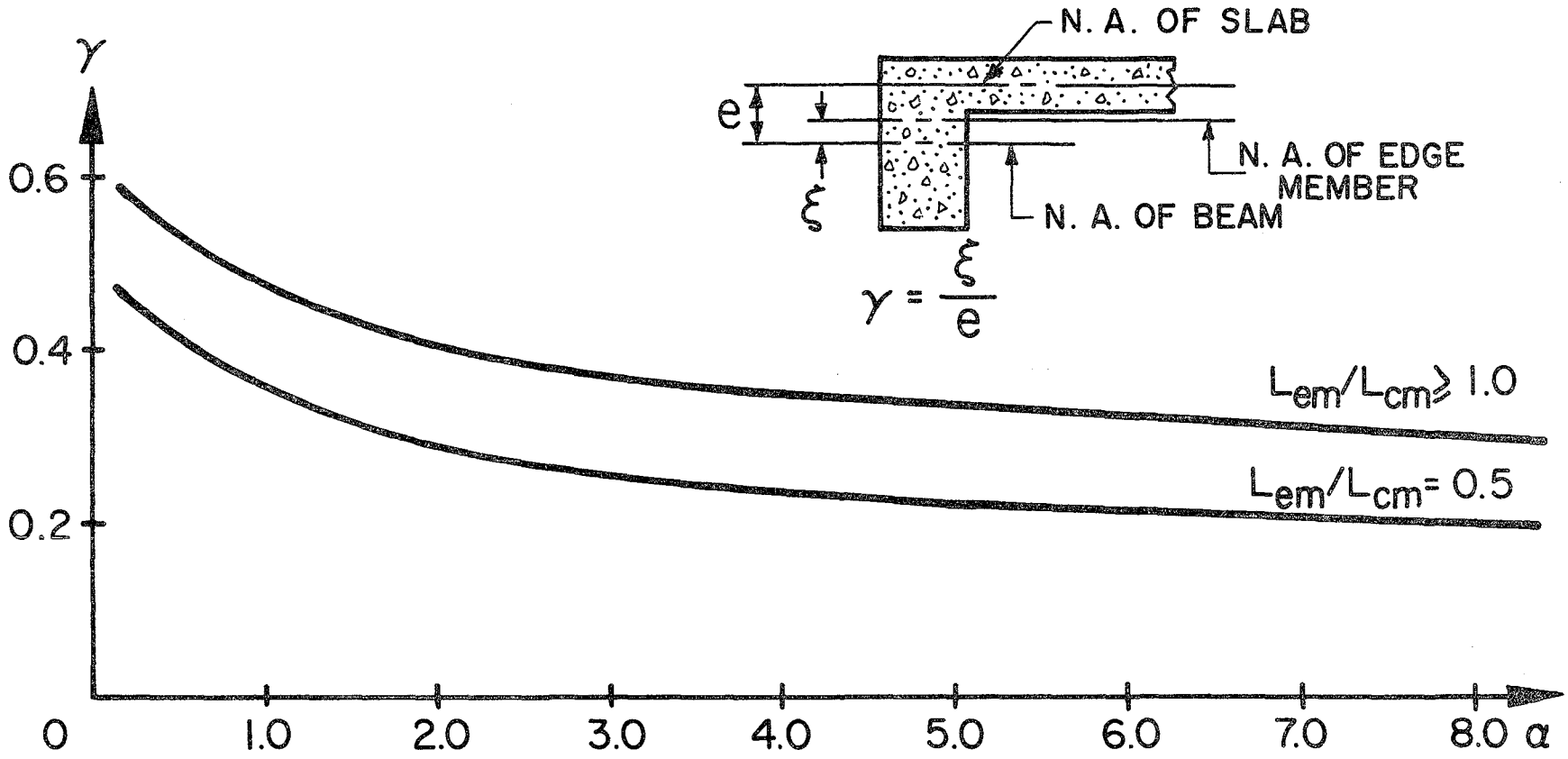

Fig. 5.3a γ vs. α for an Equivalent Edge Member of a Two-Way Slab Floor System

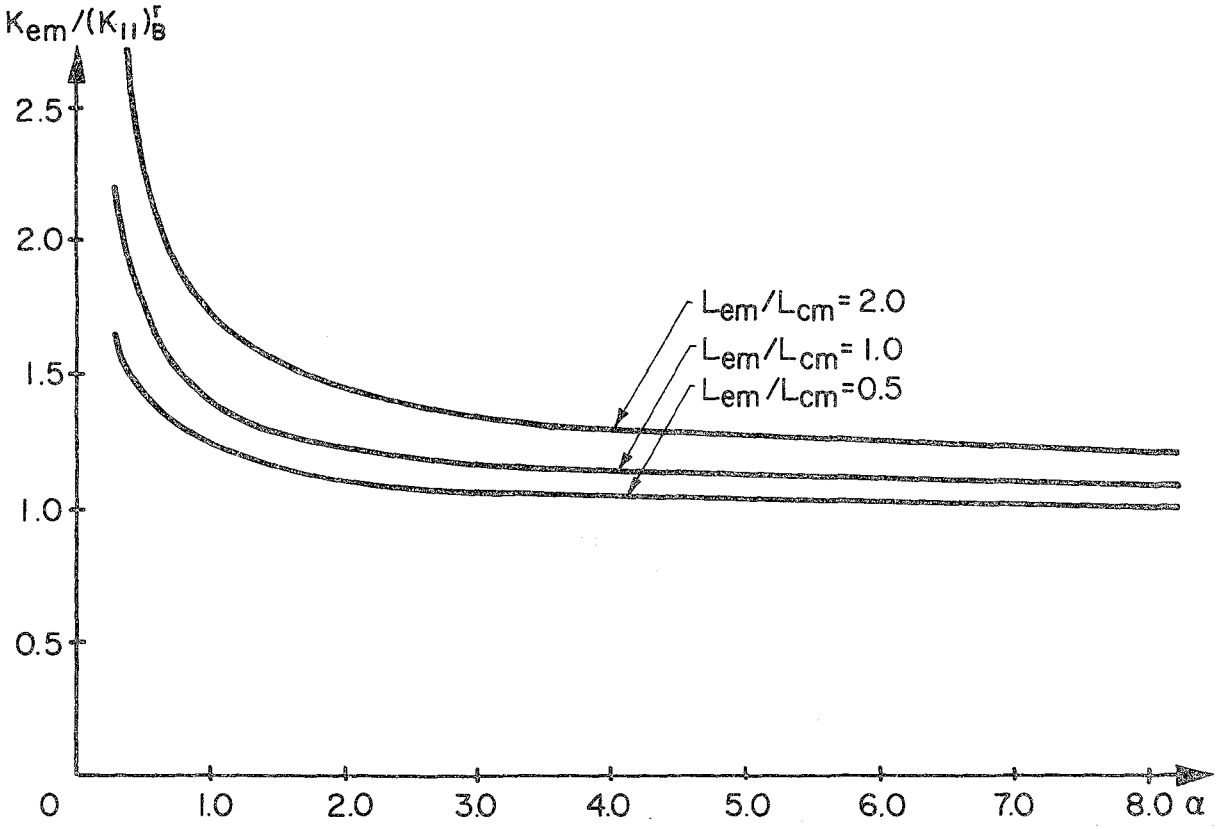

Fig. 5.3b $K_{em}/(K_{11})^r_B$ vs. α for an Equivalent Edge Member of a Two-Way Slab Floor System

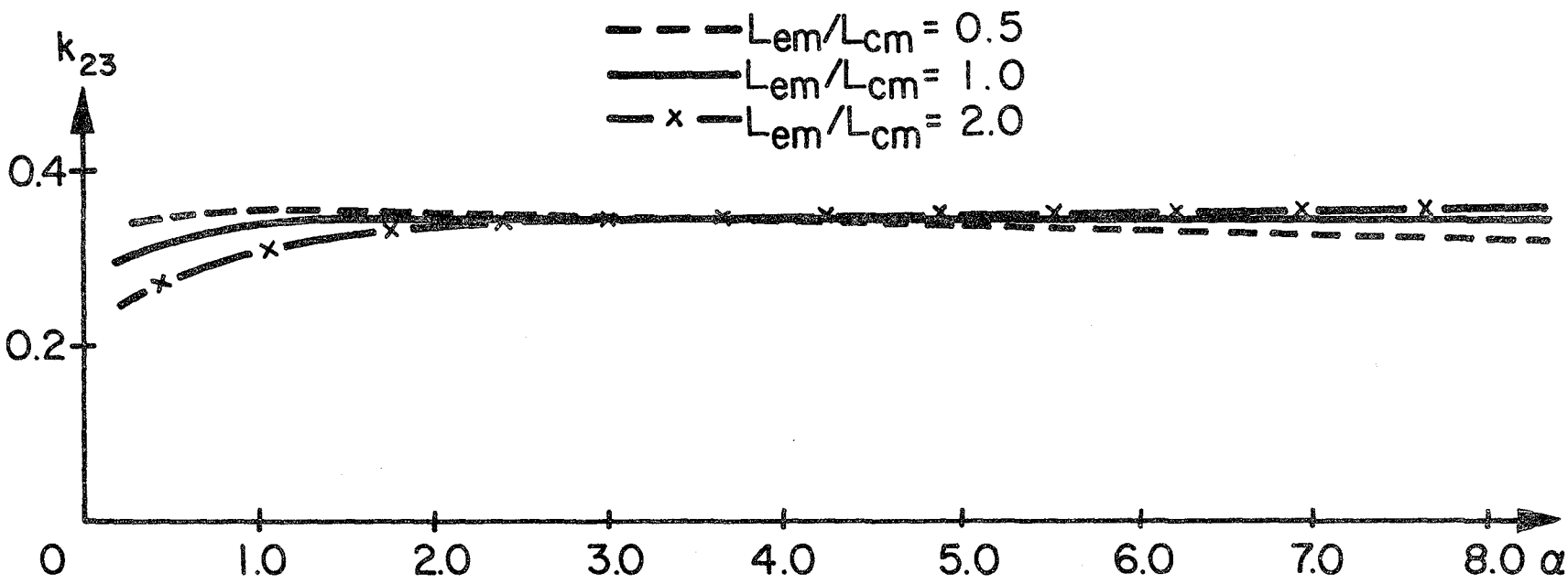

Fig. 5.3c k_{23} vs. α for an Equivalent Edge Member of a Two-Way Slab Floor System

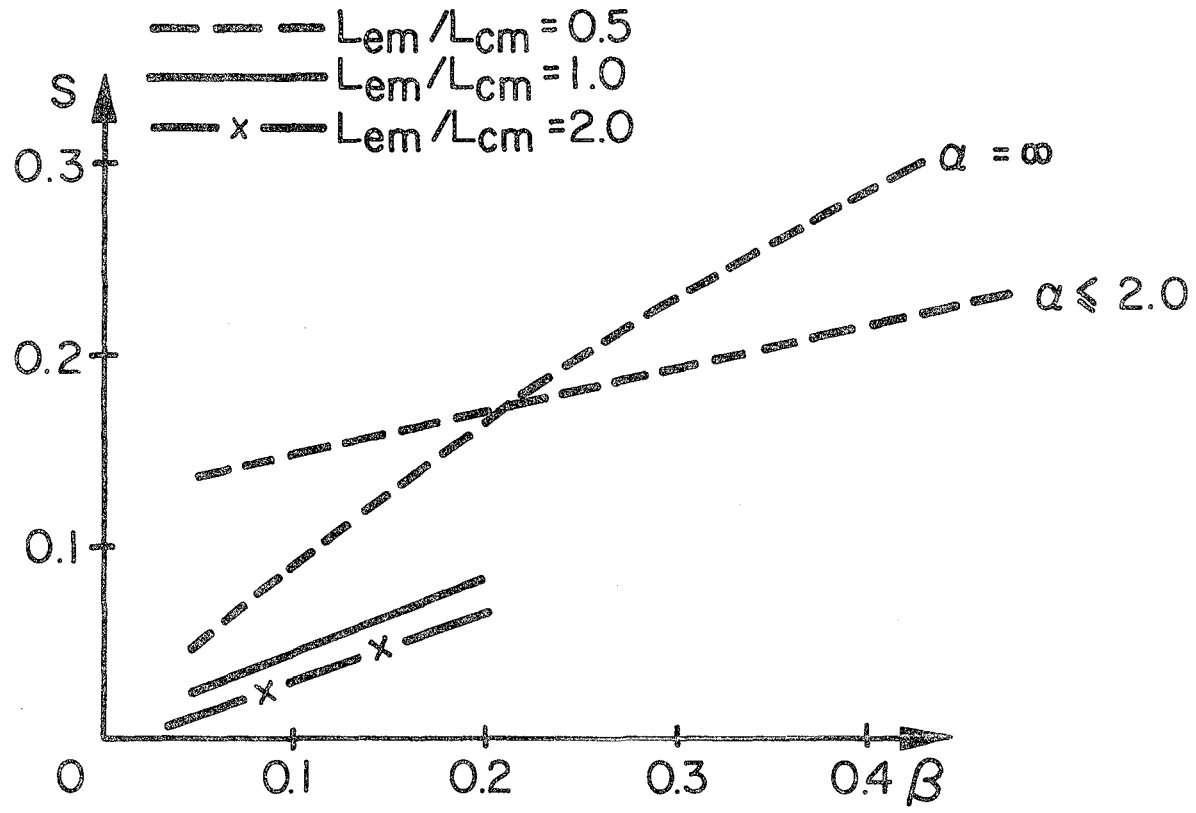

Fig. 5.3d S vs. β for an Equivalent Edge Member of a Two-Way Slab Floor System

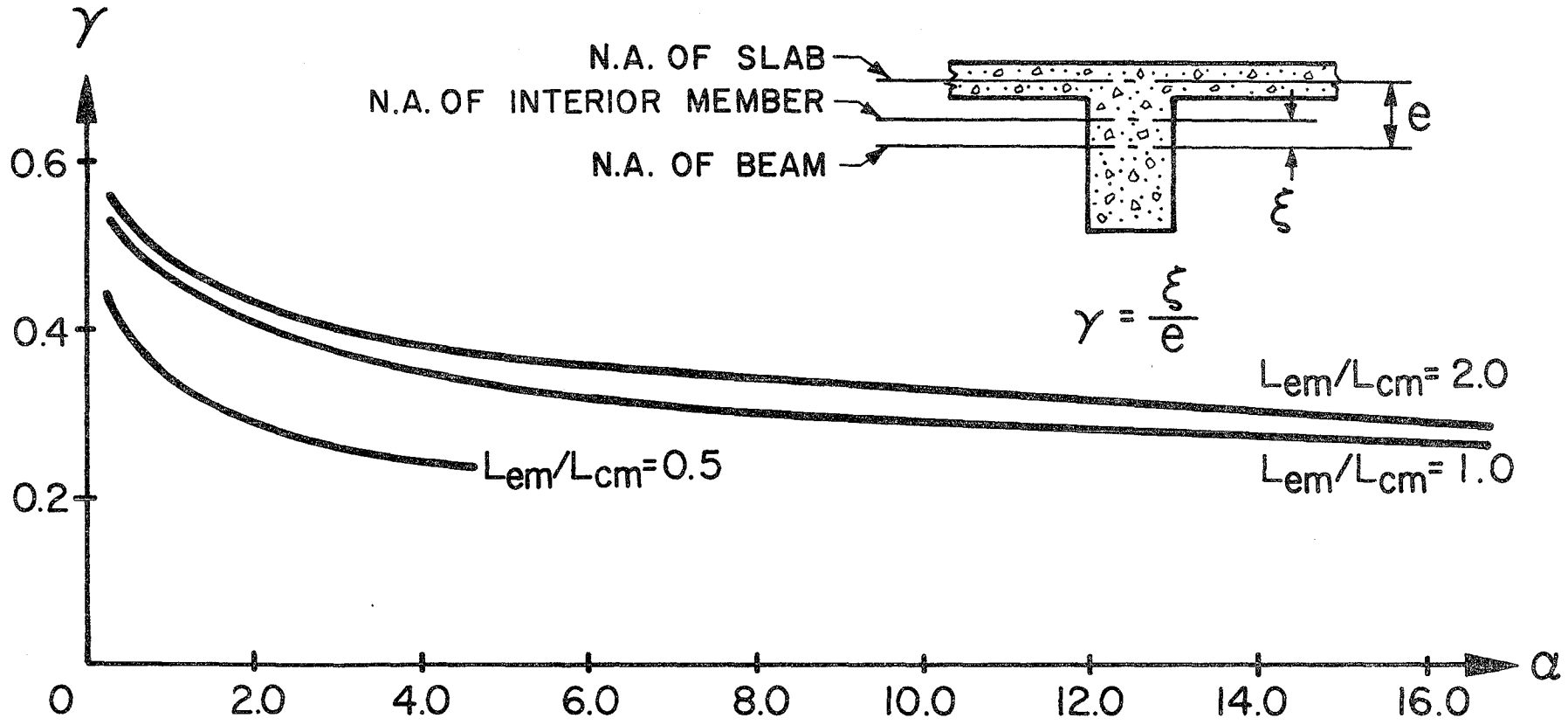

Fig. 5.4a γ vs. α for an Equivalent Interior Member of a Two-Way Slab Floor System

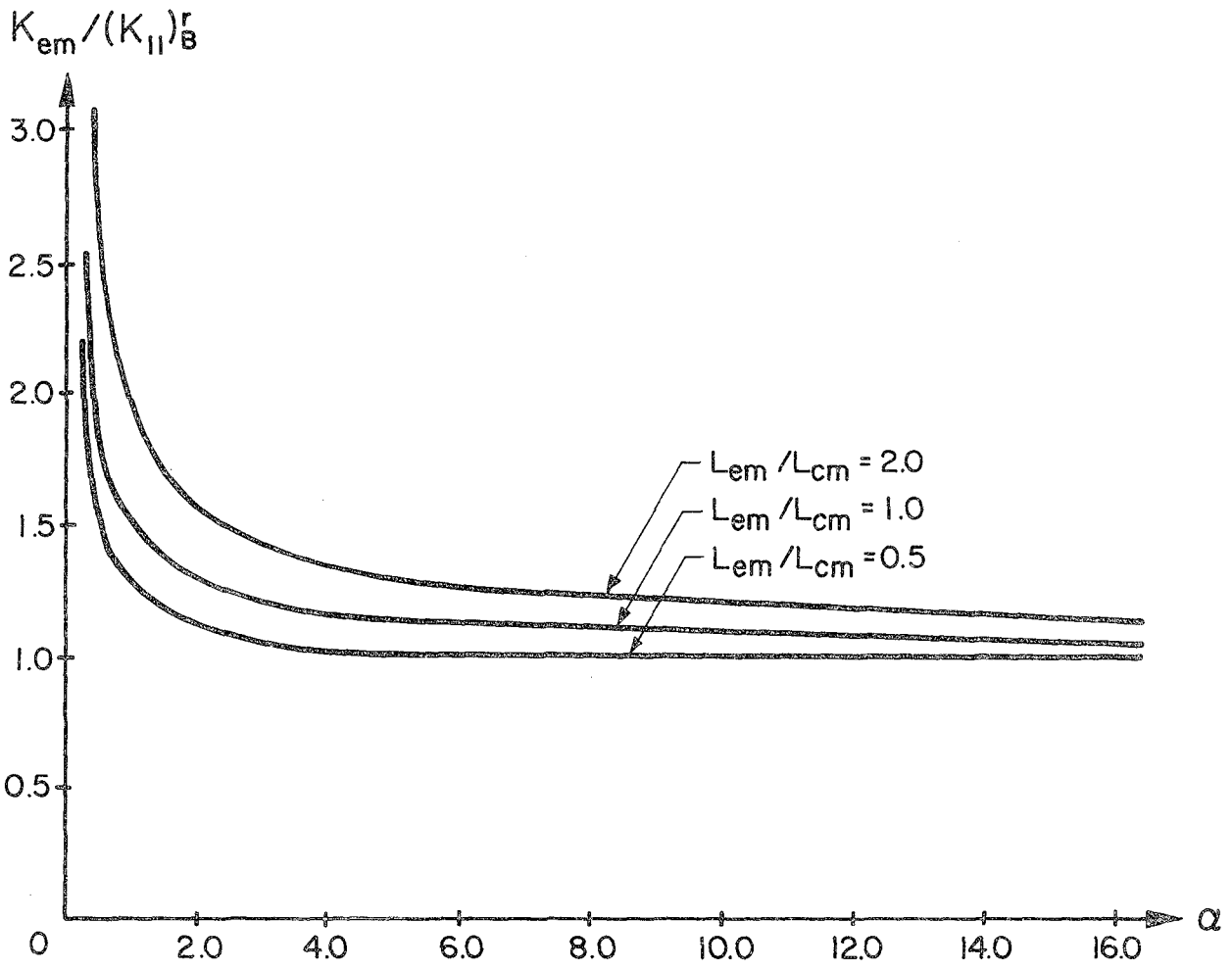

Fig. 5.4b $K_{em}/(K_{11})^r_B$ vs. α for an Equivalent Interior Member of a Floor

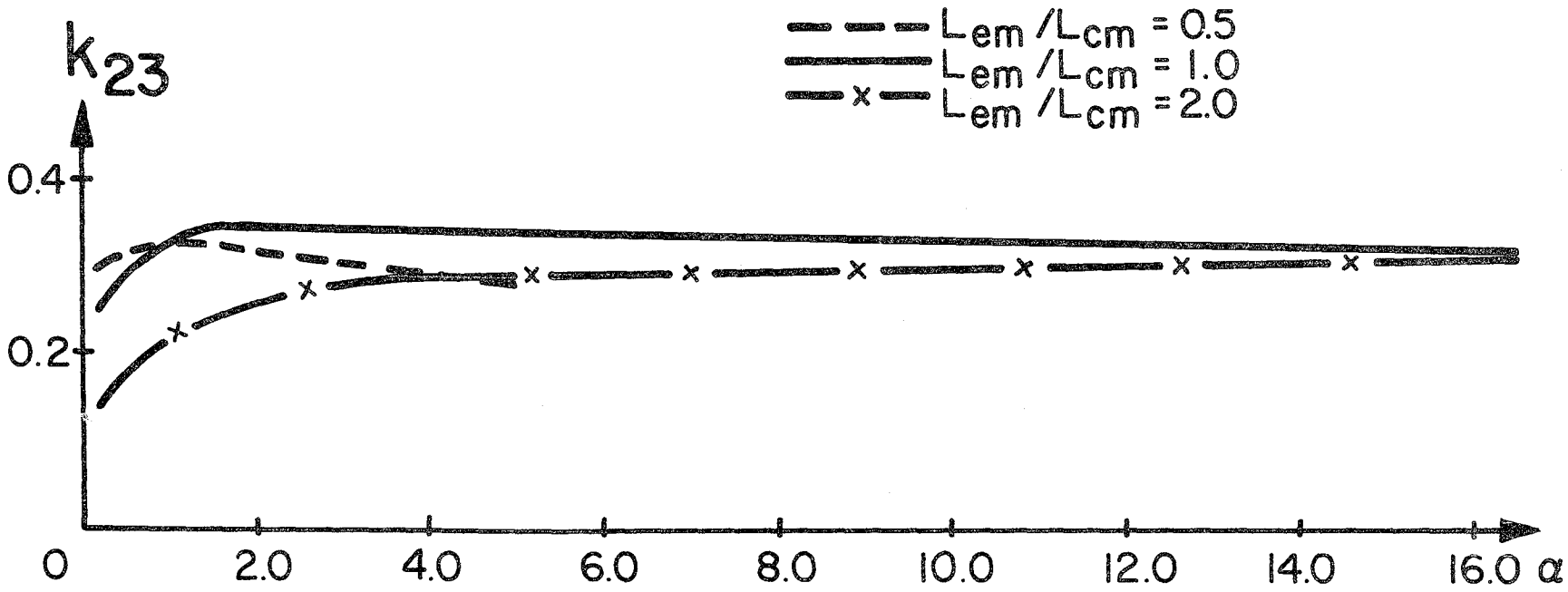

Fig. 5.4c k_{23} vs. α for an Equivalent Interior Member of a Two-Way Slab Floor

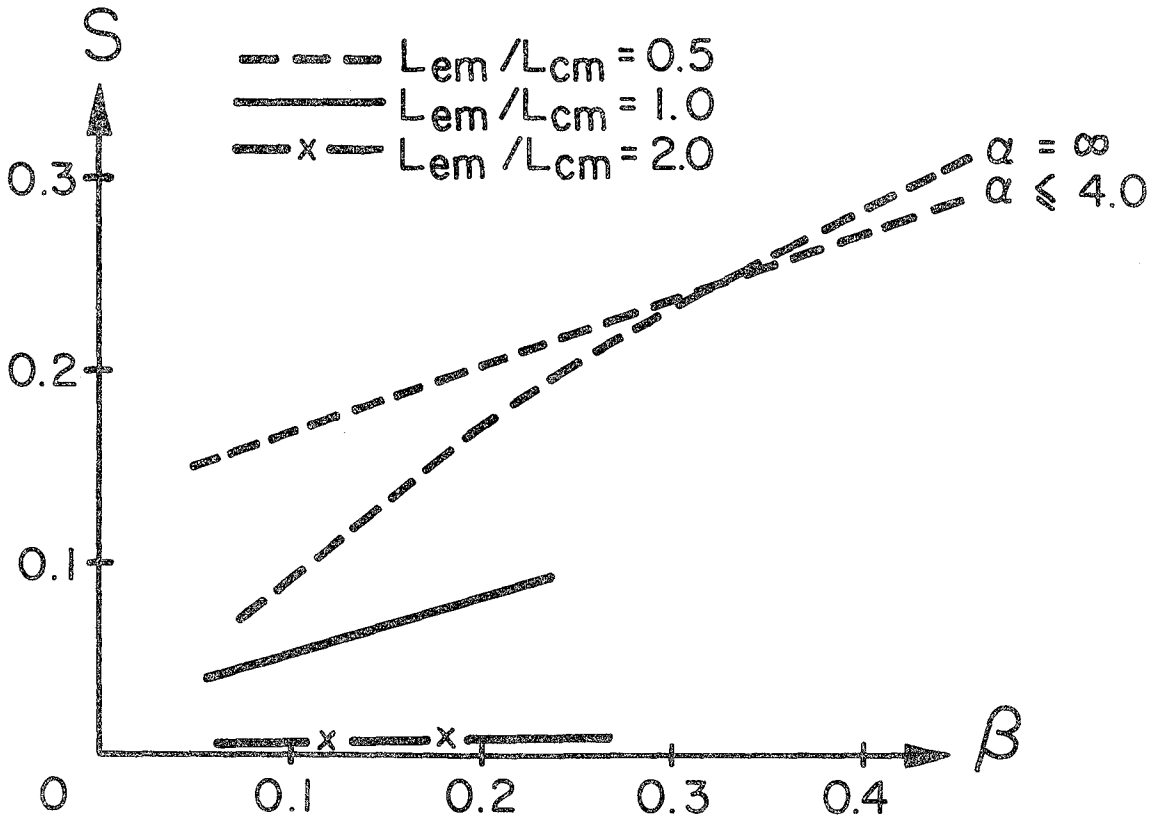

Fig. 5.4d S vs. β for an Equivalent Interior Member of a Two-Way Slab Floor System

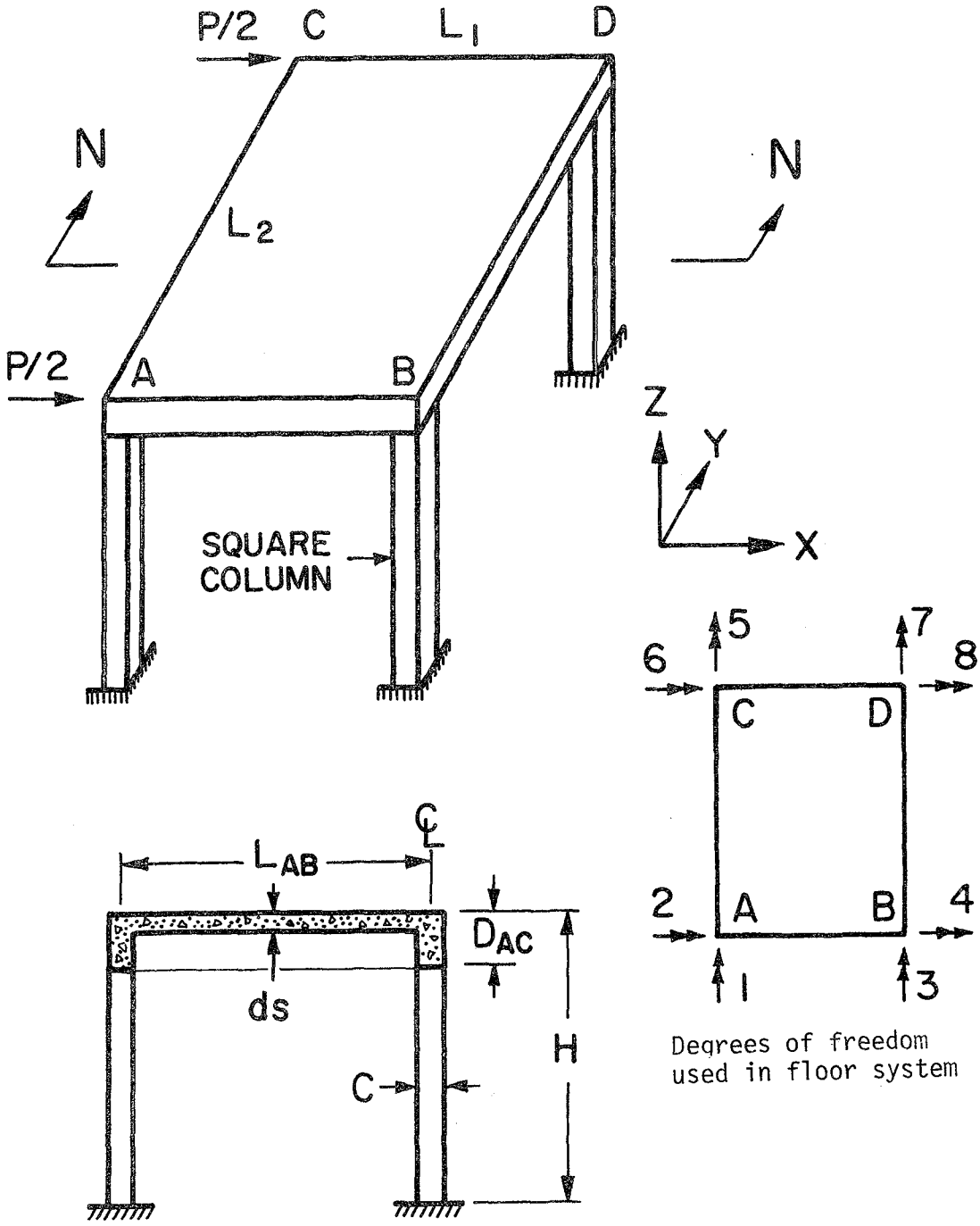

Fig. 5.5 Single-Panel, Single-Story Structure under Lateral Loading

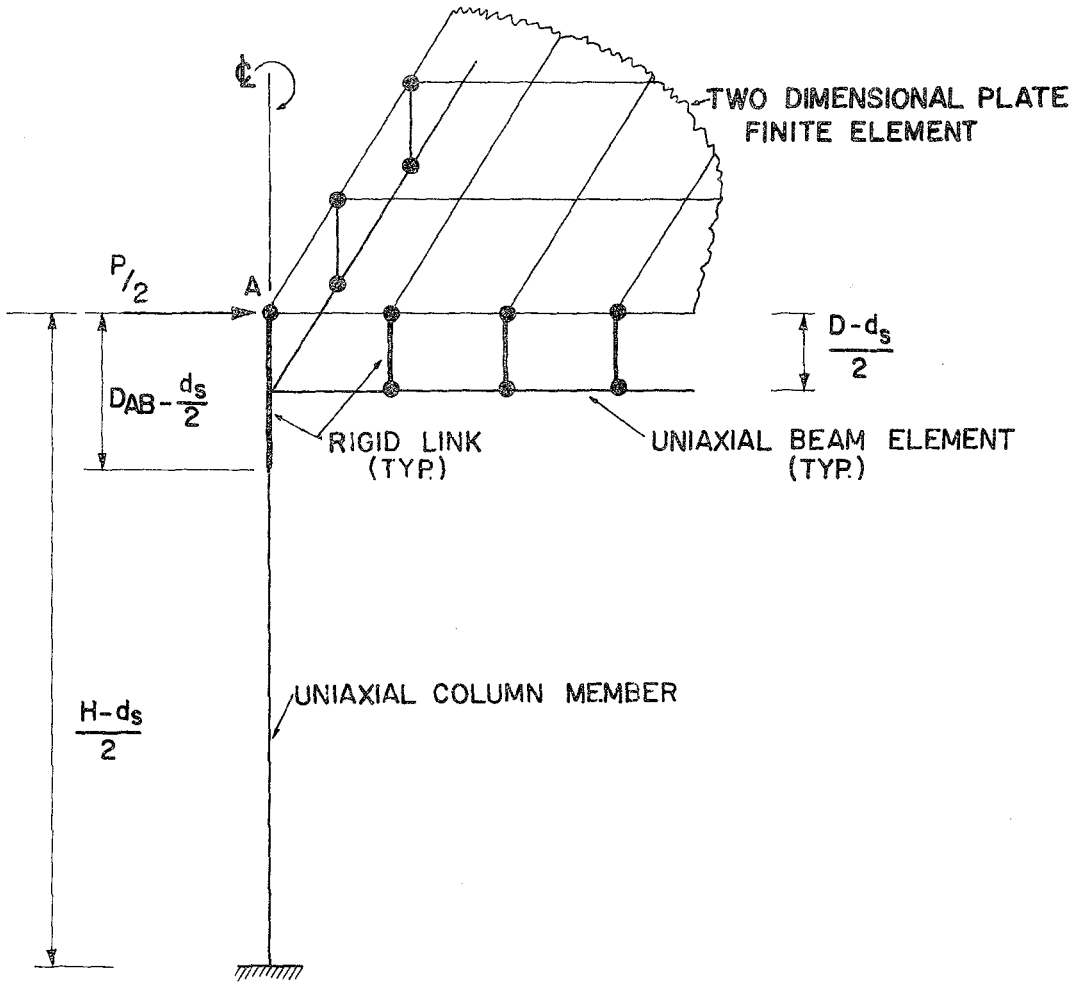

Fig. 5.6 Finite Element Model of Single-Panel, Single-Story Structure

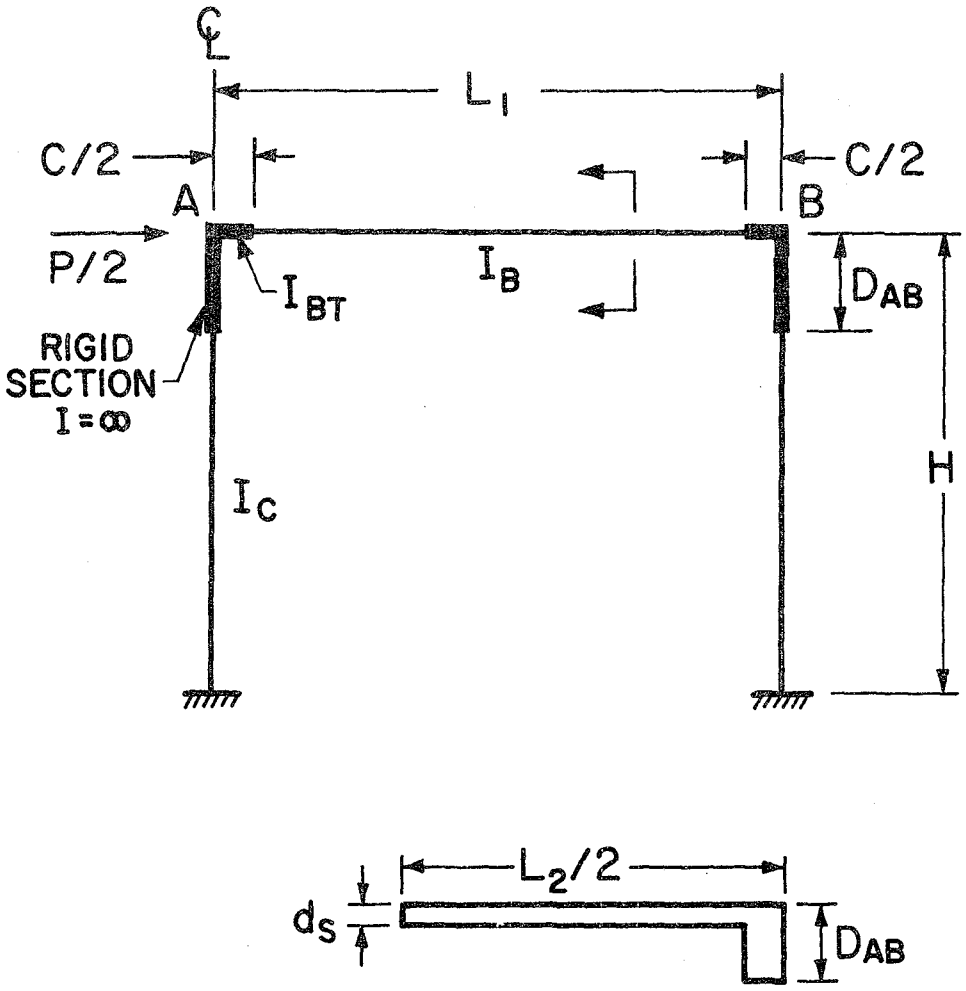

Fig. 5.7 Equivalent Frame Model of Single-Panel, Single-Story Structure

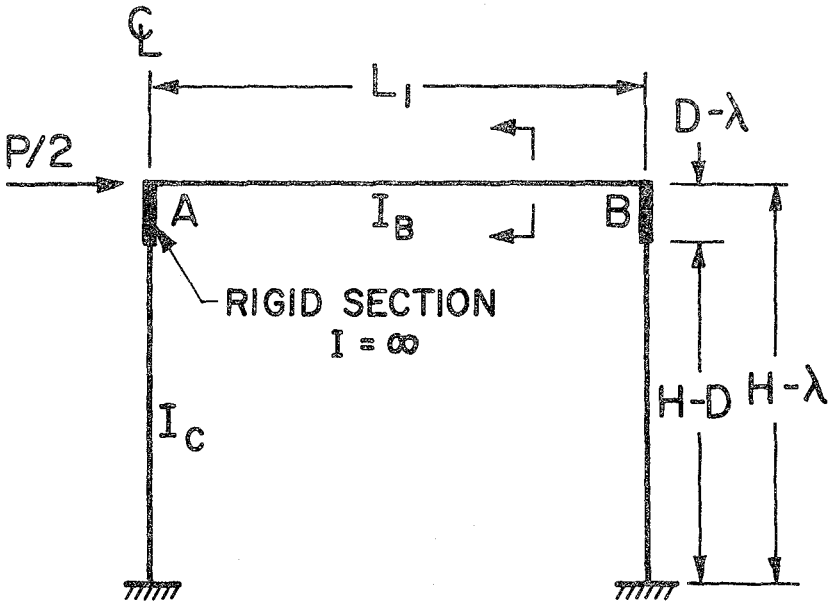

$b_f \leq 1/12(L_1)$

$b_f \leq 6\ d_s$

$b_f \leq 1/2(L_2)$

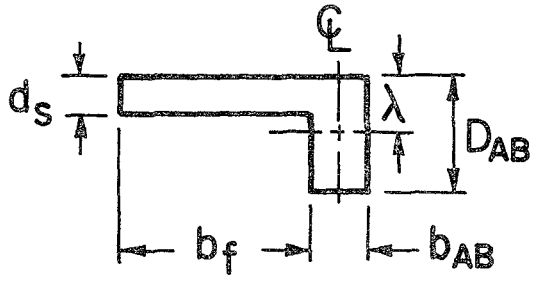

Fig. 5.8 Model of Single-Panel, Single-Story Structure Based on ACI 318-71, Section 8.7

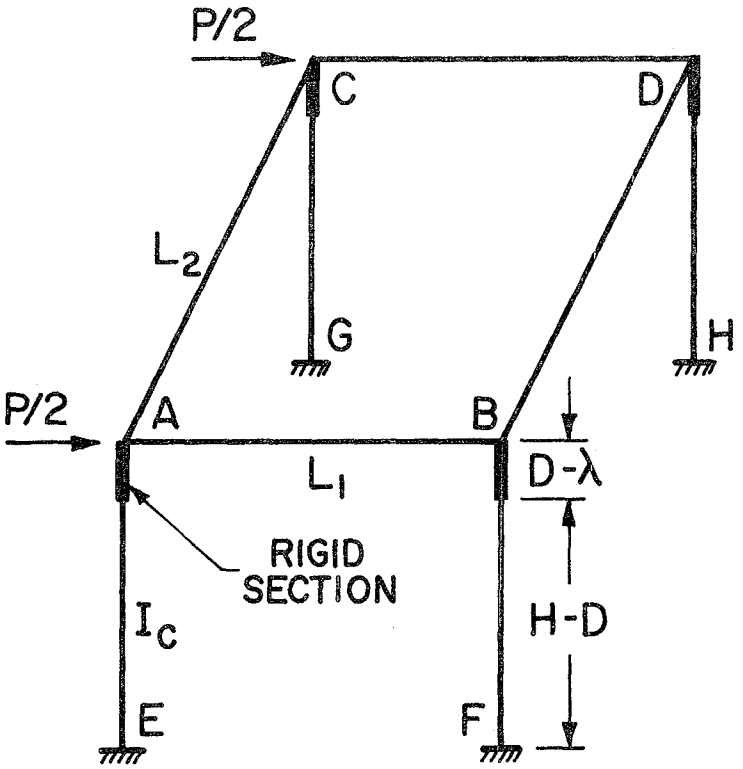

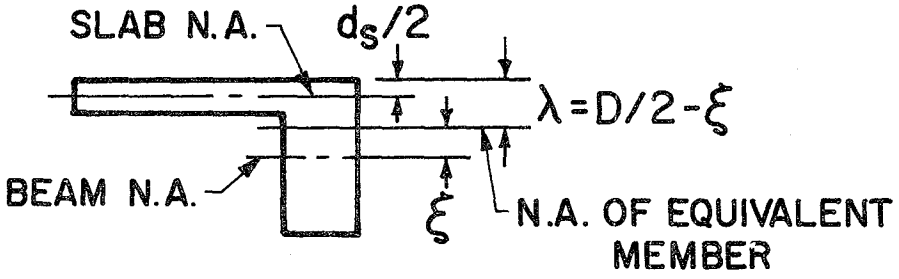

Fig. 5.9 Stiffness Matrix Method Model of Single-Panel, Single-Story Structure

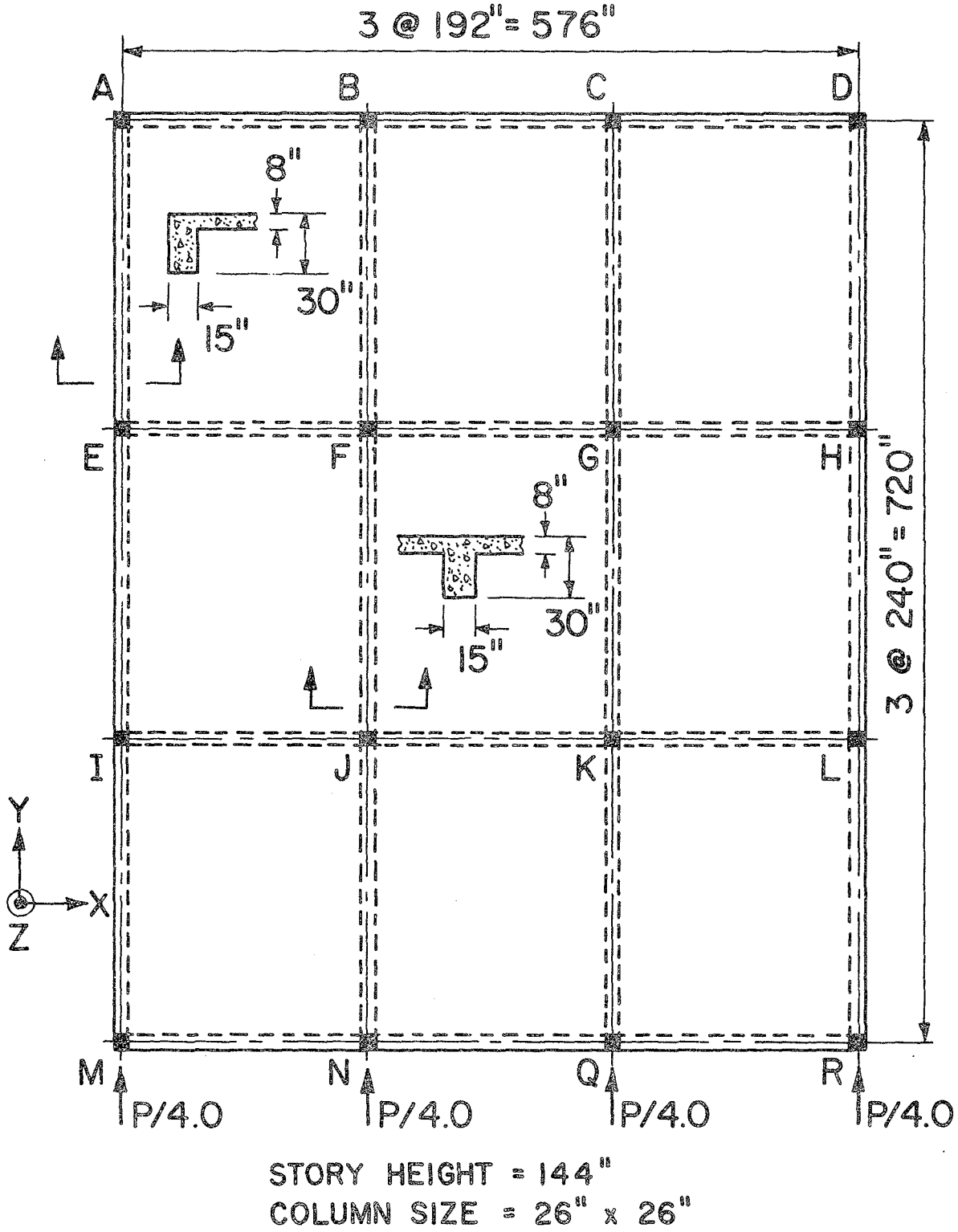

Fig. 5.10 Multi-Panel, Single-Story Structure under Lateral Loading

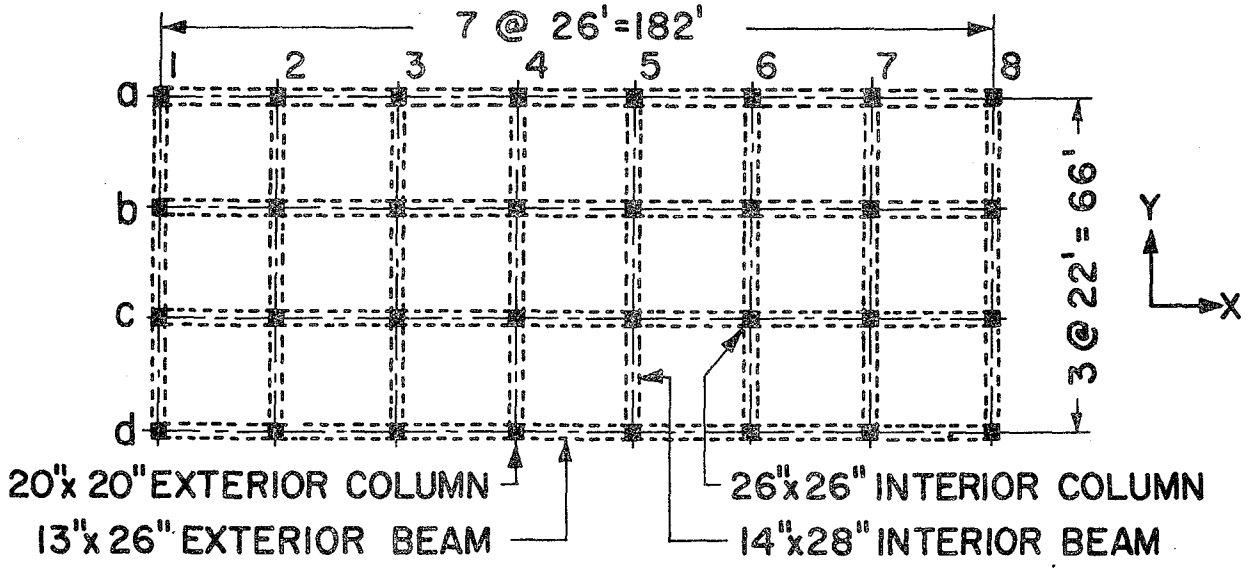

FLOOR SYSTEM PLAN OF 12-STORY BUILDING

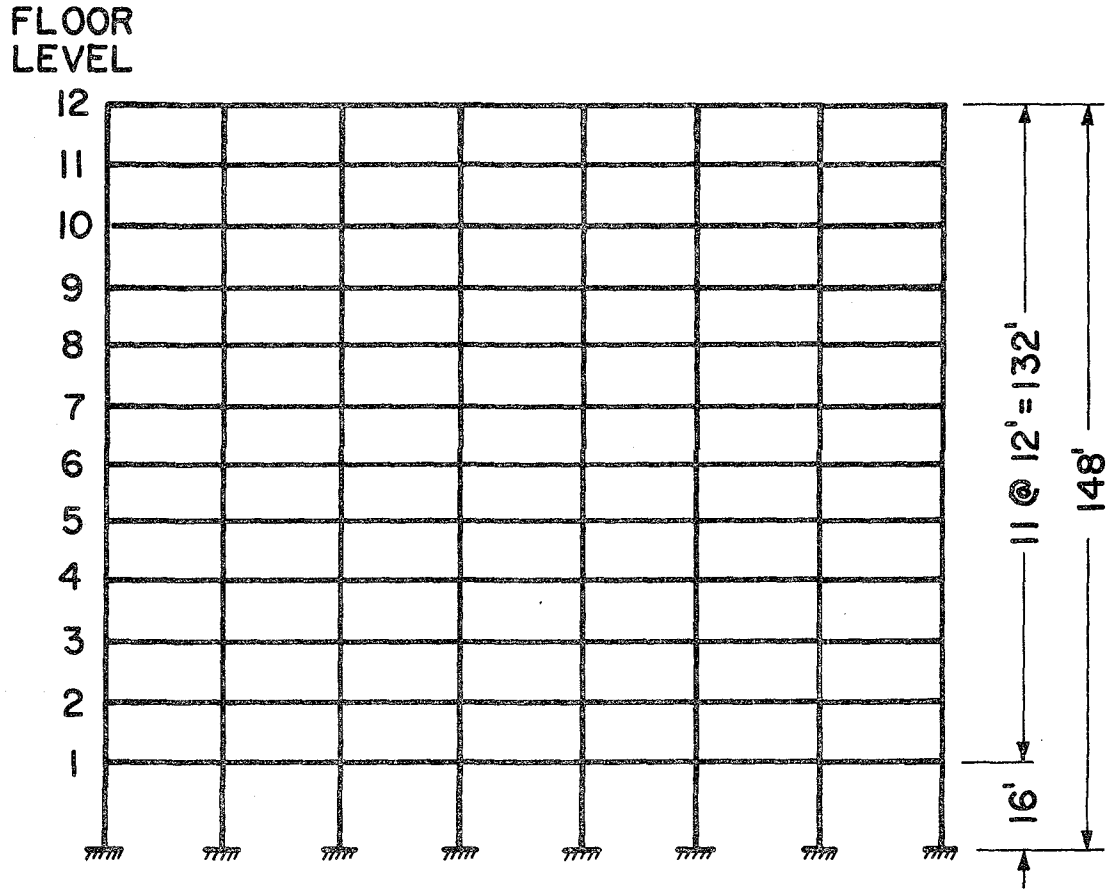

ELEVATION OF 12-STORY BUILDING

Fig. 5.11 Multistory Building

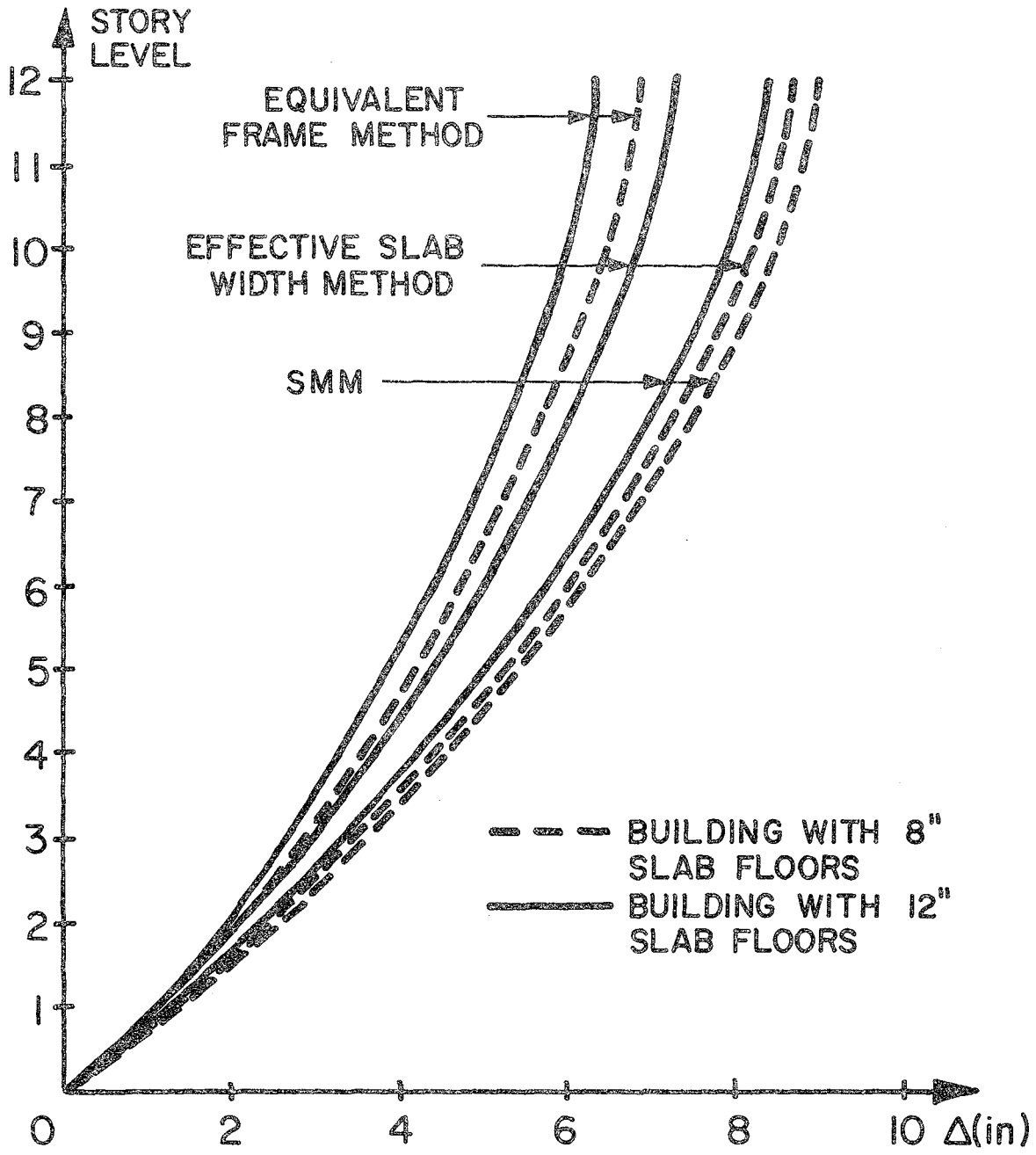

Fig. 5.12 Envelope of Maximum Displacements (SRSS) Using N-S El Centro Spectral Response with 5% Damping

Appendix A

BEAM CARRYOVER FACTORS INCLUDING INFLUENCE OF SHEAR DISTORTION IN FLEXURAL BEAM

The stiffness matrix of a prismatic member including the influence of shear distortions is:

$$K = \frac{2EI}{L(1 + 2\tau)} \begin{bmatrix} 2+\tau & 1-\tau \\ 1-\tau & 2+\tau \end{bmatrix} \tag{A.1}$$

where

$$\tau = \frac{6EI}{GA_{sh} L^2} \tag{A.2}$$

Since all beams used in this study have a depth-to-width ratio of 2:1, and material properties as defined in section 2.3.1, τ can be more easily defined as:

$$\tau = \frac{6(2)\ (1 + 0.17)\frac{D^4}{24}}{\frac{5D^2}{12} L^2}$$

$$\tau = 1.404 \frac{D^2}{L^2} \tag{A.3}$$

The stiffness matrix of eq. A.1 could also be rearranged so that:

$$K = \frac{4EI}{L} \left(\frac{2 + \tau}{2 + 4\tau}\right) \begin{bmatrix} 1.0 & \frac{1-\tau}{2+\tau} \\ \frac{1-\tau}{2+\tau} & 1.0 \end{bmatrix} \tag{A.4}$$

Given eq. A.4, when the influence of shear distortions in the flexural beam is included, the following equations must be modified:

1. The flexural stiffness k_F, as defined in eq. 2.1, is transformed to k_F' where:

$$k_F' = \frac{4EI_B}{L} \left(\frac{2 + \tau}{2 + 4\tau}\right) \tag{A.5}$$

2. The ratio β, as defined in eq. 2.6, is transformed to β' where:

$$\beta' = \beta \left(\frac{2 + 4\tau}{2 + \tau}\right) \tag{A.6}$$

3. Using eqs. A.4, A.5, and A.6, the stiffness of the bare beams $(K_{11})_B$, as defined in eq. 2.5, is transformed to $(K_{11})_B'$, where:

$$(K_{11})_B' = \frac{4EI_{FB}}{L_1} \left(\frac{2 + \tau}{2 + 4\tau}\right) + \frac{GJ_{TB}}{L_2}$$

$$(K_{11})_B' = \frac{4EI_{FB}}{L_1} \left(\frac{2 + \tau}{2 + 4\tau}\right) (1 + \beta') \tag{A.7}$$

and the bare beam carryover factor ψ_{13}, as defined in eq. 2.11, is transformed to ψ_{13}' where:

$$\psi_{13}' = \left(\frac{1 - \tau}{2 + \tau}\right) \left(\frac{1}{1 + \beta'}\right) \tag{A.8}$$

Using eqs. A.3, A.6, and A.8, the values of ψ_{13}' for some of the floors analyzed in Chapter 3 are as follows:

L_1/L_2	β	α	D (in.)	τ	β	ψ_{13}'
2.0 L_1 = 240 in.	0.064	0.8	12.74	.004	.064	.467
		3.0	17.73	.008	.065	.464
		8.0	22.66	.013	.065	.460
1.0 L_1 = 240 in.	0.064	0.8	15.15	.006	.065	.466
		3.0	21.09	.011	.065	.462
		8.0	26.95	.018	.066	.457
0.5 L_1 = 120 in.	0.064	0.8	15.15	.022	.066	.453
		3.0	21.09	.043	.068	.438
		8.0	26.95	.071	.071	.419

Appendix B

CLOSED-FORM SOLUTION OF LATERAL DISPLACEMENT USING EQUIVALENT FRAME ANALYSIS

The lateral stiffness K_L of a single-story, single-panel frame (Fig. B.1) is the force P necessary to produce a unit lateral displacement Δ at the top of the frame. The solution to the problem of finding P/Δ can be found by superimposing the solution of the two frames shown in Figs. B.1(b) and B.1(c). In the frame shown in Fig. B.1(b), the solution relating the lateral force R to the beam end moments M_B developed as consequence of the applied external moment M_F can be achieved by the use of Castigiliano's Theorem:

$$\frac{1}{2} \quad \frac{\partial U}{\partial M_B} = 0 \tag{B.1}$$

where U = complementary energy:

$$U = 2M_B \left(\frac{M_B}{K_s}\right) + 2 \left(M_F - M_B\right) \frac{\left(M_F - M_B\right)}{K_{ec}} \tag{B.2}$$

where

K_{ec} = equivalent column rotational stiffness [Fig. B.2(a)]

K_s = beam rotational stiffness [Fig. B.2(b)]

$$\frac{1}{2} \frac{\partial U}{\partial M_B} = \frac{2M_B}{K_s} - \frac{2M_F}{K_{ec}} + \frac{2M_B}{K_{ec}} = 0 \tag{B.3}$$

$$M_B = M_F \left(\frac{K_s}{K_s + K_{ec}}\right) \tag{B.4}$$

The moment in each of the columns in the frame shown in Fig. B.1(b) is $(M_F - M_B)$ and can be related to the shear in the column by:

$$\frac{R}{2} = \frac{3(M_F - M_B)}{2H} \tag{B.5}$$

$$R = \frac{3(M_F - M_B)}{H} \tag{B.6}$$

Superimposing the two frames shown in Figs. B.1(b) and B.1(c):

$$P = \frac{4M_F}{H} - R \tag{B.7}$$

Using eqs. B.4 and B.6:

$$P = \frac{M_F}{H}\left[\frac{4K_s + K_{ec}}{K_s\ K_{ec}}\right] \tag{B.8}$$

In the columns of the frame shown in Fig. B.1(c), the column moment M_F and lateral displacement Δ can be related by:

$$K_{LR} = \frac{M_F}{\Delta} \tag{B.9}$$

where K_{LR} = lateral force needed to produce unit lateral displacement in column [Fig. B.2(c)]

Using eqs. B.8 and B.9:

$$K_1 = \frac{P}{\Delta} = \left[\frac{4K_s + K_{ec}}{K_s\ K_{ec}}\right] \frac{K_{LR}}{H} \tag{B.10}$$

Member Properties: The equivalent beam as defined by the ACI Code equivalent frame method (Fig. B.3) can be shown to have the following properties:

$$I_B = \frac{d_s^3}{12}\left(\frac{L_2}{2} - \frac{D}{4}\right) + A_1\left(D - \frac{d_s}{2} - \eta\right)^2 + \frac{D^4}{24} + \frac{D^2}{2}\left(\frac{D}{2} - \eta\right)^3 \tag{B.11}$$

and

$$K_s = \frac{EL_1}{B} \tag{B.12}$$

where I_B = moment of inertia of equivalent beam

C = column width

$$A_1 = d_s \left(\frac{L_2}{2} - \frac{D}{4}\right)$$

$$A_2 = \frac{D^2}{2}$$

$$n = \frac{1}{A_1+A_2}\left[A_1\left(D - \frac{d_s}{2}\right) + A_2\,\frac{D}{2}\right]$$

$$B = F_1\left(L_1 - \frac{C}{3}\right) + F_2\left(L_1 - \frac{C}{2}\right) + F_3\left(\frac{2L_1 - 4C}{B}\right)$$

$$F_1 = \frac{C}{4I_{BT}}\left(1 - \frac{L_1-C}{L_1}\right)$$

$$F_2 = \frac{C}{2I_{BT}}\left(\frac{L_1-C}{L_1}\right)$$

$$F_3 = \frac{1}{I_B}\left[\frac{(L_1-C)^2}{4L_1}\right]$$

$$I_{BT} = \frac{I_B}{\left(1 - \frac{C}{L_2}\right)^2}$$

The rotational stiffness K_{ec} of the equivalent column (Fig. B.4) is defined by the ACI Code to be:

$$K_{ec} = \frac{(K_{ta})(K_c)}{K_{ta} + K_c} \qquad (B.13)$$

Using the conjugate beam method, it can be shown that for the column shown in Fig. B.4:

$$K_c = \frac{EI_c}{H_c - N\left[DH_c + (H_c)^2/2\right]} \qquad (B.14)$$

where

$$N = \frac{DH_c + \frac{(H_c)^2}{2}}{DH_c\left(D + \frac{H_c}{2}\right) + \frac{(H_c)^2}{2}\left(D + \frac{2H_c}{3}\right)}$$

The code also defines K_{ta} as the torsional stiffness of torsional beam (Fig. B.5) where:

$$K_{ta} = K_t \frac{I_B}{I_s} \tag{B.15}$$

and

$$4\, d_s \leq B_f \leq D - d_s$$

For definitions of I_s and K_t, see ACI 318-71 Code, section 13.4.

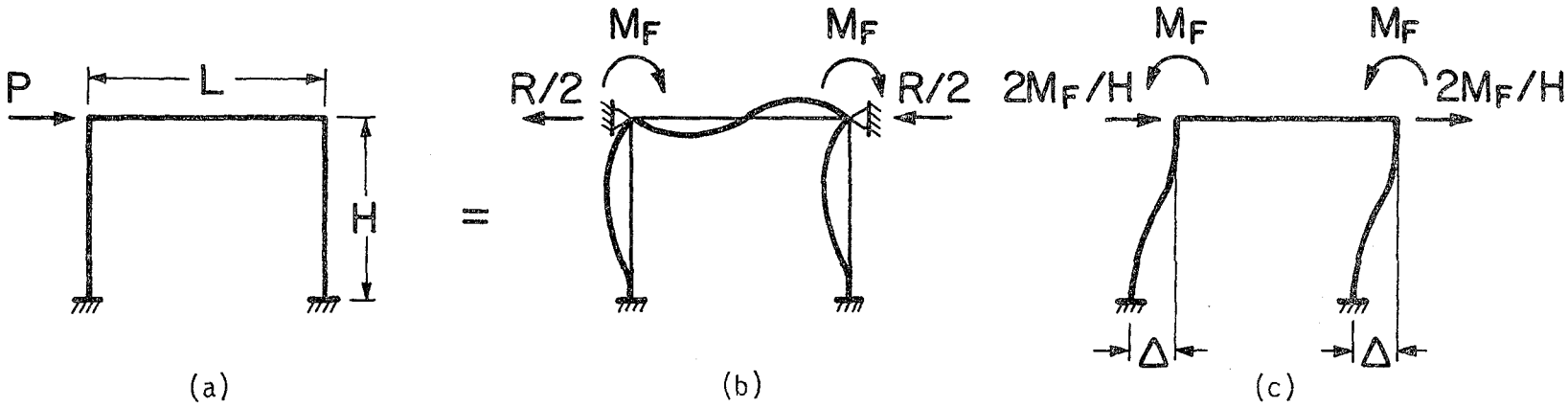

Fig. B.1 Plane Frame under Lateral Load

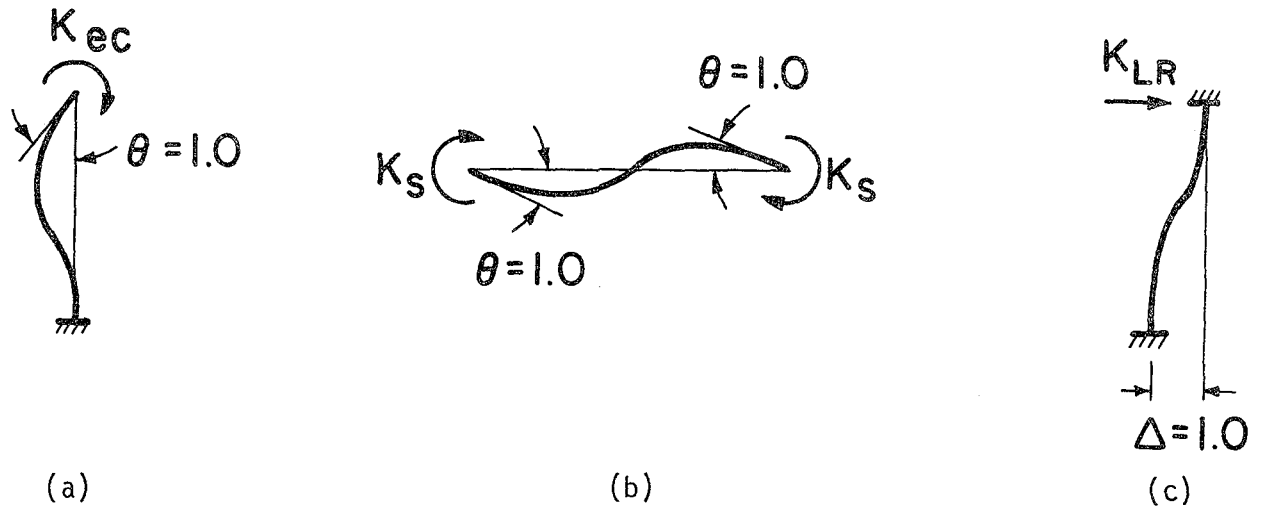

Fig. B.2 Member Stiffnesses

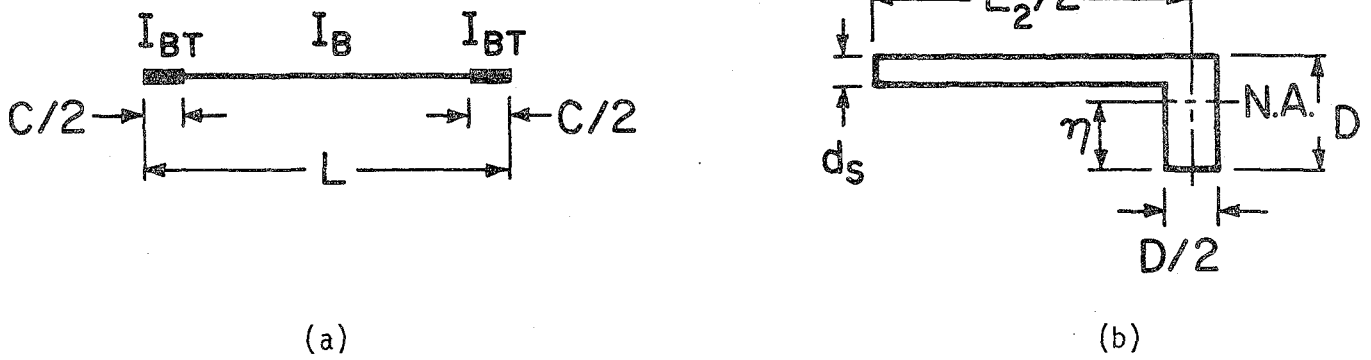

Fig. B.3 Equivalent Beam

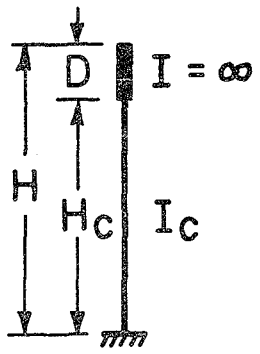

Fig. B.4 Equivalent Column

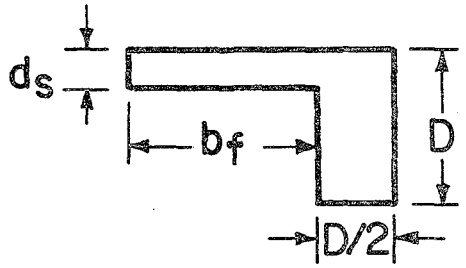

Fig. B.5 Equivalent Torsional Beam

Appendix C

CALCULATION OF LATERAL STIFFNESS OF SINGLE-STORY STRUCTURES

C.1 Single-Panel, Single-Story Structures

Following are the detailed calculations of the lateral stiffness of the single-panel, single-story structures described in Tables 5.3 through 5.6. The calculations are based on results of the computer analysis of the finite element model (Fig. 5.5), the ACI 318-71, 8.7 model (Fig. 5.8), and the SMM (Fig. 5.9).

1. Finite element model. - Given the symmetry of model and load shown in Fig. C.1, the lateral displacements Δ are such that:

$$\Delta_A = \Delta_C$$
$$\Delta_B = \Delta_D \qquad (C.1)$$

However, due to in-plane slab strains:

$$\Delta_A > \Delta_B$$
$$\Delta_C > \Delta_D \qquad (C.2)$$

The computer program produces the lateral displacements at the mid-plane of the slab Δ_{cs} and the rotation of the nodes θ_{yy}. The lateral displacement of the top of the slab Δ_T, based on the assumption that plane sections in the slab remain plane (Fig. C.1), is:

$$\Delta_T = \Delta_{cs} + \frac{d_s}{2} (\tan \theta_{yy}) \qquad (C.3)$$

Taking the average of the lateral displacements at the four columns, the lateral stiffness of the structure becomes P/Δ_{Ta} where:

$$\Delta_{Ta} = \frac{1}{2} [(\Delta_T)_A + (\Delta_T)_B] \qquad (C.4)$$

The values of Δ_{Ta} based on eq. C.4 for the structures analyzed in Chapter 5 are given in Tables C.1a through C.1d.

2. The ACI 318-71, 8.7 and the SMM. - These two models are similar, as shown in Fig. C.2. The computer program used gives the lateral displacement of the equivalent beam's neutral axis $\Delta_{N.A.}$, the moment at the top of the column M_{TC}, and the moment at the base of the column M_{BC} (Fig. C.2). Given that plane sections in the beam remain plane, the lateral displacement at the top of the slab Δ_T, as shown in Fig. C.2(b), can be calculated as:

$$\Delta_T = \Delta_{N.A.} + \lambda \tan \theta_{CT} \qquad (C.5)$$

and the rotation at the top of column θ_{CT} can be found by integrating the curvature along the length of the column, where:

$$\theta_{CT} = \frac{H-D}{2EI_c} [M_{BC} - M_{TC}] \qquad (C.6)$$

The values of Δ_T based on eq. C.6 for the structures analyzed in Chapter 5 are given in Tables C.2a through C.3d.

TABLE C.1a: LATERAL DISPLACEMENTS OF A SINGLE-PANEL, SINGLE-STORY STRUCTURE BASED ON THE FINITE ELEMENT METHOD WHERE $L_1/L_2 = 1.0$, $L_1 = 240$ in., $H = 144$ in.

C (in.)	α_{AB}	β_{AC}	d_s (in.)	Support A		Support B		Δ_T (in.)
				Δ_{CS} (in.)	θ_{YY} (rad)	Δ_{CS} (in.)	θ_{YY} (rad)	
15	0.8	.064	6.5	2.496	.01216	2.480	.01168	2.527
			9.0	1.793	.00570	1.782	.00531	1.812
		.160	6.5	2.445	.01162	2.430	.01115	2.474
15	3.0	.064	6.5	1.716	.00475	1.704	.00472	1.725
21	3.0	.064	6.5	.715	.00409	.704	.00380	.723
15	8.0	.064	6.5	1.335	.00260	1.324	.00208	1.337
		.160	6.5	1.329	.00253	1.318	.00203	1.331
20	8.0	.064	6.5	.570	.00228	.561	.00195	.572
			9.0	.408	.00109	.401	.00084	.409
		.160	6.5	.565	.00222	.555	.00190	.567
27	8.0	.064	6.5	.278	.00172	.270	.00155	.279

TABLE C.1b: LATERAL DISPLACEMENTS OF A SINGLE-PANEL, SINGLE-STORY STRUCTURE BASED ON THE FINITE ELEMENT METHOD WHERE $L_1/L_2 = 0.5$, $L_1 = 120$ in, H = 144 in.

C (in.)	α_{AB}	β_{AC}	d_s (in.)	Support A		Support B		Δ_T (in.)
				Δ_{CS} (in.)	θ_{YY} (rad)	Δ_{CS} (in.)	θ_{YY} (rad)	
15	0.4	.064	6.5	1.394	.00938	1.380	.00832	1.416
	0.8	.064	6.5	.782	.00278	.773	.00232	.786
	3.0	.064	6.5	.608	.00147	.601	.00109	.608
25	0.40	.064	6.5	.352	.00341	.340	.00302	.356
	0.80	.064	6.5	.215	.00174	.208	.00157	.216
	3.0	.064	6.5	.151	.00103	.145	.00087	.151

TABLE C.1c: LATERAL DISPLACEMENTS OF A SINGLE-PANEL, SINGLE-STORY STRUCTURE BASED ON THE FINITE ELEMENT METHOD WHERE $L_1/L_2 = 0.75$, $L_1 = 180$ in., H = 144 in.

C (in.)	α_{AB}	β_{AC}	d_s (in.)	Support A		Support B		Δ_T (in.)
				Δ_{CS} (in.)	θ_{YY} (rad)	Δ_{CS} (in.)	θ_{YY} (rad)	
25	0.8	.064	8.0	.282	.00256	.272	.00241	.287
	3.0	.064	8.0	.187	.00145	.179	.00129	.189
	8.0	.064	8.0	.127	.00083	.121	.00067	.127

TABLE C.1d: LATERAL DISPLACEMENTS OF A SINGLE-PANEL, SINGLE-STORY STRUCTURE BASED ON THE FINITE ELEMENT METHOD WHERE L_1/L_2 = 2.0, L_1 = 240 in., H = 144 in.

C (in.)	α_{AB}	β_{AC}	d_s (in.)	Support A		Support B		Δ_T (in.)
				Δ_{CS} (in.)	θ_{YY} (rad)	Δ_{CS} (in.)	θ_{YY} (rad)	
15	0.8	.064	6.5	1.752	.01382	1.735	.01344	1.788
	3.0	.064	6.5	1.157	.00681	1.143	.00632	1.171
	8.0	.064	6.5	.834	.00349	.822	.00298	.839
20	0.8	.064	6.5	.804	.00759	.788	.00734	.820
	3.0	.064	6.5	.579	.00481	.566	.00454	.588
	8.0	.064	6.5	.407	.00283	.396	.00253	.410

TABLE C.2a: LATERAL DISPLACEMENTS OF A SINGLE-PANEL, SINGLE-STORY STRUCTURE BASED ON ACI-71, 8.7 METHOD WHERE L_1/L_2 = 1.0, L_1 = 240 in., H = 180 in.

C (in.)	α_{AB}	β_{AC}	d_s (in.)	Δ_{NA} (in.)	λ (in.)	M_{TC} (K-in.)	M_{BC} (K-in.)	Δ_T (in.)
15	0.8	.064	6.5	2.440	5.279	3130.17	5112.33	2.502
			9.0	1.766	7.135	3544.84	4488.66	1.804
		.160	6.5	2.440	5.279	3130.17	5112.33	2.502
15	3.0	.064	6.5	1.604	7.852	3611.94	4333.56	1.636
21	3.0	.064	6.5	.635	7.852	2844.22	5101.28	.661
15	8.0	.064	6.5	1.260	10.778	3660.68	3988.32	1.279
			9.0	1.019	14.236	3565.12	3714.88	1.030
		.160	6.5	1.260	10.778	3660.68	3988.32	1.279
20	8.0	.064	6.5	.505	10.778	3350.20	4298.80	.523
			9.0	.374	14.236	3418.88	3861.12	.384
		.160	6.5	.505	10.778	3350.20	4298.80	.523
27	8.0	.064	6.5	.232	10.778	2560.10	5088.90	.247

TABLE C.2b: LATERAL DISPLACEMENTS OF A SINGLE-PANEL, SINGLE-STORY STRUCTURE BASED ON ACI-71, 8.7 METHOD WHERE $L_1/L_2 = 0.5$, $L_1 = 120$ in., H = 144 in.

C(in)	α_{AB}	β_{AC}	d_s (in.)	Δ_{NA} (in.)	λ (in.)	M_{TC} (K-in.)	M_{BC} (K-in.)	Δ_T (in.)
15	0.4	.064	6.5	1.417	4.983	2235.51	4327.34	1.466
	0.8	.064	6.5	.737	8.894	2823.82	3321.98	.757
	3.0	.064	6.5	.575	11.921	2804.09	3048.41	.587
25	0.4	.064	6.5	.343	4.983	517.94	6044.91	.359
	0.8	.064	6.5	.188	8.894	1790.93	4354.87	.201
	3.0	.064	6.5	.127	11.921	2215.92	3636.58	.136

TABLE C.2c: LATERAL DISPLACEMENTS OF A SINGLE-PANEL, SINGLE-STORY STRUCTURE BASED ON ACI-71, 8.7 METHOD WHERE $L_1/L_2 = 0.75$, $L_1 = 180$ in., H = 144 in.

C(in)	α_{AB}	β_{AC}	d_s (in.)	Δ_{NA} (in.)	X(in.)	M_{TC} (K-in)	M_{BC} (K-in.)	Δ_T (in.)
25	0.8	.064	8.0	.265	6.749	1094.08	5220.42	.281
	3.0	.064	8.0	.161	9.963	1922.32	4045.69	.173
	8.0	.064	8.0	.106	13.455	2247.77	3378.23	.114

TABLE C.2d: LATERAL DISPLACEMENTS OF A SINGLE-PANEL, SINGLE-STORY STRUCTURE BASED ON THE ACI-71, 8.7 METHOD WHERE L_1/L_2 = 2.0, L_1 = 240 in., H = 144 in.

C (in.)	α_{AB}	β_{AC}	d_s (in.)	Δ_{NA} (in.)	λ (in.)	M_{TC} (K-in.)	M_{BC} (K-in.)	Δ_T (in.)
15	0.8	.064	6.5	1.691	4.450	1847.88	4715.12	1.751
	3.0	.064	6.5	1.040	6.324	2536.61	3776.69	1.075
	8.0	.064	6.5	.743	8.614	2742.19	3324.61	.765
20	0.8	.064	6.5	.767	4.450	817.12	5745.88	.800
	3.0	.064	6.5	.509	6.324	1717.65	4595.65	.535
	8.0	.064	6.5	.342	8.614	2249.89	3816.91	.360

TABLE C.3a: LATERAL DISPLACEMENTS OF A SINGLE-PANEL, SINGLE-STORY STRUCTURE BASED ON THE STIFFNESS MATRIX METHOD WHERE $L_1/L_2 = 1.0$, $L_1 = 240$ in., H = 144 in.

C (in.)	α_{AB}	β_{AC}	d_s (in.)	Δ_{NA} (in.)	λ (in.)	M_{TC} (K-in.)	M_{BC} (K-in.)	Δ_T (in.)
15	0.8	.064	6.5	2.464	5.500	3106.49	5136.01	2.529
			9.0	1.761	7.189	3547.98	4485.02	1.800
		.160	6.5	2.417	5.500	3149.96	5092.54	2.480
15	3.0	.064	6.5	1.682	7.918	3536.98	4408.52	1.721
21	3.0	.064	6.5	.686	7.918	2657.68	5287.82	.717
15	8.0	.064	6.5	1.301	10.406	3624.98	4027.52	1.323
			9.0	1.030	13.389	3554.30	3725.70	1.042
		.160	6.5	1.297	10.406	3628.57	4023.93	1.319
20	8.0	.064	6.5	.539	10.406	3250.94	4401.56	.560
			9.0	.384	13.389	3386.99	3893.01	.395
		.160	6.5	.536	10.406	3260.47	4392.03	.556
27	8.0	.064	6.5	.254	10.406	2349.01	5303.49	.270

TABLE C.3b: LATERAL DISPLACEMENTS OF A SINGLE-PANEL, SINGEL-STORY STRUCTURE BASED ON THE STIFFNESS MATRIX METHOD WHERE $L_1/L_2 = 0.5$, $L_1 = 120$ in., H = 144 in.

C(in.)	α_{AB}	β_{AC}	d_s(in.)	Δ_{NA}(in.)	λ (in.)	M_{TC}(K-in.)	M_{BC}(K-in.)	Δ_T(in.)
15	0.4	.064	6.5	1.381	5.060	2287.34	4275.66	1.428
	0.8	.064	6.5	.757	8.720	2792.85	3352.65	.780
	3.0	.064	6.5	.384	11.429	2790.33	3062.18	.597
25	0.4	.064	6.5	.338	5.060	569.10	5993.90	.354
	0.8	.064	6.5	.197	8.720	1677.94	4467.57	.212
	3.0	.064	6.5	.133	11.429	2142.91	3709.59	.143

TABLE C.3c: LATERAL DISPLACEMENTS OF A SINGLE-PANEL, SINGLE-STORY STRUCTURE BASED ON THE STIFFNESS MATRIX METHOD WHERE $L_1/L_2 = 0.75$, $L_1 = 180$ in., H = 144 in.

C(in.)	α_{AB}	β_{AC}	d_s(in.)	Δ_{NA}(in.)	λ(in.)	M_{TC}(K-in.)	M_{BC}(K-in.)	Δ_T(in.)
25	0.8	.064	8.0	.265	6.766	1093.41	5221.09	.281
	3.0	.064	8.0	.169	10.371	1814.60	4153.41	.183
	8.0	.064	8.0	.112	12.808	2177.34	3448.16	.121

TABLE C.3d: LATERAL DISPLACEMENTS OF A SINGLE-PANEL, SINGLE-STORY STRUCTURE BASED ON THE STIFFNESS MATRIX METHOD WHERE $L_1/L_2 = 2.0$, $L_1 = 240$ in., $H = 144$ in.

C (in.)	α_{AB}	β_{AC}	d_s (in.)	Δ_{NA} (in.)	λ (in.)	M_{TC} (K-in.)	M_{BC} (K-in.)	Δ_T (in.)
15	0.8	.064	6.5	1.717	4.873	1801.22	4761.63	1.785
	3.0	.064	6.5	1.103	6.844	2437.06	3876.24	1.148
	8.0	.064	6.5	.781	8.987	2683.03	3384.12	.808
20	0.8	.064	6.5	.772	4.873	780.69	5782.17	.808
	3.0	.064	6.5	.541	6.844	1557.26	4756.04	.572
	8.0	.064	6.5	.368	8.987	2117.00	3950.15	.391

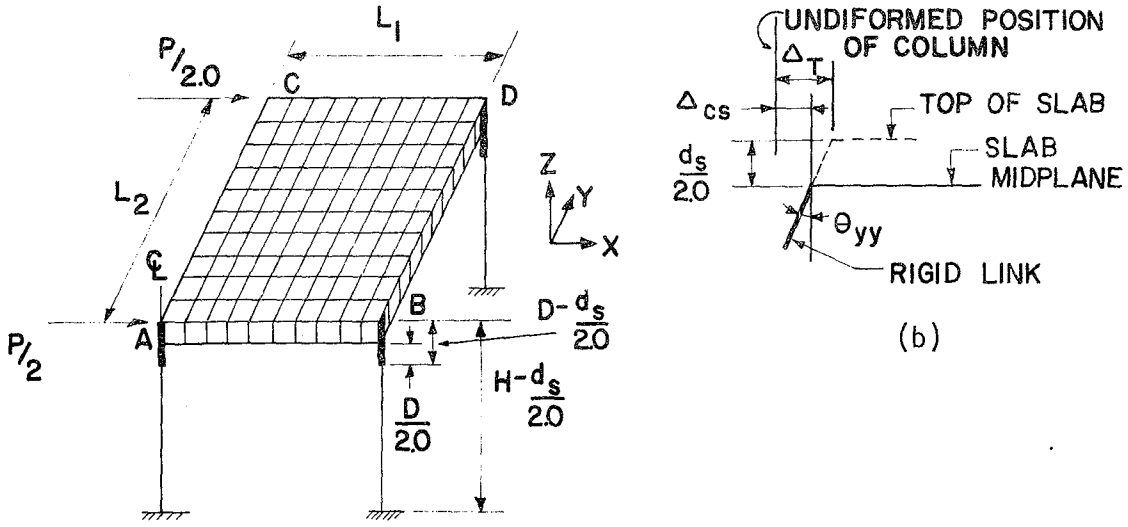

Fig. C.1 Finite Element Method Model

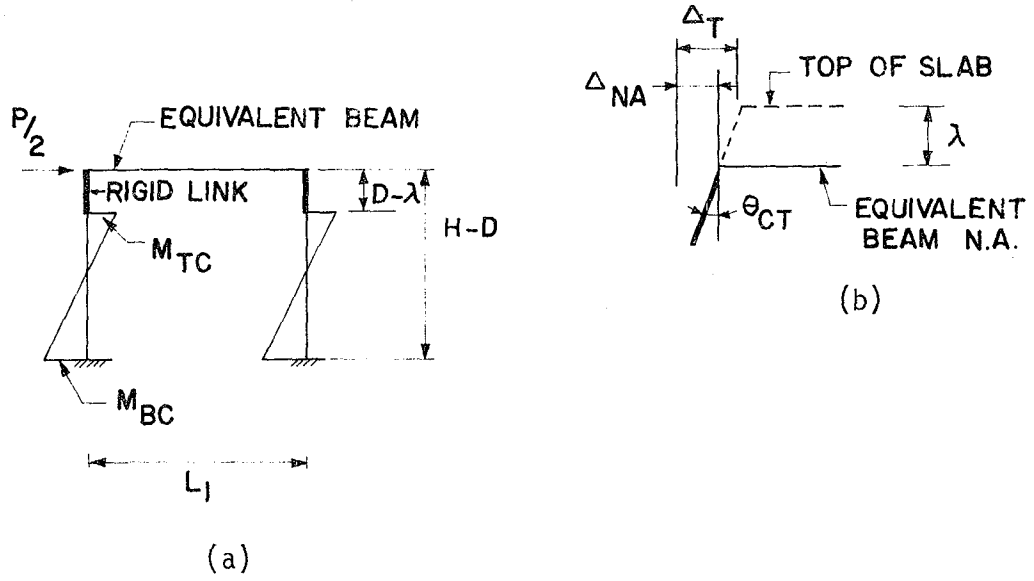

Fig. C.2 ACI 318-71, Section 8.7, and SMM Models

Appendix D

CALCULATION FOR SMM OF THE MULTI-PANEL, SINGLE-STORY STRUCTURE SHOWN IN FIG. 5.10

Since all beams in the floor are identical and slab thickness, d_s, is constant, the following values apply for all members of the model:

$$I_B = \frac{15(30)^3}{12} = 33750.0 \text{ in}^4$$

$$J_B = \frac{30(15)^3}{5} = 20250.0 \text{ in}^4$$

$$A = 15(30) = 450.0 \text{ in.}^2$$

$$e = \frac{30 - 8}{2} = 11.0 \text{ in.}$$

$$E = 3320.6 \text{ ksi}$$

$$\nu = 0.17$$

$$G = 1419.1 \text{ ksi}$$

Six different types of equivalent members are sufficient to model this floor system according to the SMM. These members are:

1. Corner member AB, CD, MN, and QR.
2. Corner member AE, DH, IM, and LR.
3. Exterior member BC and NQ.
4. Exterior member EI and HL.
5. Interior member EF, FG, GH, IJ, JK, and KL.
6. Interior member BF, FJ, JN, CG, GK, and KQ.

The stiffness matrices of the first four are determined according to the procedure given in section 5.2.1(a) and those of the last two according to the procedure given in section 5.2.1(b). Table D.1 gives the results of following the first five steps in the procedure defined in sections 5.2.1(a) and 5.2.1(b). Following are the results of the last two steps:

1. Corner member AB

$$S_{11} = \frac{1.0\ (2531423.80)}{2903798.12}\ (0.07) = 0.06$$

$$S_{22} = 1.0 - \frac{1.0\ [(2531423.80)(0.02)]}{2903798.12} = 0.98$$

2. Corner member AE

$$S_{11} = \frac{1.0\ (2903798.12)}{2531423.80}\ (0.02) = 0.02$$

$$S_{22} = 1.0 - \frac{1.0\ [(2903798.12)(0.06)]}{2531423.80} = 0.93$$

3. Exterior member BC

$$S_{11} = \frac{0.5\ (2897475.46)}{2829421.57}\ (0.05) = 0.03$$

$$S_{22} = 1.0 - \frac{0.5\ [(2897475.46)(0.03)]}{2829421.57} = 0.98$$

4. Exterior member EI

$$S_{11} = \frac{0.5\ (3207014.41)}{2448356.87}\ (0.01) = 0.01$$

$$S_{22} = 1.0 - \frac{0.5\ [(3207014.41)(0.07)]}{2448356.87} = 0.95$$

5. Interior member EF

$$S_{11} = \frac{0.5\ [(2.0)(2897475.46)]}{3207014.41}\ (0.07) = 0.07$$

$$S_{22} = 1.0 - \frac{0.5\ [(2.0)(2897475.46)(.03)]}{3207014.41} = 0.97$$

6. Interior member BF

$$S_{11} = \frac{0.5\ [(2.0)(3207014.41)]}{3897475.46}\ (0.03) = 0.03$$

$$S_{22} = 1.0 - \frac{0.5\ [(2.0)(3207014.41)(.07)]}{2897475.46} = 0.92$$

TABLE D.1: STRUCTURAL PROPERTIES OF MEMBERS FOR STIFFNESS MATRIX MODEL OF A MULTI-PANEL, SINGLE-STORY STRUCTURE

Member	α	β	$\frac{L_{em}}{L_{cm}}$	γ	ξ (in.)	$(K_{11})^r_B \left(\frac{\text{K-in.}}{\text{rad}}\right)$	$\frac{K_{em}}{(K_{11})^r_B}$	$K_{em} \left(\frac{\text{K-in.}}{\text{rad}}\right)$	k_{23}	S
AB	6.59	.08	0.80	.27	2.97	2729133.57	1.06	2903798.12	.337	.07
AE	8.24	.05	1.25	.30	3.25	2280561.98	1.11	2531423.80	.346	.02
BC	6.59	.04	0.80	.27	2.97	2669265.63	1.06	2829421.57	.337	.05
EI	8.24	.03	1.25	.30	3.25	2205726.91	1.11	2448356.87	.346	.01
EF	3.30	.05	0.80	.32	3.51	2838065.85	1.13	3207014.41	.325	.08
BF	4.12	.08	1.25	.35	3.89	2394607.82	1.21	2897475.46	.328	.03

Appendix E

EFFECTIVE SLAB WIDTH FOR SINGLE-PANEL FLOORS

The symmetry of the loading and the structure shown in Fig. 5.5 indicates that the rotations at all the column-floor joints are identical, and a point of counterflexure exists along the x-x floor centerline. Hence the floor contribution to the lateral stiffness of the frame can be modeled by two identical equivalent beams (AB and CD), provided that the moment needed to produce a unit rotation at the two ends of the equivalent beams K_b (Fig. E.1) is the same as K_s required to produce a unit rotation at the four column-floor joints.

Term K_s can be computed from the results of this investigation where:

$$K_s = (K_{11})_s \left(1 + \sum_{j=2}^{8} CF_{1j}\right) \tag{E.1}$$

Since the value of the carryover factors CF_{12}, CF_{14}, CF_{16}, CF_{17}, and CF_{18} has been shown to be small, eq. E.1 can be estimated by:

$$K_s = (K_{11})_s (1 + CF_{13} + CF_{15}) \tag{E.2}$$

It can be shown that K_s as defined in eq. E.2 can be computed from the terms of the stiffness matrix of the equivalent members AB and CD in the SMM, where:

$$K_s = K_{em} (S_{22} + k_{23}) \tag{E.3}$$

The stiffness, K_b, of a prismatic beam consisting of the floor beam and an effective slab width, b_f, (Fig. E.2) is:

$$K_b = \frac{6EI_B}{L} \tag{E.4}$$

where

$$I_B = \frac{(d_s)^3 b_f}{12} + d_s(b_f)\left(D - n\frac{d_s}{2}\right)^2 + \frac{D_w B}{13} + D_w(B)\left(n - \frac{D_w}{2}\right)^2 \tag{E.5}$$

and

$$\eta = \frac{1}{b_f(d_s) + D_w(B)} \left[b_f(d_s)\left(D - \frac{d_s}{2}\right) + \frac{B(D_w)^2}{2} \right]$$

Since we want $K_s = K_b$, using eqs. E.3 and E.4:

$$I_B = \frac{L(K_{em})\ (S_{22} + k_{23})}{6E} \qquad \text{(E.6)}$$

Using eqs. E.5 and E.6, the effective slab width, b_f, can be computed by a trial-and-error procedure.

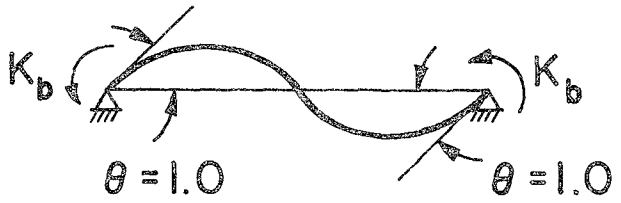

Fig. E.1 Equivalent Beam Stiffness

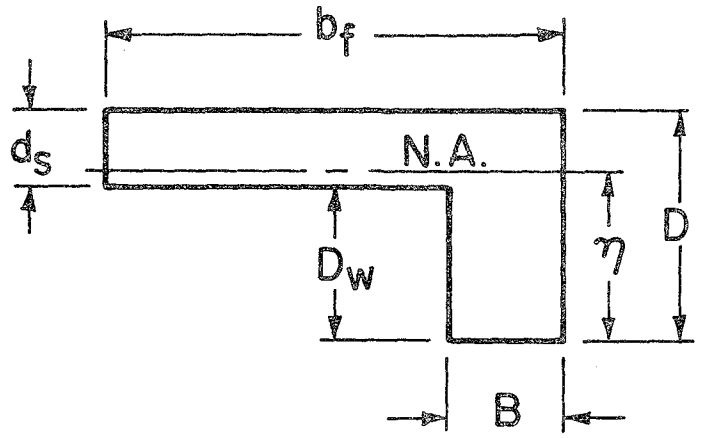

Fig. E.2 Effective Slab Width b_f

EARTHQUAKE ENGINEERING RESEARCH CENTER REPORTS

EERC 67-1 "Feasibility Study Large-Scale Earthquake Simulator Facility," by J. Penzien, J. G. Bouwkamp, R. W. Clough and D. Rea - 1967 (PB 187 905)

EERC 68-1 Unassigned

EERC 68-2 "Inelastic Behavior of Beam-to-Column Subassemblages Under Repeated Loading," by V. V. Bertero - 1968 (PB 184 888)

EERC 68-3 "A Graphical Method for Solving the Wave Reflection-Refraction Problem," by H. D. McNiven and Y. Mengi 1968 (PB 187 943)

EERC 68-4 "Dynamic Properties of McKinley School Buildings," by D. Rea, J. G. Bouwkamp and R. W. Clough - 1968 (PB 187 902)

EERC 68-5 "Characteristics of Rock Motions During Earthquakes," by H. B. Seed, I. M. Idriss and F. W. Kiefer - 1968 (PB 188 338)

EERC 69-1 "Earthquake Engineering Research at Berkeley," - 1969 (PB 187 906)

EERC 69-2 "Nonlinear Seismic Response of Earth Structures," by M. Dibaj and J. Penzien - 1969 (PB 187 904)

EERC 69-3 "Probabilistic Study of the Behavior of Structures During Earthquakes," by P. Ruiz and J. Penzien - 1969 (PB 187 886)

EERC 69-4 "Numerical Solution of Boundary Value Problems in Structural Mechanics by Reduction to an Initial Value Formulation," by N. Distefano and J. Schujman - 1969 (PB 187 942)

EERC 69-5 "Dynamic Programming and the Solution of the Biharmonic Equation," by N. Distefano - 1969 (PB 187 941)

Note: Numbers in parenthesis are Accession Numbers assigned by the National Technical Information Service. Copies of these reports may be ordered from the National Technical Information Service, 5285 Port Royal Road, Springfield, Virginia, 22161. Accession Numbers should be quoted on orders for the reports (PB --- ---) and remittance must accompany each order. (Foreign orders, add $2.50 extra for mailing charges.) Those reports without this information listed are not yet available from NTIS. Upon request, EERC will mail inquirers this information when it becomes available to us.

EERC 69-6 "Stochastic Analysis of Offshore Tower Structures," by A. K. Malhotra and J. Penzien - 1969 (PB 187 903)

EERC 69-7 "Rock Motion Accelerograms for High Magnitude Earthquakes," by H. B. Seed and I. M. Idriss - 1969 (PB 187 940)

EERC 69-8 "Structural Dynamics Testing Facilities at the University of California, Berkeley," by R. M. Stephen, J. G. Bouwkamp, R. W. Clough and J. Penzien - 1969 (PB 189 111)

EERC 69-9 "Seismic Response of Soil Deposits Underlain by Sloping Rock Boundaries," by H. Dezfulian and H. B. Seed - 1969 (PB 189 114)

EERC 69-10 "Dynamic Stress Analysis of Axisymmetric Structures under Arbitrary Loading," by S. Ghosh and E. L. Wilson - 1969 (PB 189 026)

EERC 69-11 "Seismic Behavior of Multistory Frames Designed by Different Philosophies," by J. C. Anderson and V. V. Bertero - 1969 (PB 190 662)

EERC 69-12 "Stiffness Degradation of Reinforcing Concrete Structures Subjected to Reversed Actions," by V. V. Bertero, B. Bresler and H. Ming Liao - 1969 (PB 202 942)

EERC 69-13 "Response of Non-Uniform Soil Deposits to Travel Seismic Waves," by H. Dezfulian and H. B. Seed - 1969 (PB 191 023)

EERC 69-14 "Damping Capacity of a Model Steel Structure," by D. Rea, R. W. Clough and J. G. Bouwkamp - 1969 (PB 190 663)

EERC 69-15 "Influence of Local Soil Conditions on Building Damage Potential during Earthquakes," by H. B. Seed and I. M. Idriss - 1969 (PB 191 036)

EERC 69-16 "The Behavior of Sands under Seismic Loading Conditions," by M. L. Silver and H. B. Seed - 1969 (AD 714 982)

EERC 70-1 "Earthquake Response of Concrete Gravity Dams," by A. K. Chopra - 1970 (AD 709 640)

EERC 70-2 "Relationships between Soil Conditions and Building Damage in the Caracas Earthquake of July 29, 1967," by H. B. Seed, I. M. Idriss and H. Dezfulian - 1970 (PB 195 762)

EERC 70-3 "Cyclic Loading of Full Size Steel Connections," by E. P. Popov and R. M. Stephen - 1970 (PB 213 545)

EERC 70-4 "Seismic Analysis of the Charaima Building, Caraballeda, Venezuela," by Subcommittee of the SEAONC Research Committee: V. V. Bertero, P. F. Fratessa, S. A. Mahin, J. H. Sexton, A. C. Scordelis, E. L. Wilson, L. A. Wyllie, H. B. Seed and J. Penzien, Chairman - 1970 (PB 201 455)

EERC 70-5 "A Computer Program for Earthquake Analysis of Dams," by A. K. Chopra and P. Chakrabarti - 1970 (AD 723 994)

EERC 70-6 "The Propagation of Love Waves across Non-Horizontally Layered Structures," by J. Lysmer and L. A. Drake - 1970 (PB 197 896)

EERC 70-7 "Influence of Base Rock Characteristics on Ground Response," by J. Lysmer, H. B. Seed and P. B. Schnabel - 1970 (PB 197 897)

EERC 70-8 "Applicability of Laboratory Test Procedures for Measuring Soil Liquefaction Characteristics under Cyclic Loading," by H. B. Seed and W. H. Peacock - 1970 (PB 198 016)

EERC 70-9 "A Simplified Procedure for Evaluating Soil Liquefaction Potential," by H. B. Seed and I. M. Idriss - 1970 (PB 198 009)

EERC 70-10 "Soil Moduli and Damping Factors for Dynamic Response Analysis," by H. B. Seed and I. M. Idriss - 1970 (PB 197 869)

EERC 71-1 "Koyna Earthquake and the Performance of Koyna Dam," by A. K. Chopra and P. Chakrabarti - 1971 (AD 731 496)

EERC 71-2 "Preliminary In-Situ Measurements of Anelastic Absorption in Soils Using a Prototype Earthquake Simulator," by R. D. Borcherdt and P. W. Rodgers - 1971 (PB 201 454)

EERC 71-3 "Static and Dynamic Analysis of Inelastic Frame Structures," by F. L. Porter and G. H. Powell - 1971 (PB 210 135)

EERC 71-4 "Research Needs in Limit Design of Reinforced Concrete Structures," by V. V. Bertero - 1971 (PB 202 943)

EERC 71-5 "Dynamic Behavior of a High-Rise Diagonally Braced Steel Building," by D. Rea, A. A. Shah and J. G. Bouwkamp - 1971 (PB 203 584)

EERC 71-6 "Dynamic Stress Analysis of Porous Elastic Solids Saturated with Compressible Fluids," by J. Ghaboussi and E. L. Wilson - 1971 (PB 211 396)

EERC 71-7 "Inelastic Behavior of Steel Beam-to-Column Subassemblages," by H. Krawinkler, V. V. Bertero and E. P. Popov - 1971 (PB 211 335)

EERC 71-8 "Modification of Seismograph Records for Effects of Local Soil Conditions," by P. Schnabel, H. B. Seed and J. Lysmer - 1971 (PB 214 450)

EERC 72-1 "Static and Earthquake Analysis of Three Dimensional Frame and Shear Wall Buildings," by E. L. Wilson and H. H. Dovey - 1972 (PB 212 904)

EERC 72-2 "Accelerations in Rock for Earthquakes in the Western United States," by P. B. Schnabel and H. B. Seed - 1972 (PB 213 100)

EERC 72-3 "Elastic-Plastic Earthquake Response of Soil-Building Systems," by T. Minami - 1972 (PB 214 868)

EERC 72-4 "Stochastic Inelastic Response of Offshore Towers to Strong Motion Earthquakes," by M. K. Kaul - 1972 (PB 215 713)

EERC 72-5 "Cyclic Behavior of Three Reinforced Concrete Flexural Members with High Shear," by E. P. Popov, V. V. Bertero and H. Krawinkler - 1972 (PB 214 555)

EERC 72-6 "Earthquake Response of Gravity Dams Including Reservoir Interaction Effects," by P. Chakrabarti and A. K. Chopra - 1972 (AD 762 330)

EERC 72-7 "Dynamic Properties on Pine Flat Dam," by D. Rea, C. Y. Liaw and A. K. Chopra - 1972 (AD 763 928)

EERC 72-8 "Three Dimensional Analysis of Building Systems," by E. L. Wilson and H. H. Dovey - 1972 (PB 222 438)

EERC 72-9 "Rate of Loading Effects on Uncracked and Repaired Reinforced Concrete Members," by S. Mahin, V. V. Bertero, D. Rea and M. Atalay - 1972 (PB 224 520)

EERC 72-10 "Computer Program for Static and Dynamic Analysis of Linear Structural Systems," by E. L. Wilson, K.-J. Bathe, J. E. Peterson and H. H. Dovey - 1972 (PB 220 437)

EERC 72-11 "Literature Survey - Seismic Effects on Highway Bridges," by T. Iwasaki, J. Penzien and R. W. Clough - 1972 (PB 215 613)

EERC 72-12 "SHAKE-A Computer Program for Earthquake Response Analysis of Horizontally Layered Sites," by P. B. Schnabel and J. Lysmer - 1972 (PB 220 207)

EERC 73-1 "Optimal Seismic Design of Multistory Frames," by V. V. Bertero and H. Kamil - 1973

EERC 73-2 "Analysis of the Slides in the San Fernando Dams during the Earthquake of February 9, 1971," by H. B. Seed, K. L. Lee, I. M. Idriss and F. Makdisi - 1973 (PB 223 402)

EERC 73-3 "Computer Aided Ultimate Load Design of Unbraced Multistory Steel Frames," by M. B. El-Hafez and G. H. Powell - 1973

EERC 73-4 "Experimental Investigation into the Seismic Behavior of Critical Regions of Reinforced Concrete Components as Influenced by Moment and Shear," by M. Celebi and J. Penzien - 1973 (PB 215 884)

EERC 73-5 "Hysteretic Behavior of Epoxy-Repaired Reinforced Concrete Beams," by M. Celebi and J. Penzien - 1973

EERC 73-6 "General Purpose Computer Program for Inelastic Dynamic Response of Plane Structures," by A. Kanaan and G. H. Powell - 1973 (PB 221 260)

EERC 73-7 "A Computer Program for Earthquake Analysis of Gravity Dams Including Reservoir Interaction," by P. Chakrabarti and A. K. Chopra - 1973 (AD 766 271)

EERC 73-8 "Behavior of Reinforced Concrete Deep Beam-Column Subassemblages under Cyclic Loads," by O. Kustu and J. G. Bouwkamp - 1973

EERC 73-9 "Earthquake Analysis of Structure-Foundation Systems," by A. K. Vaish and A. K. Chopra - 1973 (AD 766 272)

EERC 73-10 "Deconvolution of Seismic Response for Linear Systems," by R. B. Reimer - 1973 (PB 227 179)

EERC 73-11 "SAP IV: A Structural Analysis Program for Static and Dynamic Response of Linear Systems," by K.-J. Bathe, E. L. Wilson and F. E. Peterson - 1973 (PB 221 967)

EERC 73-12 "Analytical Investigations of the Seismic Response of Long, Multiple Span Highway Bridges," by W. S. Tseng and J. Penzien - 1973 (PB 227 816)

EERC 73-13 "Earthquake Analysis of Multi-Story Buildings Including Foundation Interaction," by A. K. Chopra and J. A. Gutierrez - 1973 (PB 222 970)

EERC 73-14 "ADAP: A Computer Program for Static and Dynamic Analysis of Arch Dams," by R. W. Clough, J. M. Raphael and S. Majtahedi - 1973 (PB 223 763)

EERC 73-15 "Cyclic Plastic Analysis of Structural Steel Joints," by R. B. Pinkney and R. W. Clough - 1973 (PB 226 843)

EERC 73-16 "QUAD-4: A Computer Program for Evaluating the Seismic Response of Soil Structures by Variable Damping Finite Element Procedures," by I. M. Idriss, J. Lysmer, R. Hwang and H. B. Seed - 1973 (PB 229 424)

EERC 73-17 "Dynamic Behavior of a Multi-Story Pyramid Shaped Building," by R. M. Stephen and J. G. Bouwkamp - 1973

EERC 73-18 "Effect of Different Types of Reinforcing on Seismic Behavior of Short Concrete Columns," by V. V. Bertero, J. Hollings, O. Kustu, R. M. Stephen and J. G. Bouwkamp - 1973

EERC 73-19 "Olive View Medical Center Material Studies, Phase I," by B. Bresler and V. V. Bertero - 1973 (PB 235 986)

EERC 73-20 "Linear and Nonlinear Seismic Analysis Computer Programs for Long Multiple-Span Highway Bridges," by W. S. Tseng and J. Penzien - 1973

EERC 73-21 "Constitutive Models for Cyclic Plastic Deformation of Engineering Materials," by J. M. Kelly and P. P. Gillis - 1973 (PB 226 024)

EERC 73-22 "DRAIN - 2D User's Guide," by G. H. Powell - 1973 (PB 227 016)

EERC 73-23 "Earthquake Engineering at Berkeley - 1973" - 1973 (PB 226 033)

EERC 73-24 Unassigned

EERC 73-25 "Earthquake Response of Axisymmetric Tower Structures Surrounded by Water," by C. Y. Liaw and A. K. Chopra - 1973 (AD 773 052)

EERC 73-26 "Investigation of the Failures of the Olive View Stairtowers during the San Fernando Earthquake and Their Implications in Seismic Design," by V. V. Bertero and R. G. Collins - 1973 (PB 235 106)

EERC 73-27 "Further Studies on Seismic Behavior of Steel Beam-Column Subassemblages," by V. V. Bertero, H. Krawinkler and E. P. Popov - 1973 (PB 234 172)

EERC 74-1 "Seismic Risk Analysis," by C. S. Oliveira - 1974 (PB 235 920)

EERC 74-2 "Settlement and Liquefaction of Sands under Multi-Directional Shaking," by R. Pyke, C. K. Chan and H. B. Seed - 1974

EERC 74-3 "Optimum Design of Earthquake Resistant Shear Buildings," by D. Ray, K. S. Pister and A. K. Chopra - 1974 (PB 231 172)

EERC 74-4 "LUSH - A Computer Program for Complex Response Analysis of Soil-Structure Systems," by J. Lysmer, T. Udaka, H. B. Seed and R. Hwang - 1974 (PB 236 796)

EERC 74-5 "Sensitivity Analysis for Hysteretic Dynamic Systems: Applications to Earthquake Engineering," by D. Ray - 1974 (PB 233 213)

EERC 74-6 "Soil-Structure Interaction Analyses for Evaluating Seismic Response," by H. B. Seed, J. Lysmer and R. Hwang - 1974 (PB 236 519)

EERC 74-7 Unassigned

EERC 74-8 "Shaking Table Tests of a Steel Frame - A Progress Report," by R. W. Clough and D. Tang - 1974

EERC 74-9 "Hysteretic Behavior of Reinforced Concrete Flexural Members with Special Web Reinforcement," by V. V. Bertero, E. P. Popov and T. Y. Wang - 1974 (PB 236 797)

EERC 74-10 "Applications of Reliability-Based, Global Cost Optimization to Design of Earthquake Resistant Structures," by E. Vitiello and K. S. Pister - 1974 (PB 237 231)

EERC 74-11 "Liquefaction of Gravelly Soils under Cyclic Loading Conditions," by R. T. Wong, H. B. Seed and C. K. Chan - 1974

EERC 74-12 "Site-Dependent Spectra for Earthquake-Resistant Design," by H. B. Seed, C. Ugas and J. Lysmer - 1974

EERC 75-24 "Testing Facility for Subassemblages of Frame-Wall Structural Systems," by V. V. Bertero, E. P. Popov and T. Endo - 1975

EERC 75-25 "Influence of Seismic History of the Liquefaction Characteristics of Sands," by H. Bolton Seed, Kenji Mori and Clarence K. Chan - 1975

EERC 75-26 "The Generation and Dissipation of Pore Water Pressures during Soil Liquefaction," by H. Bolton Seed, Phillippe P. Martin and John Lysmer - 1975

EERC 75-27 "Identification of Research Needs for Improving a Seismic Design of Building Structures," by V. V. Bertero - 1975

EERC 75-28 "Evaluation of Soil Liquefaction Potential during Earthquakes," by H. Bolton Seed, I. Arango and Clarence K. Chan 1975

EERC 75-29 "Representation of Irregular Stress Time Histories by Equivalent Uniform Stress Series in Liquefaction Analyses," by H. Bolton Seed, I. M. Idriss, F. Makdisi and N. Banerjee 1975

EERC 75-30 "FLUSH - A Computer Program for Approximate 3-D Analysis of Soil-Structure Interaction Problems," by J. Lysmer, T. Udaka, C.-F. Tsai and H. B. Seed - 1975

EERC 75-31 "ALUSH - A Computer Program for Seismic Response Analysis of Axisymmetric Soil-Structure Systems," by E. Berger, J. Lysmer and H. B. Seed - 1975

EERC 75-32 "TRIP and TRAVEL - Computer Programs for Soil-Structure Interaction Analysis with Horizontally Travelling Waves," by T. Udaka, J. Lysmer and H. B. Seed - 1975

EERC 75-33 "Predicting the Performance of Structures in Regions of High Seismicity," by Joseph Penzien - 1975

EERC 75-34 "Efficient Finite Element Analysis of Seismic Structure - Soil - Direction," by J. Lysmer, H. Bolton Seed, T. Udaka, R. N. Hwang and C.-F. Tsai - 1975

EERC 75-35 "The Dynamic Behavior of a First Story Girder of a Three-Story Steel Frame Subjected to Earthquake Loading," by Ray W. Clough and Lap-Yan Li - 1975

EERC 75-36 "Earthquake Simulator Study of a Steel Frame Structure, Volume II - Analytical Results," by David T. Tang - 1975

EERC 75-37 "ANSR-I General Purpose Computer Program for Analysis of Non-Linear Structure Response," by Digambar P. Mondkar and Graham H. Powell - 1975

EERC 75-38 "Nonlinear Response Spectra for Probabilistic Seismic Design and Damage Assessment of Reinforced Concrete Structures," by Masaya Murakami and Joseph Penzien - 1975

EERC 75-39 "Study of a Method of Feasible Directions for Optimal Elastic Design of Framed Structures Subjected to Earthquake Loading," by N. D. Walker and K. S. Pister - 1975

EERC 75-40 "An Alternative Representation of the Elastic-Viscoelastic Analogy," by Gautam Dasgupta and Jerome L. Sackman - 1975

EERC 75-41 "Effect of Multi-Directional Shaking on Liquefaction of Sands," by H. Bolton Seed, Robert Pyke and Geoffrey R. Martin - 1975

EERC 76-1 "Strength and Ductility Evaluation of Existing Low-Rise Reinforced Concrete Buildings - Screening Method," by Tsuneo Okada and Boris Bresler - 1976

EERC 76-2 "Experimental and Analytical Studies on the Hysteretic Behavior of Reinforced Concrete Rectangular and T-Beams," by Shao-Yeh Marshall Ma, Egor P. Popov and Vitelmo V. Bertero - 1976

EERC 76-3 "Dynamic Behavior of a Multistory Triangular-Shaped Building," by J. Petrovski, R. M. Stephen, E. Gartenbaum and J. G. Bouwkamp - 1976

EERC 76-4 "Earthquake Induced Deformations of Earth Dams," by Norman Serff and H. Bolton Seed - 1976

EERC 76-5 "Analysis and Design of Tube-Type Tall Building Structures," by H. de Clercq and G. H. Powell - 1976

EERC 76-6 "Time and Frequency Domain Analysis of Three-Dimensional Ground Motions, San Fernando Earthquake," by Tetsuo Kubo and Joseph Penzien - 1976

EERC 76-7 "Expected Performance of Uniform Building Code Design Masonry Structures," by R. L. Mayes, Y. Omote, S. W. Chen and R. W. Clough - 1976

EERC 76-8 "Cyclic Shear Tests on Concrete Masonry Piers, Part I - Test Results," by R. L. Mayes, Y. Omote and R. W. Clough 1976

EERC 76-9 "A Substructure Method for Earthquake Analysis of Structure - Soil Interaction," by Jorge Alberto Gutierrez and Anil K. Chopra - 1976

EERC 76-10 "Stabilization of Potentially Liquefiable Sand Deposits using Gravel Drain Systems," by H. Bolton Seed and John R. Booker - 1976

EERC 76-11 "Influence of Design and Analysis Assumptions on Computed Inelastic Response of Moderately Tall Frames," by G. H. Powell and D. G. Row - 1976

EERC 76-12 "Sensitivity Analysis for Hysteretic Dynamic Systems: Theory and Applications," by D. Ray, K. S. Pister and E. Polak - 1976

EERC 76-13 "Coupled Lateral Torsional Response of Buildings to Ground Shaking," by Christopher L. Kan and Anil K. Chopra - 1976

EERC 76-14 "Seismic Analyses of the Banco de America," by V. V. Bertero, S. A. Mahin, and J. A. Hollings - 1976

EERC 76-15 "Reinforced Concrete Frame 2: Seismic Testing and Analytical Correlation," by Ray W. Clough and Jawahar Gidwani - 1976

EERC 76-16 "Cyclic Shear Tests on Masonry Piers, Part II - Analysis of Test Results," by R. L. Mayes, Y. Omote and R. W. Clough 1976

EERC 76-17 "Structural Steel Bracing Systems: Behavior Under Cyclic Loading," by E. P. Popov, K. Takanashi and C. W. Roeder 1976

EERC 76-18 "Experimental Model Studies on Seismic Response of High Curved Overcrossings," by David Williams and William G. Godden - 1976

EERC 76-19 "Effects of Non-Uniform Seismic Disturbances on the Dumbarton Bridge Replacement Structure," by Frank Baron and Raymond E. Hamati - 1976

EERC 76-20 "Investigation of the Inelastic Characteristics of a Single Story Steel Structure using System Identification and Shaking Table Experiments," by Vernon C. Matzen and Hugh D. McNiven 1976

EERC 76-21 "Capacity of Columns with Splice Imperfections," by E. P. Popov, R. M. Stephen and R. Philbrick - 1976

EERC 76-22 "Response of the Olive View Hospital Main Building during the San Fernando Earthquake," by Stephen A. Mahin, Robert Collins, Anil K. Chopra and Vitelmo V. Bertero - 1976

EERC 76-23 "A Study on the Major Factors Influencing the Strength of Masonry Prisms," by N. M. Mostaghel, R. L. Mayes, R. W. Clough and S. W. Chen - 1976

EERC 76-24 "GADFLEA - A Computer Program for the Analysis of Pore Pressure Generation and Dissipation during Cyclic or Earthquake Loading," by J. R. Booker, M. S. Rahman and H. Bolton Seed - 1976

EERC 76-25 "Rehabilitation of an Existing Building: A Case Study," by B. Bresler and J. Axley - 1976

EERC 76-26 "Correlative Investigations on Theoretical and Experimental Dynamic Behavior of a Model Bridge Structure," by Kazuhiko Kawashima and Joseph Penzien - 1976

EERC 76-27 "Earthquake Response of Coupled Shear Wall Buildings," by Thirawat Srichatrapimuk - 1976

EERC 76-28 "Tensile Capacity of Partial Penetration Welds," by Egor P. Popov and Roy M. Stephen - 1976

EERC 76-29 "Analysis and Design of Numerical Integration Methods in Structural Dynamics," by Hans M. Hilber - 1976

EERC 76-30 "Contribution of a Floor System to the Dynamic Characteristics of Reinforced Concrete Buildings," by L. E. Malik and V. V. Bertero